OSM Cooperative Agreement #	S23AC00063
Investigators	John Quaranta, Nathan DePriest
Type of Report	Final Progress Report
Reporting Period	April 1, 2023 – March 31, 2026
Project Title	Pilot Scale Heap Leach Design for Rare Earth Element Extraction from Appalachian Coarse Coal Refuse – WV 397
Performing Organization	West Virginia University

EXECUTIVE SUMMARY

Coal mining refuse byproducts have been identified as potential sources of rare earth elements (REE). The weathering of stockpiled refuse results in the oxidation of its pyritic shale and, thus, the formation of acid mine drainage (AMD) that is enriched in REE. This research aimed to determine whether existing surface deposits of coarse coal refuse (CCR) can be managed to provide an economically attractive REE feedstock while controlling the CCR's long-term AMD liability. The study evaluated the mechanics of bench-scale leaching experiments of Appalachian CCR to extract REE. Three coal refuse feedstock types were evaluated: i) "raw" (directly from active coal preparation), ii) "fresh" (unweathered, subsurface, or new pile source), and iii) "weathered" (near surface or older pile source). Unsaturated column leaching tests, unsaturated drum leaching tests, and saturated jar tests were employed as the most appropriate bench-scale representations of field heap leaching. CCR types were tested in their current stockpiled condition without further processing. A pilot-scale design of a CCR heap leach was develop and modeled to predict seepage and stability. Objectives of the Project were as follows:

- Objective #1: Identify the kinetics of REE release from CCR and determine the key controlling variables.
- Objective #2: Develop engineering designs for a pilot-scale feasibility study for REE commercialization from coarse CCR at existing operating mine.

A summary of accomplishments on a task-by-task basis is as follows:

- Task 1.1: Coarse coal refuse selection and sample collection.
  - Selected a priority site for testing and design through a cooperation with American Consolidated Natural Resources (ACNR).
  - Conducted site visits for CCR and AMD samples collection.

- Task 1.2: Humidity cell testing.
  - Humidity cell tests were replaced with column and drum leaching tests.
  - Conducted a literature review to gather necessary information on the selected bench-scale tests.
  - Conducted column leaching tests.
  - Completed REE analysis after lab testing.
  - Completed Major metals (MM) (e.g., Fe, Al) analysis.
  - Conducted leaching on a larger scale (55-gallon tight-head plastic drum).

- Task 1.3: Predictive model development.
  - Utilized statistical techniques, such as regression analysis, to determine which variables (flow rate, pH, AMD recirculation, hydrogen peroxide addition H_2O_2, and CCR type) were statistically significant to REE extraction.
  - Performed a jar test on weathered CCR.
  - Utilized mathematical models to determine the rate-limiting step and describe the kinetics of the leaching process.

- Task 2.1: Refuse site assessment.
  - Identified critical criteria when selecting a site for heap leaching.
  - Prepared a questionnaire for comparison of two (2) ACNR study sites.
  - Applied the Analytical Hierarchy Process (AHP) decision-making theory to select the preferred project site for potential operational scale-up.

- Task 2.2: Tailings geotechnical material classification and 2-D numerical modeling.
  - Conducted as-received geotechnical testing on all types of collected CCR.
  - Conducted post-leaching and post-permeability geotechnical testing on all types of collected CCR.
  - Reviewed existing data on hydraulic pre-concentrate (HPC) from other AMD sites to inform appropriate geotextile materials for this study.

- Task 2.3. Heap pad analysis and pilot-scale design.
  - Completed a 2-D numerical seepage modeling with Plaxis LE.
  - Conducted slope stability 2-D numerical modeling with Plaxis LE using results of the unsaturated seepage models.

- Task 2.4: Environmental control and system design.
  - Obtained information on the environmental conditions present at the selected site.
  - Predict the long-term AMD generation from the CCR at the site.
  - Completed interpretation of environmental controls based on results from Task 2.1, results of acid-base accounting (ABA) analysis, and information gathered on two (2) project sites.

- Task 2.5 Technical and economic analysis.
  - Gathered existing information from column leaching tests, geotechnical classification, and numerical modeling for economic analysis.
  - Conduct a literature review to gather cost information regarding heap leach circuit units.
  - Calculated the project cost based on the conducted literature review.

The following conclusions were made based on the results of the Project:

- Weathered CCR had the highest potential for leaching when compared to the fresh and raw CCR.
- AMD as a leachant showed a better performance than the other two leachants (AMD+H_2O_2 and DI water).
- The first leaching cycle resulted in the highest percentage increase in TREE concentration.
- Multiple leaching cycles did not promote REE extraction.
- According to geotechnical lab testing, weathered refuse had the highest initial moisture content and the smallest particle size range.
- Extended drying periods (approximately 4 months) allowed for additional pyrite oxidation and REE compounds accumulation at the surface of the solid refuse, which doubled the total REE concentration in the collected leachate.
- REE concentration in leachate increased as the contact time between the leaching solution and the solid particles is extended under saturated conditions.
- Cerium (Ce), neodymium (Nd), and lanthanum (La) were the most abundant REEs in both weathered and fresh CCR. Scandium (Sc) and yttrium (Y) were only abundant in the weathered coal refuse.
- Concentrations of total major metals (TMM) (e.g., Fe and Al) from the refuse followed the same trends seen with total REE. Aluminum (Al), Iron (Fe), and Calcium (Ca) had the highest concentrations in leachate collected from the six columns.

- Blacksville #2 Coal Mine was suitable for the construction of a pilot-scale heap leach pad, as it contained the oldest CCR piles and has existing infrastructure for AMD control.
- Wetting the material before leaching reduced the percentage loss of the applied leaching solution during the first leaching cycle to nearly zero.
- Moisture migration through the geomembrane liner was possible; thus, a double liner system accompanied by a low-permeability clay layer was recommended.
- Constructing a toe berm tie-in around the perimeter of the leach pad footprint and maintaining a uniform distribution of the applied leachant favors the stability of the pile (FOS 1.6).
- The lowest capital and operation cost options available were those that do not involve material processing (e.g., crushing).

The experimental results successfully evaluated the hypothesis of this Project. Bench-scale leaching tests conducted to achieve the goal of the Project have confirmed that REE and CM concentrations in AMD can be increased when AMD is used to leach CCR to produced a REE/CM-enriched pregnant leaching solution (PLS).

The Project successfully demonstrated that CCR can be managed to provide an economically attractive REE feedstock while controlling its long-term AMD liability. We identified that leaching primarily occurred during the first leaching cycle, making the REE compounds readily available due to past weathering exposure. The discovery that weathered refuse has the best potential for REE extraction was a remarkable finding, as this refuse was initially discounted because it visually looked as the most exhausted type of the three coal refuse materials evaluated. Along with REE/CM, major metals (MM) (e.g., iron, aluminum) are also leached during the process.

Additional work conducted during the drum leaching tests provided more valuable conclusions. The extended drying period of approximately 4 months allowed for additional pyrite oxidation and doubled the amount of TREE within the PLS discharge. These findings are of particular relevance for abandoned, or closed and reclaimed coal mines, primarily due to the availability of the two major components: weathered refuse containing REE/CM and pyrite generating AMD. The implementation of heap leaching for manufacturing REE/CM at such sites could serve as a sustainable practice, helping to achieve multiple benefits, such as the responsible management of tailing piles for REE/CM materials and mitigating the long-term environmental consequences of AMD generation.

We believe that the findings of this Project support further expanding the overall REE/CM investigation into a pilot-scale heap leach demonstration using weathered CCR. Concurrent bench-scale testing to optimize individual site operational characteristics is advised before progressing to field-scale application. During this step, the essential criterion to determine the optimal drying duration can be determined for repeating maximizing TREE loads in the PLS.

The numerical modeling through PLAXIS LE showed that PLS flow within the heap structure was steady throughout the permeable and weathered coal refuse. Limit-equilibrium analysis for slope stability concluded that a balanced and surface uniform irrigation combined with slope toe reinforcement results in a substantial role to maintaining slope stability.

We developed a site selection criteria process to assist with the selection of coal mine refuse sites that have beneficial or favorable site ground topography, deposit, and other characteristics to aid in the development of an engineering and operational design. Selecting the best candidate for constructing a leach pad was made possible through multi-criteria decision-making techniques

(e.g., Analytical Hierarchy Process [AHP]). Blacksville #2 was recommended as the best option for any future potential operational scale-up of this project. Coal refuse tailings and AMD at the Crest Pond, available at the Hughes Hollow Impoundment, can be managed and used as part of the implemented design, which adds additional environmental measures to the site.

Abandoned coal mines are not considered a point source of pollution under the Clean Water Act because their source of pollution is not regulated. Therefore, their discharge results in a negative impact on groundwater and streams for extended periods. The developed criteria process could be easily applied to identify other mine sites suitable for leaching implementation, based on site characteristics and coal refuse age.

A significant conclusion to our research indicates that a design strategy can be applied to a coal refuse-based heap-leaching process to extract REE and CM while ensuring pyrite oxidation through intentional drying periods, thereby maximizing REE production while exhausting the pyrite within the refuse, resulting in minimizing the AMD environmental legacy.

BACKGROUND

Acid mine drainage (AMD)

AMD is considered one of the most serious environmental problems in the mining industry (Skousen et al., 2000a). As a result of mine drainage contamination, large numbers of fish and other aquatic organisms have been killed, and natural vegetation has been destroyed over the years (Bigham and Nordstrom, 2000). In the United States alone, there are possibly 500,000 inactive or abandoned mines. It is estimated that mine effluents have severely damaged nearly 19,300 km of streams and more than 72,000 ha of lakes and reservoirs (Bigham and Nordstrom, 2000). Coal refuse has a high pyrite content, which is expected to result in AMD generation over a long time period (Skousen et al., 2000a). AMD is recognized as harmful to the environment, as it is known for its low pH, high acidity, and high level of harmful elements such as aluminum (Al), iron (Fe), and manganese (Mn) (Skousen et al., 2000a). When pH is 2 to 4, and acidity is 1000 to 100,000 mg/L, the environmental consequences of the generated AMD are generally considered moderate (Akcil and Koldas, 2006).

Various research initiatives are being undertaken by the mining industry, universities, and research institutions to understand its causes and treatment. When sulfide-containing materials, such as sulfide-aggregated rocks, are exposed to weathering conditions, AMD is generated (Akcil and Koldas, 2006). This natural process can be accelerated or promoted by mining because large quantities of sulfide minerals deep in the earth are exposed after mining (Gaikwad and Gupta, 2007; Skousen et al., 2019). Pyrite (FeS_2), also known as pyritic sulfur or iron pyrite, is a disulfide and is the most common sulfide mineral in coal refuse. As the pyritic sulfur is exposed to the natural environment (air and water), it undergoes an oxidation process to form sulfuric acid (H_2SO_4) and dissolved iron (Gaikwad and Gupta, 2007; Skousen et al., 2019). Equation 1 explains the general reaction of pyrite oxidation to sulfuric acid.

$$\underset{\text{Pyrite}}{4\ FeS_2} + \underset{\text{oxygen as oxidant (air)}}{15\ O_2} + \underset{\text{water}}{14\ H_2O} \longrightarrow \underset{\text{Yellowboy}}{4\ Fe(OH)_3} + \underset{\text{Sulfuric Acid}}{8\ H_2SO_4} \qquad \text{(Equation 1)}$$

Equations 2 to 5 describe the individual reactions that drive AMD formation. Ferrous iron, sulfate, and hydrogen are formed during the oxidation of pyrite in the first reaction in the process (Equation 2). Most ferrous iron is then oxidized to ferric iron if the surrounding environment is sufficiently

oxidizing, which depends on oxygen concentration, pH, and bacterial activity and availability (Equation 3). It is pH that determines the formation of ferric hydroxide ($Fe(OH)_3$) precipitate (solid). At pH 3.5 and above, solids form, but at pH below 3.5, little or no solids precipitate (Equation 4). The oxidation of additional pyrite may be achieved using the little ferric iron Fe^{3+} that is left in solution (Equation 5) (Akcil and Koldas, 2006; Gaikwad and Gupta, 2007).

$$2FeS_2 + 7O_2 + 2H_2O \rightarrow 2Fe^{2+} + 4SO_4^{2-} + 4H^+ \quad \text{(Equation 2)}$$

$$4Fe^{2+} + O_2 + 4H^+ \rightarrow 4Fe^{3+} + 2H_2O \quad \text{(Equation 3)}$$

$$4Fe^{3+} + 12H_2O \rightarrow \mathrm{Fe(OH)_3} + 12H^+ \quad \text{(Equation 4)}$$

$$FeS_2 + 14Fe^{3+} + 8H_2O \rightarrow 15Fe^{2+} + 2SO_4^{2-} + 16H^+ \quad \text{(Equation 5)}$$

The rate of AMD formation can be affected by several factors, such as the surface area and particle size of rocks containing sulfide minerals, pH, and temperature (Gaikwad and Gupta, 2007). Small-sized particles have a higher surface area when compared to large-sized particles, which means they are more likely to contact weathering agents. For that reason, rock tailings with very fine particles or crushed tailings tend to weather faster than boulders with larger particles. Moreover, low pH and high temperature accelerate chemical reactions because metals are more soluble at higher temperatures, and biological oxidation is higher at pH 3.5 or lower. Depending on what heavy metals are present in the solution, AMD can vary in color. When Fe is the dominant element, AMD tends to be yellow-to-red-to-brown, which is known as “yellow boy.” However, AMD tends to have a milky-white color when Al is the dominant element and a black color when it is rich in Mn (Bigham and Nordstrom, 2000). Other major elements (MM) that can be present in AMD are Calcium (Ca), Magnesium (Mg), Cobalt (Co), Lithium (LI), Sodium (Na), Nickel (NI), Silicon (SI), and Zinc (Zn). In addition to the MM present in AMD, the formed acid can also leach rare earth elements (REEs) from coal refuse, as AMD shows higher REE concentrations (Honaker et al., 2018).

AMD can be treated in various ways, but the most common method is to use chemicals, such as calcium carbonate (limestone) and calcium hydroxide (hydrated lime), primarily for pH neutralization. Significant AMD is often left untreated because most treatments are either inadequate or expensive (Gaikwad and Gupta, 2007). We proposed recirculating AMD through CCR to exhaust its pyritic shale while enriching the generated leachate with REE. If proven successful, the proposed work can provide the triple benefits of highly efficient refuse management, a controlled environment for AMD treatment, and the creation of sustainable sources of REE over the long term. The concept of accelerating pyrite oxidation through AMD circulation is considered novel and has not been reported in the literature to our best knowledge.

Mine tailings and rare earth elements (REE)

Prior to delivery to power plants, market-ready pre-combustion coal must undergo a process known as preparation to remove impurities, such as non-combustible components, as well as crushing to size the coal for combustion. Preparation plants separate material into products (coal) and reject streams (coal refuse). Currently, coal waste is managed by practices such as onsite treatment and fine coal refuse tailing impoundments. The current practices have resulted in many issues, such as acidification and elevated total dissolved solids in receiving waters, toxic chemicals leaching, and structural failures, all of which pose threats to the environment and public health (Colín-Torres et al., 2014; Hudson-Edwards et al., 2024; Sun et al., 2018; P. Wang et al.,

2019). Recently, there has been increased interest in the use of coal mine tailings as a potential feedstock of valuable elements, especially heavy and light REE (Allen et al., 2019; Honaker et al., 2014, 2018; Lange et al., 2017; Lin et al., 2017; Luttrell et al., 2016; Xiao et al., 2015; Yang, 2019a). The search and increased attention to the adoption of domestic feedstocks for REE extraction in the United States have become a priority since 2009, when export restrictions on key REEs were placed by foreign governments, which led to some international supply chain concerns (Lange et al., 2017; Honaker et al., 2018).

REEs are a group of 17 elements and are divided into two groups based on their atomic weights: heavy rare earth elements (HREEs) and light rare earth elements (LREEs). HREEs are yttrium (Y), gadolinium (Gd), terbium (Tb), dysprosium (Dy), holmium (Ho), erbium (Er), thulium (Tm), ytterbium (Yb), and lutetium (Lu). LREEs are scandium (Sc), lanthanum (La), cerium (Ce), praseodymium (Pr), neodymium (Nd), promethium (Pm), samarium (Sm), and europium (Eu). REEs are critical to modern technologies (e.g., electronic displays, health care, and green energy technologies) (Lange et al. 2017; Lin et al. 2017). Over the next two decades, Nd and Dy demand is expected to increase by more than 700% and 2,600%, respectively, due to the development of industries such as electric vehicles, smartphones, and renewable energy (Honaker et al., 2018). The United States Department of Energy (USDOE) identified Nd and Dy as essential for future supply, along with Y, Tb, and Eu (Honaker et al., 2018; USDOE, 2011).

Most REEs associated with coal preparation plants have been identified in mine refuse (Lange et al., 2017; Lin et al., 2017; Honaker et al., 2018). For example, a 2014 field study determined the amount of REE in streams generated by 20 coal processing plants in Kentucky (KY), Pennsylvania (PA), Virginia (VA), and West Virginia (WV) (Honaker et al., 2014; Luttrell et al., 2016). The majority of the REEs by weight were reported to the coal refuse streams, which provided a target for maximizing REE recovery from pre-combustion coal sources (Honaker et al., 2014). In addition, the run-of-mine feeds from this group of plants contained sufficient REEs to satisfy the annual US consumption of these high-value elements (Luttrell et al., 2016).

The weathering of refuse results in the oxidation of its pyritic shale and, thus, the formation of acidic liquid discharge (leachate) enriched in REEs. Honaker et al. (2018) analyzed natural leachates generated from CCR and found that REEs are concentrated in the leachate samples (> 300 ppm) as opposed to the solid refuse feedstock. High-value and critical REEs (i.e., Nd, Dy, Y, Eu, Tb) are selectively leached into the solution that can be readily recovered by downstream separation and purification processes. The elevated concentration of REEs in the generated leachate is evidence of the potential to extract these valuable elements from coal refuse (Honaker et al., 2018; Zhang and Honaker, 2018).

The research team at West Virginia University's (WVU) West Virginia Water Research Institute (WVWRI) has identified AMD as a promising source for REEs (Ziemkiewicz et al. 2016). Ziemkiewicz et al. (2018) indicated that AMD discharges in the Northern and Central Appalachian coal basins have the potential to produce about 1,000 tons per year of REE oxides. This value represents approximately 5% of the total US demand and would satisfy the United States Department of Defense needs. Therefore, in addition to using loose coal mine refuse as an alternative ore, leaching with acids naturally produced from coal refuse has the potential to be an economical method of extracting REEs. Vass et al. (2019) established a typical distribution of REE within AMD based on a field survey study of 155 samples. The leachate generated from coal refuse via leaching has a water chemistry similar to that of AMD, since both are formed following pyrite oxidation in a natural process. Consequently, the hypothesis underlying this project is that pyrite oxidation can be accelerated, and REE extraction from CCR can be enhanced, through the recirculation of AMD. Once AMD is enriched, REE concentrations that

make recovery economical, WVU's patented recovery process (Patent no. US 10,954,582 B2) can be implemented (Ziemkiewicz, 2021). This process can create both a heavy and light mixed rare oxide (MREO) with valuable concentrations of elements such as Tb and Dy (Ziemkiewicz et al. 2023).

Grain Size Distribution (GSD) effect on REE extraction

Ore particle size and hydraulic conductivity strongly affect heap leaching efficiency and kinetics (Allen et al., 2019). Literature specifies particle sizes for heap leaching to range between 5 to 100 mm. This range is specified for the leaching of Cooper (Cu), Nickel (Ni), Uranium (U), and Gold (Au) (Ghorbani et al., 2016). REEs and other minerals contained in coal can be more easily leached and recovered by reducing the particle size of the used ore (Yang, 2019b). This section includes a summary of some previous studies that show the impact of ore particle size on REE extraction from coal byproducts.

The effect of particle size on REE leaching recovery from fire clay coal was studied (Yang and Honaker, 2020) along with other factors, such as leaching time, temperature, and solid concentration. A dry whole sample analysis of the fire clay coal showed a total containment of 242 parts per million (ppm) of REE, whereas dry ash analysis indicated a total of 1331 ppm of REE. To achieve a top particle size of 1 mm, a jaw crusher and hammer mill were used. Around eight samples with a range of 80% passing mesh 80 (0.177 mm) were leached with sulfuric acid solution. The results showed that mineral matter with high concentrations of REE was released by reducing the particle size. The study indicated that by reducing the size of particles, more REEs were recovered through leaching, and more REEs were reported in the leach feed.

In a study by Zhang et al. (2018) on REE extraction from a fire clay coal source, particle sizes were reduced from 90%, passing 84.3 microns (0.0843 mm) to 4.5 microns (0.0045 mm). Using froth flotation, wet high-intensity magnetic separation (WHIMS), and leaching, REEs were concentrated and recovered from samples in this study. Mineral matter within the sample was also released by grinding the material using a laboratory jaw crusher and hammer mill. A modest increase in the total REE content from 500 ppm to 1000 ppm was observed after froth flotation. However, a sequence of froth flotation of the released mineral matter due to 110 minutes of grinding resulted in a concentrate containing 7000 ppm of total REEs. Thus, grinding the material using an attrition mill to release the mineral matter led to a 60% recovery of REEs. Over 80% of REEs were recovered by leaching with nitric acid.

Allen et al. (2019) studied the extraction of REE from coal feed sources. CCR was used in the study, and the material was crushed before use. The goal of the study was to achieve an 8% recovery of REE by the use of ores with small particle sizes and different leaching conditions. The crushing process was done using a laboratory jaw crusher, a roll crusher, a pulverizer, and a grinding mill. The study intended to test coarse refuse samples with a high ash content (approximately 95% passing sieve # 200) and samples with various sulfur contents (ranging from <0.4% to around 40%). Data showed that ash content ws very high in all the tested samples, varying from 84 to 95%. Samples also contained particle sizes bigger than 1 inch (25 mm). Leaching tests were performed using ferric sulfate and bacterial leaching solution in large columns. The results of the study indicated a 10% REE recovery after 90 days of leaching.

Yang et al. (2019) studied the impact of particle size on REE recovery. One of the main goals of the study was to improve recovery through reducing the particle size of the ore. Coarse coal reject stream contains a type of rock known as middlings; this core rock was used as the feed in this study along with coarse refuse samples. Using a jaw crusher, hammer mill, and

pulverizer, the feed for leaching tests was reduced to 177 µm (80 mesh). An attrition mill was also used to grind a representative sample for improving mineral liberation evaluation. Sulfuric acid solution was used in the leaching test. The results showed that grinding nearly doubled LREE leaching recovery; however, no significant impact on the leaching recovery of HREEs was observed after crushing the tested material.

Column leaching tests

Column leaching tests can be employed to better simulate water or any other solution (e.g., AMD) flux in a heap leach pad (Ghorbani et al., 2016). In a column leaching test, recovery versus time is collected for the ore being evaluated so that scale-up to industrial scale can be validated. It is a laboratory method where solid samples are placed in plastic or glass columns. Columns can range in diameter from 10 cm to 1 m and are usually used during metallurgical evaluations (Galla et al., 2008; Ghorbani et al., 2016). The columns are fed with the leaching solution at the top continuously to maintain leaching performance. The effluent discharge is collected at the bottom of the columns after percolation. The leaching solution is uniformly distributed over the surface of the ore, while a constant flow rate is maintained throughout the testing process (Iasillo et al., 2013). Leaching solution can be delivered to the column at a constant flow rate using a variety of devices, such as intravenous drip apparatus, syringe pumps, and constant head tanks. The pregnant leaching solution (PLS) is then analyzed for the elements of interest (Galla et al., 2008; Iasillo et al., 2013; Allen et al., 2019). If soluble precious metals are no longer present in the column effluent after a certain number of days, the test procedure will be stopped. Among the important test parameters provided by the column test are the overall precious metal extraction and reagent consumption (Iasillo et al., 2013).

A wide range of columns are used in literature. Column diameters range from 10 cm to 2 m, while column heights range from 50 cm to 6 m (Ghorbani et al., 2016). **Table 1A, Appendix A,** shows the different sizes of columns used in previous studies. According to sampling theory, the maximum ore particle size is related to column diameter. It is generally recommended that the leaching column should have a diameter three to four times larger than the largest particle of the tested material (Iasillo et al., 2013). Generally, columns with 150 to 300 mm diameters and an ore height ranging from 1.5 to 3 meters can be used in the leach test when larger quantities of ore are available. This test requires a charge of 90 to 360 kg per column. According to the literature, short columns leached faster than long columns due to an unlimited reagent supply (Ghorbani et al., 2016). Shorter columns receive more reagent per mass of reacting ore per unit time of irrigation; thus, a faster leach will be achieved. However, when two different ores are leached, their reagent requirements will differ (Lizama et al., 2005).

Heap pad construction

Prior to constructing a heap pad, a geotechnical investigation must be conducted to evaluate the site's suitability and address any issues that may impact construction. Aspects that need to be addressed include groundwater and surface runoff, the availability of borrow materials on site, and land slope (Pyper et al., 2019).

A typical heap leach pad consists of layers of the ore of interest, a drainage and protection layer through which air injection and solution collection pipes are placed, a geomembrane liner, and the prepared foundation layer. The primary function of the liner is to improve leachate recovery and ensure environmental containment of the leachate and ore (Lupo, 2010). Two types of liner systems are usually adopted: single-composite and double-composite. A single-composite consists of one layer of geomembrane liner, whereas a double-composite consists of two

geomembrane liners with a leak detection layer in between (Whitehorse, 2012; Pyper et al., 2019). According to Lupo (2010), geomembrane liners made out of High-Density Polyethylene (HDPE) or Low-Density Polyethylene (LLDPE) are both considered suitable candidates for acidic leachate containment. Lupo (2010) also indicated that there is a strong interdependent relationship between parameters of the liner system used to construct a heap pad, which can affect the liner performance and eventually the performance of the leach pad itself. These interdependent parameters can affect environmental containment, leachate collection, and the stability of the heap. Some of these parameters include hydraulic and mechanical properties of the liner, slope of the surface, any settlement in the foundation, and the friction between the geomembrane liner and any material in direct contact with the liner. Currie and Parra (2010) reported that LLDPE geomembrane is an ideal liner for leach pads because of its improved elongation and frictional resistance.

There are three configurations for constructing a heap leach pad: standard pads, valley-fill pads, and on/off pads (Ghorbani et al., 2016). Standard pads occupy large surface areas, which can reach 124 acres (0.5 km²), and are known for their low capital cost (Ghorbani et al., 2016). It is typical for them to be between 13 and 33 ft. (4- and 10-m) high. A standard pad site is considered suitable if it is a featureless ground surface uniformly sloped with a grade of 0.5% to 2.0% towards a collection system or pond. A flat grade should be applied at the front edge of the heap, approximately 98 to 164 ft (30 to 50 m), when the ground slope exceeds 3% to prevent failure (Kappes, 2002). Heap pads are typically built in layers (lifts), with ore particle sizes ranging from large rock fragments to fine sizes (crushed) (Ghorbani et al., 2016; Pyper et al., 2019). For safety considerations, a slope of less than 2H:1V (27 degrees) is recommended for the side slope between heap benches.

Valley fill pads are usually built in steep topography where the foundation slope can be very steep and reach 40-50%. They are more expensive compared to the other types, and they are more appropriate for hard, durable ores. It is typical for valley fill pads to have internal solution storage double-lined with a detection system; thus, they require a pumping system (Ghorbani et al., 2016; Pyper et al., 2019).

On/off pads are usually ideal for handling ores that cannot be stacked very high. In this type, the material is removed at the end of the leaching cycle, and a fresh ore load is placed and leached. This double handling of ore is what affects and increases the operational cost of this type of pad; however, it is generally less expensive to construct compared to the other two types. Other aspects that might add to the cost of construction are liner damage due to the frequent handling of material, and the necessity to build multiple cells (at least three pads) to ensure ongoing operation (Ghorbani et al., 2016; Pyper et al., 2019).

Heap bioleaching is another type of leaching that requires a microbial process to extract metals, such as copper and gold, from low-grade ores (Leahy et al., 2006). Maintaining oxygen diffusion is crucial in heap bioleaching. Low-pressure air blowers or fans installed at the toe of the heap are commonly used to maintain aeration in such cases. Then, air is blown into the heap through perforated piping that is connected to the air blowers or fans. These pipes are usually buried in the ore or within the drainage layer underneath the ore (Ghorbani et al., 2016).

Stacking the ore of interest through the construction process can be achieved through three primary methods: truck stacking, conveyor stacking, and excavator stacking. Truck and conveyor stacking are the most common types, whereas excavator stacking is utilized when truck stacking can cause problems with permeability (Pyper et al., 2019).

Numerical modeling of heap leach pads

Numerical modeling has been used in the literature to evaluate heap leach pad design (Dixon and Petersen, 2003; Leahy et al., 2006; Petersen and Dixon, 2007; Bouffard, 2008; Bouffard and Dixon, 2009; Marsden and Botz, 2017). More details about some of the studies are provided in the following paragraph.

The air sparging effect on the heap bioleaching process was investigated by Leahy et al. (2006) through a steady-state 2-D model built using a computational fluid dynamics solver. Copper leaching is affected by airflow rate and sparging placement (for a typical spacing of 1-4 m). Liquid flow rate and permeability also influenced the leaching process.

A complex computational fluid dynamics model coupled with a leach kinetic model was employed by McBride et al. (2018) to simulate a virtual three-dimensional heap of low-grade complex copper sulfide ore. The ore was leached with a leaching solution that contained sulfuric acid along with other components, such as ferric ions and ferrous ions. The heap occupied an area of 2 ft by 79 ft (54 m by 24 m) and was constructed in three lifts, each 30 ft (9 m) in height. A small particle size was not adopted in the modeling, as it caused issues with permeability. The leach period was simulated over a two-year period. The thermal effect on copper recovery was tested by applying internal and external temperatures. The applied external temperature was tested using two scenarios: low (5 °C to 10°C) and high (20 °C to 30 °C). In two scenarios, copper recovery was relatively high but increased slightly with higher temperatures. However, it was concluded that the internal thermal kinetics dominate copper recovery over the long term, while external temperatures have only a small impact. Continuous and pulse (combining irrigation with resting pulses) irrigations were also investigated. Pulse irrigation slightly increased copper recovery per unit volume of applied leach solution (by approximately 12%) compared to continuous irrigation.

Differences between 2-D and 3-D Factor of Safety (FOS) in slope stability analysis were addressed by Reyes et al. (2014). The analysis was performed to evaluate translational failure in heap leaching. The translational failure, which involves the horizontal sliding of ore masses, is the most common type of failure mechanism in heap leaching (Reyes et al. 2014). The general limit equilibrium (GLE) method was employed to conduct the 2-D analysis using standard 2-D LE software. In contrast, the SVSLOPE-3D software package was used for the 3-D GLE analysis. The results of the study showed a significant increase in 3-D FOS compared to 2-D FOS, with static analyses increasing by 20%-49% and pseudo-static analyses increasing by 74%-86%.

OBJECTIVES

The overall goal of the proposed work was to determine whether CCR can be managed to provide an economically attractive REE feedstock while controlling its long-term AMD liability.
We identified and experimentally quantified the REE source amount and the extraction potential of three coarse coal refuse processing streams. We developed prototype engineering design and operation strategies for constructing and operating heap leach pads to efficiently extract the REE in an environmentally beneficial process with a coal company operating in West Virginia and Pennsylvania.

Objective #1: Identify the kinetics of REE release from coarse coal refuse and determine the key controlling variables.

The WVU research team has identified AMD as a promising source for REE. Our research thus far has identified that the majority of REE in raw coal are associated with pyritic shales that, in

turn, are rejected to the refuse stream during processing. Refuse is enriched in pyritic sulfur (0.5 to 12%) which, after exposure, oxidizes to form sulfuric acid. The acid leaches REE and other metals that report to the AMD stream (Vass et al. 2019 a,b). Due to its high pyrite content, coal refuse is a major source of long-term AMD generation (Skousen et al., 2000a) and may generate AMD for many decades after placement. Under the OSMRE Acid Mine Drainage Policy of 1997, Refuse must be treated to prevent long term AMD generation, usually by alkaline amendment or capping (Ziemkiewicz and Skousen, 1992). Refuse disposal is regulated within the SMCRA permit and construction of refuse storage facilities under MSHA safety guidelines. Using a common kinetic test method, column testing, we will determine the rates of AMD and REE generation and the extent to which both are controlled by key management variables such as AMD recirculation and hydrogen peroxide (H_2O_2) addition. We will use these rate variables to generate predictive extraction models to forecast pyrite reaction rates and REE production rates.

Objective #2: Develop engineering designs for a pilot-scale feasibility study for REE commercialization from coarse coal refuse at existing operating mine.

We will develop engineering designs for construction of pilot-scale heap leach pad design and the REE Preconcentrate sludge collection will be handled using Tencate® composite geobags. We will identify operating parameters for the process that simultaneously oxidizes the refuse's pyrite and collects the leaching solution for downstream pH treatment and selective high-grade REE preconcentrate sludge production. The engineering design will compare and contrast the constructability, operation, and REE preconcentrate production based on REE extraction data from three different coarse coal waste product streams: raw, fresh, and weathered. We will address field site selection requirements and identify the environmental controls necessary to benignly operate a heap leach mine facility based on a CCR feedstock. We will collaborate with ACNR and Tencate to develop engineering designs for a pilot-scale coarse coal REE heap leach process and identify parametric operating parameters. The ability to dewater AMD sludge (commonly found up to 2500 % gravimetric moisture content) is necessary to produce a REE preconcentrate which may be economically and environmentally appropriate for shipment to the down-stream REE refining facility. We will develop a Techno-Economic Analysis (TEA) report based on the engineering process design and scalability.

STATEMENT OF WORK

The proposed Statement of Work (SOW) was provided on a task-by-task basis in the Project Narrative. Humidity Cell testing, planned for Task 1.2 in the project proposal, was replaced with column leaching tests based on a literature review of leaching studies. The end date of the project was modified to March 31, 2026, based on a No-Cost Extension Request (NCE) submitted to the Office of Surface Mining (OSM) for review on February 12, 2025, and approved on April 11, 2025. An updated Project schedule, including revised scope for Tasks 1.2 (Humidity cell testing), 2.3 (Heap pad analysis and pilot-scale design), 2.4 (Environmental control and system design), and 2.5 (Technical and economic analysis), was provided in the NCE. The revised schedule extended the end date for these tasks to Quarter 12 (Year 3, Quarter 4) to support the revised scope.

ACCOMPLISHMENTS

Deliverables

Performance progress reports

A total of eleven (11) Quarterly Performance Progress Reports (PPR) were submitted ahead of deadline to the OSM via GrantSolutions and email on a quarterly basis. The Final PPR for the Project, which covers the entire Project performance period (4/1/2023 through 3/31/2026), is provided herein.

Technical publication

The Project team submitted a conference paper and proceedings to the 2025 Heap Leach Solutions Conference. Dr. Nate DePriest provided an oral presentation on 10/20/2025, and the associated paper was published in the conference proceedings. PhD student Zainab Jawad also presented the key findings of the project at the 2026 WVWRI Seminar Series on February 26 and during the WVU annual research week (rapid fire and poster competitions) on April 9th and 10th, 2026 (**Appendix G**). A manuscript summarizing the key findings of the project was developed and submitted to a refereed journal for review in March 2026. A copy of the accepted paper will be provided to OSM once available.

Fact Sheet

A Fact Sheet for the Project was provided to OSM via email on 3/23/2026.

Communication and visits with OSM

Communication between the Project team and OSM was maintained on a regular basis. Multiple in-person visits were conducted with OSM, Applied Sciences Program, project technical reviewer (PTR) Steve Ball, for the purpose of monitoring progress throughout the project. The PTR joined the Project team during the first visit to the site (Blacksville # 2 Mine) on August 17, 2023. The purpose of this visit was to familiarize him with the site during the collection of CCR and AMD samples (Task 1.1). The Project team later met with Steve Ball in April 2024 at WVU to present preliminary key findings after the first round of column leaching tests. The Project team also received a visit from the PTR to the high bay of the National Research Center for Coal and Energy (NRCCE) building at WVU, where column testing was underway, to review the performance of the second round of leaching tests (Task 1.2). The Project team met with Steve Ball on 1/31/2025 to discuss further results and the scope of the NCE submitted to OSM. Mr. Steve Ball also attended the final PhD dissertation defense of student Zainab Jawad, which covered the project's methodology, main results, key findings, and recommendations. Follow-up site visits were conducted with Steve Ball on 8/21/2025 and 1/14/2026.

A meeting with ACNR was held in January 2025 to provide them with a broader update on the project and seek their assistance in completing two questionnaires that were created during Quarter 6 (refer to **Appendix C** and **Appendix D**) for two ACNR study sites (ACNR Blacksville Number 2 Mine and ACNR Marion County Mine). A brief presentation was prepared for the meeting. Their feedback on the two questionnaires was input into an analysis using the Analytical Hierarchy Process (AHP) to quantify and compare the two study sites based on a mathematical approach to achieve the goals of Task 2.1.

Task 1.1 Coarse coal refuse selection and sample collection

Monongalia County Mine – weathered and fresh CCR

The Monongalia County Mine (formally known as "Blacksville #2 Coal Mine "; hereafter referred to as the "site") is located in Monongalia County, West Virginia (WV) (39º 42' 40.38" N, 80º 17' 34.86" W) (**Figure 1.1.1**) and operated by ACNR. The site was selected for proximity to Morgantown, WV, the existence of a recently completed but not yet reclaimed refuse pile (Hughes Hollow), and the collaboration of the mine operator.

Hughes Hollow is the coal refuse impoundment located at the site, permit number U004684, located at (39º 43' 22.89" N, 80º 17' 33.53" W) (**Figure 1.1.2**). CCR tailings locations are also pointed out in **Figure 1.1.2**. Per ACNR, the impoundment received fine coal refuse slurry until 2016, when the backfilling process started. Backfilling was completed in 2019, but the area has not yet been reclaimed. **Figure 1.1.3** shows the impoundment area filled with CCR.

The first visit to the site was conducted on August 17, 2023, to obtain samples needed for the geotechnical laboratory and column leach testing. Other visits to the site were conducted to ACNR's Blacksville # 2 Coal Mine on October 27, 2023, June 26, July 16, and 18, 2025, to obtain samples. Our primary contact for most visits was Nicholas Hegedus, a Project Engineer at ACNR. The team visiting the site included project team members from WVU and the WVWRI.

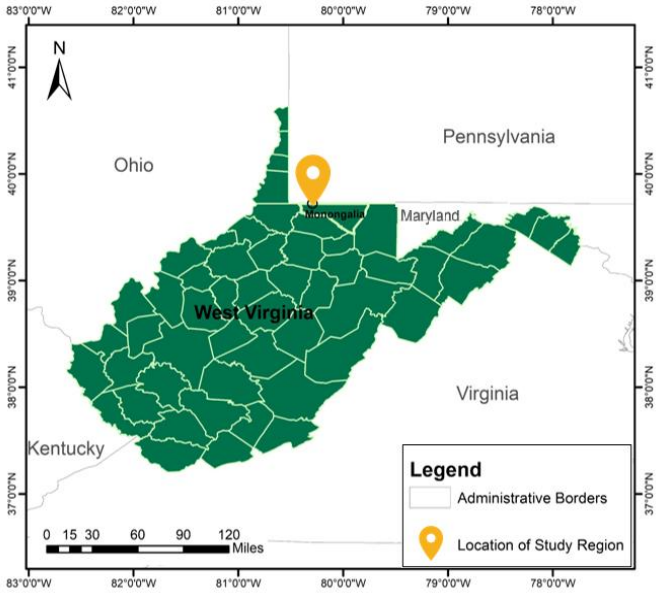


Figure 1.1.1: Location Map - Blacksville #2 Coal Mine located in Monongalia County, WV.



Figure 1.1.2: Hughes Hollow coal refuse impoundment at Blacksville #2 Coal Mine (Google Earth, 2023).


Figure 1.1.3: Hughes Hollow backfilled with CCR.

During the first visit, two types of samples were intended to be collected: “weathered” (near-surface or older pile source) and “fresh” (unweathered, subsurface, or newer pile source). According to ACNR, all refuse at Blacksville #2 (Hughes Hollow and adjacent piles) is at least 2 years old. We were advised that the old tailings would have a brownish color to it, while newer tailings would have more of a black color.

CCR used to backfill the impoundment was first tested as a potential source of samples at a depth of 2 feet; the CCR contained a high proportion of fines and tended to be cohesive when tested by hand, which made it a poor candidate. We were advised by ACNR that CCR tailings available at the site have a drier consistency and are less cohesive compared to backfilling (**Figure 1.1.4**). Thus, old tailings (height 5 to 6 feet) were chosen to be the source for the weathered samples, while newer tailings (height 6 to 7 feet) placed at the site were the source for the fresh samples. With the help of an excavator available at the site performing maintenance work, samples were obtained from these CCR tailings (**Figure 1.1.5**). Eight (8) 5-gallon buckets of weathered samples were collected at a depth of 3 to 4 feet from the oldest tailings available at the site; five buckets were to be used for the geotechnical laboratory testing, and three buckets were used for column leach testing. Another eight buckets of CCR were also obtained from the newest tailing on site as

the fresh sample, with five buckets for the geotechnical laboratory testing and three buckets for the column leaching tests.

During the second visit to the site (October 27, 2023), four (4) 5-gallon buckets of weathered CCR samples and four (4) 5-gallon buckets of fresh CCR samples were collected from the same piles chosen during the first visit. During another visit (June 26, 2025), twenty-seven (27) 5-gallon buckets of weathered CCR samples were collected at a depth of 3 to 4 feet from the oldest piles (weathered refuse). On July 16, 2025, three (3) more 5-gallon buckets of weathered CCR samples were also collected.



Figure 1.1.4: CCR has a dry consistency and is less cohesive.

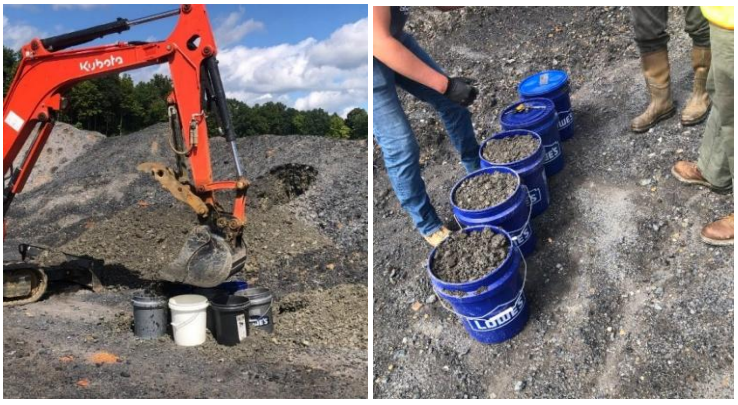


Figure 1.1.5: Obtaining fresh samples from the newer CCR tailings available at the site.

Water from ponds at Hughes Hollow was collected for REE liquid analysis during the first visit (August 17, 2023). Two upper ponds (Low Gap and Crest Pond) are located in the NE and SW corners of the impoundment, respectively, and the polishing pond (Toe Pond) is located at the toe of the impoundment (**Figures 1.1.6 and 1.1.7**). Water quality conditions, such as pH and conductivity, were tested onsite by the WVWRI team to determine how acidic the water is. pH levels for the upper two ponds (Low Gap and Crest Pond) were around 2.3, while the lower toe polishing pond had a pH of 2.6. Based on pH, all ponds were deemed good candidates for further testing. REE analysis then identified which pond was the best source of AMD to serve as a leachant for the column leaching tests.

The WVWRI team members collected additional AMD samples from the Crest Pond for the column leaching tests during the second visit (October 27, 2023). The team collected eight (8) 5-gallon buckets of AMD. An additional two (2) 5-gallon buckets of AMD were collected from the Crest Pond on June 3rd, 2024 (**Figure 1.1.8**). Water quality conditions were tested onsite and

were as follows: pH = 2.60 and Conductivity = 2,291 µS/cm. Also, between July 16 and 18, 2025, six (6) 5-gallon buckets of AMD were collected using a mobile pump provided by on-site workers.



Figure 1.1.6: Aerial view of three AMD source ponds at Hughes Hollow (Google Earth, 2023).


Figure 1.1.7: Three AMD source ponds at Hughes Hollow. Left to right: Toe Pond, Low Gap, Crest Pond.


Figure 1.1.18: AMD testing and collection from the Crest Pond at Blacksville #2 Coal Mine.

Marion County Mine – raw CCR

The secondary study area was the Marion County Mine, formerly known as Loveridge Mine, located in Marion County, WV, USA (39° 36' 17.5" N 80° 17' 03.3" W) and is also operated by ACNR (**Figure 1.1.19**). Six (6) 5-gallon buckets of CCR samples were collected. The samples were picked up from the main office of the Marion County Mine preparation plant, as no site visit

was conducted due to heavy operations on the site. The site was selected because it is actively generating refuse. Thus, the collected refuse (hereafter referred to as the “raw CCR”) has never experienced any weathering conditions. A very fresh CCR needed to be tested as the fresh sample tested before is at least 2 years old, meaning it has been subjected to weather conditions for two years, yet is still fresher than the weathered sample, which was sitting out at the site for a longer time. A complete assessment of leaching potential was achieved once the raw CCR was tested for leaching.



Figure 1.1.19: Loveridge Mine in Marion County, WV (Google Maps).

Task 1.2 Humidity cell testing

Humidity cell testing, which was planned in the project proposal, was replaced with column leaching tests.

Column leaching test methodology

Column diameter selection

A small diameter column of 2 inches (5 cm) that is 3 feet (91 cm) long was tested to check the ease with which the ore particles will sit in such a diameter (**Figure 1.2.1**). The percolation of water through the ore (CCR) in the column was also tested. A cut piece of filter sock, as a single layer of net, was used at the bottom of the column to prevent the outlet from clogging. The results showed that using this diameter, larger particles with a diameter greater than 0.75 inches (20 mm) should be avoided, as they might create large gaps within the packed ore in the column. Based on the results of the experiment and the literature review of column sizes used in leaching tests, it was decided that the diameter of the columns intended for the test should be increased to 4 inches (10 cm). Thus, a 4-inch (10 cm) diameter PVC pipe was purchased and used in the column leaching test. The selected columns provided a diameter-to-particle size ratio of 101.6/20 = 5.08, which satisfies the minimum ratio (4) specified in the literature and is considered a rule of thumb to avoid undue side wall seepage effects (Potter 1981; Iasillo et al. 2013; Van Staden and Petersen 2018).

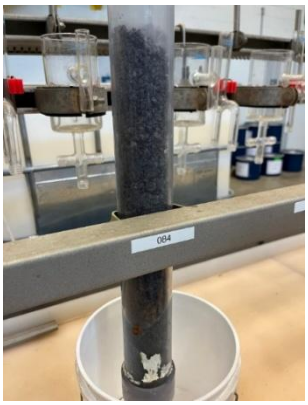


Figure 1.2.1: CCR placed in a small diameter column of 2 inches (5 cm).

Weathered and fresh CCR

Leaching tests were conducted in PVC columns with a 4-inch (10 cm) diameter and a 3-foot (91 cm) length. The setup consisted of six columns, each containing CCR of both types (fresh and weathered). A coupling fitting of 6 inches was attached to one of the two open ends of each column, followed by a PVC reducer bushing (male spigot x female NPT). Then, another two different-sized reducers were added, followed by a PVC barb hose fitting connector adapter of 3/8 in (9.5 mm) to gradually reduce the flow and collect the solution exiting that end into a beaker (**Figure 1.2.2**).



Figure 1.2.2: Coupling fitting and reducers attached to one end of each column.

We used non-woven geotextile with an apparent opening size (AOS) of 0.15 mm as the filtration or drainage layer before adding the CCR in each column (**Figure 1.2.3**). This type of geotextile is known for its robustness, making it suitable for heavy-duty filtration applications, and was used in our study to emulate field conditions. It is non-reactive to AMD or H_2O_2 used in the test and can also provide a highly permeable zone to collect the solution percolating through the material within the column.



Figure 1.2.3: Non-woven geotextile (1100N) used as a filtration layer in the column setup.

The leaching tests were performed for six weeks, with a one-week break after the third cycle to allow for the analytical data processing to that point. During the first three weeks, the test was completed by conducting one leaching cycle per week, followed by sample collection for analytical testing after each cycle. Two leaching cycles were performed each week during the last two weeks (weeks 5 and 6), and sample collection was conducted after the second cycle in week 6. More details about the leaching cycles are provided later in this section. With approximately 16 lb (7.3 kg) of material filling each column, leachants (recirculated AMD, DI water, and recirculated AMD+H_2O_2) were applied through the open end of the columns. **Table 1.2.1** shows the CCR type and leachant used in each column.

Table 1.2.1: Type of CCR placed in each column and type of leachant used in the test.

Column Number	Type of CCR	Leachant Used	Amount of CCR (lb.)	Column Name
1	Weathered	Recirc AMD	16.1	AMD-W
2	Fresh	Recirc AMD	16.0	AMD-F
3	Weathered	DI Water	16.4	DI-W
4	Fresh	DI Water	16.4	DI-F
5	Weathered	Recirc AMD+H_2O_2	16.0	H2O2-W
6	Fresh	Recirc AMD+H_2O_2	16.6	H2O2-F

Calculations were performed to determine the volume of leachant needed to saturate the material in the columns. The volume of voids within both types of CCR was calculated based on the initial void ratio (*e*) and porosity (*n*) using equations 6 through 8 listed below. **Table 1.2.2** shows calculated *e* and *n* for both types of CCR. **Table 1.2.3** shows the volume of voids within each type of CCR and the equivalent volume of solution to fill voids. The equivalent volume of solution needed to fill the voids within a column ranged from 1.3 to 1.9 liters.

$$e = \frac{G_S \gamma_w}{\gamma_d} - 1 \qquad \text{(Equation 6)}$$

$$n = \frac{e}{1+e} \qquad \text{(Equation 7)}$$

$$n = \frac{V_V}{V} \qquad \text{(Equation 8)}$$

Where: e=Initial void ratio, G_s= Specific gravity, γ_w =Unit Weight of water, γ_d=Dry unit weight, n=porosity, V_v= Volume of voids, and V= Total volume

Table 1.2.2: Geotechnical Properties of CCR.

Physical Properties	**Fresh CCR**	**Weathered CCR**
Specific Gravity, G_s	2.28	1.99
Dry Unit Weight, γ_d (KN/m^3)	15.55	15.40
Unit Weight of water, γ_w (KN/m^3)	9.81	9.81
Initial Void Ratio, e_o	0.44	0.27
Porosity, n	0.30	0.21
Degree of Saturation, S	0.59	0.97

Table 1.2.3: Volume of voids and the equivalent volume of solution needed to fill voids.

Column Name	**Height of empty part (in.)**	**Total Volume of CCR (in^3)**	**Volumes of voids (*Vv*) (in^3)**	**Volume of Solids (*Vs*) (in^3)**	**Equivalent Volume of Solution needed to fill voids (L)**
AMD-W	1.75	430.4	90.9	339.5	1.5
AMD-F	7.5	358.1	109.2	249.0	1.8
DI-W	7	364.4	76.9	287.5	1.3
DI-W	7	364.4	111.1	253.4	1.8
H_2O_2-W	6.25	373.8	78.9	294.9	1.3
H_2O_2-F	5.75	380.1	115.9	264.3	1.9

The leachant volume was also estimated based on a scale-up to field demonstration conditions. The AMD source at Blacksville (Crest Pond) has a proximate volume of 3.3 acre-feet (ac-ft), which is equivalent to approximately 1 million liquid gallons (1 Mgal). A future heap pad field demonstration size was assumed to be 2 acres in area by 10 feet high. The 1 Mgal of AMD available in the Crest Pond would be equivalent to approximately 40% of the total volume of the pad. Applying that same proportion of 40% to the scale of the column leaching test would result in 1 L (1000 mL) of leachant volume needed for the given CCR volume. The leaching tests were carried out with the volume of leachant that was estimated based on a scale-up to field demo (1 L) for consistency and simulation of field conditions. The following subsections describe the week-to-week methodology for the column leaching tests.

Week 1 (11/8/2023)

During the first week of the test, one leaching cycle was performed. Raw AMD collected from the Crest Pond was used as the leachant in columns 1, 2, 5, and 6 (AMD-W, AMD-F, H_2O_2-W, and H_2O_2-F, respectively). No H_2O_2 was added to the leachant percolated in columns 5 and 6 during the first cycle. A Masterflex L/S digital pump (**Figure 1A, Appendix A**) was used to move the AMD to the top of the columns with an application flow rate of 50 mL/min. Soft-walled tubing connected to the two ends of the pump transferred AMD from 1000 mL beakers to the open end of the columns, where it was distributed through showerheads (**Figure 1.2.4**). DI water was used as the leachant in columns 3 and 4 (DI-W and DI-F). 1000 mL of DI water was applied manually for 1 minute through the open ends of the columns (**Figure 1.2.4**).

Under the six columns, 1000 mL beakers were placed to collect the leachate discharging from each column, while the elapsed time was measured. pH readings were taken for the raw AMD

and the collected leachate when the test ended. A Mettler Toledo Seven 2 Go Pro was calibrated and used to take the pH readings (**Figure 1.2.4**). Approximately 350 mL of the leachate was collected from each beaker upon completion of the test (**Figure 2A, Appendix A**), and later samples were sent to the analytical lab at the NRCCE building, WVU. The remaining leachate from columns 1,2, 5, and 6 was covered with parafilm to be used in the second leaching cycle (week 2), while the remaining leachates from columns 3 and 4 were discarded.

Week 2 (11/15/2023)

In the second week of the test, one leaching cycle was performed. AMD that was percolated through the CCR during the first week of the test was used as the leachant in columns 1 and 2 (referred to as recirculated AMD). Some raw AMD collected from the Crest Pond was added to the recirculated AMD to maintain a total volume of 1000 mL. pH readings were taken before and after adding the raw AMD. The leachant used in columns 5 and 6 was a mixture of recirculated AMD from week 1, raw AMD from Crest Pond, and 100 mL of H_2O_2 (**Table 2A-Appendix A**)**.** The prepared leachant was placed in four beakers, and the digital pump was used to move the leachant from the beakers to the top of the columns.

Fresh DI water was used as the leachant for columns 3 and 4. About 1000 mL of DI water was applied manually through the open ends of the columns. A volume of 250 mL of leachate was collected from each beaker when the test was over, and samples were sent to the analytical lab. The remaining leachates from columns 1, 2, 5, and 6 were covered with parafilm to be used during the third week (cycle 3), while the remaining leachates from columns 3 and 4 were discarded.

Week 3 (11/21/2023)

The same process and leachant blend used in week 2 was followed in week 3 for columns 1, 2, 5, and 6, while DI water was used as the leachant in columns 3 and 4 (**Table 2A, Appendix A**).

Week 4 (11/28/2023)

No leaching cycle was conducted during the fourth week. Results from weeks 1 through 3 were collected and compared so informed decisions could be made on the efficiency of performing one leaching cycle per week. Based on the results from weeks 1 through 3, the project team decided that, moving forward, it would be best to perform the test with an increased number of leaching cycles. It was decided that multiple leaching cycles should be conducted during weeks 5 and 6 before the next analytical sample testing.

Week 5 (12/6/2023)

During the fifth week, two leaching cycles were performed. Raw AMD from Crest Pond was added to recirc AMD from the third cycle (week 3) and used as the leachant in columns 1 and 2. The leachant used in columns 5 and 6 was a mixture of recirc AMD from week 3, raw AMD from the Crest Pond, and 100 mL of H_2O_2. Fresh DI water was used in columns 3 and 4 (1000 mL each). Upon the completion of the first cycle, leachates collected from columns 3 and 4 were discarded, while leachates collected from the other four columns (1, 2, 5, and 6) were used as part of the leachant in the second cycle. Fresh DI water was used in columns 3 and 4 (1000 mL each) during the second cycle (**Table 2A, Appendix A**). When the second cycle was completed, leachates from columns 3 and 4 were discarded, and the other four beakers placed under columns 1, 2, 5, and 6 were covered with parafilm to be used in the following week (week 6). No samples were collected for analytical testing during week 5.

Week 6 (12/13/2023)

Two leaching cycles were conducted during the sixth week, following the same process and leachant blend as week 5 for columns 1, 2, 5, and 6. DI water was percolated through CCR placed in columns 3 and 4 (**Table 2A, Appendix A**). When the second cycle was completed, samples of 250 mL were collected from each beaker placed under the six columns for analytical testing. Later, the remainder of the leachate collected from columns 3 and 4 were discarded, whereas the remainder of the leachate collected from columns 1, 2, 5, and 6 were kept for any possible future use.

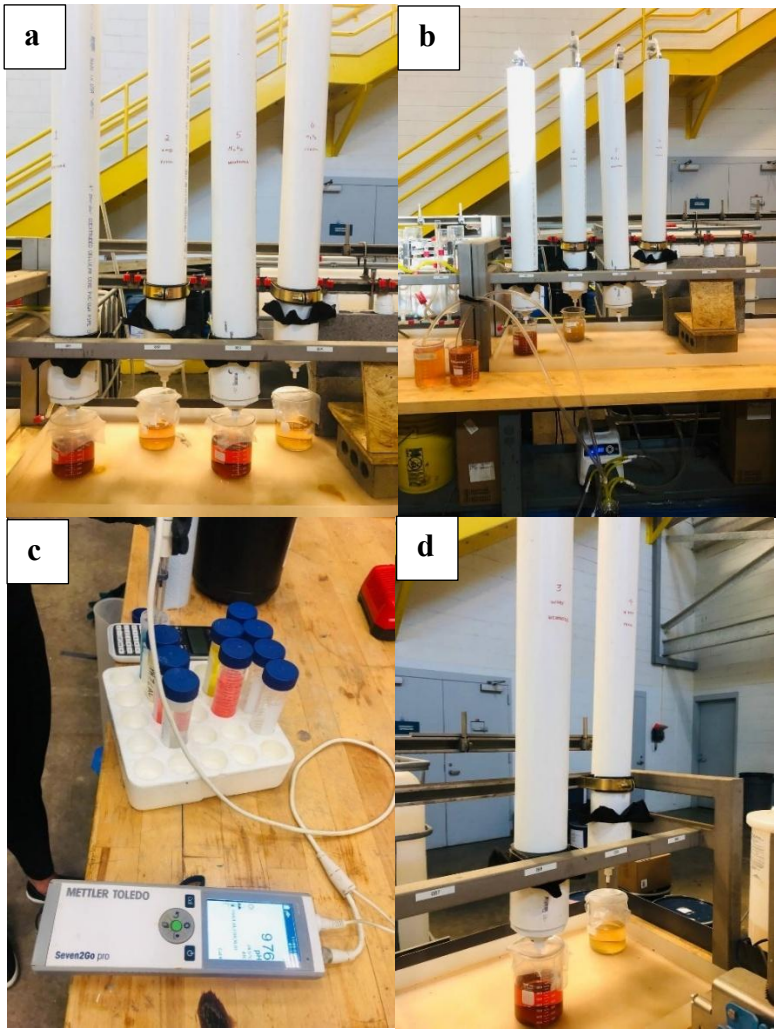


Figure 1.2.4: a) Column leaching test setup (columns 1, 2, 5, and 6), b) Soft-walled tubing connected to the two ends of the pump transfers AMD from beakers to the open end of the columns, c) Mettler Toledo Seven 2 Go Pro being calibrated before taking pH readings and d) Column leaching test setup (columns 3 and 4).

When the test was terminated after the sixth week, the six columns were disassembled. The material in each column was taken out and split into three layers. Layers were placed in trays, labeled, and sent to the geotechnical lab for post-grain size distribution (post-GSD) testing. More details about the post-leaching GSD are provided in Task 2-2. Additionally, six solid samples were

collected from the middle layer of each column for post-leaching TREE concentration in refuse solids (**Figure 1.2.5**).



Figure 1.2.5: Six (6) solid samples collected for post-leaching TREE concentration in refuse solids.

Raw CCR

Leaching tests were conducted using the same PVC columns that were used to leach the weathered and fresh CCR [diameter of 4 inches (10 cm) and a length of 3 feet (91cm)]. The setup consisted of two columns in which raw CCR was placed (**Figure 1.2.6**). **Table 1.2.4** provides details on the leachants used in each column and the amount of CCR placed. Based on leaching results from weathered and fresh CCR, it was decided that the leaching procedure to be tested is a frequent leaching cycle. The plan was to leach as frequently as possible so that the next leaching cycle proceeds when the discharge from columns ceases after a cycle. Frequent leaching needs to be tested to determine whether multiple leaching cycles (e.g., 100) can accelerate weathering conditions and thus speed up pyrite oxidation. During the first leaching cycle for column 1 (AMD-R), CCR was leached with 1000 mL of AMD from the Crest Pond. In the remaining leaching cycles, recirculated AMD was supplemented with raw AMD (from the Crest Pond) as needed so that the leachant volume was 1000 mL (1L). **Table 3A, Appendix A** shows volumes of raw AMD and recirculated AMD used as part of the leachant in column 1 during 10 leaching cycles. Column 2 (DI-R) was leached with fresh 1000 mL of DI water during every leaching cycle. Leachate samples were sent to the lab for analytical testing after cycles 1 and 10. Around 30 leaching cycles were completed for both columns, but the test was terminated after receiving the results of leaching cycle # 10.

Table 1.2.4: Type of CCR placed in each column and type of leachant used in the test.

Column Number	Type of CCR	Leachant Used	Amount of CCR (lb.)	Column Name
1	Raw	Recirc AMD	20.1	AMD-R
2	Raw	DI water	20.2	DI-R



Figure 1.2.6: Column leaching test setup-raw CCR.

Drum leaching test methodology

The drum leaching tests were performed to eliminate the possibility of restricting walls and preferential pathways that might have affected the column-leaching test results. Liquid molecules encounter attractive and repulsive forces in all directions, caused by the surrounding molecules and elements (Sophocleous, 2010). The attractive force between molecules of the same substance is cohesion, whereas the attractive force between molecules of different substances is known as adhesion. When the adhesion between the leachant molecules and the walls of the column outcompetes the cohesion among the leachant molecules, the leachant will find preferential pathways along the inner walls of the column. This possibility can be eliminated by using a vessel with a larger diameter (e.g., 55 Gallon Tight Head Plastic Drum), as the walls will have less restrictive impact on the flow.

The setup consisted of two (2) 55-gallon tight-head plastic drums, in which weathered CCR was placed. Weathered CCR was selected as the best candidate ore based on results obtained during the column leaching tests. The drums were placed upside down on concrete blocks, and a containment pallet was placed underneath the two drums to prevent and manage any possible discharge spills. One of the bung holes on top of each drum was used as the outlet, where a 2" PVC male adapter was attached, followed by a PVC valve to control the discharge. Layers of GFF were placed at the bottom of the drums, followed by non-woven geotextile bags. The purpose of using geotextile bags was to contain the CCR and prevent the movement of any fine particles through the outlet. The bottom of each drum was cut open to allow for the AMD application. The design and setup of the drum leaching test are shown in **Figures 1.2.7 and 1.2.8**.

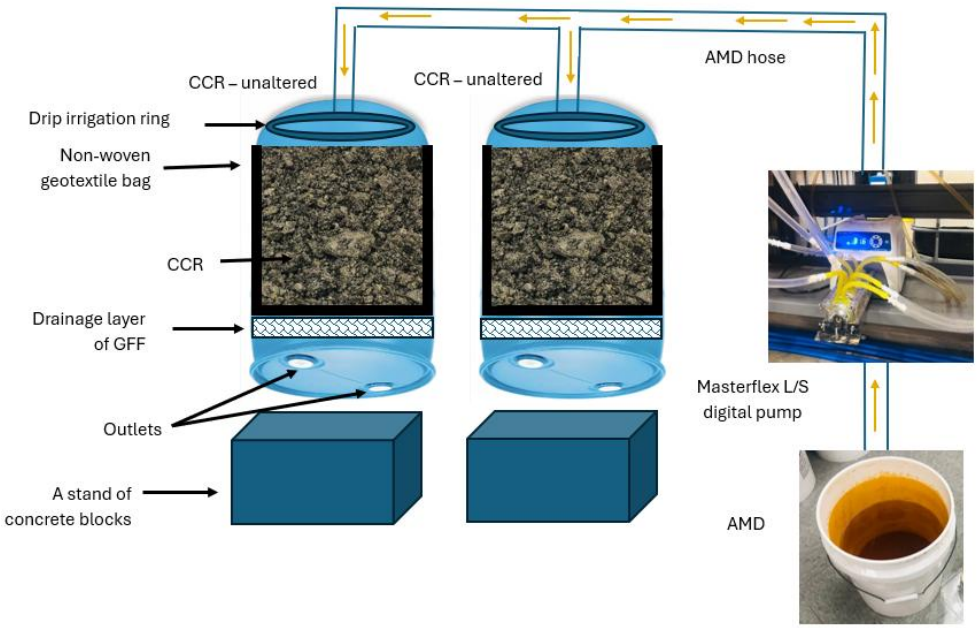


Figure 1.2.7: Schematic of the drum leaching test design.



Figure 1.2.8: Drum leaching test setup.

Phase 1: Mimicking column leaching plan

Phase 1 of the drum leaching test was performed over a period of three weeks following the same leaching schedule adopted during the column leaching tests. Over the three weeks, the test was completed by conducting one leaching cycle per week, followed by sample collection for analytical testing after each cycle (**Figure 3A, Appendix A**). With approximately 375.9 lb. (171 kg) and 363.5 lb. (165 kg) of material filling each drum (**Table 4A, Appendix A**), leachant (AMD) was applied through the open end of the drums. The amount of CCR added filled each drum to the top, leaving an empty part of about 13 cm at the top to make it easy for the irrigation tubing to sit at the top of the CCR.

Approximately 6 gallons (22.7 L) of AMD were used as the leachant in each drum, providing the same CCR:AMD ratio as in the column tests. About 1.3 gallons (5 L) were added to the leachant to fill the bottom of each drum to the berm of the outlet. This was done only during the first week of leaching. The digital pump used in the column leaching test was set to deliver AMD to the top of the drums at an application flow rate of 50 mL/min. The recirculated AMD was supplemented with raw AMD from the Crest Pond during leaching cycles 2 and 3, resulting in a total of 6 gallons (22.7 L) of leachant. **Table 5A, Appendix A** shows the exact measurements of recirculated and raw AMD used each week (weeks 1, 2, and 3).

Phase 2: Alternate wetting and drying periods

Phase 2 of the drum leaching test evaluated alternating wetting and drying periods. The last leaching cycle of phase 1 (leaching cycle 3, performed on 8/5/2025) and the first leaching cycle of phase 2 (leaching cycle 4, performed on 12/8/2025) were separated by approximately a four-month period. The four months provide a good indication of the influence of an extended drying period on REE extraction in both drums. After the first leaching cycle of phase 2 (leaching cycle 4), drum 1 underwent another drying period of 2 weeks (from 12/8/2025 to 12/22/2025), whereas drum 2 underwent a wetting period of 2 weeks (from 12/8/2025 to 12/22/2025).

A shorter drying period (two weeks) was evaluated with drum 1. The CCR within drum 1 was leached with AMD collected at the end of phase 1, and a sample was collected at the end of the cycle and sent to the analytical lab for testing. The recirculated AMD was supplemented with raw AMD from the Crest Pond to achieve a total of 22.7 L of leachant. The drum was then left open for 2 weeks to allow the material to air-dry. At the end of the two-week drying period, the material was leached with AMD (leaching cycle 5). Another sample was collected at the end of the leaching cycle and sent to the lab for testing.

An extended wetting period was evaluated with drum 2. The CCR within drum 2 was leached with AMD collected at the end of phase 1, and a sample was collected at the end of the cycle and sent to the analytical lab for testing (**Figure 4A, Appendix A**). This followed the same method used with drum 1. After the first leaching cycle, humidified air was applied for 6 hours, and the drum was then sealed for 2 weeks (**Figures 1.2.9, 1.2.10, and 1.2.11**). A perforated pipe was placed in the middle of the material and connected to the humidifier pipe to allow for a larger area of exposure to humidified air. At the end of the two-week wetting period, drum 2 was leached with AMD (leaching cycle 5), and another sample was collected by the end of the cycle and sent to the lab for testing.

By the end of leaching cycle 5, both drums underwent another 2-month drying period to evaluate the influence of a mid-term drying period on leaching performance. By the end of the 2-month period, both drums were leached with AMD (leaching cycle 6).



Figure 1.2.9: Humidified air applied to the CCR within drum 2.



Figure 1.2.10: Perforated pipe placed in the middle of drum 2.

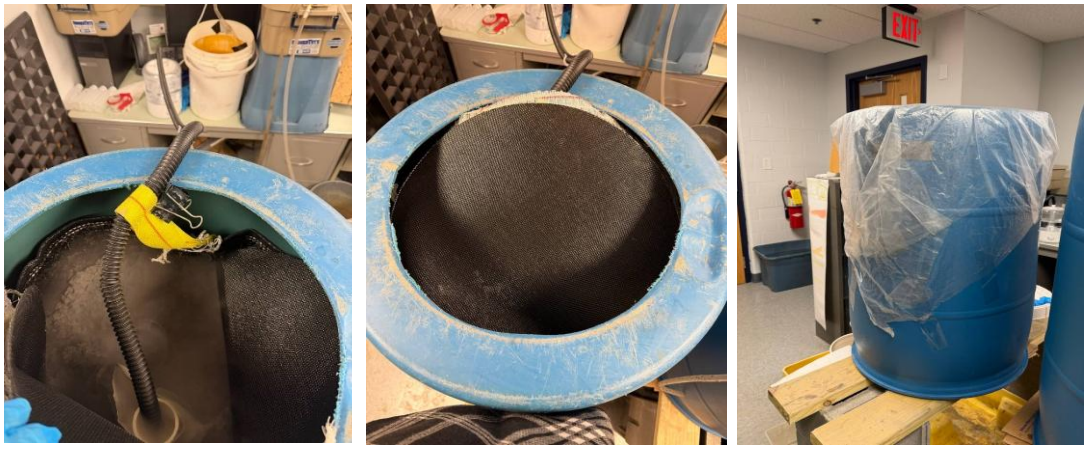


Figure 1.2.11: Drum 2 was sealed for two weeks after applying humidified air.

Column leaching test results

Weathered and fresh CCR

Weathered refuse had a higher leaching potential when compared to fresh CCR. The increase in TREE concentrations was always higher in leachate collected from weathered CCR columns as compared to fresh CCR, regardless of leachant type (**Figure 1.2.12**). TREE concentrations present in all used leachants and collected leachate are presented in **Table 6A, Appendix A**.

The majority of REE leaching occurred in the first leaching cycle (**Figure 1.2.12 and Table 6A, Appendix A**). The first leaching cycle resulted in an increase in TREE concentration of 252%, 178%, 229%, and 116% in leachate collected from columns AMD-W, AMD-F, H_2O_2-W, and H_2O_2-F, respectively. Beyond the first leaching cycle, the percentage increase of TREE concentration in collected leachate ranged from 13% to 50%. Columns DI-W and DI-F showed a constant decrease in leachate TREE concentration after the first leaching cycle. Multiple leaching cycles conducted in weeks 5 and 6 had no substantial impact on TREE content compared to a single leaching cycle (cycles 1 to 3) (**Figure 1.2.12**).

Comparing the performance of the three leachants, recirculated AMD and recirculated AMD+H_2O_2 leached more TREE than DI water. During the first three leaching cycles, AMD-W had the highest cumulative percentage of leached TREE from the solid (**Figure 5A, Appendix A**). However, recirculated H_2O_2-W had the highest percent of leached TREE from the solid after four additional leaching cycles. Column DI-F, which had the highest outflow rate, yielded the lowest cumulative percentage leached from the solid.

Weathered refuse columns had a lower outflow rate than those filled with fresh refuse. The outflow rate did not follow a specific trend. AMD-W and DI-W columns had an increase in outflow flow rate after the first leaching cycle, while column H_2O_2-W had a decrease in flow rate. The H_2O_2-F column had an increase in outflow rate after the first leaching cycle, and then the flow rate decreased again after the third leaching cycle. Column AMD-F showed a relatively constant outflow rate, and column DI-F showed a constant high outflow rate ranging between 150 to 270 mL/min throughout the testing period. DI-W and H_2O_2-W showed a unique behavior of flow rate slowing down and water ponding during leaching cycles 5 and 7, which are the second cycles of leaching performed in weeks 5 and 6 (**Figure 6A, Appendix**).

Based on the percentage TREE increase in leachate collected during the first leaching cycle that produced the most REEs, it was concluded that the pH of DI water (approximately 5) did not adversely affect the performance of leaching tests conducted with DI water as the leachant. The pH readings of leachate collected from all columns showed a decrease (minimum value of 1.72 and maximum value of 2.36) (**Figure 7A, Appendix A**). Leachate pH remained within the same range for all three tests after the first cycle. Additional pH readings of the leachant and leachate from every column during the six weeks of testing are presented in **Table 7A, Appendix A**.

Field-scale TREE load was estimated based on the volume of AMD available in the Crest Pond at Blacksville Number 2 Coal Mine [approximately 6,167 m^3 (3 ac-ft)] (**Figure 8A, Appendix A**). TREE loads formed by leaching weathered CCR with recirculated AMD and recirculated AMD+H_2O_2 were higher than those of leaching fresh CCR using the same leachants. Beyond the first leaching cycle, TREE loads generated by leaching fresh CCR with recirculated AMD and recirculated AMD+H_2O_2 stayed relatively constant or decreased slightly (-5%). However, TREE loads produced by leaching weathered CCR indicated a slight increase (5% to 10%) after multiple leaching cycles with recirculated AMD and recirculated AMD+H_2O_2.The highest TREE load, approximately 50 lb (23 kg), was associated with multiple leaching cycles of weathered CCR with recirculated AMD+H_2O_2 (**Figure 8A, Appendix A**). In addition, TREE load decreased as the number of leaching cycles with DI water increased, and the column with the highest outflow rate (DI-F) was associated with the lowest TREE load, approximately 4.4 lb (2 kg).

Cerium (Ce), neodymium (Nd), and lanthanum (La) were the most abundant REEs in both weathered and fresh CCR. Meanwhile, scandium (Sc) and yttrium (Y) were abundant only in weathered coal refuse (**Figure 1.2.13 and Tables 8A through 11A, Appendix A**).

Total major metals (TMM) followed similar trends to those seen with TREE. Weathered CCR leached a larger amount of TMM than fresh refuse, regardless of leachant type. The majority of TMM leaching occurred in the first leaching cycle (highest percentage increase in TMM concentration of 259%) (**Table 12A, Appendix A**). Recirculated AMD and recirculated AMD+H_2O_2 leached more TMM than DI water and yielded the highest cumulative percentage of leached TMM from the solid phase. Multiple leaching cycles did not increase TMM concentration compared with single cycles. Al, Fe, and Ca had the highest concentration in leachate collected from the six columns (**Figure 1.2.13**). Weathered CCR leached a higher level of Fe when compared to fresh refuse.

TREE concentrations within the refuse increased in all but one (AMD-F) of the columns when compared to the starting TREE values for both fresh and weathered CCR (**Figure 1.2.14**). The percentage change in TREE concentration in solid collected from columns AMD-W, AMD-F, DI-W, DI-F, H_2O_2-W, and H_2O_2-F were 29.0%, -3.2%, 12.1%, 0.5%, 17.4%, and 11.6%, respectively.

Raw CCR

Raw CCR behavior differed from that of the weathered and fresh CCR. As AMD percolated through the material, the refuse acted as a filter, and the leachate was observed as clear water exiting column AMD-R (**Figure 9A, Appendix A**). A similar observation was made for column DI-R, with the exception that the leachate had fines that caused the water to become dark; this difference is likely due to the high flow rate through the column (300 mL/min). The leachate was clear after the fines settled. Leachate pH after each leaching cycle (6.6 to 7.2) indicated that the solution was alkaline (**Table 13A, Appendix A**). The results from the analytical lab supported the visual observation of the collected leachate. The alkalinity of the leachate collected from both columns was high (approximately 67 to 129 mg/L for column AMD-R and 30 to 35 mg/L for column

DI-R), whereas the acidity was low (<4.09) (**Table 13A, Appendix A**). No REEs were leached from column AMD-R, and REE present in AMD was sorbed into the solid particles rather than being released from them after one leaching cycle (change in TREE concentration from column AMD-R = -479 mg/L) (**Fig. 1.2.12 and Table 14A, Appendix A**).

The collected amount of REE from column DI-R was insignificant (6 mg/L) and declined after the first leaching cycle (**Table 14A, Appendix A**). Compared to weathered and fresh CCR, small amounts of TMM were leached out of the raw CCR (**Table 15A, Appendix A**). Based on the results of cycles 1 and 10, and visual examination of collected leachate up to cycle 30, it was decided to terminate the experiment.

Column AMD-R had a constant outflow rate of approximately 40 mL/min throughout 30 leaching cycles. Column DI-R also had a constant, average outflow rate of approximately 300 mL/min until cycle 25. A decrease in outflow rate to approximately 250 mL/min was then observed.

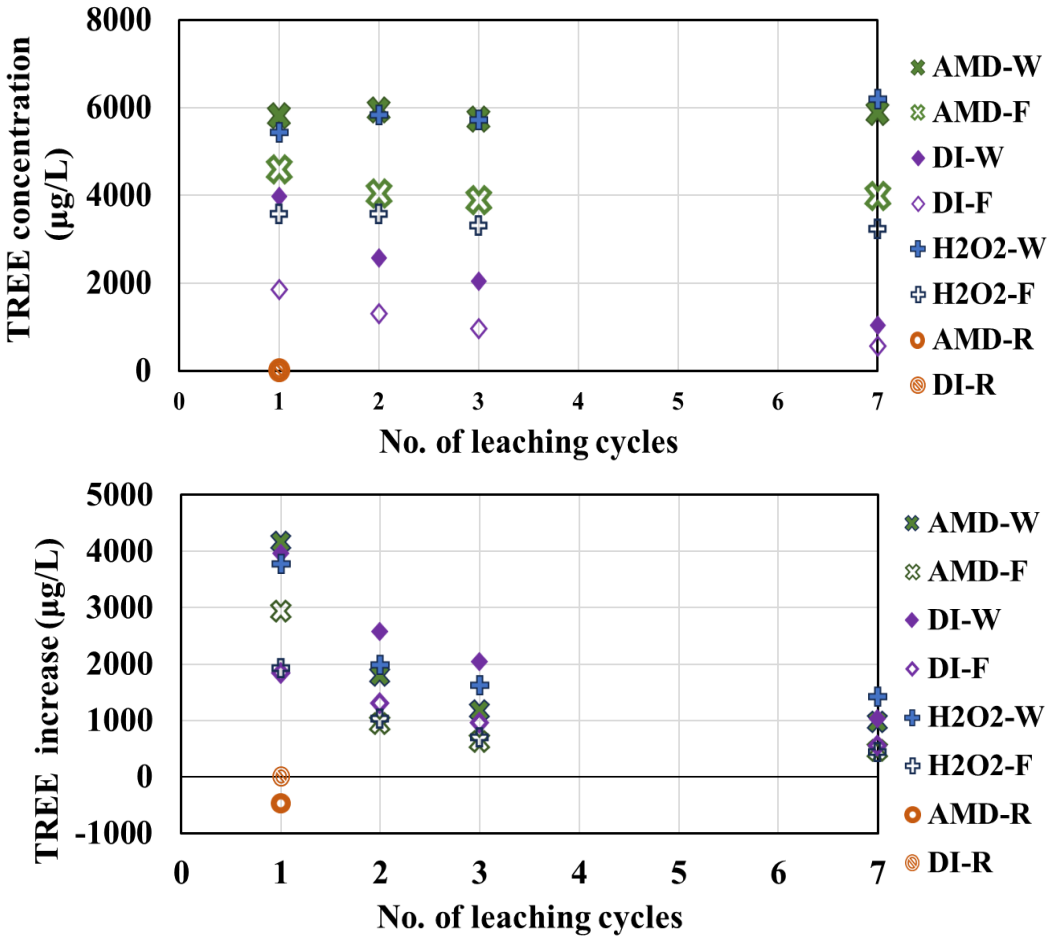


Figure 1.2.12: TREE concentration in collected leachate (top) and increase in TREE (bottom) in column leaching tests.

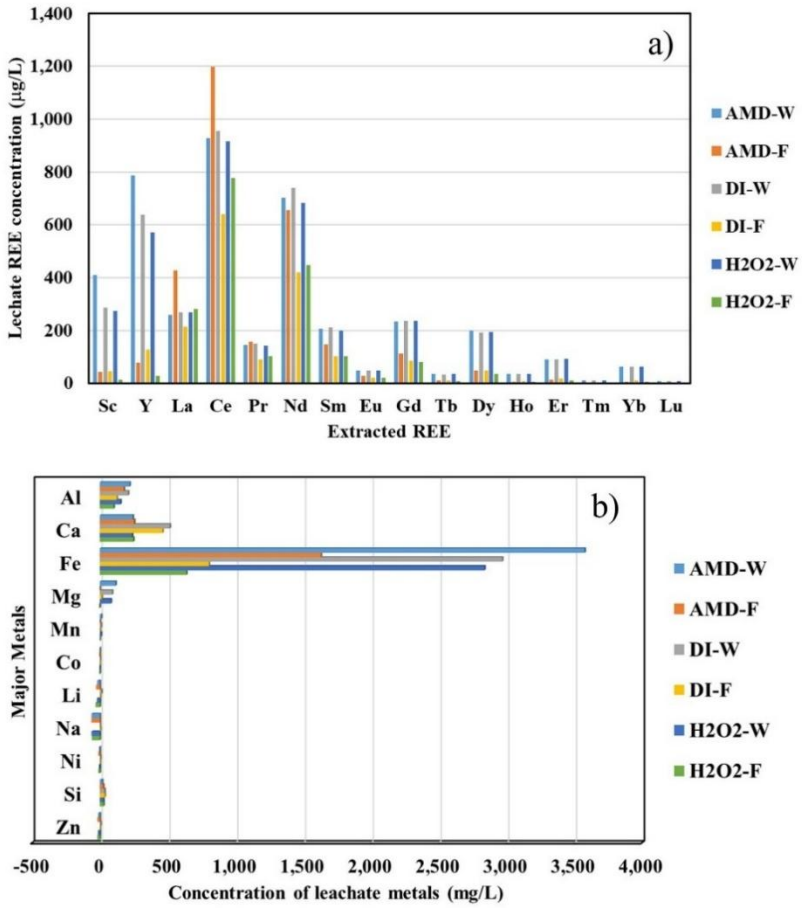


Figure 1.2.13: Column leaching tests: a) Individual REE concentration, and b) MM concentration in leachate collected from six columns after one leaching cycle.

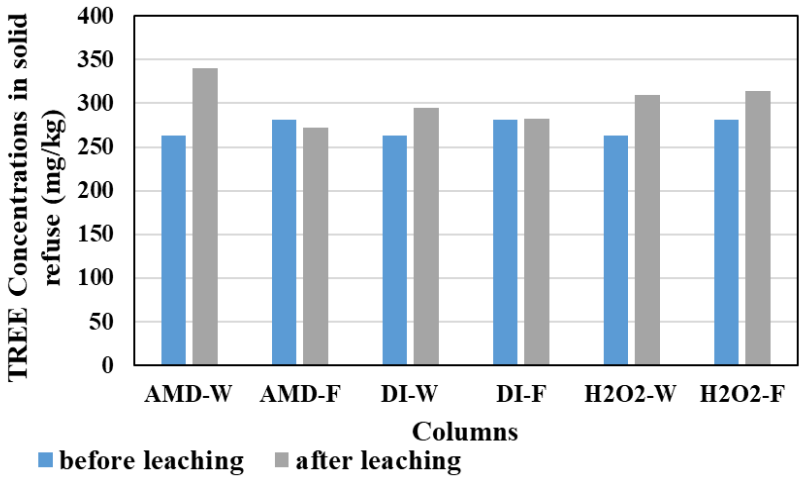


Figure 1.2.14: TREE Concentration in solid before and after leaching in column leaching tests.

Drum leaching test results

Phase 1: Mimicking column leaching plan

The first phase of drum leaching tests confirmed the results of the column leaching test. Leaching behavior was consistent across the two bench-scale tests (columns and drums) (**Figure 1.2.15**). Weathered refuse filling both drums showed a high leaching potential. The majority of REE leaching occurred in the first leaching cycle (**Figure 1.2.16 and Table 16A, Appendix A**). Subsequent leaching (one week apart) with recirculated AMD did not promote additional leaching. The first leaching cycle resulted in a 366% and 209% increase in TREE concentration in the leachate collected from drums 1 and 2, respectively. Beyond the first leaching cycle, the percentage increase of TREE concentration in collected leachate from drum 1 was 36% and 2% after leaching cycles # 2 and 3, respectively. Similarly, the percentage increase of TREE concentration in collected leachate from drum 2 was 52% and 2% after leaching cycles 2 and 3, respectively.

The highest TREE load was associated with the first leaching cycle in drum 1 (44 lb. or 20 kg) (**Figure 1.2.17**). Similar to results from the column leaching tests, high percentage of TREE leaching during the first leaching cycle (366% for drum 1 and 209% for drum 2) reflected a low value of cumulative percentage of leached TREE from the solid phase (1.4% for drum 1 and 0.8% for drum 2) (**Figure 1.2.17**).

Both drums had similar outflow rates (between 33.3 to 50 mL/min). The pH of leachate stayed relatively constant for both drums after the first cycle (approximately 2.0) (**Figure 1.2.17**). Almost all individual REEs were more abundant in drum 1 compared to drum 2 (**Figure 1.2.18**). The differences in results between the two drums could be attributed to differences in the amount of CCR in each drum [approximately 377 lb (171 kg) and 364 lb (165 kg) in drum 1 and drum 2, respectively].

It should be noted that during the first leaching cycle, there was a five-hour residence time. However, the residence time was approximately 30 minutes during the second and third leaching cycles. The CCR was placed into the drums one week prior to the leaching process, which allowed for some water evaporation within the pore space. As the material became dry, it needed more time to absorb the AMD and reach a saturation level at which AMD could flow through the pore space. When the second leaching cycle was performed, approximately 10 to 11 L of raw AMD was added to the recirculated AMD to achieve the required 22.7 L of leachant. Only 1.2 to 1.6 L of raw AMD needed to be added to the recirculated AMD for the third leaching cycle as the material maintained its full saturation due to trapped AMD at the bottom of the drum.

Phase 2: Alternate wetting and drying periods

The outflow rates during phase 2 of the drum leaching tests were consistent across both drums (33.3 to 50 mL/min), and no significant differences were observed in their outflow patterns. When resuming leaching after a pause of approximately four months between phases 1 and 2, TREE increased sharply. The response in leaching performance to this extended drying period was observed in the first leaching cycle of phase 2 (leaching cycle 4). Leachate TREE concentration increased by 115% for drum 1 and 118% for drum 2 (**Figure 1.2.16**). Leaching cycle 4 doubled the amount of TREE within the leachate, increasing the percentage leached from solid placed in drum 1 and drum 2 to 2.47% and 2.04%, respectively (**Figure 1.2.17**). It appeared that the leaching performance seen in the first leaching cycle, identified in the early stages of the project as the one that could produce the most significant amount of TREE, may be repeated through an

extended drying period. The second and third leaching cycles in phase 2 (leaching cycles 5 and 6) showed a similar pattern to the later cycles in phase 1, with a limited increase in TREEs of approximately 50% and 40% (**Figure 1.2.16**). Extended wetting via humidification (drum 2) did not provide any significant benefits (**Figure 1.2.16**).

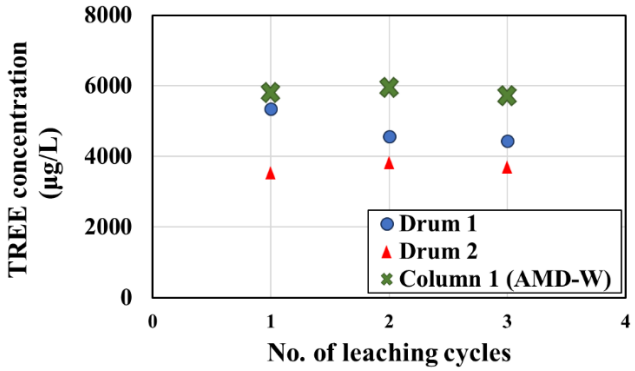


Figure 1.2.15: TREE concentration in leachate-drum leaching (phase 1) and three cycles of column leaching

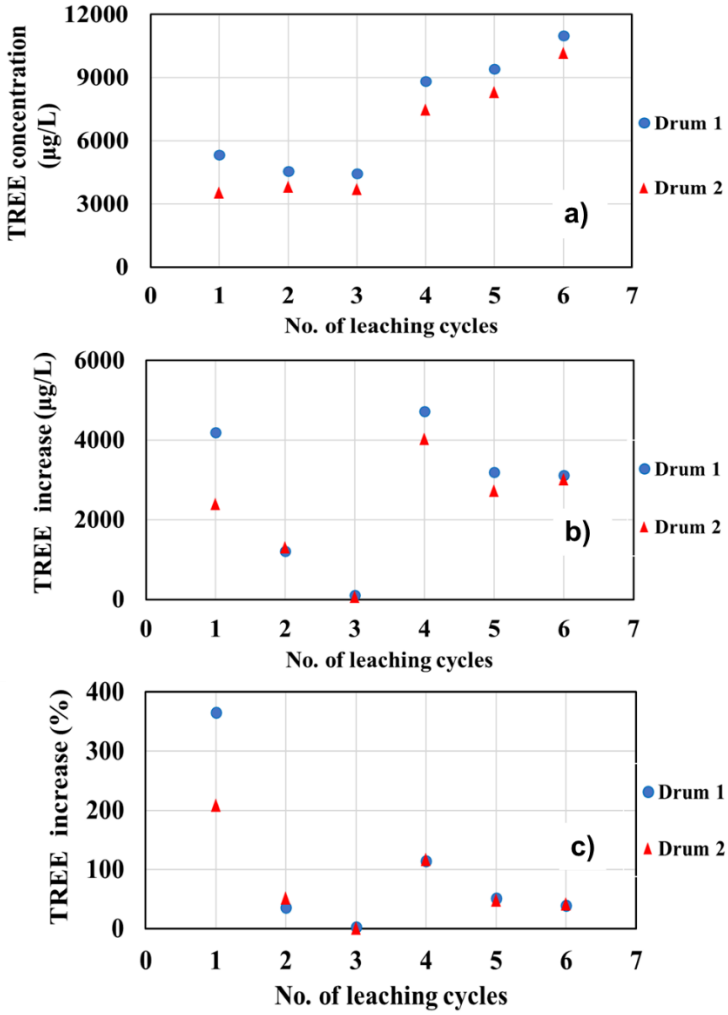


Figure 1.2.16: Drum leaching test results: a) TREE concentration in leachate, b) TREE increase, and c) percent TREE increase.

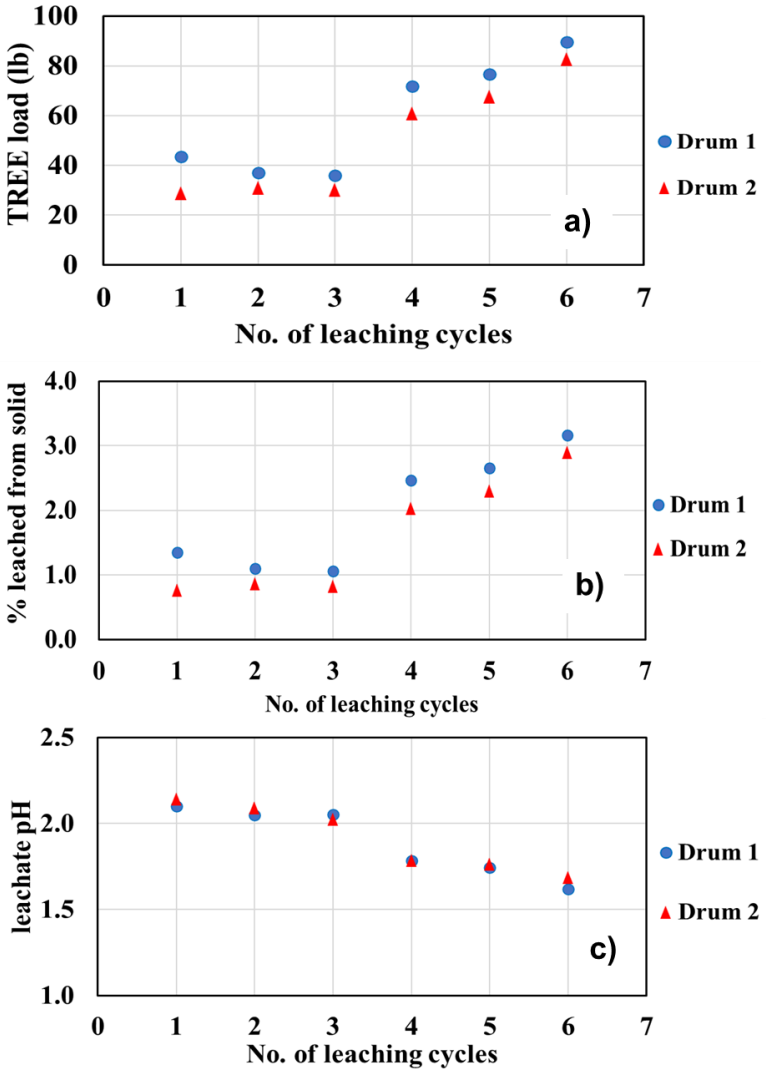


Figure 1.2.17: Drum leaching test results: a) TREE load, b) percent leached from solid, and c) leachate pH.

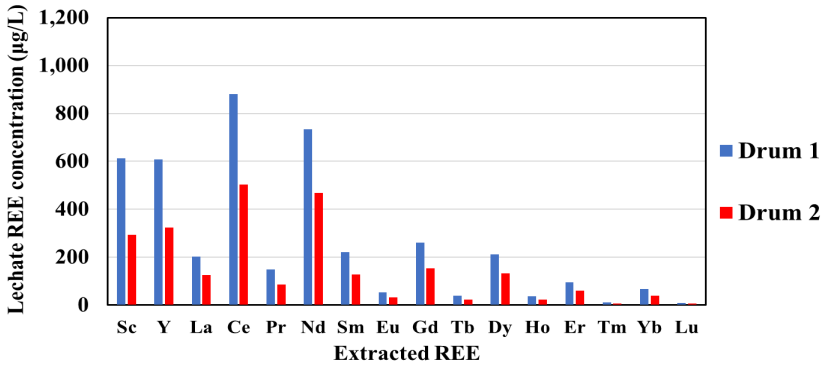


Figure 1.2.18: Individual REE concentration in collected leachate-drum leaching test.

Leaching tests discussion

Refuse age

Results indicated that the more weathered the refuse was, the more REE could be extracted. Comparing the results among the three types of CCR, the best TREE leaching results were associated with the weathered CCR, which had been on site for at least five years. Meanwhile, raw refuse that experienced no weathering (raw CCR, 0 years old) yielded poor or negative outcomes for TREE content in collected leachate, regardless of the leachant type used.

Particle size

Weathered CCR had the smallest particle-size range compared to fresh and raw CCR, which is the first key factor explaining the high leaching potential. Previous studies indicated that as coal mine waste is subject to environmental factors (rainwater and oxygen), its physical characteristics change, such as changes in surface color, growing tendency to fracture, and a decrease in particle size (Fabiańska et al., 2024). Physical degradation is a result of mechanical weathering, which takes place due to variations in temperature (thermal cycling), freeze and thaw cycles (water volumetric expansion due to freezing), and forces of wind and rainfall (Eppes, 2022). These factors develop and change pressure and stress within large particles, which lead to cracking and eventually breaking down into smaller particles in a process known as fragmentation and a phenomenon known as slaking (D'Appolonia, 2009a). Stresses produced by mechanical weathering break molecular bonds in rocks along a defined plane without modifying their chemical composition (Eppes, 2022). When overburden material is fragmented or broken down, the weatherable surface area of minerals is increased (Jain et al., 2021). Leaching characteristics and particle liberation within a given sample are known to be impacted by particle size (Allen et al., 2019; Yang, 2019a; Yang and Honaker, 2020; Zhang and Honaker, 2018). The smaller the particle size, the more surface area is available for leachant contact and REE liberation (Yang and Honaker, 2020). It should be noted that the main goal was not to test the particle size effect but rather to test the potential of leaching CCR under its current sitting conditions (identified by a soil group symbol of GW) without further processing (e.g., crushing). Thus, it was concluded that using the weathered refuse as it sits on site has a high potential for leaching, as it has the smallest particle-size range due to weathering.

Moisture content

In addition to a decrease in particle size, spoil slaking has other effects, such as a decrease in material strength and an increase in moisture content (D'Appolonia, 2009a). Geidel (1979) and Jain et al. (2021) showed that contaminants (e.g. AMD and/or salt) loads produced and released from coal mine waste are dependent on *in situ* moisture content. This *in situ* moisture content is also considered an important factor contributing to the high leaching potential of the weathered refuse. The weathered CCR had the highest initial moisture content (18%) compared to the fresh and raw CCR (14% and 7%, respectively). The higher moisture content helps to ensure oxidation.

Pyrite oxidation

Another important factor that might have had a substantial impact on results is that pyrite oxidation has already taken place at least within the outer layer of the weathered refuse, and oxidation products, such as REE compounds, have already become available at the surface of the solid particles. Introducing an acid enriched in hydrogen ions (H+), such as AMD in this case, can break down those compounds and release the REE into the leachate. This resulted in the release of

what are referred to as the “easy-to-leach” REEs (Cao et al., 2018; Yang and Honaker, 2020; Ait Brahim et al., 2022). This quick reaction was evident through the first leaching cycle of the column and drum test (Phase 1) and the first leaching cycle of the drum test (Phase 2, leaching cycle 4).

Outflow rate

The weathered CCR had the smallest particle size range (D_{30}=2.5 mm, D_{50}=4.8 mm, and D_{60}=6.0 mm) and contained more fine particles compared to the other types. This distribution of fines can clog the pores between large CCR particles, reducing the movement of solution through the solids. This difference in particle size distribution was illustrated by the difference in outflow rates among the columns. The weathered refuse had the lowest outflow rate compared to other types.

Stored acidity

Refuse that has been exposed to weathering conditions has what is known as existing or stored acidity, which can be easily released into the surrounding environment (Daniels et al., 2018). The stored acidity is present as soluble acidic components, including soluble sulfate salts. Generally, sulfate salts are soluble in water and build up on coal waste during dry seasons due to water evaporation (Daniels et al., 2018). They release acidity and metals during rainfall events (Pope et al., 2012). When DI water with a pH of approximately 5 was used as the leachant, the stored acidity contributed greatly to reducing the pH and releasing the REE along with other major metals.

Leaching frequency

The results of this study showed that multiple leaching cycles that are one week apart would not promote REE extraction under these test conditions. The results show that pyrite oxidation is time-dependent, and REE compound accumulation on the surfaces of the refuse solid particles is allowed through drying periods. This was evident through the 4-month drying period that separated phases 1 and 2 of the drum leaching test and doubled the amount of TREEs in the collected leachate. Thus, frequent leaching may interrupt the process and prevent the accumulation of REE compounds on the surface. This finding is consistent with previous studies done on salt leaching and acid generation from coal mines (Geidel, 1979; Jain et al., 2021). Geidel (1979) investigated AMD release and found that acidity is generated primarily by oxidation of pyrite, followed by dissolution and chemical reactions to break down weathering compounds. Geidel (1979) also found that time-dependent kinetics control the process, and the amount of acidity produced depends directly on the time interval between leaching cycles. Increasing the interval between flushings increased the amount of acidity released, while frequent flushings produced mild acidic leachate.

TREE concentration in solids post-leaching

Three possible scenarios can explain the increased amount of TREE concentrations in solids post-leaching. The first is that REE may be sorbed back to the solid. This scenario can be explained by diffusion, which is mainly controlled by Brownian motion (random movement). This molecular motion and collision should cause the natural movement of REE from the leachate back into the pore space or the water layer surrounding individual solid particles. This scenario is more likely when the test is conducted under saturated conditions, allowing diffusion to occur. Some pooling was observed in columns AMD-W and H_2O_2-W, which might explain this increase in these two columns. This scenario explains what happened during the leaching of the raw CCR, as almost all the REE available within the AMD was sorbed back into the material. The second

scenario involves the migration of REE from one location to another as the leachant is percolating through the material; it is possible that REE will be carried from one location to another. The last scenario is a variation in the samples collected. That is a very likely possibility, as variability may be found in coal refuse within the same disposal area, and that is due to factors such as variation in feed coal. Individual prep plants often process more than one coal seam, so refuse materials within the same disposal area often differ greatly (Daniels et al., 2018; D'Appolonia, 2009).

Task 1.3 Predictive Model Development

Statistical analysis

Results and data from the column leaching test for TREE were analyzed to determine the best statistical approach to presenting the outcomes. **Figure 1.3.1** shows a boxplot representation of the TREE concentrations in leachates collected from the six columns. The results of the boxplot showed that there is little to no difference between the TREE concentration of columns leached with AMD and columns leached with AMD+H_2O_2. It also showed that the highest leaching amounts of REE were associated with weathered CCR leached using either AMD or AMD+H_2O_2. The lowest amounts of TREE resulted from the percolation of DI water through fresh CCR.

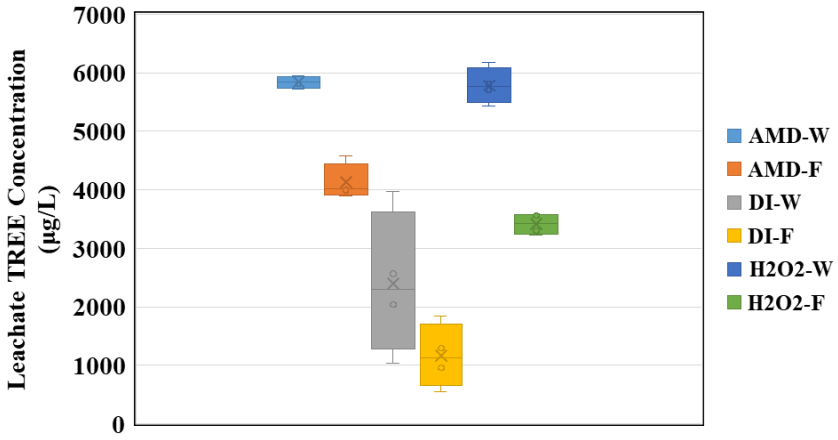


Figure 1.3.1: TREE content in leachate collected from six columns during the first leaching cycle.

The distribution of data collected from the column leaching test lacks symmetry as the highest amounts of TREE were seen in the first leaching cycle and decreased in the following weeks (weeks 2 through 6). As the data obtained did not have a normal distribution, nonparametric tests (e.g., ANOVA and Mann–Whitney test) were used to determine whether there were any significant differences in the results of the three types of leachants (AMD, AMD+H_2O_2, and DI water) and the two groups (fresh and weathered) by comparing the means of TREE concentrations correlated with each group.

The One-way ANOVA test was conducted for TREE concentrations across the three leachants (**Table 1B, Appendix B**). Results from the first leaching cycle were considered, as the most significant amount of REE was leached during the first cycle. The null hypothesis that the three different groups were all equal was tested using the one-way ANOVA (**Table 2B, Appendix B**). The null test showed that there is no statistically significant difference between the results of the three different leachants, as $F < F_{critcical}$ and p-value > 0.05. The Mann-Whitney test was applied to results from the two groups of CCR: weathered and fresh (**Table 3B, Appendix B**). The results

showed that the difference between the means of the two groups is statistically significant with $U_{stat} < U_{critical}$ and a p-value < 0.05. The effect of leachant pH and flow rate on TREE leaching was tested by applying the regression analysis. The results indicated that the pH had no effect on the TREE results, with a p-value of 0.7 and R^2 of 0.02. The results showed that 54% of the results can be explained by the flow rate.

CCR jar test

Methodology

A jar test was performed to study the leaching trends over time, develop an REE concentration versus time curve, and determine the solution-solid contact time during a flushing cycle (**Figure 1.3.2**). This test was completed as a modification to ASTM C1308-21 (ASTM, 2008). Jar tests have been carried out in scientific publications to facilitate the leaching of metals (Neupane and Donahoe, 2013).

This test was conducted using the weathered CCR (solid TREE concentration of 263.4 mg/kg), as it was identified in the column leaching tests as having the highest leaching potential. The Crest Pond at Blacksville # 2 coal mine was the source of the AMD (aqueous TREE concentration of 488.6 μg/L at the time of testing). Five containers were filled with approximately 2 kg of weathered CCR (**Figure 1.3.3**). The CCR was submerged in AMD for increasing time intervals of 30 minutes (min), 1 hour (h), 2 h, 4 h, and 8 h. Five factors remained constant throughout the test: temperature (25°C), GSD (D_{30}=2.5 mm, D_{50}=4.8 mm, and D_{60}=6.0 mm), leachant type (AMD), leachant amount (1 L), and pH (2.6). CCR leachate was then filtered through a layer of non-woven geotextile (1100 N; apparent opening size [AOS] of 0.15 mm) (**Figure 1.3.4**). The filtrate from each container was collected and delivered the same day of testing to the Analytical Lab for REE concentrations (EPA 200.8) and major metals concentrations (EPA 200.7) (**Figure 1B, Appendix B**).

The TREE concentration determined from the jar test was proportionally scaled up to the field scale based on calculated CCR mass in a pile. The heap pad field demonstration size was assumed to be 8,093.7 m^2 (2 acres) in area by 3 m (10 ft). Using the unit weight of the weathered CCR (12.4 kN/m^3) determined in the lab under a reduced compaction energy of 67.84 kJ/m^3 (1,416 $ft\text{-}lb/ft^3$), the mass of CCR that is within the heap was calculated as 10,115 metric tons (11,150 US tons).

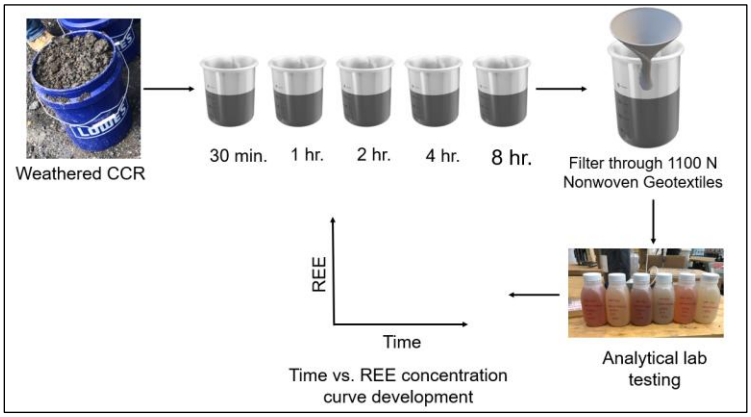


Figure 1.3.2: Weathered CCR jar test flow chart.

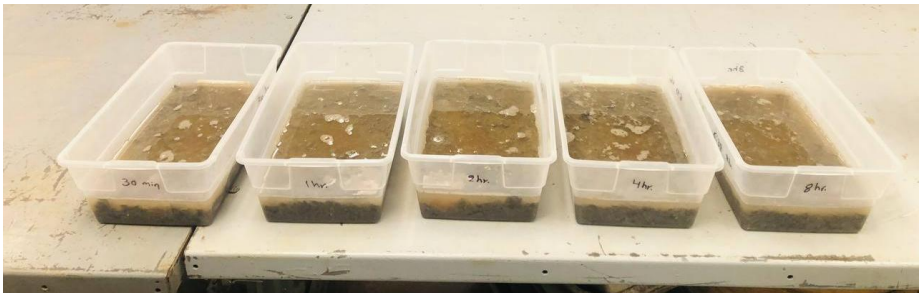


Figure 1.3.3: Five containers filled with weathered CCR submerged with 1000 mL of AMD.



Figure 1.3.4: Filtration of jar test leachate using 1100N nonwoven geotextile.

Kinetic analysis of leaching

A fluid-particle heterogeneous reaction can explain the leaching process (Ait Brahim et al., 2022). As a result of the direct contact of the solid ore with the leachant, this reaction occurs, generating a product from the solid. The process includes several stages: i) leachant diffusion across the liquid boundary layer surrounding particles within the ore, ii) leachant diffusion across the porous space of the product layer, iii) product formation by surface reaction, iv) substance released from the surface, and v) product diffusion through the product layer followed by diffusion across the liquid layer surrounding particles. When the process follows a steady state, the reaction rate of each stage is relatively equal. The leaching mechanism and the rate-determining stages are commonly described using mathematical models (e.g., Safari et al. 2009; Zhu et al. 2017; Cao et al. 2018; Ruan et al. 2019; Yang and Honaker 2020; Kuppusamy and Holuszko 2022; Ait Brahim et al. 2022). In coal, coal rejects, and fly ash, the shrinking core model is applied to describe leaching dynamics (Zhu et al., 2017; Ruan et al., 2019). The shrinking core model is defined as follows (Equation 6) in the event of a chemically controlled process:

$1 - (1-\alpha)^{1/3} = k_r t$ (Equation 6)

However, when the inner diffusion reaction controls the process, the kinetic equation is defined as (Equation 7):

$1 - 2/3\ \alpha - (1- \alpha)^{2/3} = k_r t$ (Equation 7)

where α = the leaching efficiency at time t, and k_r = the rate constant.

Data from the jar test were fit to Equations 6 and 7 to determine the rate-limiting step and describe the kinetics of the leaching process.

Results and discussion

Figure 1.3.5 shows the difference in color between the leachant used in the test and the collected leachate from the five jars. The filtered leachate had a pH of 2.1. REE concentration in the leachate increased as the contact time was extended. Due to the prolonged contact time, more REE had the opportunity to dissolve into the solution chemically (**Table 1.3.1**; **Figure 1.3.6**). The increase in REE concentration from leachant to leachate ranged between 644% (Jar 1) and 845% (Jar 5). This increase, however, accounted for only 1% to 2% of the CCR solid concentration, indicating a poor leaching efficiency of 0.60% to 0.78%.

The 2 kg of CCR used in the lab to perform the jar test yielded a total concentration of TREE of 4,130 μg/L through the longest contact time of 8 h. Based on the assumption that leaching efficiency in the field is similar to that in the lab, approximately 21 kg (46 lb) of TREE is estimated to be achieved in the field.

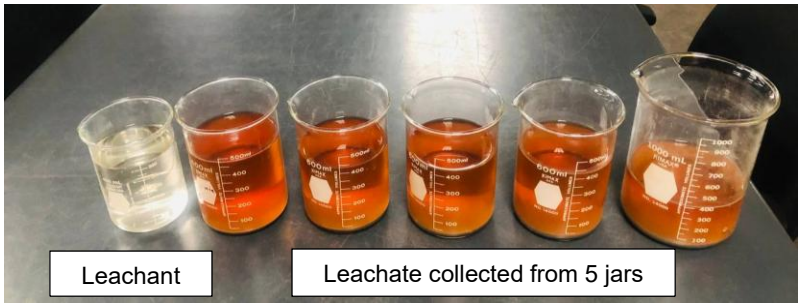


Figure 1.3.5: Jar test leachant (far left) and leachate collected from each jar.

Table 1.3.1: Jar test results.

Jar Number	Time Interval (h)	Leachate TREE concentration (μg/L)	Increase in TREE concentration (μg/L)	Increase in TREE concentration (%)	Cumulative leached from solid (%)
1	0.5	3,634	3,146	644	1
2	1	3,783	3,295	674	1
3	2	3,795	3,307	677	1
4	4	4,242	3,754	768	1
5	8	4,618	4,130	845	2

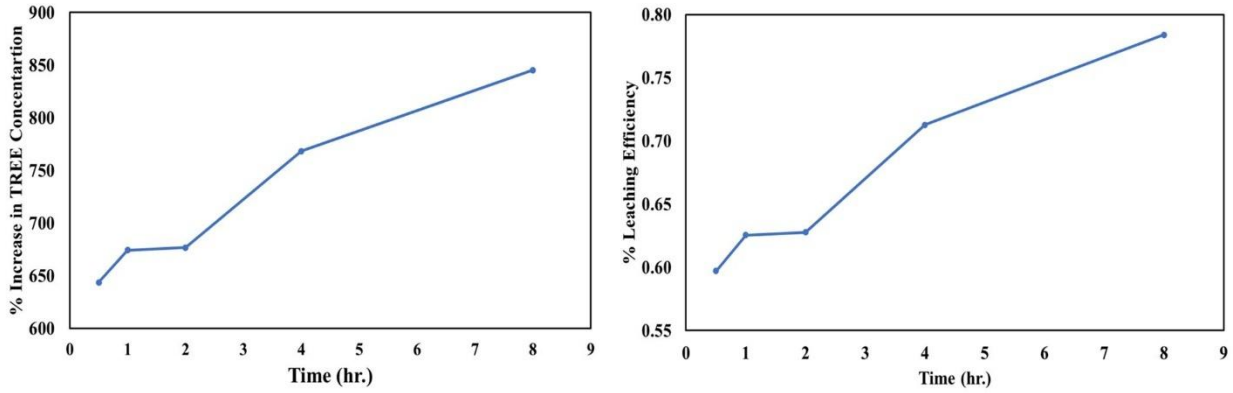


Figure 1.3.6: Percent increase in TREE concentration (left) and leaching efficiency (right) in jar tests.

Saturated jar tests of CCR confirmed that extended contact time produces more REE. After the 30-min and 1-h time intervals, the TREE concentration in leachate increased by 644% and 674%, respectively. Comparing the 1-h to 2-h time interval, no substantial increase in REE concentration was observed (**Figure 1.3.6**). Doubling the time interval showed an increase of 14% when comparing the 2-h to 4-h, and 10% when comparing the time intervals of 4-h to 8-h. This behavior can be explained as follows: during the first 1-h, the hydrogen ion H^+, abundant in the AMD and responsible for its acidity, had a quick reaction kinetics with ion exchangeable REEs available at the surface of the solid particles, causing the breakdown of REE-bearing minerals and releasing REEs (Cao et al., 2018; Yang and Honaker, 2020; Ait Brahim et al., 2022). This is known as the "easy-to-leach" REEs, which are usually released as soon as the leaching process begins. During the time period from 1 h to 2 h, the increase in TREE concentration was very limited due to a diffusion process of acid into the particles (**Figure 1.3.6**). During this period, the leaching efficiency did not change. All REE available at the surface of the particles had already been leached by this time, so no increase in REE concentration was seen until the acid diffusion into the particles had occurred. When this happened, the REE concentration rapidly increased. The increase in REE concentration seen after the diffusion period was due to the reaction of H^+ with the readily dissociable REE compounds contained within the particles. This finding was consistent with results from another study done on leaching REE from coal fly ash (Cao et al., 2018).

The square of the correlation coefficients (R^2) of the two fitted models (chemical reaction controlled and inner diffusion reaction control) for TREE were 0.965 and 0.973, respectively. Both models could describe the leaching process of REE from CCR; however, the inner diffusion control mechanism can be considered the predominant mechanism, as the model yielded a higher value of R^2, suggesting that the rate of the reaction is primarily limited by diffusion. For all individual REEs, the R^2 values of the inner diffusion-controlled model were greater than those of the chemically controlled model (**Tables 1.3.2 and 1.3.3**). The leaching rate constants for all individual REEs were in the same order regardless of the model used for fitting: Tb> Gd> Dy> Ho> Y> Er> Tm> Yb> Lu for HREE, and Eu> Sm> Nd> Sc> Pr> Ce> La for LREE (**Figure 1.3.7**). Compared to the other elements, Tb is the easiest HREE to release from the weathered CCR, whereas Eu is the easiest LREE to leach.

It is important to note that the determined mechanisms of leaching are based on fully saturated leaching conditions. The diffusion mechanism may differ under unsaturated leaching conditions, as the leachant will not have the same time to diffuse through the porous space of the solid particles.

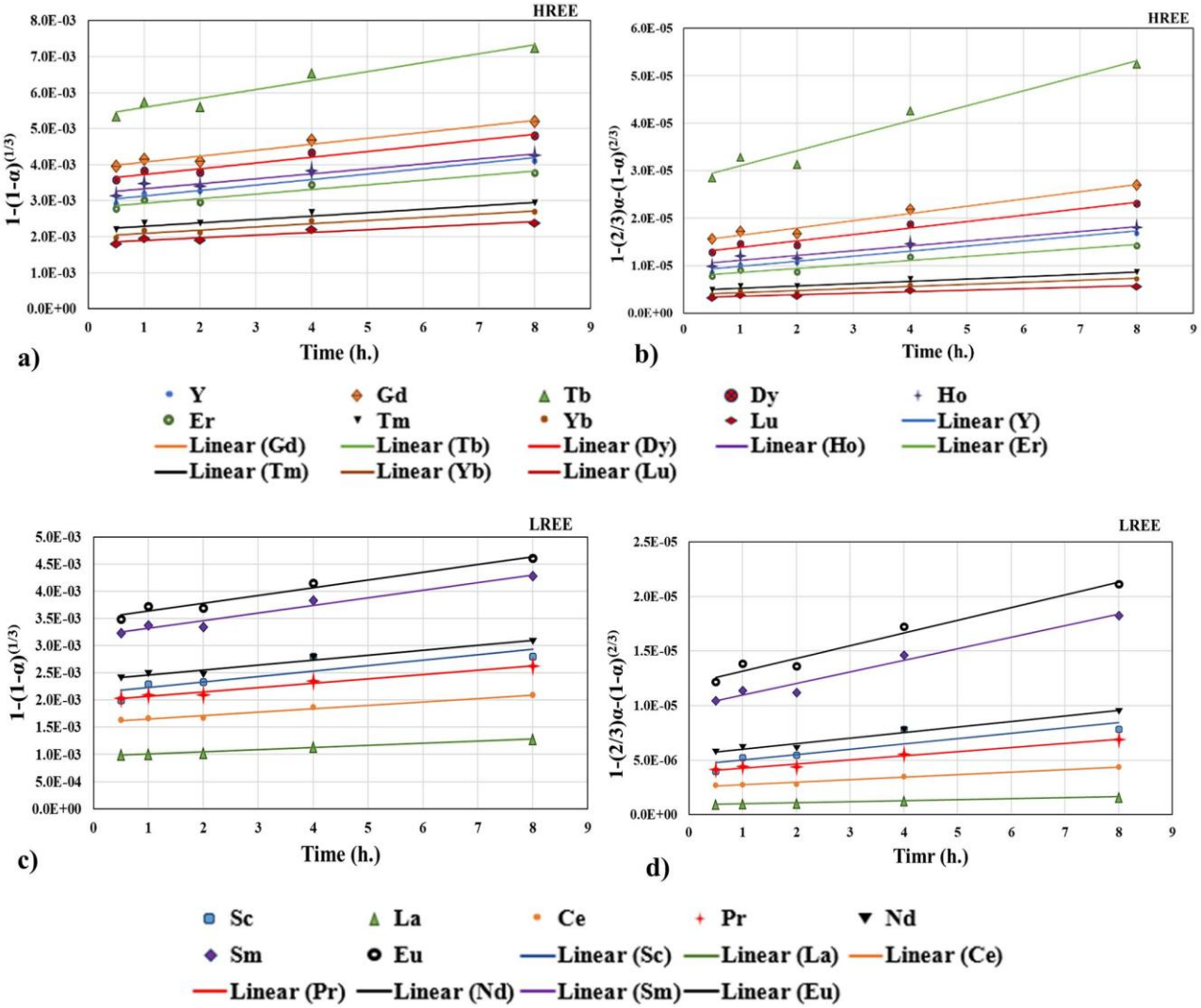


Figure 1.3.7*:* Kinetic modeling of individual (HREE) (a and b) and (LREE) (c and d).

Table 1.3.2: The square of the correlation coefficient (R^2) and the corresponding rate constant (*kr),* of two fitted models for individual HREE.

HREE	Chemically controlled		Inner diffusion-controlled	
	kr	**R^2**	***kr***	**R^2**
Yttrium (Y)	2.0×10^{-4}	0.923	1.0×10^{-6}	0.942
Gadolinium (Gd)	2.0×10^{-4}	0.960	2.0×10^{-6}	0.967
Terbium (Tb)	3.0×10^{-4}	0.946	3.0×10^{-6}	0.957
Dysprosium (Dy)	2.0×10^{-4}	0.957	1.0×10^{-6}	0.967
Holmium (Ho)	1.0×10^{-4}	0.931	1.0×10^{-6}	0.947
Erbium (Er)	1.0×10^{-4}	0.932	8.0×10^{-7}	0.945
Thulium (Tm)	9.0×10^{-5}	0.953	5.0×10^{-7}	0.966
Ytterbium (Yb)	9.0×10^{-5}	0.934	4.0×10^{-7}	0.949
Lutetium (Lu)	7.0×10^{-5}	0.916	3.0×10^{-7}	0.930

Table 1.3.3: The square of the correlation coefficient (R^2) and the corresponding rate constant (*kr*) of two fitted models for individual LREE.

LREE	Chemically controlled		Inner diffusion-controlled	
	kr	R^2	*kr*	R^2
Scandium (Sc)	1.0×10^{-4}	0.741	5.0×10^{-7}	0.755
Lanthanum (La)	4.0×10^{-5}	0.988	9.0×10^{-8}	0.989
Cerium (Ce)	6.0×10^{-5}	0.979	2.0×10^{-7}	0.981
Praseodymium (Pr)	8.0×10^{-5}	0.974	4.0×10^{-7}	0.978
Neodymium (Nd)	9.0×10^{-5}	0.965	5.0×10^{-7}	0.971
Samarium (Sm)	1.0×10^{-4}	0.968	1.0×10^{-6}	0.974
Europium (Eu)	1.0×10^{-4}	0.962	1.0×10^{-6}	0.970

Task 2.1 Refuse site assessment

Methodology

Construction of macro-scale heap leach operations requires large surface areas to accommodate material transfer. Sites also require infrastructure to distribute, collect, and process the REE-enriched PLS into a hydraulic pre-concentrate (HPC) solid precipitate. Ground topography and deposit volume conditions can vary greatly from one site to another; thus, it is essential to validate candidate sites for heap leaching using subjective criteria applicable to all sites. The purpose of this task was to develop a site selection criteria process to assist with the selection of coal mine refuse sites that have beneficial or favorable site ground topography, deposit volume, and other characteristics to support a CCR REE heap leach design and operation.

The most important criteria to be considered when selecting a site for heap leaching are identified in published literature as follows: site size, topography, environmental considerations (e.g., AMD containment and treatment), haulage distance, construction materials source, wildlife and vegetation, and meteorological conditions (Nasab et al., 2007). Two known sites (ACNR Blacksville Number 2 Mine and ACNR Marion County Mine) were compared according to the listed criteria in a hierarchical structure (**Figure 2.1.1**). One additional factor (CCR age) was included in this project because it was identified as a critical factor in heap leaching REEs from CCR. Questionnaires were prepared for the two (2) study sites and developed based on the most important criteria identified in the literature. The questionnaires were sent to ACNR for review and feedback. The questionnaires for Blacksville Number 2 and Marion County are provided in **Appendix C** and **Appendix D**, respectively.

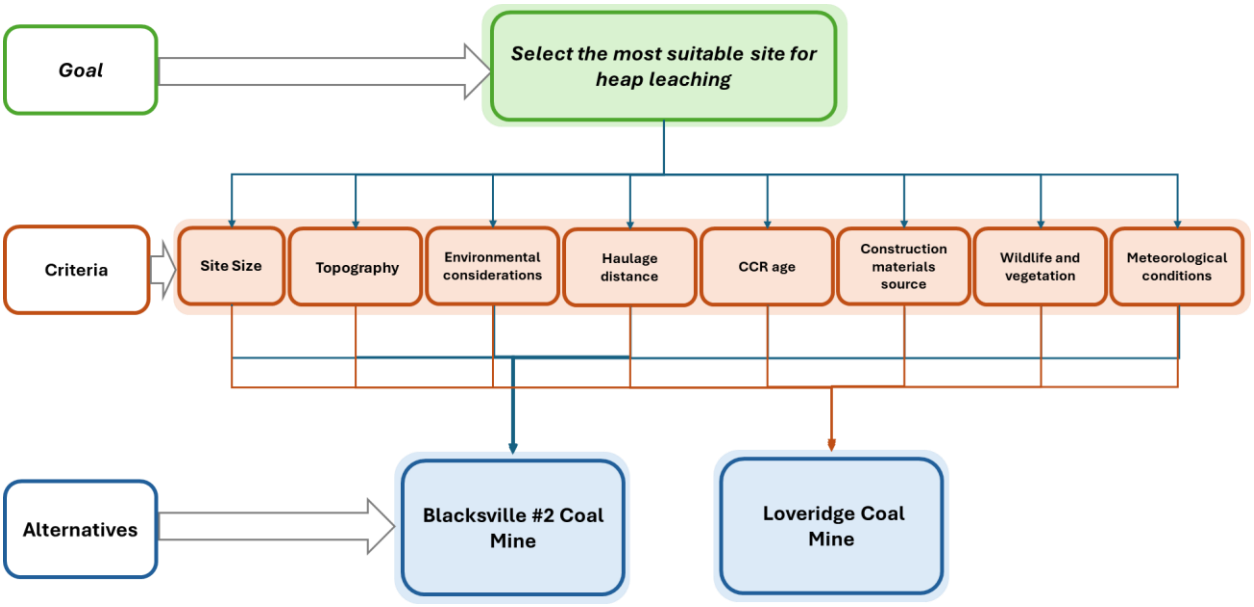


Figure 2.1.1: Hierarchical structure for the evaluation of two selected sites for heap leaching according to defined criteria.

Considering the interrelationships between these criteria, identifying a site using independent criteria is challenging (Soltani-Mohammadi and Amini, 2013). Multi-criteria decision-making techniques (e.g., Analytical Hierarchy Process [AHP]) are considered helpful in such cases (Goepel, 2019; Soltani-Mohammadi and Amini, 2013). AHP was used to quantify and compare the two study sites. This technique is used to analyze complex decisions based on a mathematical approach (Darko et al., 2019). AHP was applied using feedback from ACNR on the developed questionnaires. The criteria were weighed, and the two site alternatives were compared. The degree of importance of every criterion for the selection of the heap leach pad site was determined based on published literature (Goepel, 2019; Soltani-Mohammadi and Amini, 2013).

Table 2.1.1 illustrates the degree of importance of criteria for heap leach site selection. A numerical rating from 1 to 9 was followed to explain the verbal judgments of preference. **Table 2.1.2** explains the pairwise comparison scale that was defined by Saaty (1977) and reported in the literature (Soltani-Mohammadi and Amini, 2013; Yıldırım, 2019; Cavallo and Ishizaka, 2023). Environmental considerations and CCR age were given the highest degree of importance, followed by site size and topography. Because weathered refuse showed the highest leaching potential and the refuse will be sitting on site, haulage distance was assigned the lowest degree of importance.

Each criterion defined in the project was verbally compared with the other criteria in a respective hierarchy level, and their corresponding evaluation values were entered into a squared matrix (**Table 1E, Appendix E**).

Table 2.1.1: The degree of importance of criteria for heap leach site selection.

Criteria	Very low	Low	Average	High	Very high
Site Size				✓	
Topography				✓	
Environmental considerations					✓
Haulage distance	✓				
CCR age					✓
Construction materials source			✓		
Wildlife and vegetation			✓		
Meteorological conditions		✓			

Table 2.1.2: Pairwise comparison scale (Saaty, 1977; Soltani-Mohammadi and Amini, 2013; Yıldırım, 2019; Cavallo and Ishizaka, 2023).

Value	Semantic meaning
1	The two decision items have the same importance
3	The selected decision item is weakly more important than the other one
5	The selected decision item is strongly more important than the other one
7	The selected decision item is very strongly more important than the other one
9	The selected decision item is absolutely more important than the other one
2, 4, 6, 8	Intermediate values

Results

The weights of criteria representing their relative importance (global priority) were determined (**Table 2.1.3**). A consistency ratio (CR) of zero was also determined to ensure the consistency of the pairwise comparison matrix.

Blacksville #2 and Loveridge overall scores were 0.65 and 0.35, respectively (**Table 2.1.4**). Based on the analysis results, the Blacksville #2 mine was selected as the best candidate site. Both sites had similar qualifications, particularly in terms of size, topography, and environmental characteristics such as AMD treatment. However, CCR age played a significant role in affecting the overall score. Blacksville Number #2 contains the oldest piles of refuse, which is preferred based on earlier results of the study.

Table 2.1.3: Weights of criteria, representing their relative importance (global priority).

Criteria	Site Size	Topography	Environmental considerations	Haulage distance	CCR age	Construction materials source	Wildlife and vegetation	Meteorological conditions	Priority	Average
Site Size	0.08	0.14	0.08	0.14	0.05	0.09	0.20	0.15	0.12	0.1
Topography	0.04	0.07	0.08	0.14	0.05	0.14	0.20	0.15	0.11	0.1
Environmental considerations	0.39	0.36	0.39	0.24	0.49	0.27	0.25	0.23	0.33	0.3
Haulage distance	0.02	0.02	0.06	0.03	0.04	0.02	0.02	0.02	0.03	0.0
CCR age	0.39	0.36	0.19	0.24	0.25	0.27	0.25	0.26	0.28	0.3
Construction materials source	0.04	0.02	0.06	0.07	0.04	0.05	0.02	0.08	0.05	0.0
Wildlife and vegetation	0.02	0.02	0.08	0.07	0.05	0.14	0.05	0.08	0.06	0.1
Meteorological conditions	0.02	0.02	0.06	0.07	0.04	0.02	0.02	0.04	0.04	0.04
Sum	1.0	1.0	1.0	1.0	1.0	1.0	1.0	1.0	1.0	1.0

Table 2.1.4: Weight of criteria (global priority) and weight of criteria of each alternative (local priority).

Criteria	Site Size	Topography	Environmental Considerations	Haulage distance	CCR age	Construction materials source	Wildlife and Vegetation	Meteorological Conditions
Overall Priority	0.12	0.11	0.33	0.03	0.28	0.05	0.06	0.04
Blacksville #2	0.33	0.67	0.67	0.667	0.88	0.333	0.33	0.667
Loveridge	0.67	0.33	0.33	0.333	0.13	0.667	0.67	0.333

Blacksville #2	0.65
Loveridge	0.35

Task 2.2 Tailings geotechnical material classification and 2-D numerical modeling

Hydraulic conductivity and ore particle size have a significant influence on heap leaching efficiency and kinetics (Free, 2020). Thus, it is essential to investigate several geotechnical properties, particularly index and engineering properties, so that coal refuse heap leach pads can be designed more efficiently. Bench-scale geotechnical laboratory testing was performed to determine the coal refuse particle size distribution, in addition to other physical properties.

Testing was carried out in two phases. As received, baseline parameters of the collected CCR were assessed during the first phase. The second phase determined the leaching effect on the grain-size distribution of the refuse, which, in turn, may determine the potential for fine-particle intrusion and clogging.

There are two classifications of geotechnical soil properties: index and engineering. Moisture content, specific gravity, grain size distribution (GSD), Atterberg limits, and unit weight are considered the five index properties. Hydraulic conductivity is considered an engineering property (Tolikonda, 2010). The properties of the CCR were determined in triplicate in accordance with American Society for Testing and Materials (ASTM) protocols (**Table 2.2.1**).

Table 2.2.1: Soil tests and corresponding ASTM protocol.

Test Name	ASTM
Physical Properties	
Moisture Content	D-2216
Specific Gravity	D-854
Particle or Grain Size Distribution (GSD)	D-422
Atterberg limits	D-4318
Soil Classification USCS	D-2487
Compaction	
Standard Proctor	D-698
Permeability	
Hydraulic Conductivity	D-5856

Geotechnical properties

The oven-dried average moisture content of the raw samples was 7%, and the average moisture contents of the fresh and weathered samples were approximately 14% and 18%, respectively (**Table 2.2.2**). In contrast, air drying for 4 days resulted in average moisture contents of 6%, 11%, and 13% for the raw, fresh, and weathered CCR, respectively. The weathered CCR had the lowest G_s (1.99) among the three types (**Table 2.2.2**). Values of G_s were within the most common values defined by the Mine Safety and Health Administration (MSHA) for CCR (D'Appolonia 2009) and reported in the literature (Quaranta and Tolikonda, 2011; Stevens, 2016). The raw CCR was classified as poorly graded gravel with sand (group symbol GP). The fresh and weathered refuse was identified as well-graded gravel with sand (group symbol GW) (**Table 2.2.2** and **Figure 2.2.1**). The weathered refuse had the highest degree of saturation calculated based on determined air-dried moisture content (13%) and dry density (15.4 kN/m^3). Additional information about the geotechnical properties (individual tables and figures) is provided in **Appendix F**.

Table 2.2.2: Summary of CCR mean geotechnical physical properties.

Geotechnical properties	Raw	Fresh	Weathered
Initial moisture content-oven dried, ω_{oven} (%)	7	14	18
Initial moisture content-air dried, ω_{air} (%)	6	11	13
Specific gravity, G_F	2.20	2.30	1.99
Particle diameters corresponding to 10% finer by weight, D_{10} (mm)	2.0	0.7	0.7
Particle diameters corresponding to 30% finer by weight, D_{30} (mm)	5.0	3.0	2.5
Particle diameters corresponding to 50% finer by weight, D_{50} (mm)	8.5	6.0	4.8
Particle diameters corresponding to 60% finer by weight, D_{60} (mm)	12.0	8.1	6.0
Uniformity coefficient, C_u	6.0	11.6	8.6
Coefficient of curvature, C_c	1.0	1.6	1.5
Group symbol	GP	GW	GW
Dry unit weight, γ_d (kN/m^3) -Standard Compaction	16.7	15.5	15.4
Initial Void Ratio, e_o	0.25	0.44	0.27
Porosity, n	0.20	0.31	0.21
Degree of saturation (%), S	47.4	58.2	97.4

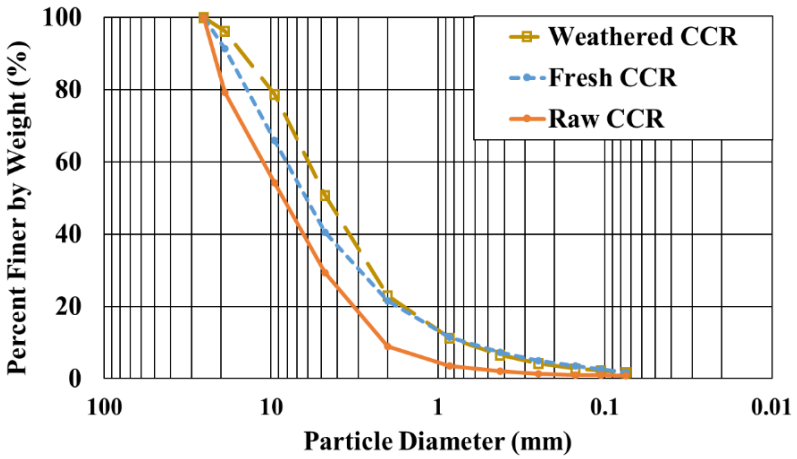


Figure 2.2.1: Average particle size distributions of three types of CCR (raw, fresh, and weathered) - as received.

Hydraulic conductivity

Hydraulic conductivity measurements followed ASTM D-5856 Standard Test Method for Measurement of Hydraulic Conductivity of Porous Material Using a Rigid-Wall, Compaction-Mold Permeameter. By varying the water content and compaction energy in the permeability cell, the CCR samples were compacted to specified densities. The test was performed using two different compaction energies: i) regular compaction (12,375 ft-lb/ft^3); and ii) reduced compaction (1,416 ft-lb/ft^3). At the end of the permeability test, samples were removed from the rigid wall cell, cut into layers, and placed in trays to be dried for post permeability-GSD test. The permeability sample subjected to standard compaction energy (12,375 ft-lb/ft^3) was divided into three layers, whereas the permeability sample subjected to reduced compaction energy (12,375 ft-lb/ft^3) was cut into two layers. Results from the post-permeability GSD test were compared to the GSD test done prior to the permeability test in order to determine if changes in material properties had occurred. Post-permeability GSD tests can evaluate any potential increase in the percentage of fine particles due to compaction and any fine particle movement within the structure of the sample due to the flow of the solution (Tolikonda and Quaranta, 2012). Specimens were crushed in a manner that would result in a post-GSD less than 4.75 mm in size.

Tables 2.2.3 and **2.2.4** summarize the hydraulic conductivity test results for all CCR types with two different compaction energies: standard and reduced. The permeability of the reduced compaction samples was one order of magnitude higher than the permeability of the standard compaction sample for fresh and weathered refuse, which is consistent with published literature (Tolikonda and Quaranta, 2012). No change or reduction in hydraulic conductivity was observed during the test period (**Figures 8F-10F, Appendix F),** suggesting minimal fine-particle movement. A stable equilibrium condition was observed for samples compacted with reduced energy (1,416 ft-lb/ft^3).

Table 2.2.3: Hydraulic conductivity of all CCR samples (Standard Compaction).

Properties	Raw	Fresh	Weathered
Dry Density, kN/m^3 (pcf)	16.7 (106.3)	15.51 (98.7)	15.3 (97.3)
Compaction Energy (ft-lb/ft^3)	12,375	12,375	12,375
Number of Blows/Layer	25/3	25/3	25/3
Gradient	5	5	5
Average k, cm/sec (m/sec)	1.18e-03 (1.18e-05)	2.9e-04 (2.9e-06)	3.48e-04 (3.48e-06)

Table 2.2.4: Hydraulic conductivity of all CCR samples (Reduced Compaction).

Properties	Raw	Fresh	Weathered
Dry Density, kN/m^3 (pcf)	14.7 (93.5)	14.2 (90.3)	12.4 (78.9)
Compaction Energy (ft-lb/ft^3)	1,416	1,416	1,416
Number of Blows/Layer	4/2	4/2	2/2
Gradient	5	5	5
Average k, cm/sec (m/sec)	2.16e-03 (2.16e-05)	3.9e-03 (3.9e-05)	3.8e-03 (3.8e-05)

Grain Size Distribution (GSD)

Post-leaching GSD

Upon termination of the column leaching test, the columns were disassembled. The material in each column was taken out and split into three layers. Layers were placed in trays to be air dried for four days before testing for post-leaching GSD (**Figure 2.2.2**).

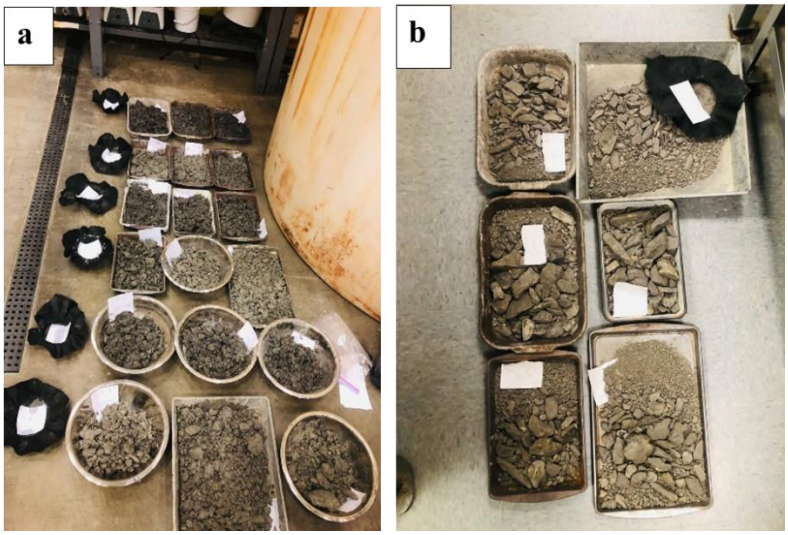


Figure 2.2.2: CCR in each column divided into three layers to be tested for post-leaching GSD: a) fresh and weathered CCR, and b) raw CCR.

Post-leaching GSD indicated a shift in the curve toward larger particle sizes compared to the as-received GSD curve, which indicates the agglomeration of small particles. The most substantial shift was observed in either the middle or bottom layers across most columns (**Figures 2.2.3 and**

2.2.4). Agglomeration occurs when particles of the material adhere loosely to each other (Merkus, 2009; Tolikonda and Quaranta, 2012; Iasillo et al., 2013). Dlamini (2015) reported that agglomeration that occurs during the leaching process is expected to improve the permeability and recoveries of metals by combining fine particles into larger ones. Also, agglomeration can improve the leaching of the element of interest (e.g., copper recovery) as it provides good control of the leachant flow (Dlamini 2015; Ghorbani et al. 2016; Wang et al. 2021; Yin et al. 2021). At the same time, studies that investigate the extraction of REE from coal byproducts emphasized the fact that coarse or aggregated particles would have a small area of interface, which has a negative impact on REE leaching (Yang, 2019a; Yang and Honaker, 2020). Results from the current study also showed that particle aggregation did not work in favor of leaching REE.

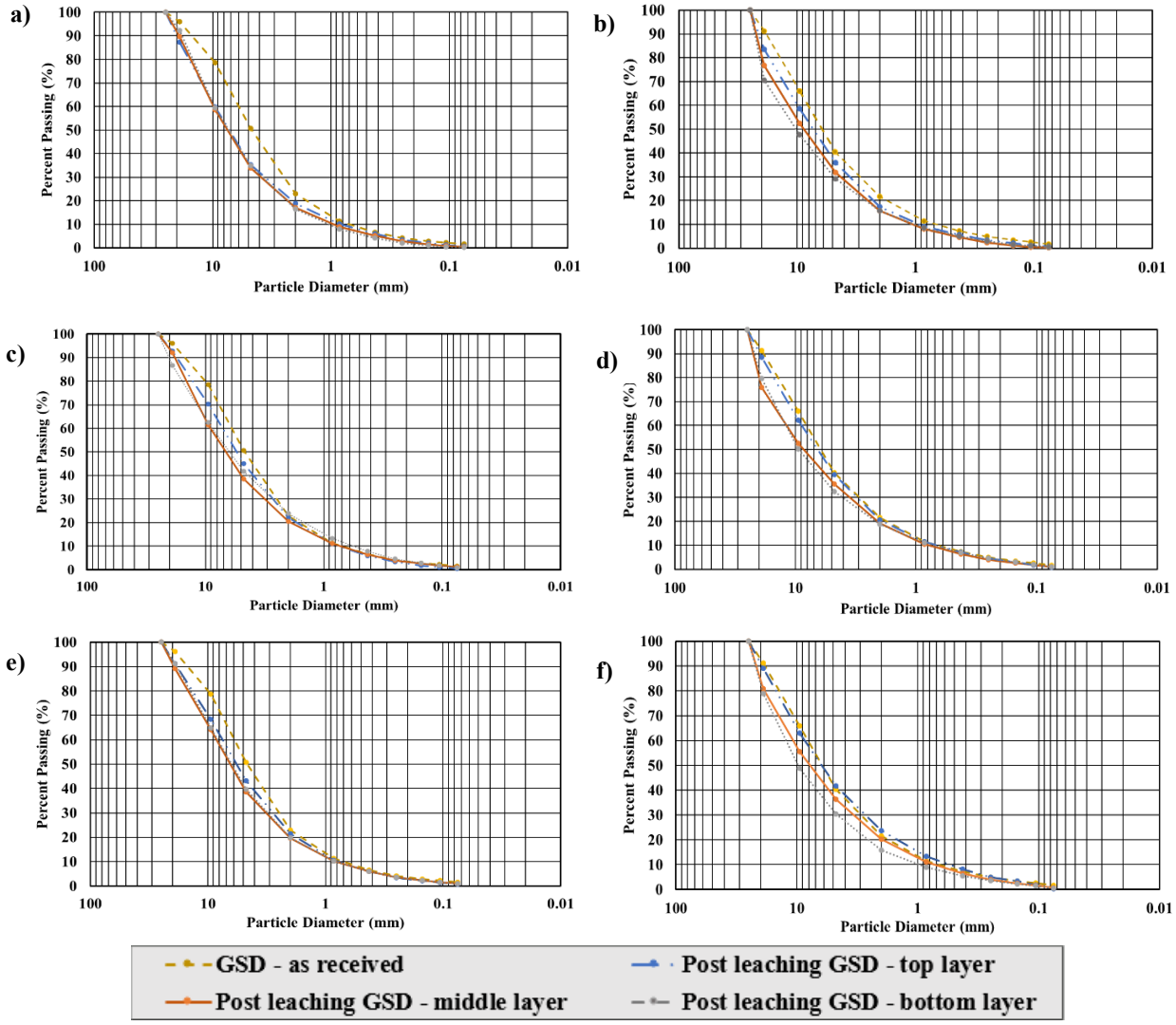


Figure 2.2.3: Post-leaching vs. as-received average grain size distribution (fresh and weathered CCR): a) AMD-W, b) AMD-F, c) DI-W, d) DI-F, e) H_2O_2-W, and f) H_2O_2-F.

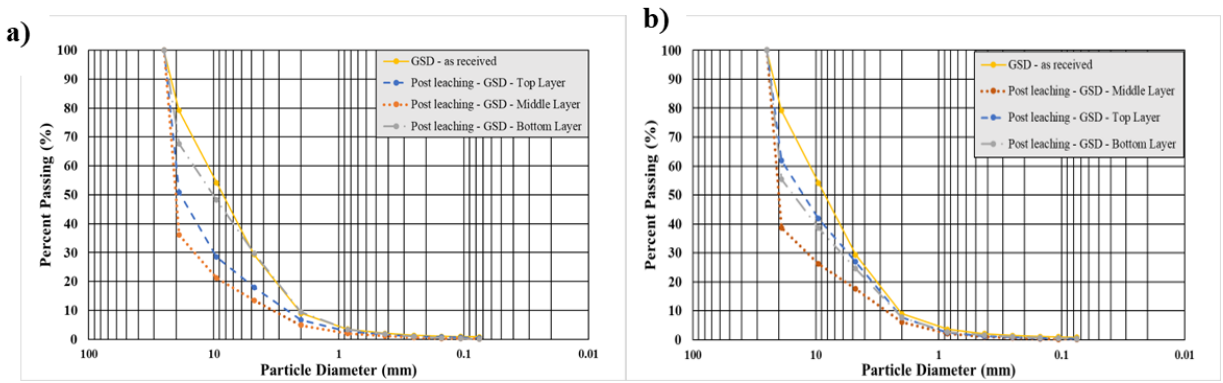


Figure 2.2.4: Post-leaching vs. as-received average grain size distribution (raw CCR): a) AMD-R, and b) DI-R.

Post-permeability GSD

GSD curves for all types of CCR compacted samples showed an overall and consistent movement (**Figure 2.2.5 and 11F, Appendix F**). A shift to the right in the post-GSD curve indicates an increase in fines, which was caused by the compaction effort resulting in particle crushing and slaking.

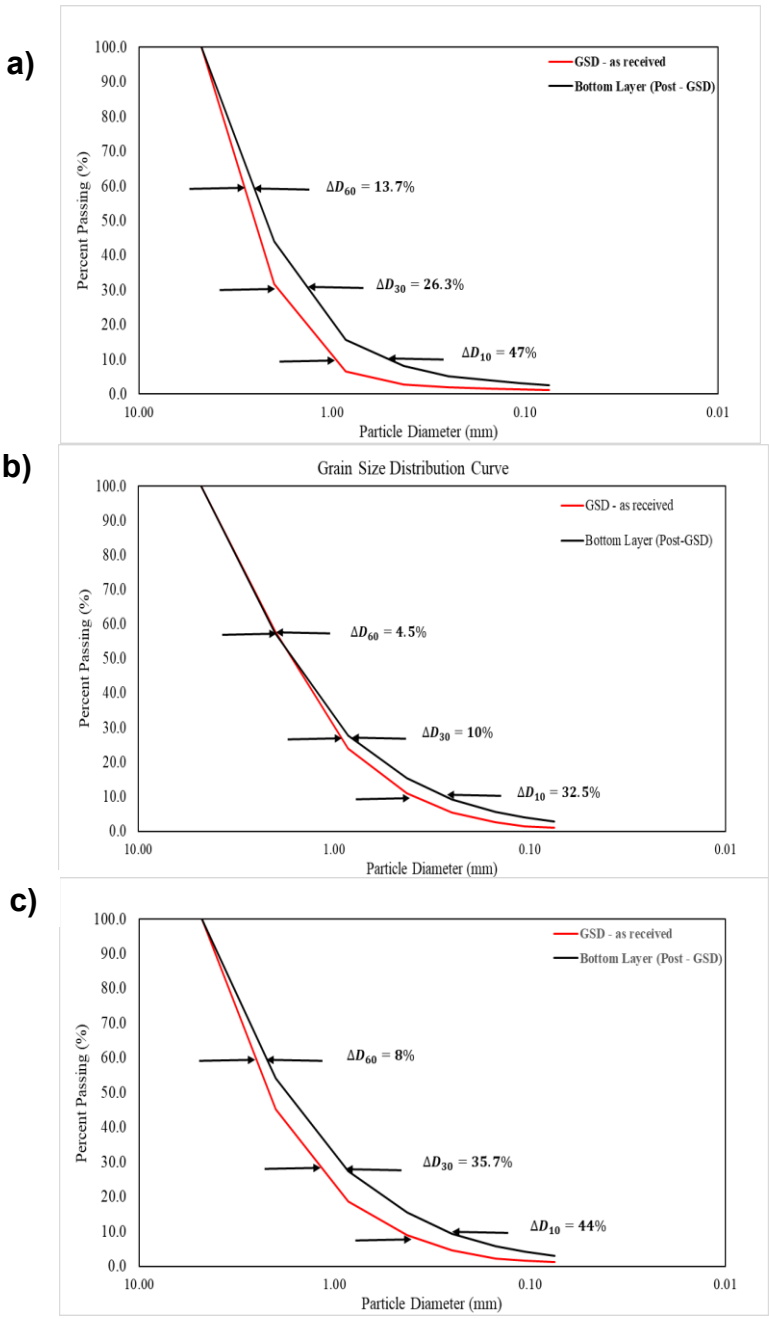


Figure 2.2.5: Grading envelope (as-received versus post-permeability bottom layer) – standard compaction (12,375 ft-lbs/ft^3): a) raw CCR, b) fresh CCR, and c) weathered CCR.

Geotextile material selection

In practice, recovery of REE from CCR leachate would require production of HPC via selective precipitation. HPC storage would consist of geotubes manufactured by Solmax. A literature review of previous research and recent projects was conducted to verify the geotextile materials appropriate for HPC filtration and dewatering at the study sites in this project.

A column filtration test (CFT) study by Tyson (2023) quantified the hydraulic conductivity and filtration efficiencies of conventional AMD sludge with woven and nonwoven geotextile fabrics.

Five (5) geotextile fabrics were assessed in the study: GT500 (woven), 1100N (nonwoven), 140NC (nonwoven), MD88 (nonwoven typar), and MD7407 (nonwoven typar). AOS, filtration efficiency, and fabric applications were taken into consideration. AMD sludge was collected from two West Virginia Department of Environmental Protection (WVDEP) AMD treatment sites: Omega (Morgantown, WV) and T&T (Albright, WV). Geotextiles were wrapped and tightened to the bottom of a column. AMD sludge was poured into the column, and filtrate was collected in a graduated cylinder placed under the column. Results showed that the highest filtration efficiency (>91%) was achieved using the 1100N nonwoven geotextile. The study recommended the use of 1100N fabric for filtration and dewatering in any future geotextile bag designs. A woven geotextile (e.g., GT500), however, is commonly used by WVDEP for capture and dewatering of conventional AMD sludge.

A CFT study was conducted by Houde (2024) to identify filtration and dewatering characteristics of both AMD sludge and HPC generated from coal-based AMD at the Richard Mine (Morgantown, WV). Four (4) polymer doses were evaluated: 0 ppm, 2 ppm, 4 ppm, and 10 ppm. Three (3) geotextile fabrics were evaluated: two (2) nonwovens (NW1 and NW2) and one (1) woven (W1). Results showed that the nonwoven geotextile outperformed the woven geotextile in filtration in all cases. When the test was performed with AMD sludge, NW2 had the highest average filtration efficiency of 80.3% and an average hydraulic conductivity of 1.17×10^{-3} cm/s, whereas the NW1 fabric had a filtration efficiency of 77.2% and an average hydraulic conductivity of 7.15×10^{-4} cm/s. When HPC was tested, NW1 had the highest average filtration efficiency of 79.2% and an average hydraulic conductivity of 1.01×10^{-4} cm/s, while NW2 had an average filtration efficiency of 66.9% and an average hydraulic conductivity of 1.75×10^{-4} cm/s. Results indicated that the woven geotextile (W1) had the lowest filtration efficiency of approximately 50%.

A study by Bird (2024) investigated the use of geotextiles for filtering and dewatering HPC from hardrock-based AMD at the Horseshoe Bend Water Treatment Plant (HsB WTP) in Butte, Montana. Eight (8) CFTs were performed using one (1) woven geotextile and one (1) nonwoven geotextile. Geotextile filtration efficiencies were similar; the woven geotextile had a slightly higher filtration efficiency (92.9%) compared to non-woven fabric (90.1%). Geotubes using these same geotextiles were also evaluated onsite at pilot scale. HPC was pumped from the treatment plant directly into woven and composite (woven and nonwoven) geotubes. All geotubes were effective in filtration and performed similarly in dewatering. Woven geotextiles were recommended for future applications. While nonwoven geotextiles are necessary for filtration of HPC from coal-based AMD, woven geotextiles are adequate for HPC from hardrock-based AMD due to the larger particle size.

Based on the results of these three (3) research studies, it is recommended to use a composite geotextile (woven outer layer with nonwoven inner layer) for the HPC storage system in this study. Composite bags have consistently performed adequately in filtration of coal-based HPC.

Task 2.3 Heap pad analysis and pilot-scale design

Numerical modeling methodology

A two-dimensional modeling analysis was conducted to characterize the moisture movement within the proposed heap pad and assess the stability of the ore heap. The proposed heap leach pad was assumed to cover an area of 2 acres (8,094 m^2) and four lifts/layers of CCR. Each CCR lift was 10 ft (3 m) high. More details about the design information are provided in following sections. The numerical modeling and analysis were achieved using PLAXIS LE (PLAXIS LE, 2023). PLAXIS LE is a limit equilibrium software. It includes different modules that can be used

for solving geotechnical engineering problems, analyzing groundwater seepage, and evaluating the global stability of engineered structures. It enables users to analyze seepage movement under both saturated and unsaturated conditions. It also allows for choosing among classic methods for slope stability analysis, which slice slopes to analyze forces within (PLAXIS LE, 2023).

Groundwater analysis

To understand and evaluate the movement of water or AMD through the proposed heap pad, time-dependent (transient-state) two-dimensional seepage models were created using the finite element groundwater module in PLAXIS LE 2D. The analysis determined the distribution of pore pressures within the heap, which is crucial for assessing stability and identifying potential issues, such as piping. The groundwater software module was used for the analysis of the flow of water in unsaturated CCR. In PLAXIS, flow through saturated soil follows Darcy's Law, according to which water flow through soil is proportional to the hydraulic gradient. In the case of soil in an unsaturated state, hydraulic conductivity is related to soil saturation by a mathematical function (e.g., Fredlund and Xing model) (Fredlund et al., 2012).

Three model geometries were developed. Model 1 was developed to represent the column leaching test. The objective of Model 1 was to simulate laboratory conditions and calibrate the model. The model was created by defining the necessary material properties and specifying the desired boundary conditions. The profile geometry was established in AutoCAD Civil 3D (**Figure 2.3.1**) and then imported to Plaxis LE. The column had similar dimensions to those used in the lab [diameter of 4 in (10.16 cm) and a length of 3 ft (91.44 cm)].

The other two models were designed with distinct layers: a foundation layer (compacted coal refuse), a geomembrane layer, a layer of gravel, a non-woven geotextile layer (1100 N; AOS of 0.006 inches or 0.15 mm), and CCR layer/s through which leachate would be introduced and allowed to flow. The purpose of the nonwoven layer is to filter the liquid from the coal refuse so that it does not end up in the settling pond. The gravel layer allows for the leachate to flow through it after being filtered and guides the liquid towards the settling pond. The geomembrane layer is used to prevent the leachate from flowing through the gravel and entering the surrounding environment. Model 2 was developed to represent the first lift of the proposed heap pad. The lift had a height of 10 ft. (3 m) and a base length of 295 ft (90 m). The side slope angle was 2:1 horizontal to vertical (H:V), or 26.6 degrees. The base of the stack was designed with a 2% gradient slope, allowing for a near-flat pad while also supporting the outflow in a specific direction.

Model 3 was created to represent the proposed heap pad with four CCR lifts. The model consisted of the same five layers that were created in Model 2, with three more lifts of CCR added. For the first (bottom) layer, the maximum run was 295 ft (90 m). Above this, the second layer of coal refuse maximum run was 235 ft (72 m). The maximum run for the third and fourth layers was 175 ft (53 m) and 115 ft (35 m), respectively. The side slope angles of the layers were 26.6 degrees to comply with a 2H:1V ratio. From the top of these side slopes, the next layer did not begin until a run of 10 ft (3 m) had been completed. Each lift of CCR was 10 ft (3m) in height. The foundation and the gravel layers had thicknesses of 20 ft. (6 m) and 1.7 ft (0.5 m). The geomembrane and the non-woven geotextile layers were assumed to have a thickness of 1 ft (0.3 m) each. This assumption was adopted to maintain a gradual transition in layer thicknesses and avoid convergence/solution issues that can occur with smaller numbers (e.g., 0.09 inches [0.03 m]). The profile geometry of these models was established in AutoCAD Civil 3D (**Figure 2.3.1**). The models were created by defining the necessary material properties and specifying the desired boundary conditions.

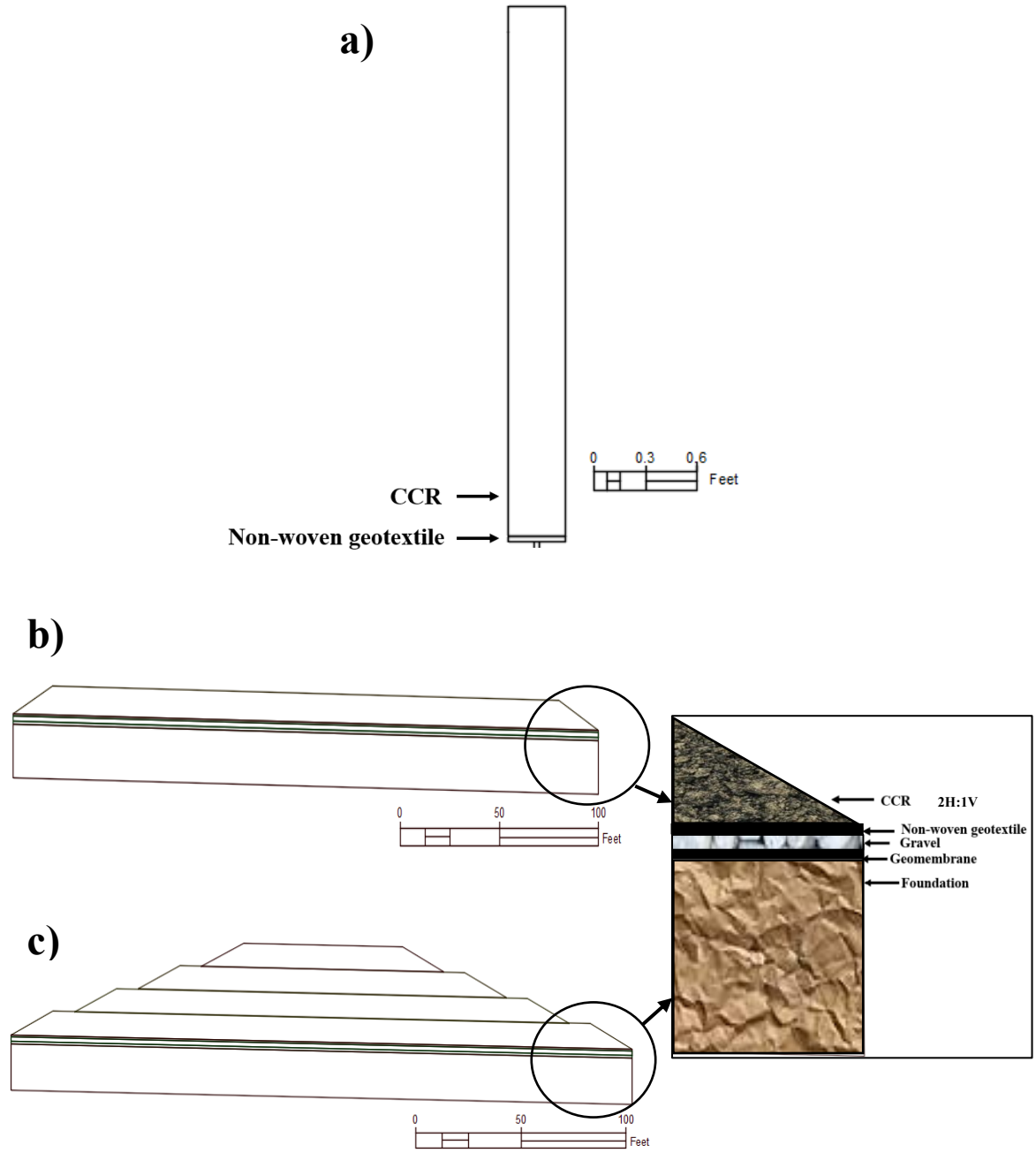


Figure 2.3.1: Column and Heap leach stack models a) Model 1, b) Model 2, and c) Model 3.

The permeability values of different layers were defined based on previous literature (Das, 2010; Koerner, 2012; Tolikonda and Quaranta, 2012; Smith, 2023; **Table 2.3.1**). Saturated volumetric water content was assumed to be 0.4 for the CCR, nonwoven geotextile, and the gravel layers. Whereas the geomembrane and shale layers were assigned saturated volumetric water content values of 0.2 and 0.1, respectively. These values fall within the ranges defined in the literature (Das, 2010; J. D. Quaranta and Tolikonda, 2011; Dompierre et al., 2023; TenCate., 2025). Each model was processed under unsaturated soil conditions. In unsaturated soil, flow is determined by a mathematical function relating hydraulic conductivity to soil saturation (e.g., Fredlund and Xing model). Models 1 and 2 were processed for four days. The CCR was modeled under

unsaturated conditions using the Fredlund and Xing, (1994) equation for the soil-water characteristic curve (SWCC) (Equation 8) (Huang et al., 1998; Li et al., 2009). The SWCC describes the relationship between the soil's matric suction and moisture content.

The equation uses volumetric water content (θ_w), saturated volumetric water content θ_s, soil matric suction corresponding to residual water content, and four fitting parameters (a_f, n_f, m_f, and hr) to develop the SWCC (Fredlund et al., 1994; Huang et al., 1998). The SWCC controls flow when the pore-air and pore-water pressures vary as the moisture content changes (Fredlund et al., 2012). The SWCC typically has a transition point known as the air-entry value (AEV). The flow within the system is controlled by the saturated hydraulic conductivity above the AEV. As a result, the system would have the highest permeability at saturation and a decrease in permeability once the AEV is exceeded.

Soil grain size data is typically used to estimate the fitting parameters in the Fredlund et al. (1994) equation. A D_{10} value of 0.11 mm (0.004 inches) was used in Equation 9. This value was adopted from Torres Hernandez, (2011) and Stevens (2016) for granular soils. This value represents the maximum recommended size. The computed fitting parameters were as follows: a_f=9.62, n_f=4.72, m_f=0.79. Using the developed SWCC (**Figure 2.3.2**), the permeability function was determined (**Figure 2.3.3**) according to Fredlund et al., (1994) (Equation 13) (Huang et al., 1998).

$$\theta_w = \theta_s \left(1 - \frac{\ln\left(1+\frac{\psi}{h_r}\right)}{\ln\left(1+\frac{10^6}{h_r}\right)}\right)\left(\frac{1}{\left(\ln\left[e+\left(\frac{\psi}{a_f}\right)^{n_f}\right]\right)^{m_f}}\right) \quad \text{(Equation 8)}$$

$$a_f = -967.21 * D_{10}^2 + 218.37 * D_{10} - 2.7 \quad \text{(Equation 9)}$$

$$n_f = 10^{\left(-0.0075a_f^3+0.1133a_f^2-0.3577a_f+0.3061\right)} \quad \text{(Equation 10)}$$

$$m_f = 0.0058a_f^3 - 0.0933a_f^2 + 0.4069a_f + 0.3481 \quad \text{(Equation 11)}$$

$$hr = 100 \quad \text{(Equation 12)}$$

where,

θ_w: Volumetric water content
ψ: Soil matric suction (soil suction value)
θ_s: Saturated volumetric water content
D_{10}: Soil diameter at which 10% of the soil weight is finer
a_f *:* Curve fitting parameter, which is a function of AEV of the soil, a_f =1.28 if D_{10}<0.020 mm
n_f : Curve fitting parameter, which is a function of the water extraction rate of the soil when the AEV is exceeded
m_f : Curve fitting parameter, which is a function of the residual moisture content of the soil
hr : Curve fitting parameter, which is a function of the soil suction at which residual moisture content occurs

$$k(\psi) = \frac{\int_{\ln(\psi)}^{b} \frac{\theta(e^y)-\theta(\psi)}{e^y}\theta'(e^y)dy}{\int_{\ln(\psi_{aev})}^{b} \frac{\theta(e^y)-\theta_s}{e^y}\theta'(e^y)dy} \quad \text{(Equation 13)}$$

where,

$k(\psi)$: Coefficient of permeability as a function of soil suction, ψ: Soil matric suction, b: ln (1,000,000), y: Dummy variable representing the logarithm of soil suction, ψ_{aev}: Air entry value, and $\theta(\psi)$: Volumetric water content as a function of matrix suction

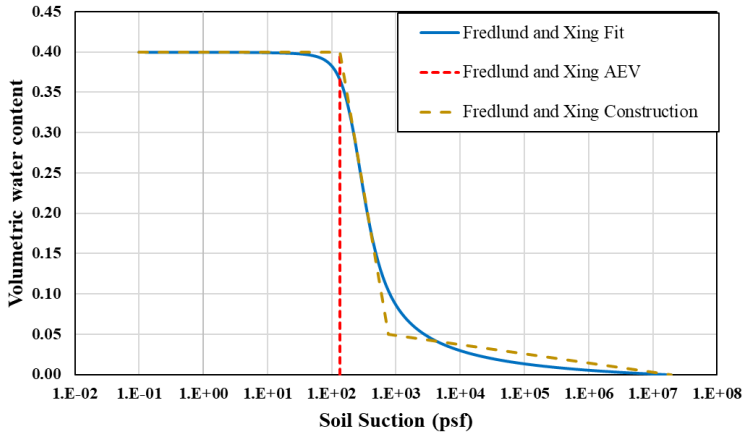


Figure 2.3.2: CCR soil-water characteristic curve (SWCC) determined according to Fredlund et al. (1994).

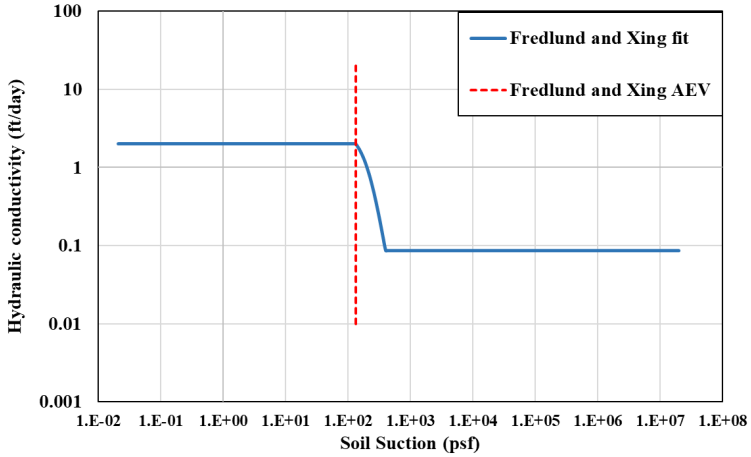


Figure 2.3.3: CCR permeability function determined according to Fredlund et al. (1994).

Table 2.3.1: Assigned material properties in numerical model.

Layers	Permeability, (k) (ft/day)	Permeability, (k) (cm/min)	References
CCR	2	0.04	(Quaranta and Tolikonda, 2011)
Non-woven Geotextile	2.268×10^{3}	48	(TenCate., 2025)
Gravel	5.669×10^{3}	120	(Das, 2010)
Geomembrane Liner	2.835×10^{-4}	6×10^{-6}	(Koerner, 2012; Dompierre et al., 2023)
Shale	2.830×10^{-5}	5.9×10^{-7}	(T. Smith, 2023)

Boundary conditions were assigned to each model based on flow conditions. Boundary conditions defined for the current model included flux, zero-flux, and review boundary. A flux boundary was defined where fluid flow is introduced. A zero-flux boundary was defined where no flow is permitted. A review boundary was defined at the point where the flow exited the system.

Fluid flow was introduced at a flux boundary (indicated by the red lines and circles in **Figures 2.3.4 through 2.3.6**). A zero-flux boundary was defined where no flow was permitted. A review boundary was defined where the flow exited the system, as indicated by the green lines and squares in **Figures 2.3.4 through 2.3.6**. The bottom right side of the gravel layer was assigned a review boundary, which represents the outlet. The geomembrane layer was assigned a review boundary in both models to test the ability of the material to prevent any solution from penetrating the foundation beneath.

A flux of 1 $ft^3/day/ft^2$ (0.3 $m^3/day/m^2$) was applied to the CCR in model 1 for 2 hours, which is equivalent to one leaching cycle in the lab. The initial head was specified at 0 ft (0 m). A flux of 10 $ft^3/day/ft^2$ (3 $m^3/day/m^2$) was applied to the CCR layers in models 2 and 3 for four days. The initial head was specified at -10 ft (-3 m). Model 3 was run under a second condition (Case 2) where the flux was applied for four days, followed by a one-day break, and another four days of application. This case was needed to study the percentage loss of the solution when the material is already saturated. The cases that were run are shown in **Table 2.3.2**.

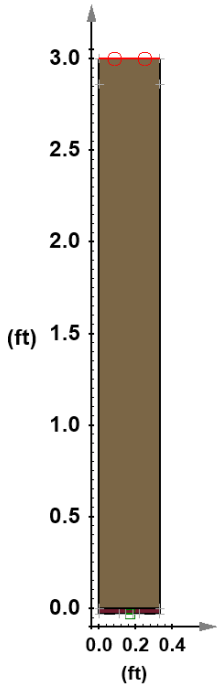


Figure 2.3.4: Column model and boundary conditions (Model 1); red lines with circles represent flux boundary; green square represents a review boundary.

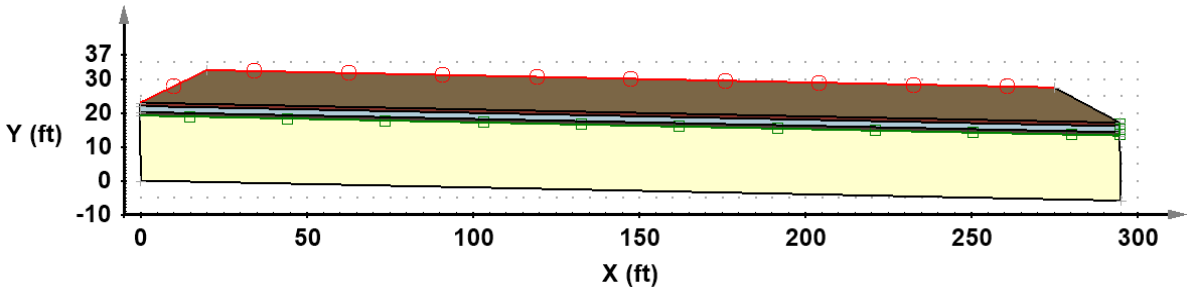


Figure 2.3.5: Heap leach stack model and boundary conditions (Model 2, one CCR lift); red lines with circles represent flux boundary; green lines with squares represent a review boundary.

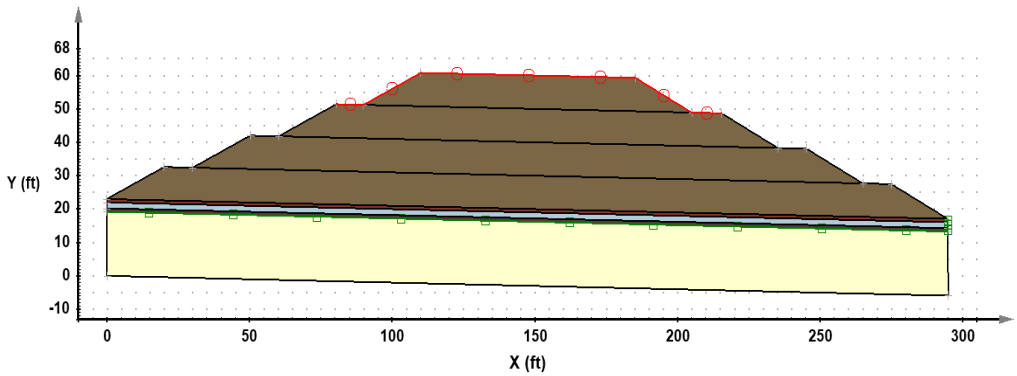


Figure 2.3.6: Heap leach stack model and boundary conditions (Model 3, four CCR lifts); red lines with circles represent flux boundary; green lines with squares represent a review boundary.

Table 2.3.2: Conceptual Seepage Models and cases created using Plaxis LE 2D.

Models	Cases	Model Assembly	CCR layers/lifts	Height per lift (ft)	Leaching period (day)
2	--	A foundation layer, a geomembrane layer, a gravel layer, a non-woven geotextile layer (1100N), and a CCR layer (s).	1	10	4
3	Case 1		4	10	4 days
	Case 2		4	10	9 (with a one-day break)

Slope stability analysis

The heap leach stack, consisting of four layers (Models 3 [Cases 1 and 2]), were tested for a factor of safety (FOS) against sliding to determine the feasibility of the proposed dimensions and number of lifts.

A 2-D model space was created in PLAXIS LE for the slope stability module. The slip direction was set as left to right to check for the global stability of the pile at the outlet direction. To construct this model, the start and end points of each polyline were joined to form a polygon. Later, the parameters and characteristics for the layers included in the design were assigned. The input parameters needed included the unit weight, cohesion, and the angle of internal friction (phi) (**Table 2.3.3**). The parameters were obtained from previous literature (**Table 2.3.4**). The cohesion

for all the created layers was assigned a value of 0 psf (0 kPa) as the worst-case scenario to be tested. For this project, the general limit equilibrium (GLE) methods were selected as the framework and calculation method for slope stability, which accounts for forces and moments in equilibrium. The slope search methods were selected and applied to the entire structure to locate the slip surface with the lowest FOS based on the defined input parameters and the condition of the structure (PLAXIS LE, 2023).

Table 2.3.3: Assigned material characteristics in Plaxis 2D LE models for slope stability analysis.

Layers	Unit Weight (lb/ft³)	Cohesion (psf)	Phi (deg)
CCR	93.4	0	32.8
Non-woven Geotextile	25.5	0	7
Gravel	145.0	0	45
Geomembrane Liner	50.0	0	3
Shale	131.3	0	34.2

Table 2.3.4: Material characteristics in published literature for coarse coal refuse, clay, shale, gravel, non-woven geotextile, and geomembrane liner.

References	Unit Weight (lb/ft³)	Notes	Cohesion (kPa)	Cohesion (psf)	Phi (deg)
CCR					
Quaranta and Tolikonda, 2011	93.96	Reduced Compaction	--	--	--
	119.87	Standard Compaction	--	--	--
Hegazy et al. 2004	125.4	Standard Compaction	13	271.5	34
Smith, 2023	120	Standard Compaction	0	0	31.5
Stevens, 2016	92.9	Reduced Compaction	--	--	--
	101.21	Standard Compaction	--	--	--
Clay					
Smith, 2023	123	--	8.62	180	30
Shale					
Smith, 2023	137	--	0	0	30
Stevens, 2016	125.7	--	2	41.8	38.3
Gravel					
Smith, 2023	145	--	0	0	45
Das, 2010	--	--	--	--	34-48
Non-woven geotextile					
TenCate. n.d.	8.7	--	3445	71,950.3	--
Koerner, 2012	25.5	--	--	--	--
Geomembrane liner					
TenCate. 2024	50	--	--	--	--
Koerner, 2012	--	--	--	--	3

Numerical modeling results

Groundwater analysis

In Model 1, approximately 950 mL was applied to the column, and around 450 mL of effluent exited the column (**Figure 2.3.7**). The percentage difference between the applied and collected amounts was approximately 50%. A lag time of approximately 20 minutes was observed (represented by the flat section of the outflow curve). Results for flow gradient, hydraulic conductivity, and degree of saturation for Model 1 are shown in **Figures 2.3.10 through 2.3.12**.

Approximately 10,791 ft^3 (306 m^3) of leachant was applied to the lift in Model 2, and approximately 9,913 ft^3 (280 m^3) of effluent exited the structure (**Figure 2.3.8**). The percentage difference between the applied and collected amounts was approximately 8%. A lag time of approximately 9.6 hours was observed (represented by the flat section of the outflow curve). As the leachant was applied to the lift, the pressure head gradually increased. As four days of flushing passed, the pressure head was approximately 11 to 44 ft (3 to 13 m) throughout the lift, with the top left part having a pressure head in the range of 44 to 78 ft (13 to 24 m) (**Figure 2.3.13** Day 4). A steady incremental increase in pore water pressure was also observed during the four days of leaching. At the end of day 1, the pore water pressure was in the range of 0 to 2,000 psf (0 to 96 kPa) at the top part of the heap and achieved a range of 2,000 to 3,000 psf (96 to 144 kPa) throughout the lift by day 4 of applying the leachant (**Figure 2.3.14** Day 4). On day 1 of leaching, the hydraulic conductivity (*k*) was in the range of 1.67 to 2.5 ft/day (0.5 to 0.7 m/day) at the top part of the heap and approximately 0 at the bottom, where the leachant had not yet reached. It then reached that range (1.67 to 2.5 ft/day or 0.5 to 0.7 m/day) throughout the entire lift by 4 days of application (**Figure 2.3.15,** Day 4). The degree of saturation was approximately zero throughout the first lift (**Figure 2.3.16**, initial condition) and gradually increased to a value of 1 as the leachant was applied (**Figure 2.3.16**, Day 4).

As three more lifts of CCR were added in Model 2-Case 1, the lag time was extended to 40 hours (**Figure 2.3.9**). Approximately 5,440 ft^3 (154 m^3) was applied to the heap in this case, and approximately 2,854 ft^3 (81 m^3) of effluent was discharged from the heap through the outlet. A percentage difference of approximately 48% was observed. It appeared that the leachant flowed along expected pathways without encountering any issues. The pressure head was in the range of 33 to 133 ft (10 to 40 m) in the top two lifts during the first day of applying the leachant (**Figure 2.3.17** Day 1) and ranged from 67 to 167 ft (20 to 50 m) in the same two lifts during days 2 to 4 of application (**Figure 2.3.17** Days 2, 3, and 4). Pore-water pressure increased from 0 psf (0 kPa) (**Figure 2.3.18** initial condition) to the range of 0 to 4,000 psf (0 to 192 kPa) (**Figure 2.3.18** Day 1) in the two top lifts of the heap. On days 2, 3, and 4 of application, the pore water pressure stayed in the range of 6,000 to 8,000 psf (287 to 383 kPa) in the two top lifts of the heap, and in the range of 2000 to 4,000 psf (96 to 192 kPa) in the two bottom lifts of the heap (**Figure 2.3.18** Days 2, 3, and 4).

Furthermore, the hydraulic conductivity and degree of saturation of the heap increased incrementally over the four-day period as the leachant was introduced to the heap. The hydraulic conductivity was in the range of 1.67 to 2.5 ft/day (0.5 to 0.7 m/day) throughout the heap (**Figure 2.3.19** Day 2 through 4). And stayed in the range of approximately 0 to 1.3 ft/day (0 to 0.4 m/day) in dry and/or partially saturated areas that the leachant did not research on the left and right sides of the heap (**Figure 2.3.19** Day 4). The hydraulic conductivity of the gravel layer was in the range of 4 to 5 ft/day (1.2 to 1.5 m/day) (**Figure 2.3.19** Days 2, 3, and 4).

The degree of saturation was approximately zero throughout the heap (**Figure 2.3.20**, initial condition) and gradually increased to a value of 1 as the leachant was applied (**Figure 2.3.20**, Day 4). Dry and/or partially saturated areas on the left and right sides of the heap showed a degree of saturation in the range of 0.0 to 0.3 (**Figure 2.3.20**, Day 4).

The geomembrane layer played a key role in preventing the penetration of any solution into the foundation in both models (**Figures 2.3.16 and 2.3.20**, Day 4).

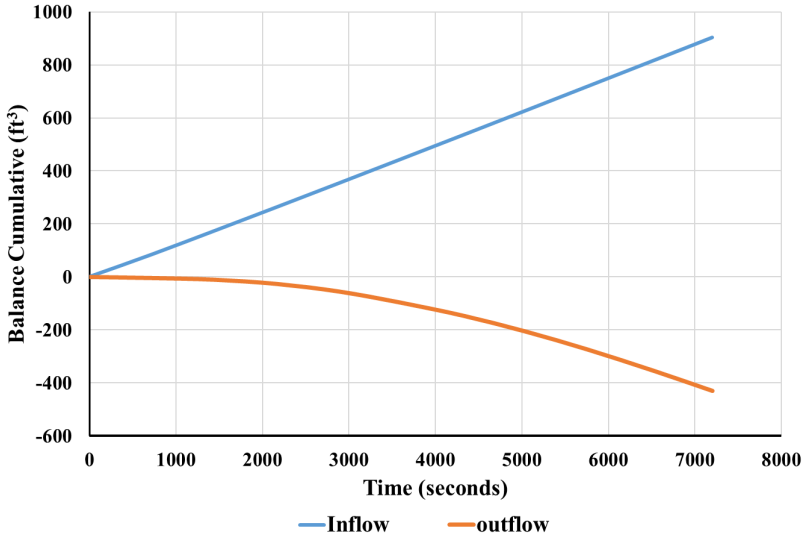


Figure 2.3.7: Amounts of leachant applied and collected for Model 1 (column).

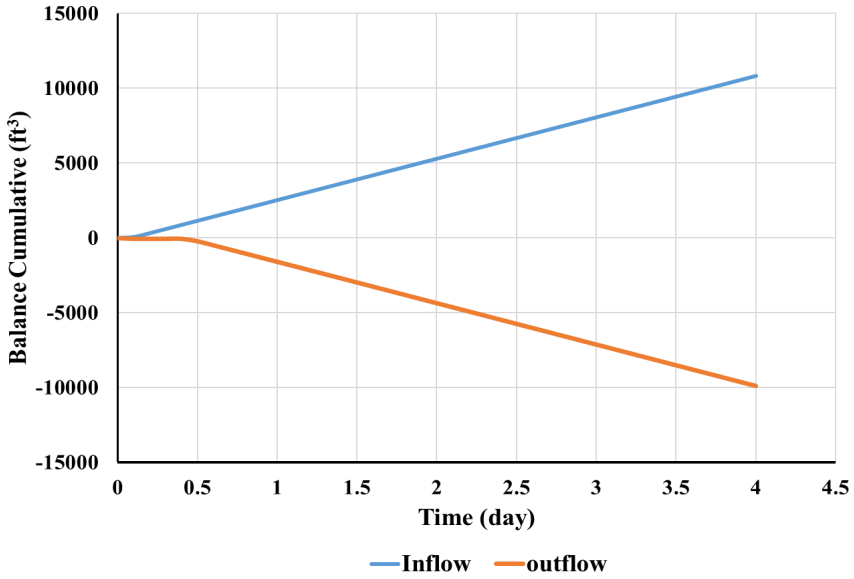


Figure 2.3.8: Amounts of leachant applied and collected for Model 2 (one lift of CCR).

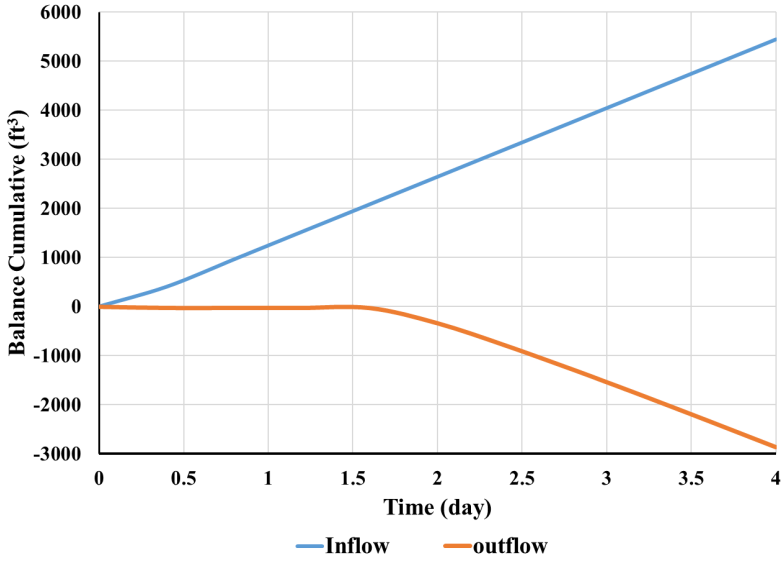


Figure 2.3.9: Amounts of leachant applied and collected for Model 3 (Case 1).

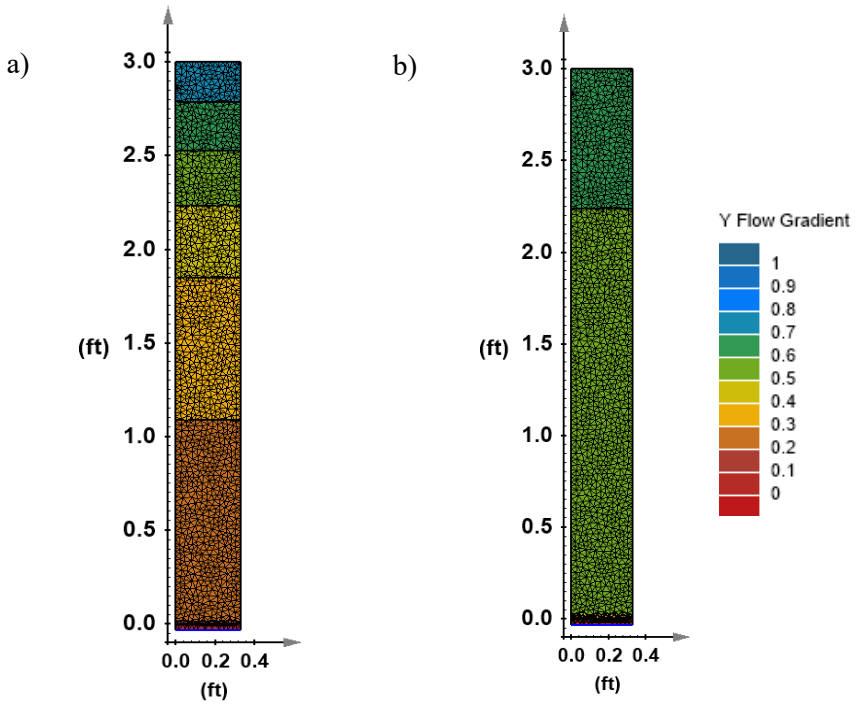


Figure 2.3.10: Flow gradient – Model 1 (column). a) after one hour of applying water and b) after 2 hours of applying water.

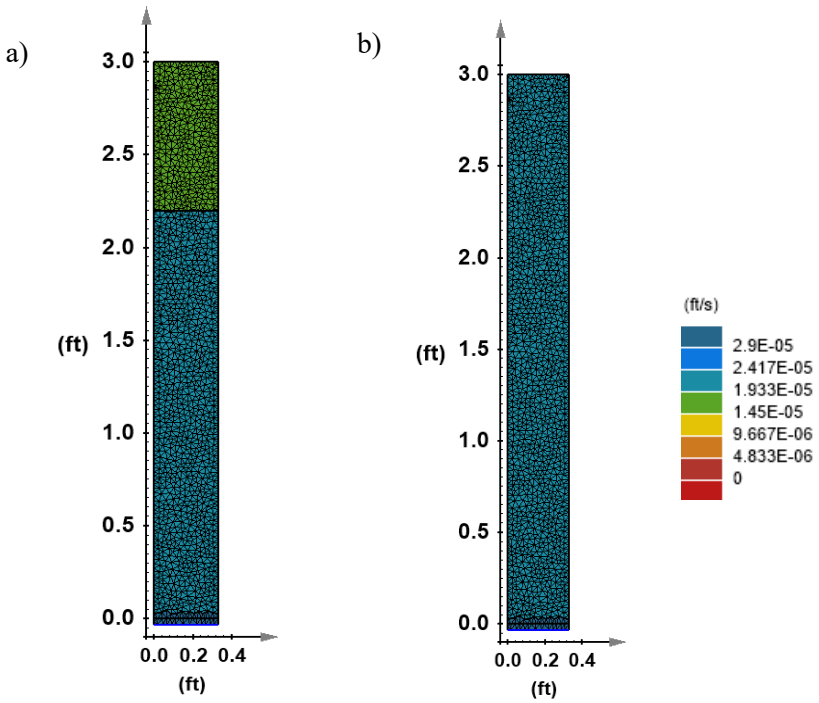


Figure 2.3.11: Hydraulic conductivity – Model 1 (column). a) after one hour of applying water and b) after 2 hours of applying water.

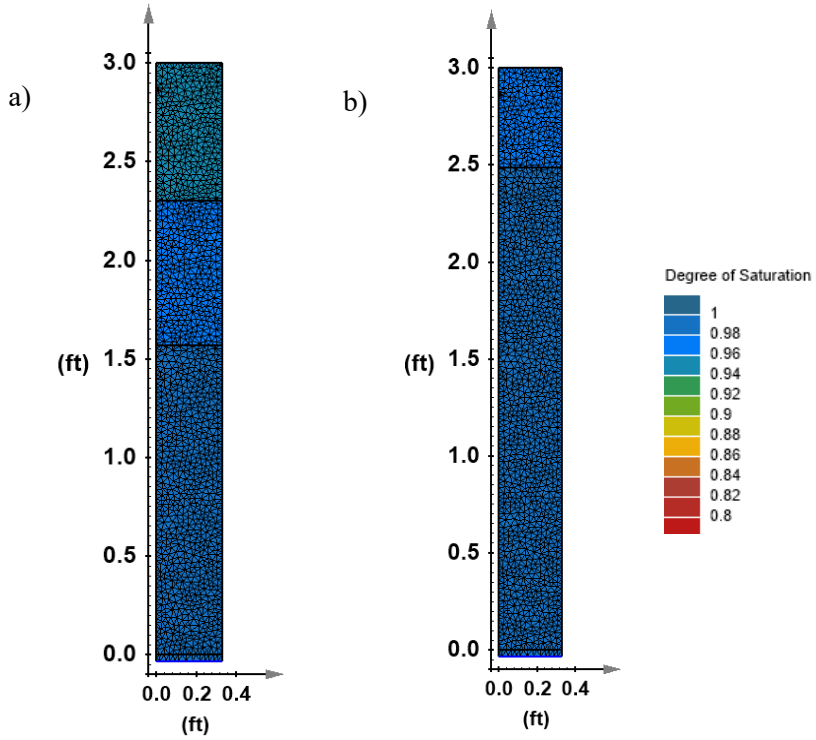


Figure 2.3.12: Degree of saturation – Model 1 (column). a) after one hour of applying water and b) after 2 hours of applying water.

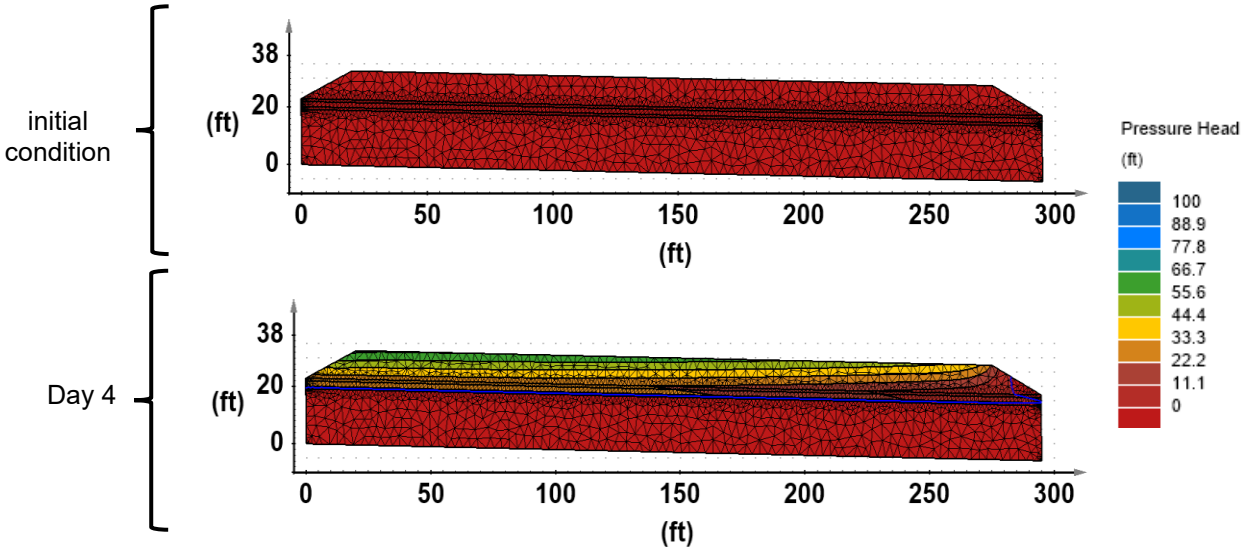


Figure 2.3.13: Pressure head – Model 2, one CCR lift.

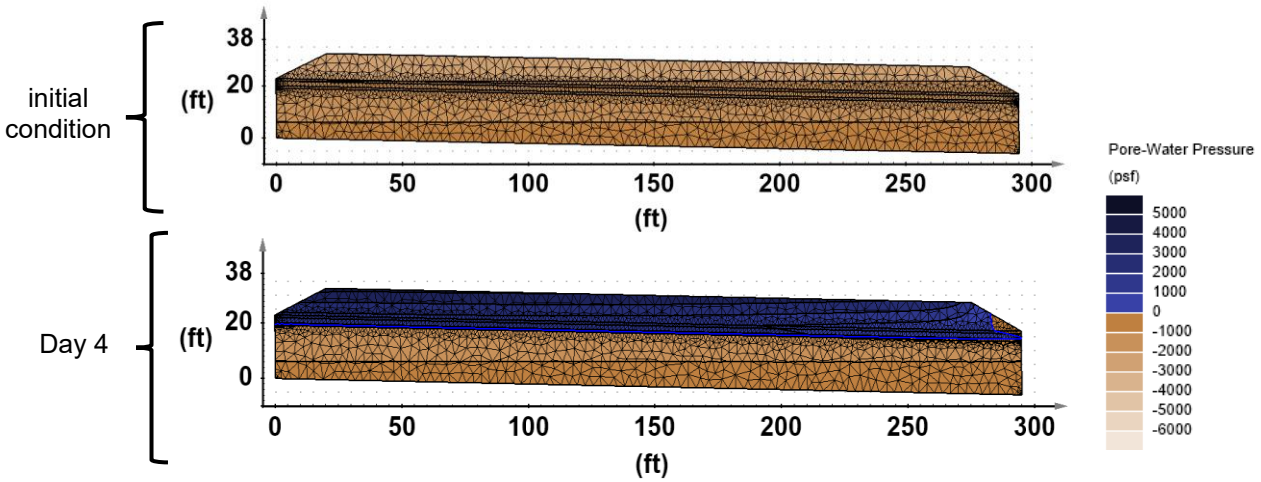


Figure 2.3.14: Pore-water pressure – Model 2, one CCR lift.

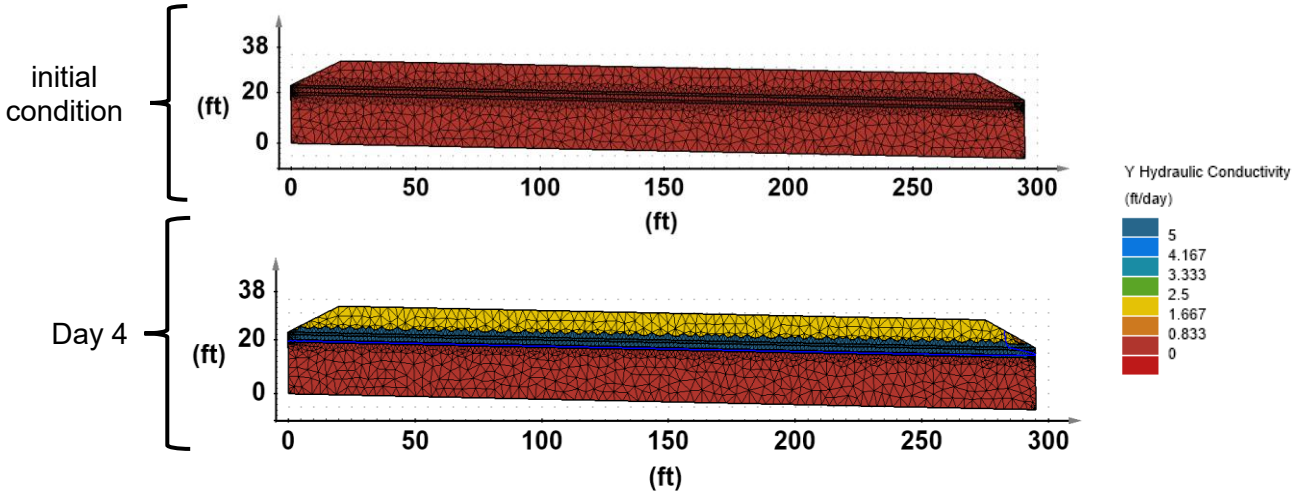


Figure 2.3.15: Hydraulic conductivity – Model 2, one CCR lift.

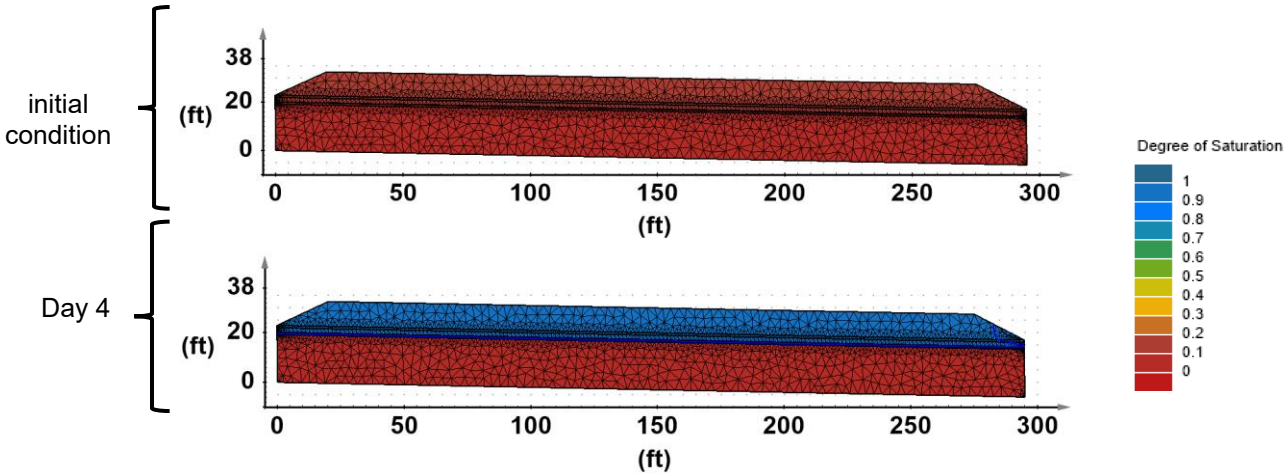


Figure 2.3.16: Degree of saturation – Model 2, one CCR lift.

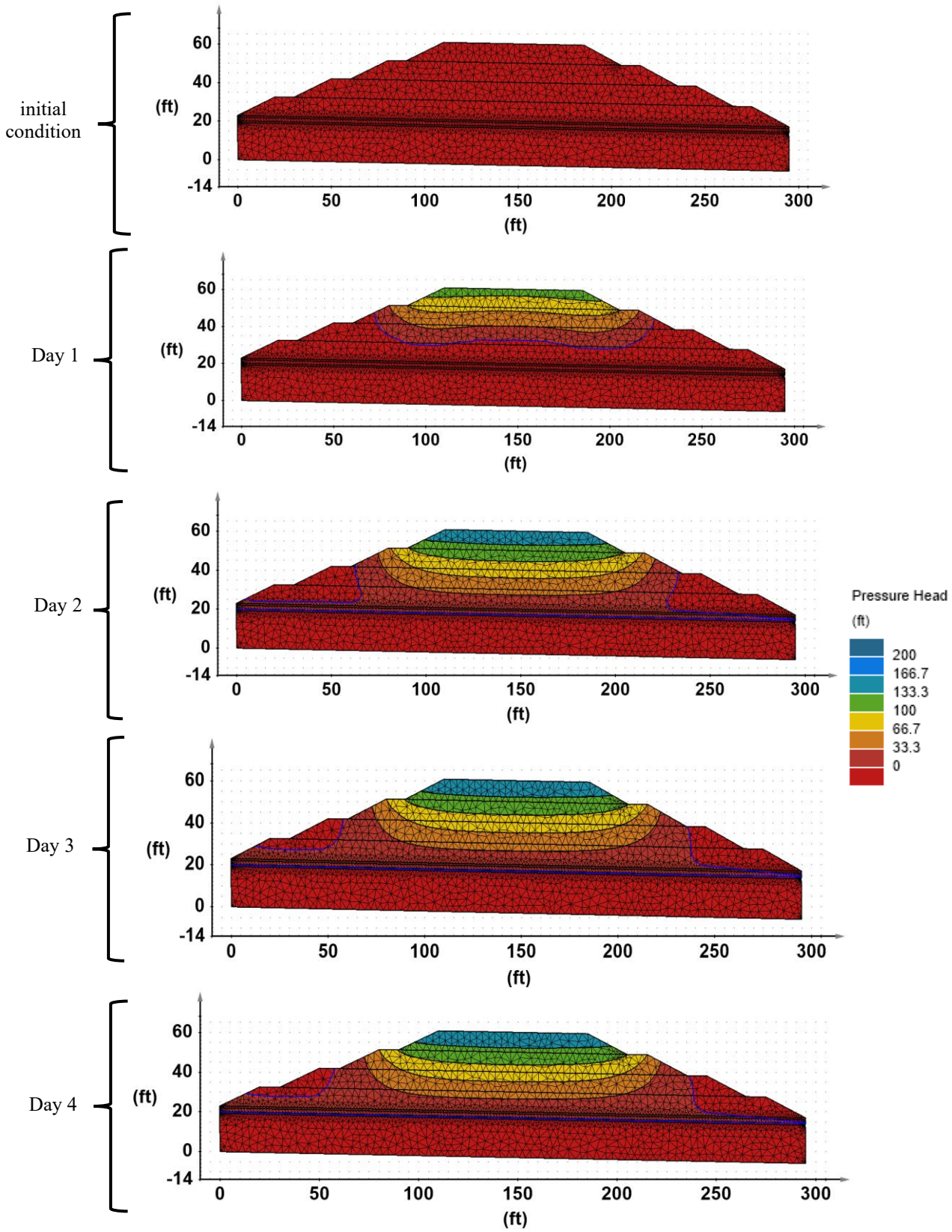


Figure 2.3.17: Pressure head – Model 3, four CCR lifts.

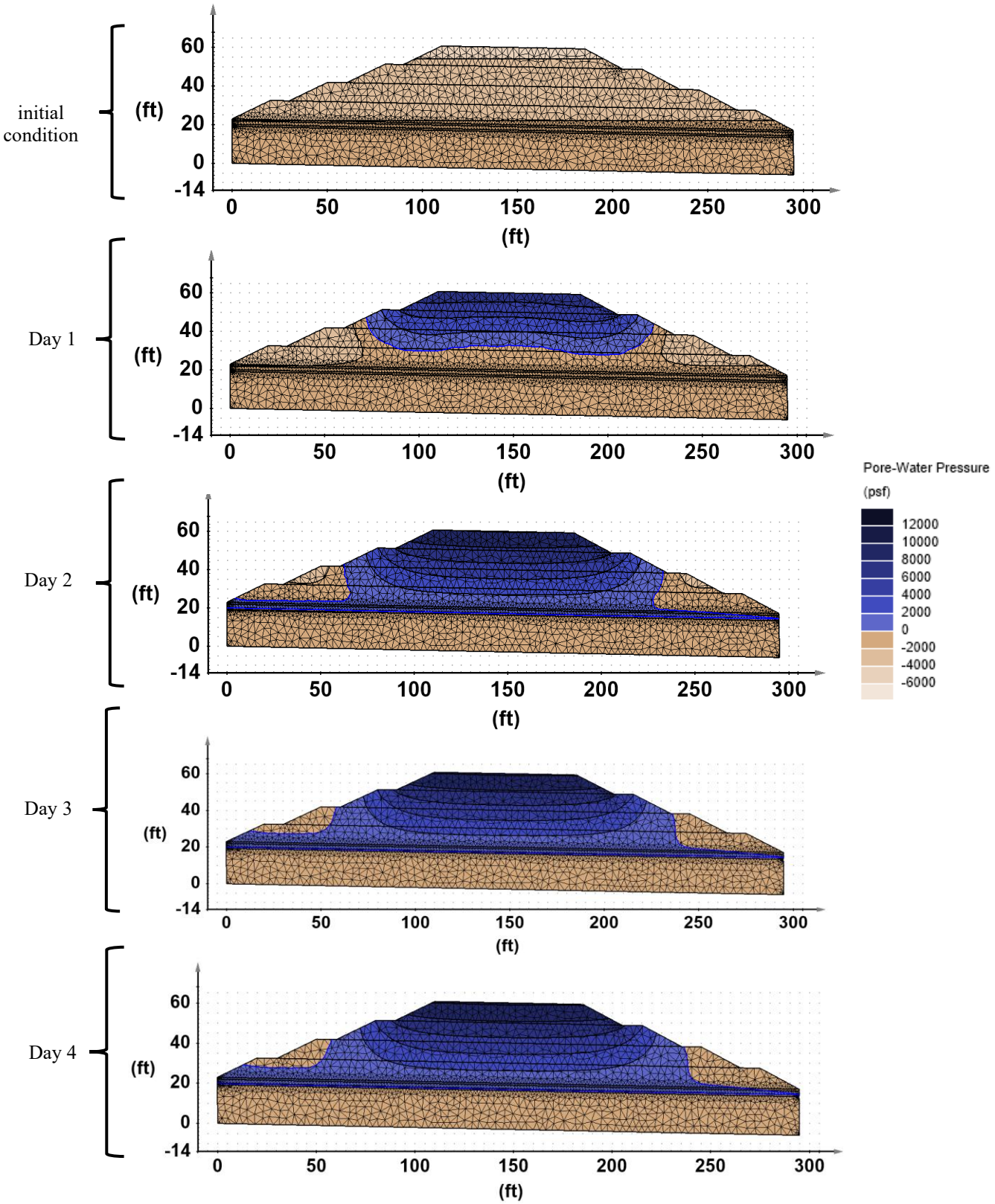


Figure 2.3.18: Pore-water pressure – Model 3, four CCR lifts.

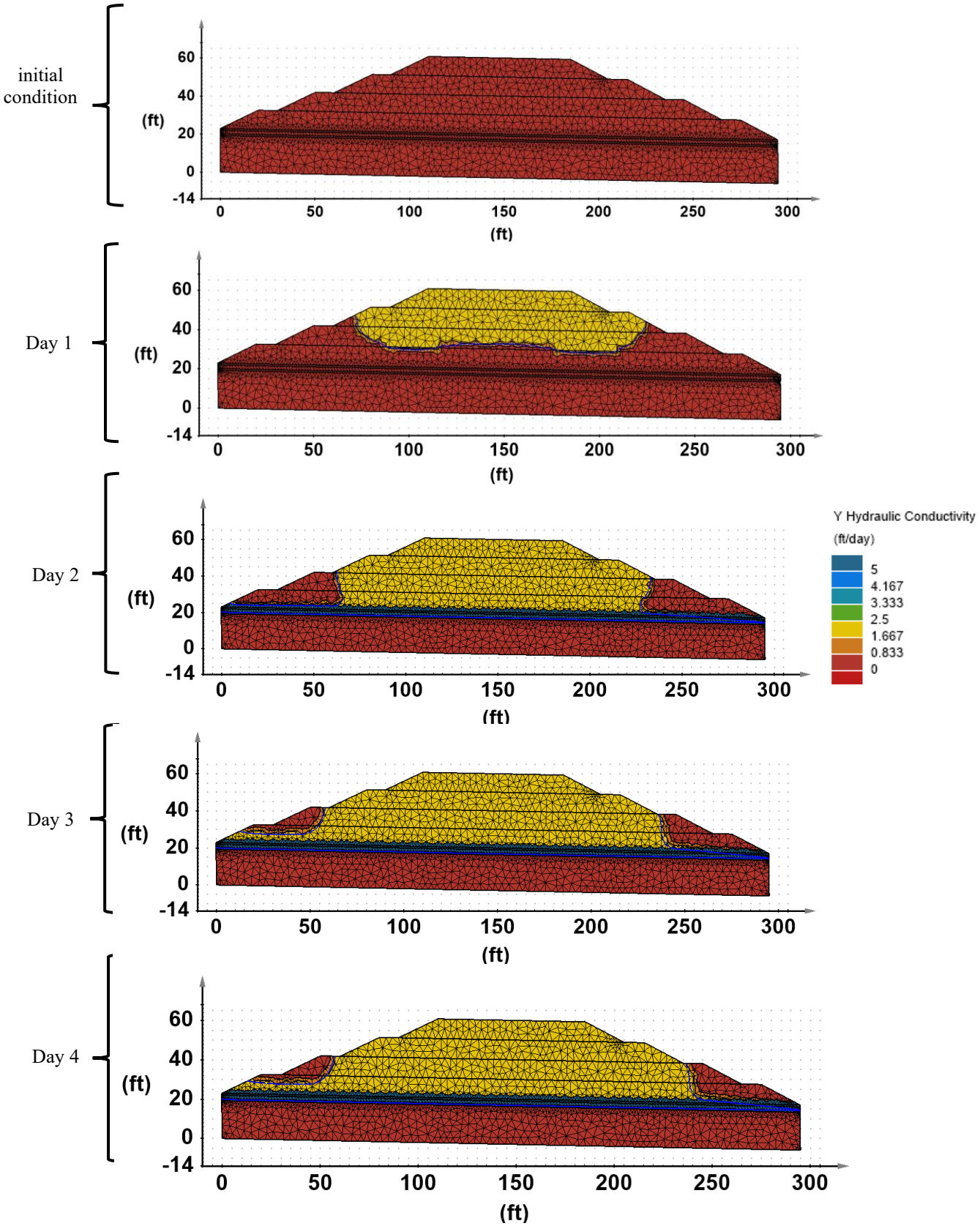


Figure 2.3.19: Hydraulic conductivity – Model 3, four CCR lifts.

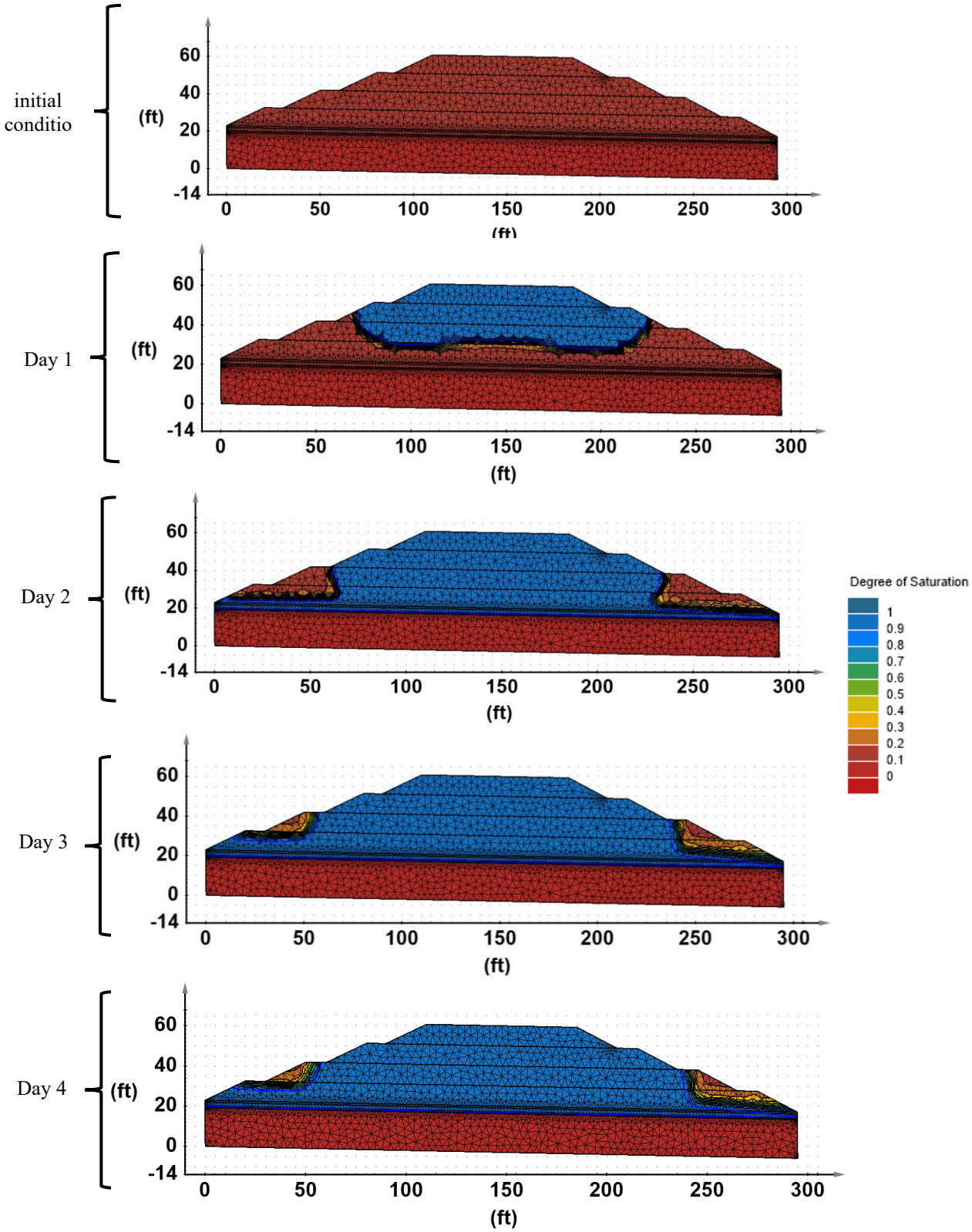


Figure 2.3.20: Degree of saturation – Model 3, four CCR lifts.

Figure 2.3.21 shows the cumulative applied and collected solution in Model 3 – Case 2, which was run under an extended leaching period of 9 days with a one-day break. Approximately 5,440 ft^3 (154 m^3) of leachant was applied to the heap during the first four days of leaching, with approximately 2,852 ft^3 (80 m^3) of effluent exiting the heap through the outlet. After the one-day break, approximately 5,627 ft^3 (159 m^3) of leachant was applied to the heap, with around 5,626 ft^3 (159 m^3) discharging from the heap (**Figure 2.3.21**). The determined percentage difference between the cumulative applied and collected solution after the first four days of leaching was 48%, whereas the percentage difference between the cumulative applied and collected solution after the second round of 4 days was about 0%. This indicates that the material remained partially saturated even after the one-day break, and once the material was saturated, the entire applied volume was collected as a discharge. This finding was consistent with observations made in the lab during the column leaching test. During multiple leaching cycles (2 leaching cycles per week), the collected discharge volume was equivalent to the leachant volume. This was also evident by the degree of saturation results (**Figure 2.3.25**/ Day 5), where the material maintained some saturation during that one-day break.

When the leachant was introduced to the heap, pressure head, pore-water pressure, and degree of saturation showed some incremental increase that progressed over the 4-day time period (**Figures 2.3.22, 2.3.24, and 2.3.28** Days 1 to 4). As a result of the cessation of inflow on day 5, a reduction in the pressure head (approximately zero) was observed (**Figure 2.3.23**/ Day 5). In addition to the reduction in the pressure head, pore-water pressure was dissipated (**Figure 2.3.25**/ Day 5). As water percolated through the material, hydraulic conductivity was in the range of 1.67 and 2.5 ft/day (0.5 to 0.7 m/day) (**Figure 2.3.26** Days 1 - 4). A reduction in hydraulic conductivity to between 0.00 and 1.67 ft/day (0.00 to 0.5 m/day) was observed across the top of the heap as leachant inflow ceased on day 5 (**Figure 2.3.27**/ Day 5). The degree of saturation was in the range of 0.4 to 0.7 within the top part of the heap when the inflow ceased on day 5 (**Figure 2.3.29** Day 5) and went back to reach a value of approximately 1 when the leachant continued to be applied on days 6, 7, 8, and 9 (**Figure 2.3.29**).

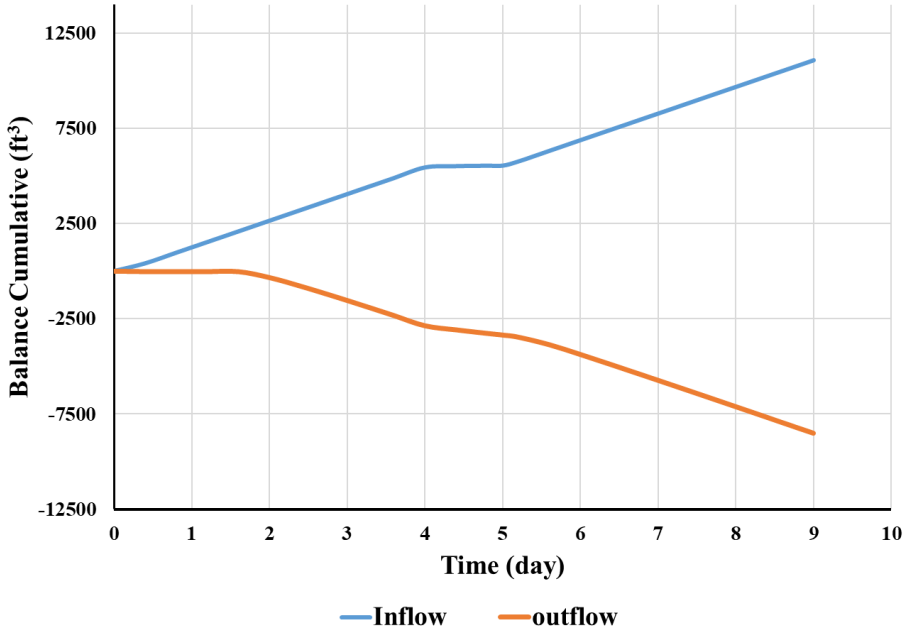


Figure 2.3.21: Inflow and outflow for Model 3 Case 2.

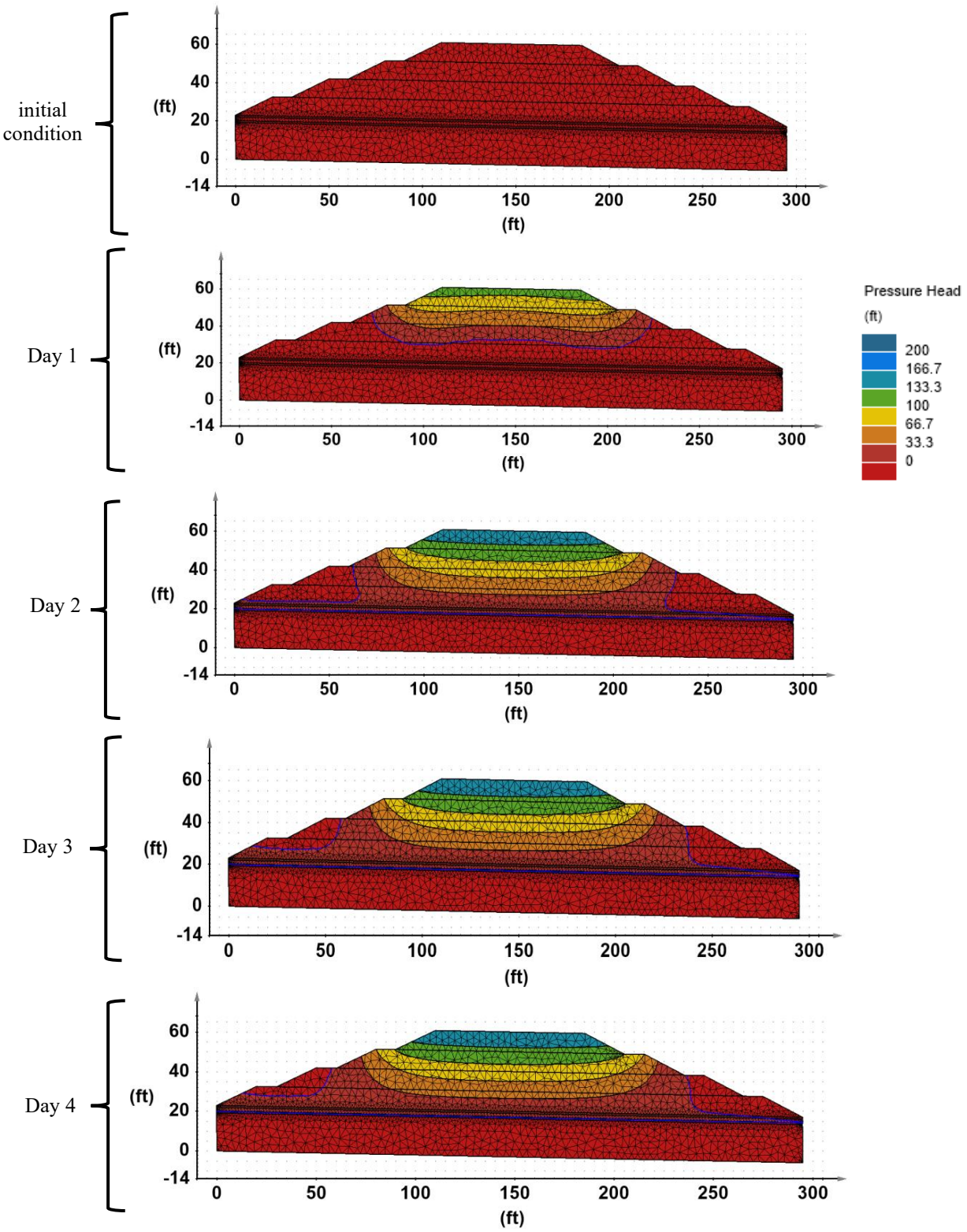


Figure 2.3.22: Pressure head - Day 1 to 4 – Model 3 Case 2 (8 days of leaching).

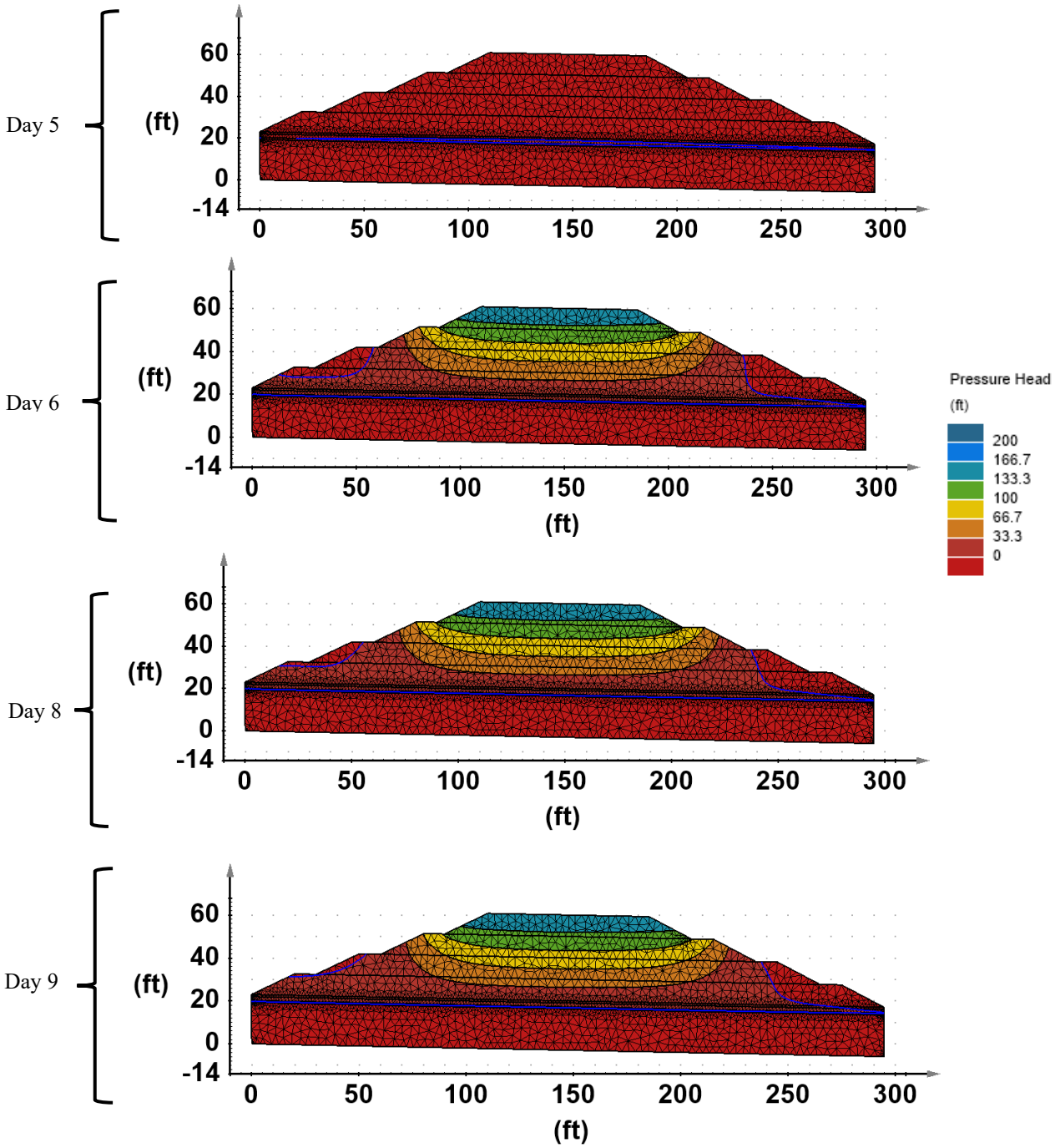


Figure 2.3.23: Pressure head - Day 5 to 9 – Model 3 Case 2 (8 days of leaching).

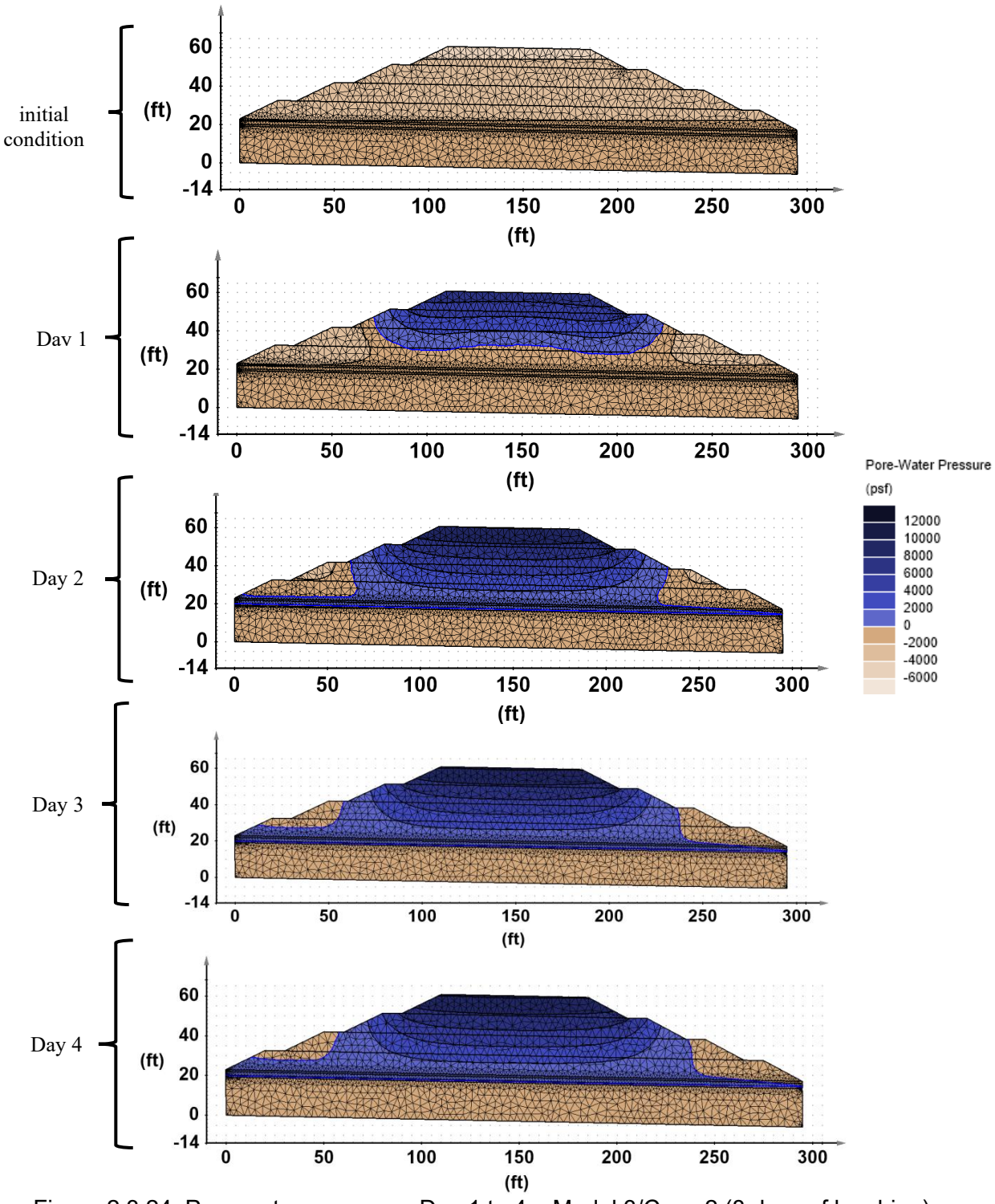


Figure 2.3.24: Pore-water pressure - Day 1 to 4 – Model 3/Case 2 (8 days of leaching).

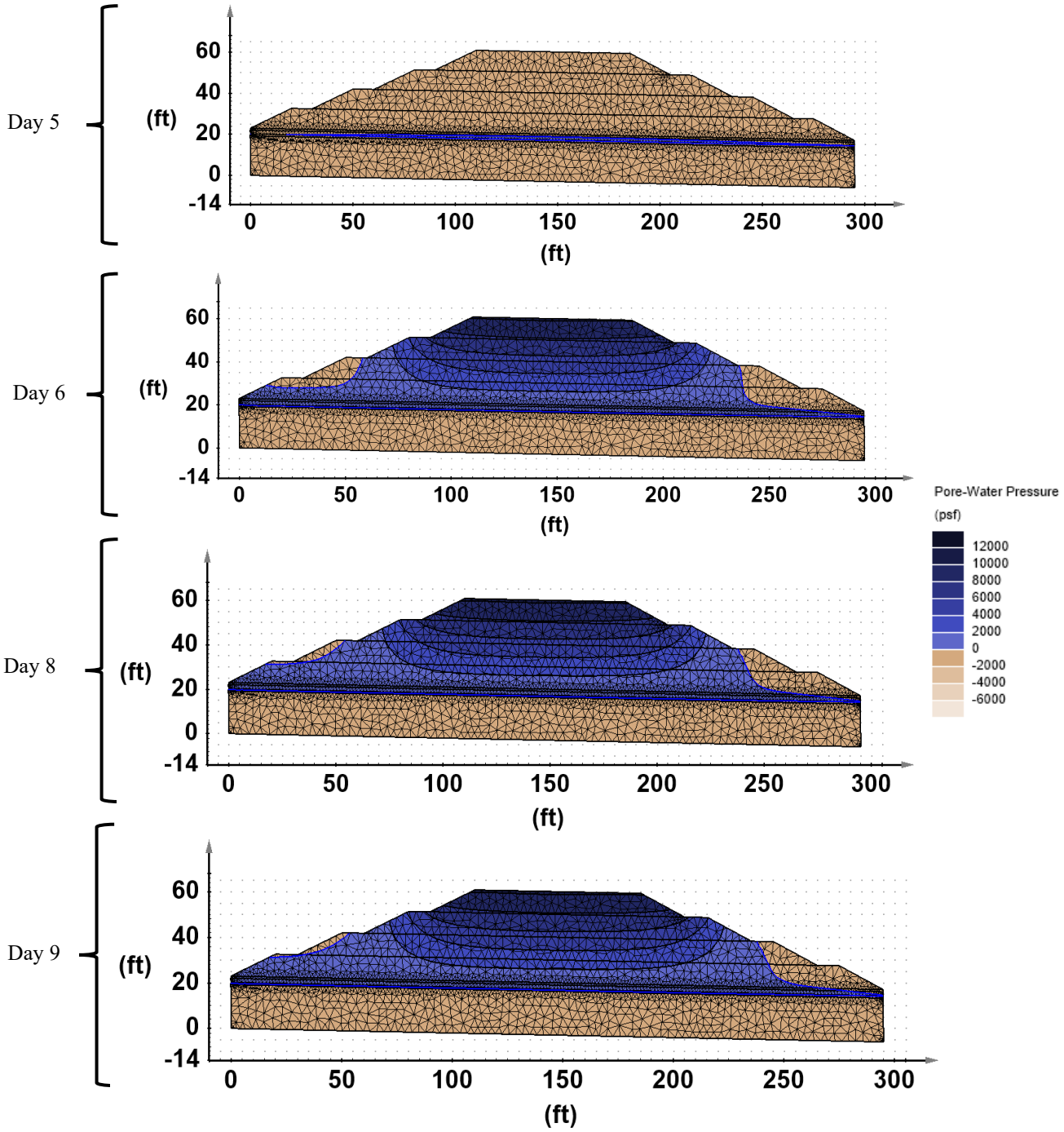


Figure 2.3.25: Pore-water pressure - Day 5 to 9 – Model 3 Case 2 (8 days of leaching).

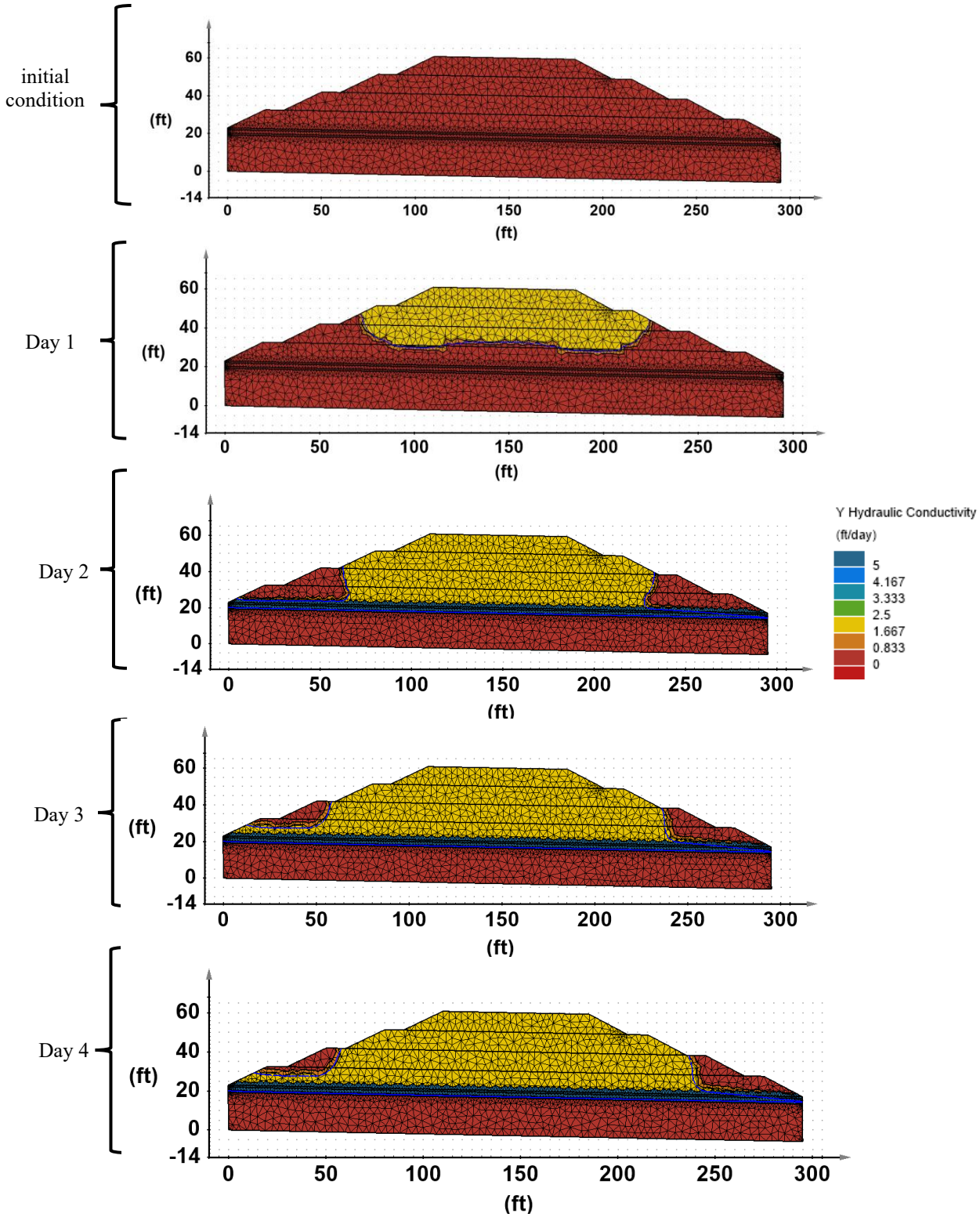


Figure 2.3.26: Hydraulic conductivity - Day 1 to 4 – Model 3 Case 2 (8 days of leaching).

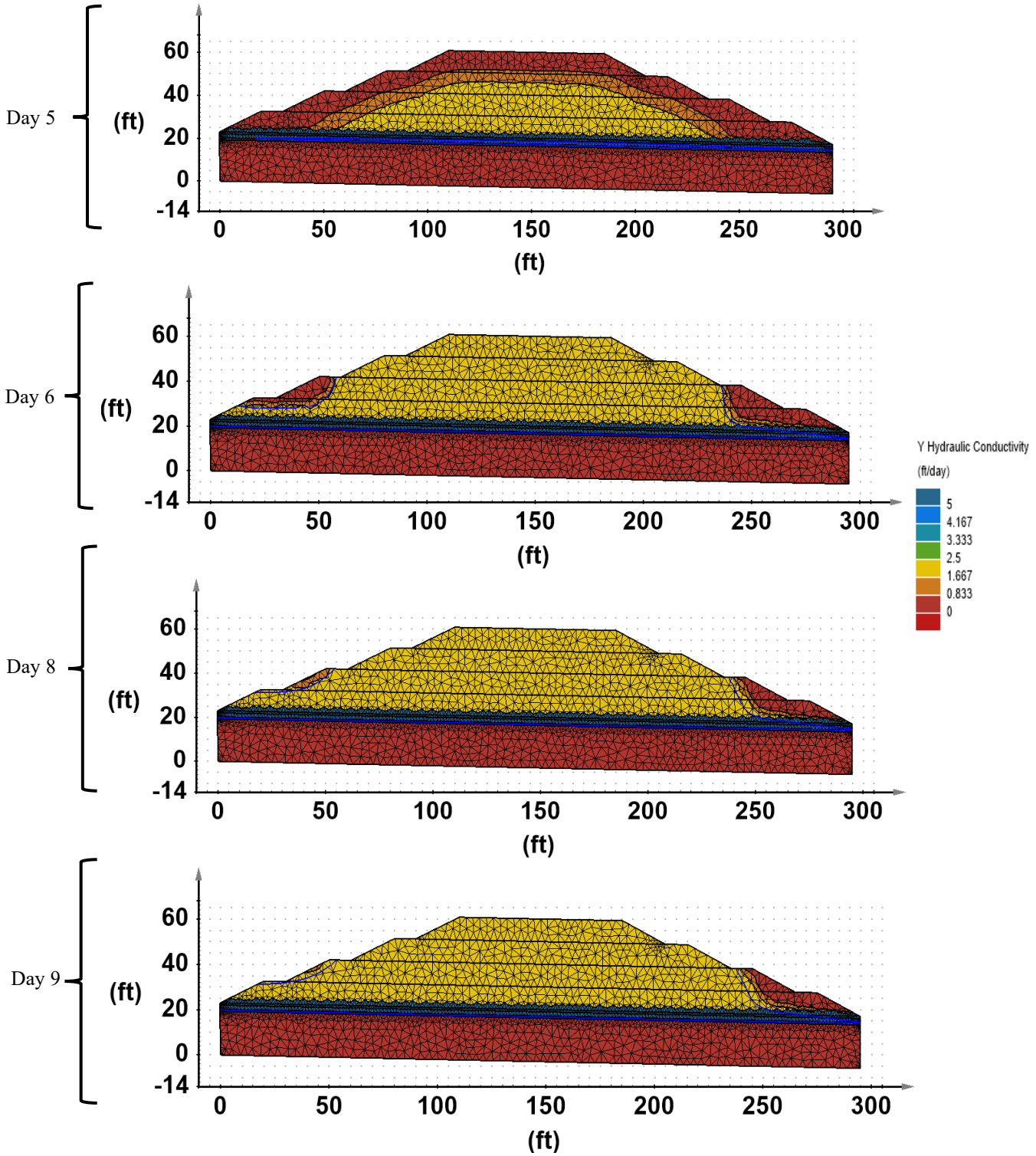


Figure 2.3.27: Hydraulic conductivity - Day 5 to 9 – Model 3 Case 2 (8 days of leaching).

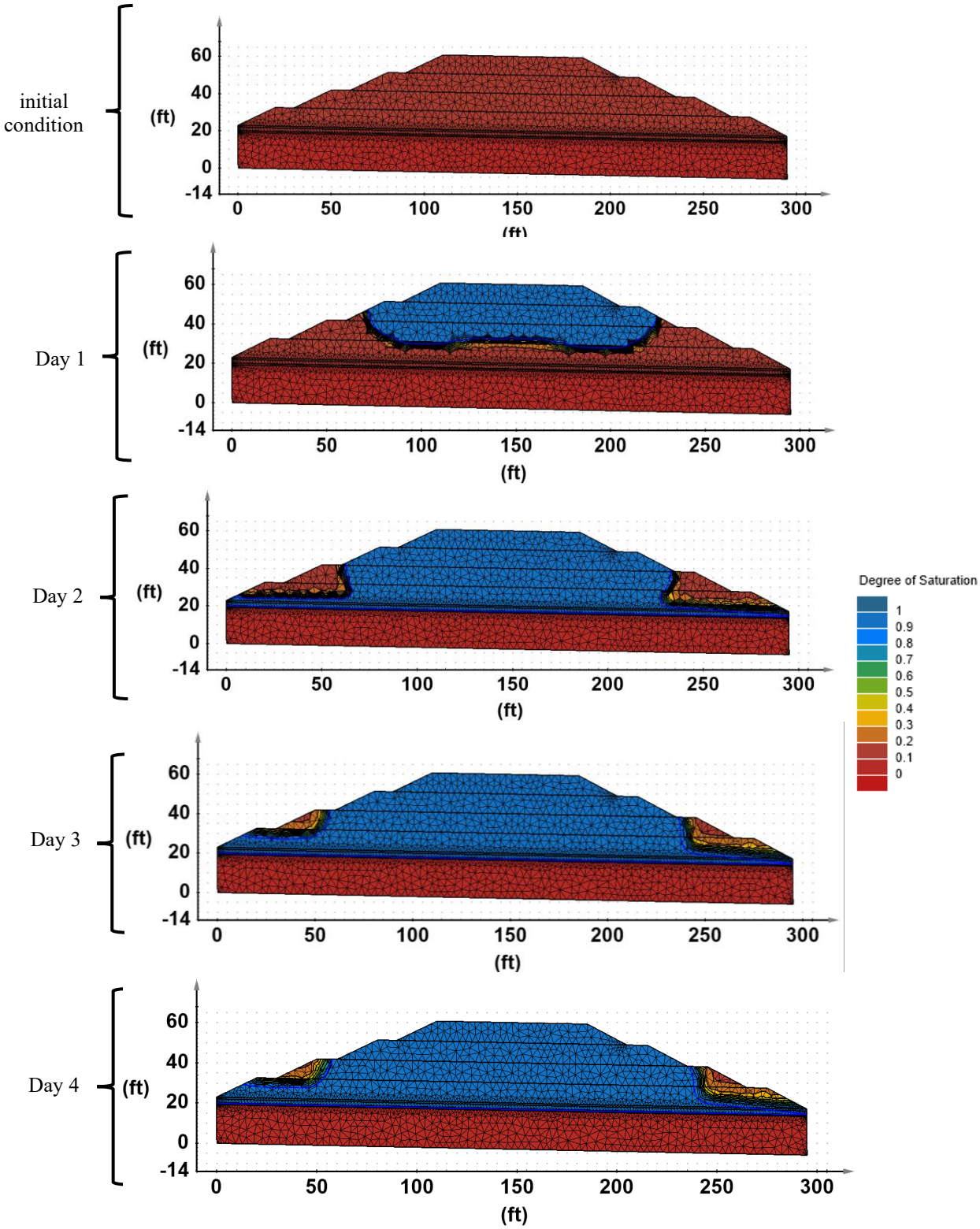


Figure 2.3.28: Degree of saturation - Day 1 to 4 – Model 3 Case 2 (8 days of leaching).

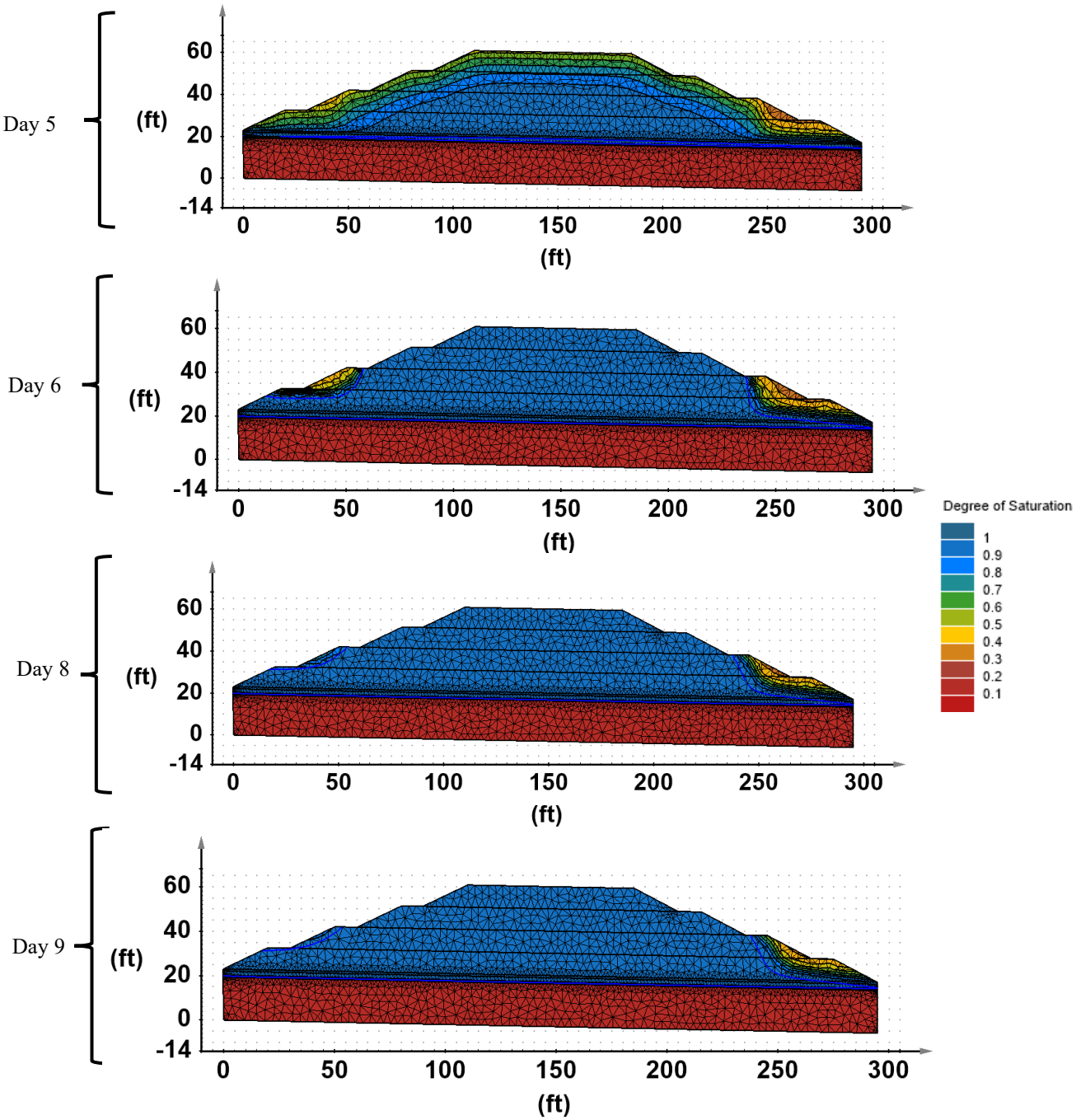


Figure 2.3.29: Degree of saturation - Day 5 to 9 – Model 3 Case 2 (8 days of leaching).

Slope stability analysis

Slopes FOS is determined as the ratio between the forces that resist movement and those that encourage movement. For structures, the ideal minimum FOS against sliding is established as 1.5, and it is considered a standard benchmark (B. Das, 2010; Inabah and Sukamta, 2025). With this comparison, the results of the slope stability analysis indicate that the structure would not maintain this requirement under its current condition. A potential sliding surface through the CCR layer was observed in both cases of Model 3. The calculated FOS of the critical slip surface was

0.902 for Case 1 (**Figures 2.3.30** and **Table 2.3.5**) and 0.877 for Case 2 (**Table 2.3.5**). This failure slope was identified along dry zones on the side of the heap. As the leachant was applied to the top lift only, two areas on the sides of the slope remained dry as the leachant did not reach them. As the leachant percolated through the heap, saturated areas became heavier as the pore space filled with the liquid. Dry areas adjacent to the wet areas would then work against the stability of the slope as they would be lighter in weight and the particles would hold together by the friction between the grains alone.

Different scenarios were performed to address the issue of the failure plane and to enhance the global FOS of the model. The first scenario was extending external irrigation. In the first scenario, solution irrigation was extended to the external surface of all the layers to avoid partially saturated and dry areas (**Figure 2.3.31**). The results of this scenario indicated that this approach could increase the strength of the slope against sliding as the design maintained a minimum FOS of 1.62 (**Figure 2.3.32**). However, the critical surface in this case was deeper and heavier (**Table 2.3.6**).

In the second scenario, external and internal irrigations were combined. Incorporating internal irrigation in addition to external irrigation (**Figure 2.3.33**) seemed to further improve the FOS against sliding. The design maintained a minimum FOS of 2.04 when the second scenario was applied; however, the critical slope surface (FOS=2.04) was deeper, heavier, and extended to the deep foundation underneath the pile as the material became heavier (**Figure 2.3.34** and **Table 2.3.6**).

Slope reinforcement and improving the FOS could also be achieved by adding a toe berm, which is another common approach that has been investigated and reported in the literature (Agarwal et al., 2018; Kay and Panayides, 2023; Basta et al., 2024). Thus, the third scenario that was performed was the addition of a toe berm at the very bottom of the pile to provide stability (**Figure 2.3.35**). Previously tested scenarios were rerun with the added toe berm (**Table 2.3.8**). The results showed that adding the toe berm did work in favor of the stability of the pile as it added weight and resistance to the base of the slope. This was evident by the increased global FOS in the rainfall event model (**Tables 2.3.7** and **2.3.8**). The model was processed with two 100-year storm events that were performed back-to-back, with a break. An application rate of 0.5 $ft^3/day/ft^2$ (0.05 $m^3/day/m^2$) was applied in this case based on information from the National Oceanic and Atmospheric Administration (NOAA, 2025).

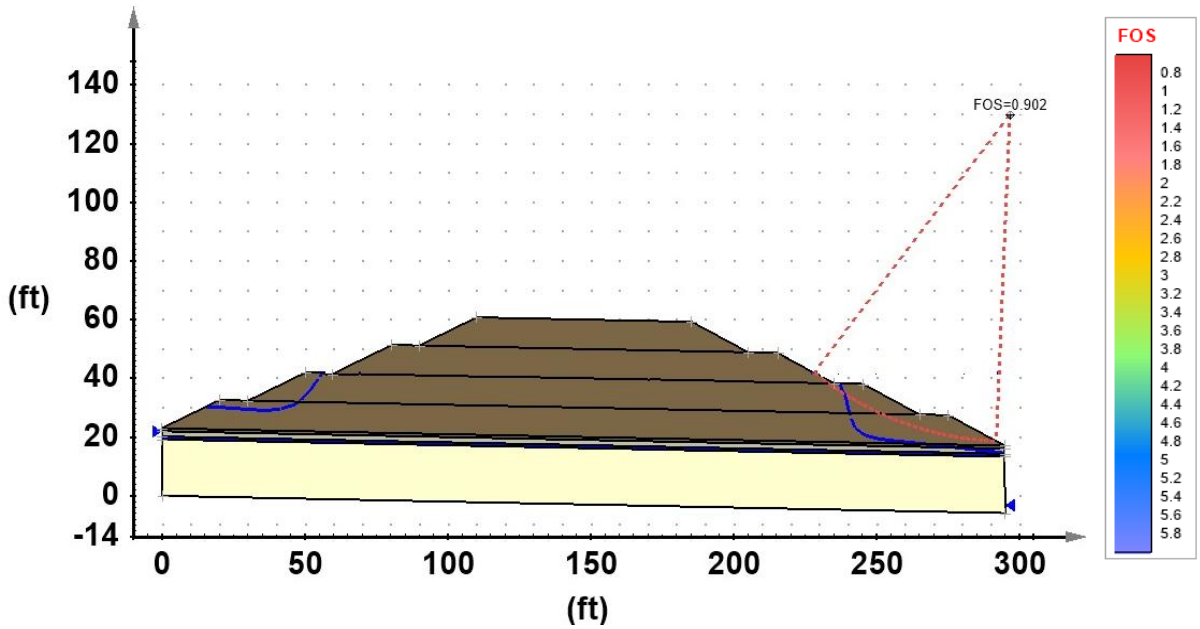


Figure 2.3.30: Critical slip surfaces for the slope after 4 days of irrigation (Model 3 Case 1).

Table 2.3.5: Sliding mass characteristics for slope stability models.

GLE Analysis	Model 3 (Case 1)	Model 3 (Case 2)
FOS	0.902	0.877
Total weight (lb)	3.13×10^4	3.16×10^4
Total volume (ft^3)	3×10^2	3×10^2
Total Activating moment (lb-ft)	1.94×10^6	2×10^6
Total Resisting Moment (lb-ft)	1.75×10^6	1.76×10^6
Total Activating Force (lb)	1.69×10^4	1.75×10^4
Total Resistive Force (lb)	1.53×10^4	1.54×10^4

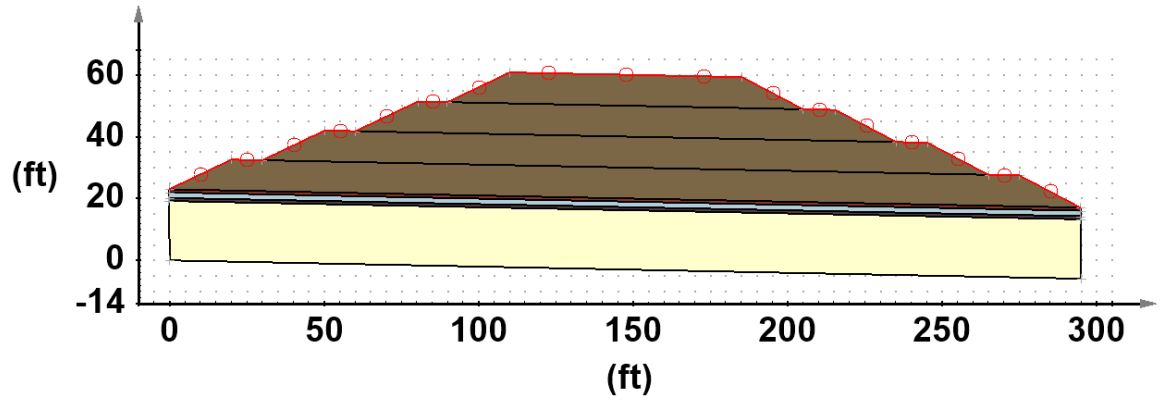


Figure 2.3.31: Extended external irrigation scenario; red line indicates irrigation (flux).

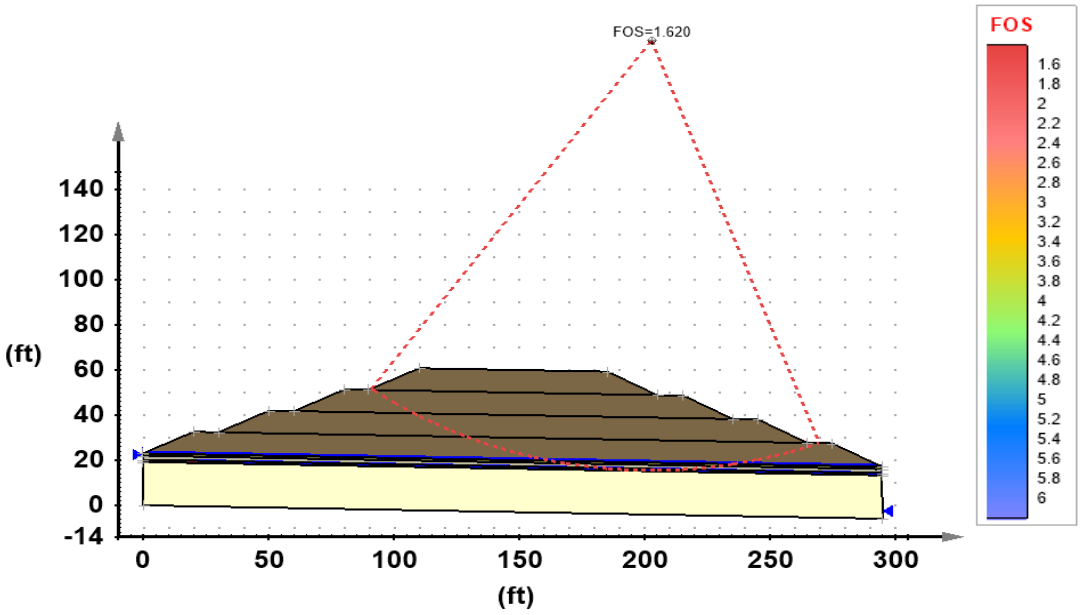


Figure 2.3.32: Critical slip surfaces for the slope after applying the extended external irrigation scenario.

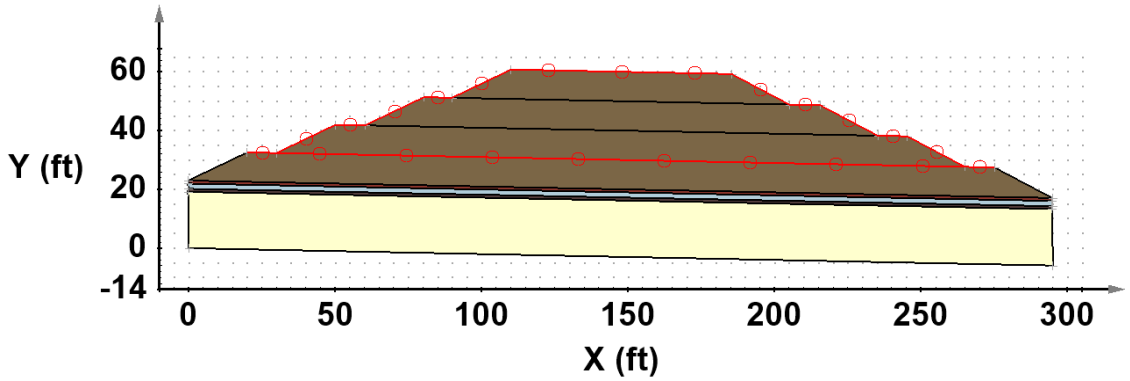


Figure 2.3.33: External and internal irrigations scenario; red line indicates irrigation (flux).

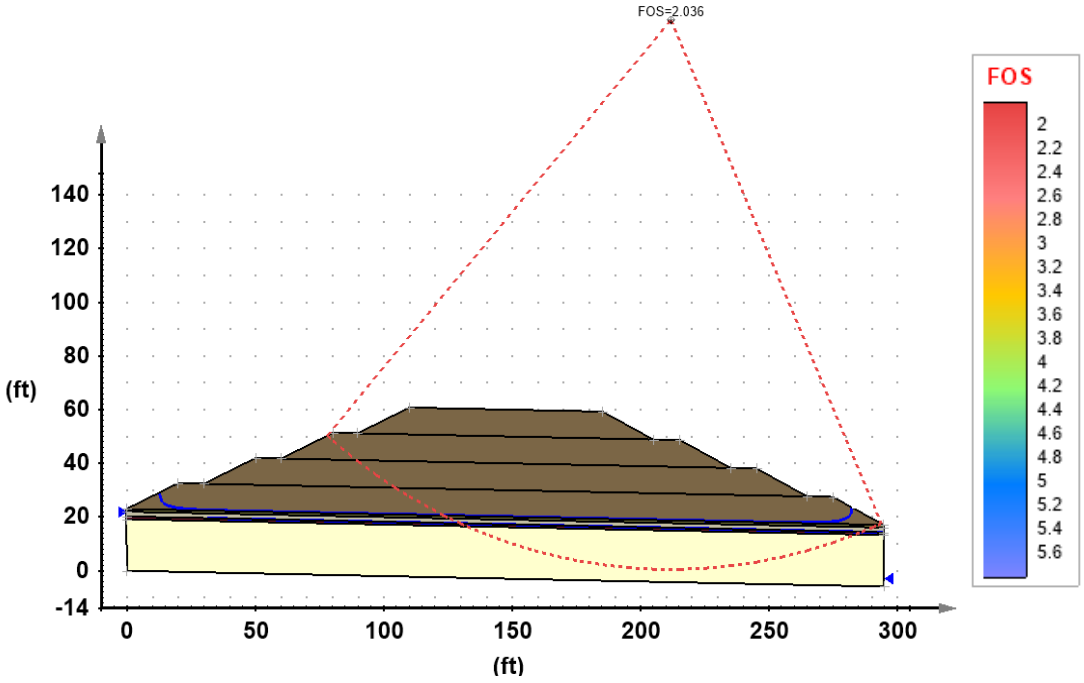


Figure 2.3.34: Critical slip surface for the slope after applying the external and internal irrigations scenario (FOS = 2.036).

Table 2.3.6: Sliding mass characteristics for irrigation scenarios.

GLE Analysis	Extended external irrigation	External and internal irrigation
FOS	1.620	2.036
Total weight (lb)	1.94×10^{6}	3.54×10^{6}
Total volume (ft^3)	4.8×10^{3}	7.74×10^{3}
Total Activating moment (lb-ft)	1.14×10^{8}	2.72×10^{8}
Total Resisting Moment (lb-ft)	1.84×10^{8}	5.53×10^{8}
Total Activating Force (lb)	5.89×10^{5}	1.31×10^{6}
Total Resistive Force (lb)	9.54×10^{5}	2.67×10^{6}

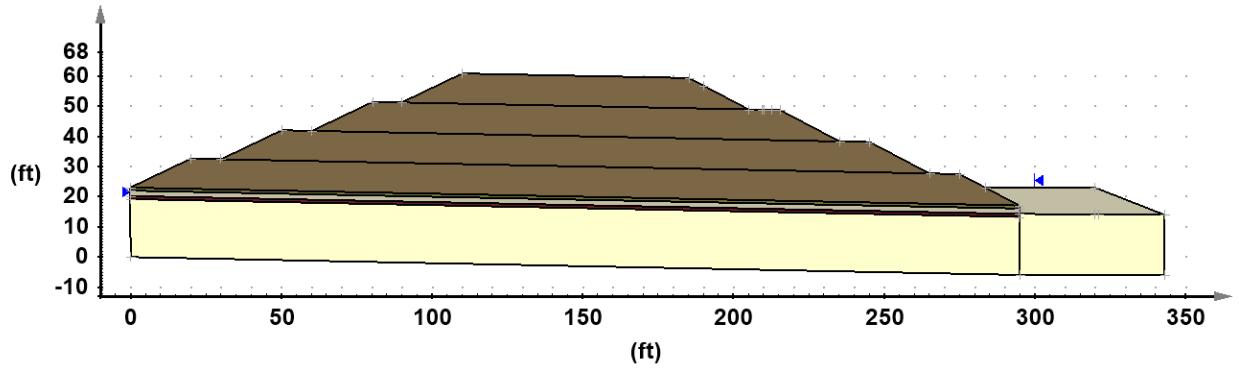


Figure 2.3.35: A toe berm at the very bottom of the pile to provide stability.

Table 2.3.7: Sliding mass characteristics for toe berm scenario.

GLE Analysis	Rainfall event (no berm)	Rainfall event (with a berm)
FOS	0.974	1.626
Total weight (lb)	7.22×10^3	7.40×10^3
Total volume (ft^3)	8.08×10	7.92×10
Total Activating moment (lb-ft)	3.23×10^4	5.75×10^4
Total Resisting Moment (lb-ft)	3.15×10^4	9.36×10^4
Total Activating Force (lb)	2.03×10^3	2.53×10^3
Total Resistive Force (lb)	1.98×10^3	4.12×10^3

Table 2.3.8: Model 3 Case 1 - Different scenarios of irrigation and stability results.

Irrigation	Berm	Volume of applied fluid (ft^3)	Volume of discharge (ft^3)	% loss	FOS	Note
Irrigation is applied to the top layer only	None	5,440	2,854	48	0.90	--
External irrigation is applied to all the heap	None	12,238	9,958	19	1.62	--
External irrigation is applied to all the heap and internal irrigation to the first lift	None	28,782	27,084	6	2.04	Critical surface extending to the foundation layer
Rainfall event	None	937	9	99	0.97	--
Irrigation is applied to the top layer only	Berm	5,440	2,854	48	1.02	--
External irrigation is applied to all the heap	Berm	12,238	9,958	19	1.66	--
External irrigation is applied to all the heap and internal irrigation to the first lift	Berm	28,782	27,084	6	1.98	Critical surface extending to the foundation layer
Rainfall event	Berm	937	9	99	1.63	--

Numerical modeling discussion

Results of the transient seepage models indicated that the applied solution flowed through expected pathways (**Figure 2.3.36**). No blockage in the flow paths was detected. However, moisture migration through the geomembrane liner layer was clearly visible (**Figure 2.3.37**). The migrated moisture did not penetrate through the compacted foundation. This finding highlighted the importance of the use of a double liner system of two LDPE geomembrane: two (2) 60 mil (1.5mm) layers with a 1-ft (0.3 m) thick compacted low-permeability soil (clay). A geosynthetic

clay liner (GCL) can be used as an alternative to the clay layer (Pyper et al., 2019). The permeability of the GCL is typically in the range of 2.8×10^{-3} to 2.8×10^{-5} ft/day (1×10^{-6} to 1×10^{-8} cm/s). This finding is consistent with results reported by Erickson and Breckenridge (2025), where 2-D finite element seepage modeling of a gold heap leach facility showed a moisture migration through a breach in the HDPE geomembrane layer. The moisture migration was stopped by a secondary backup underliner layer of low-conductivity clay layer (LCCL). The HDPE layer was designed as an impermeable layer (Erickson and Breckenridge, 2025).

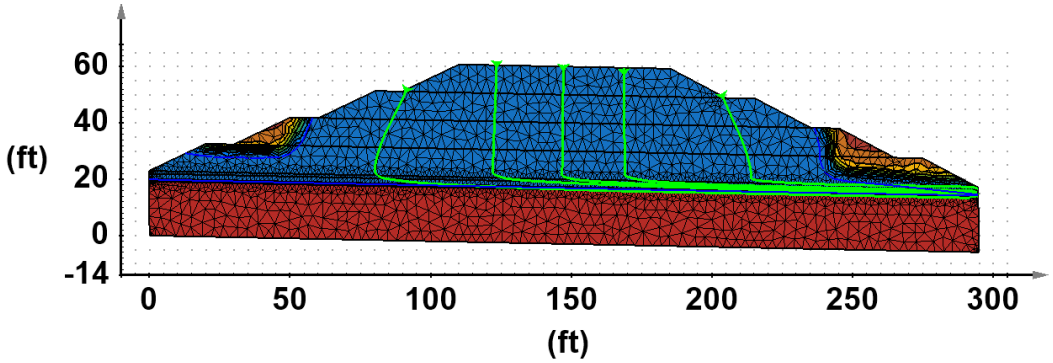


Figure 2.3.36: Flow lines of applied solution through the heap.

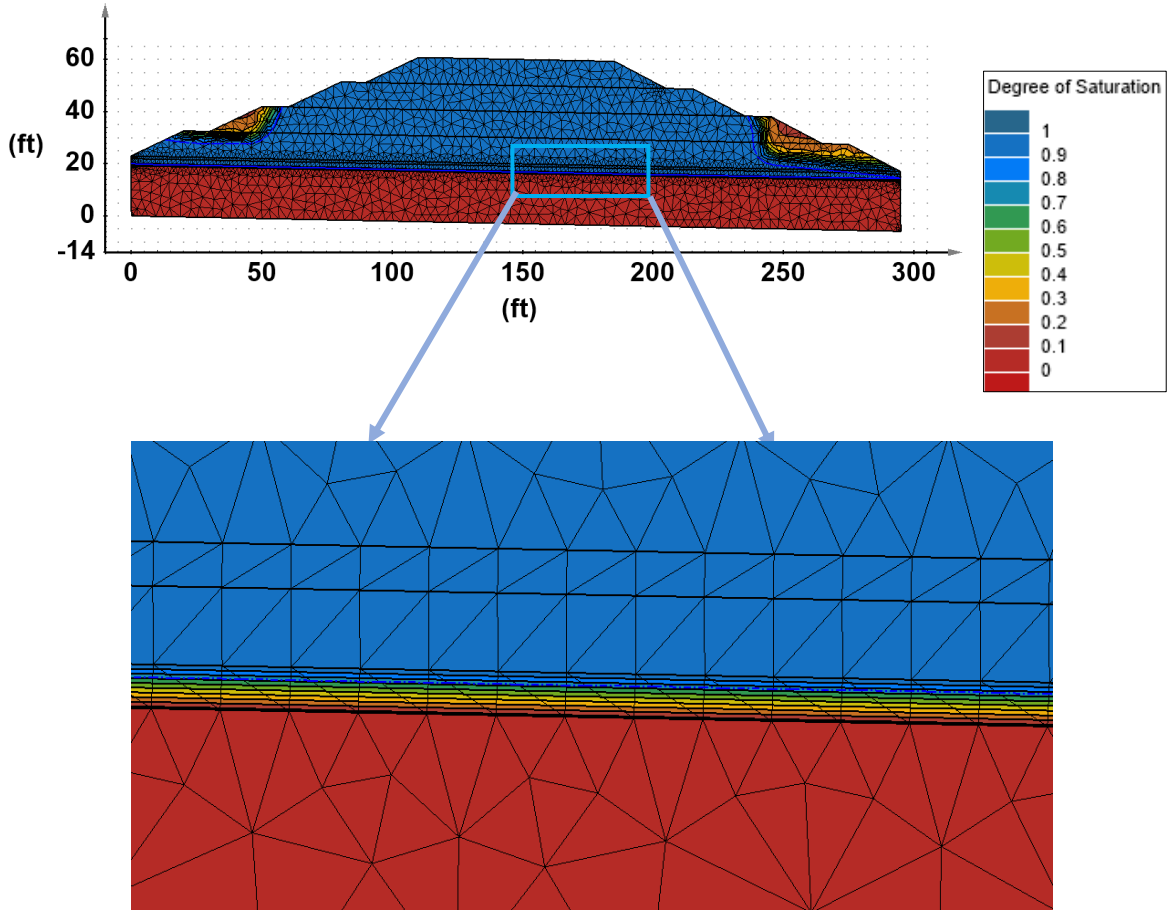


Figure 2.3.37: Moisture migration through the geomembrane conceptual layer.

The flow through the CCR progressed under saturated hydraulic conductivity, flow remained steady throughout the modeling period (4 and 9 days), and no solution surface ponding was detected. During the 40-hour lag time, the solution spread across the surface of the solid, saturating the pore space and coating the solid particles. As the material became saturated, the applied solution tended to flow unimpeded, as shown by vertical flow lines in **Figure 2.3.36**. The solution percentage loss was necessary to saturate the material before free discharge could exit the system. This was evident through the second leaching cycle of 4 days performed in Model 2-Case 2, as the material stayed saturated during the one-day break, allowing the solution to drain freely through the system with approximately 0% loss. This finding aligns with lab observations, as the outflow rate was approximately consistent.

Non-uniform surface coverage of solution application across the heap was observed as the solution was applied to the top lift of the heap. Some dry and/or partially saturated areas were observed. Uniform coverage is essential in heap leaching as it allows for optimum wetting, leading to maximal metal extraction. The non-uniform distribution of the solution resulted in areas that were heavier and settled faster compared to areas with less irrigation, which can create critical potential failure surfaces. Achieving uniform coverage involves extending the applied flux to the external surface of all the layers. Combining external irrigation with an internal irrigation plan resulted in higher FOS for the built design; however, the critical surface extended below the liner layer to the deep foundation. This is an indication of the increased weight of the slope with irrigation strategy.

Based on the results, the toe berm contributed to the stability of the pile by adding weight (driving forces) and resistance to the base of the slope. Pourverdi et al. (2025) analyzed a failing heap leaching structure and concluded that combining toe reinforcement and load reduction minimized deformations and mass displacements. The heap leach pad operation plan can play an essential role in identifying the irrigation period. In the current research, the heap leach pad operational plan has not been finalized, as additional testing is needed to identify the most suitable irrigation strategy to ensure optimal REE extraction. However, in terms of stability, the results suggest that the irrigation plan should maintain a balance between uniform wetting and avoiding the addition of extra weight to the slope to ensure stability. External irrigation to all exposed surfaces of the heap lifts seemed to be the suitable irrigation option according to the results.

The following points are recommended to be considered based on highlights from the results of the study:

1. Ensuring that external irrigation is uniformly implemented.
2. Utilizing a double liner system at the base of the pad or a single geomembrane liner followed by a GCL layer.
3. Wetting the heap to fill void volume before a leaching cycle can result in 0% loss of the applied leachant.
4. Constructing a toe berm tie-in around the perimeter of the pad footprint to ensure stability of the pad.

Task 2.4 Environmental control and system design

Environmental control

Methodology

Environmental control is a critical aspect for the survival of industries that are process-based (Jämsä-Jounela, 2001). The primary environmental concern associated with heap leach facilities relates to the failure to contain process solutions within the heap leach circuit. This is of top priority, as containment failures would have a potential negative impact on human health and ecosystems (Ghorbani et al., 2016). Identifying the long-term environmental aspects of the CCR heap leaching (potential for the continuous production of acidic drainage) is critical in the process. The environmental controls to be investigated were the capability of the heap pad design and the selected site to contain the process solutions. Results from the Acid-Base Accounting (ABA) analytical procedure conducted in the analytical lab at WVU were used to predict the future drainage quality of the tested CCR (weathered, fresh, and raw). Results from seepage analysis performed using PLAXIS LE were used to predict the suitability of the geomembrane liner to contain the collected leachate. Furthermore, the suitability of the selected site for drainage containment was evaluated based on feedback and information received from decision-makers and people in charge (ACNR personnel) on questionnaires created for the Blackville #2 Coal Mine (provided in **Appendix C**).

ABA is an analytical procedure that predicts whether a rock at a specific location can produce excessive acid or alkaline drainage. In this test, acid formation potential and acid neutralizing capacity are indicated and measured, and thus, post-mining drainage quality can be determined (Skousen et al., 2002; Fosu et al., 2020). Scientists at WVU developed this procedure in the 1960s. This test predicts post-mining water quality by determining acid production potential (AP), neutralization potential (NP), Net Neutralization Potential (NNP), and the Neutralization Potential Ratio (NPR) (Fosu et al., 2020). AP is determined as the product of the percentage of pyritic sulfur present in the ore and the factor of 31.25 kg $CaCO_3$/ton, which represents the amount of ($CaCO_3$) necessary for neutralizing the acid generated by the complete oxidation of all of the sulfur in one ton (1,000 kg) of the ore (Skousen et al., 2000a; Brookhian et al., 2022). Maximum acid potential (MAP) is determined using the same calculation, but based on the percentage of total sulfur (Skousen et al., 2000a). Total sulfur accounts for any acid-generation sulfides in addition to pyrite [e.g., Pyrrhotite ($Fe_{1-x}S$), Arsenopyrite (FeAsS), and Tennantite ($Cu_{12}As_4S_{13}$)]. NP is a measure of acid consumption capacity, and thus, the amounts of acid-neutralizing compounds in the sample (e.g., carbonates) are measured through NP. A negative value of NP is an indicator of the deficiency of acid-neutralizing minerals. NNP is determined by subtracting AP from NP and represents the ability of a sample to produce AMD or neutralize free acid, whereas NPR is the ratio of NP to AP (Brookhian et al., 2022).

Results

Even though raw CCR measured the highest AP and MPA values (**Table 2.4.1**), it does not indicate a higher potential for acidity production compared to weathered and fresh CCR. According to the literature, there is a poor correlation between MPA and post-mining water quality and an intermediate one between NP and water quality. However, NNP and NPR proved to be the most accurate predictors. In a study by Skousen et al. (2002), predictions of water quality using NNP and NPR were identical for 50 out of 56 cases.

Based on guidelines for defining strata as either acid or alkaline-generating, when the NPP value is < 0 tons/1000 tons and the NPR value is < 1, it is expected to produce acidic drainage (Skousen et al., 2000b, 2002; Brookhian et al., 2022). Fresh and raw CCR had NNP values were less than zero (-26.88 and -65.91 tons/1,000 tons, respectively) and NPR values less than 1 (-0.23 and 0.28, respectively) (**Table 2.4.1**). Weathered CCR had an NNP value of more than 20 (43.34 tons/1000 tons) and an NPR value of more than 3, which indicates a potentially acid-neutralizing sample. It should be noted that the calculated AP that was used to determine NNP was estimated based on the percent of pyritic sulfur and not the percent of total sulfur. The use of total sulfur to determine NNP and NPR values for the weathered refuse put the weathered refuse within the acid-generating category ranges.

Prior to any reactions, the paste pH is measured in a mixture of sample and DI water. The value indicates whether the sample material contains readily available acidity or alkalinity. In other words, paste pH can determine the acidity status of a sample (Fosu et al., 2020). Sulfide oxidation may be indicated by the paste pH value, which is also considered an important sign of weathering. A paste pH value of less than 6.5 indicates that the sample under test has already been weathered and has formed acidic sulfate salts (Fosu et al., 2020). Weathered and fresh CCR samples had paste pH values of <6.5 (4 and 2.7, respectively), which is consistent with the information gathered on both samples. The raw CCR sample had a paste pH value of 9, which indicates that the raw sample has never experienced any weathering conditions. **Table 2.4.2** summarizes the post-leaching ABA results for samples collected from the middle layers of the six columns (AMD-W, AMD-F, DI-W, DI-F, H_2O_2-W, and H_2O_2-F, respectively). All columns (except column#1) had a negative value for NNP and NPR values of < 1, which indicates a higher potential for the continuous production of acidic drainages. The most substantial acidic production potential was associated with column # 3, which was filled with weathered CCR and leached with DI water. This indicates that the leached CCR is still able to produce AMD as suitable conditions (e.g., oxygen, humidity, and time) are present.

Table 2.4.1: ABA and Sulfur Forms Analysis for all types of CCR collected (weathered, fresh, and raw).

CCR Type	Total Sulfur %	Pyritic Sulfur %	Sulfate Sulfur %	Organic Sulfur %	Pyritic Sulfur % of Total Sulfur	Calcium Carbonate Equivalent in Tons/1000 Tons of Material				Paste pH	NPR	
						Potential Acidity (AP)	Maximum Potential Acidity (MPA)	Neutralization Potential (NP)	Net Neutralization Potential NNP		Np/MPA	NP/AP
Weathered	2.50	0.49	1.74	0.27	19.7	15.41	78.1	58.75	43.34	4.0	0.75	3.81
Fresh	2.45	0.70	1.47	0.29	28.5	21.88	76.6	-5.00	-26.88	2.7	-0.07	-0.23
Raw	3.97	2.93	0.70	0.34	73.7	91.41	124.1	25.50	-65.91	9	0.21	0.28

Table 2.4.2: ABA and Sulfur Forms Analysis for post-leaching CCR with six columns.

Columns	Total Sulfur %	Pyritic Sulfur %	Sulfate Sulfur %	Organic Sulfur %	Pyritic Sulfur % of Total Sulfur	Calcium Carbonate Equivalent in tons/1000 tons of Material				Paste pH	NPR	
						Potential Acidity (AP)	Maximum Potential Acidity (MPA)	Neutralization Potential (NP)	Net Neutralization Potential NNP		Np/MPA	NP/AP
AMD-W	1.24	0.21	0.72	0.31	17.1	6.63	38.8	14.00	7.37	3.7	0.36	2.11
AMD-F	2.17	0.66	1.00	0.51	30.2	20.47	67.8	1.00	-19.47	2.7	0.01	0.05
DI-W	6.98	4.75	1.59	0.64	68.0	148.28	218.1	7.50	-140.78	2.9	0.03	0.05
DI-F	2.50	0.87	0.99	0.65	34.7	27.13	78.1	1.50	-25.63	2.7	0.02	0.06
H_2O_2-W	2.42	0.86	1.10	0.46	35.7	27.00	75.6	12.75	-14.25	2.6	0.17	0.47
H_2O_2-F	1.91	0.71	0.82	0.37	37.3	22.22	59.7	0.75	-21.47	2.6	0.01	0.03

Based on the refuse site assessment results, Blacksville #2 was selected as the best option for any future potential operational scale-up of this project. Coal refuse tailings available at the Hughes Hollow Impoundment are linked to leachate generation following the same principles of heap leaching during rainfall events. Considering the drainage quality prediction conducted through the ABA analytical procedure, all types of samples available at the site have already undergone weathering and have formed acidic sulfate salts. The refuse piles at Hughes Hollow fall into the category of acidic-generating samples and indicate a higher potential for the continuous production of acidic drainage. According to ACNR, the generated AMD is under control and handled as follows (**Figure 2.4.1**): Water from Hughes Hollow gravity flows to what is considered the mine's "Beaver Pond". An active treatment plant at Beaver Pond treats the collected AMD with hydrated lime. The AMD at the Beaver Pond is fed with water from the mine's Sedimentation Pond 2 and from a recirculation pump that is stationed on the west end of the Beaver Pond. Water from Hughes Hollow is mixed with the mentioned sources. A combination of pumps transfers water from the Beaver Pond to the mine's Freshwater Impoundment, located west of the Beaver Pond. The water within the Freshwater Impoundment is allowed to naturally flow into Dunkard Creek. The AMD treatment system is located in West Virginia under WVDEP Article 3 Permit No. O1011193.

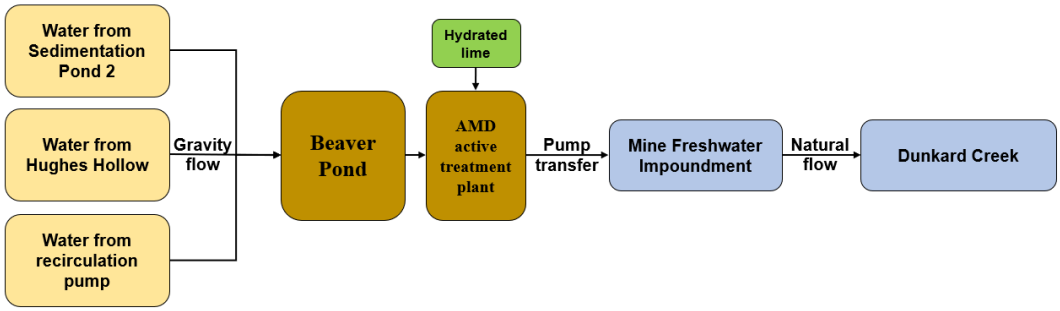


Figure 2.4.1: Block flow diagram of the AMD handling process at the Blacksville #2 Coal Mine.

ACNR also stated that the mine has redundant pumps to manage significant storm events and/or potential pump failures. However, they pointed out that failed pumps could lead to AMD discharge. At the same time, the mine is seeking approval to install additional ditching on the east side of the cap of Hughes Hollow to handle any overflow of the Low Gap Pond (located at the northeast side of the impoundment). The mine had never experienced any problems containing the AMD within the ponds at the site, as all sediment control structures are designed to pass a 10-year, 24-hour storm. Furthermore, ACNR reported that the ditches and ponds have not presented any known hazards to wildlife or birds. Water is treated to below effluent levels before it is discharged into any streams. Also, there are no additional inherent potential impacts from this site on local communities that are not typical of coal refuse sites. Currently, an Engineered Work Plan (EWP) is in place for this structure.

The seepage analysis performed using PLAXIS LE showed that a layer of geomembrane, in addition to the low-permeability foundation (compacted CCR), acted as an impervious surface. These layers prevented the percolation of AMD into the foundation, thereby ensuring the containment of the solution. No external chemical acids will be introduced to the site for the purpose of heap leaching; AMD is being used as the leaching solution and is naturally generated on-site. No waste management is required, as the waste in this process will be the exhausted coal refuse, which is already available and stored on-site. Further steps in the heap leach circuit

(e.g., generating HPC from PLS via two-stage pH adjustment) will be handled through closed tanks, which provide an additional measure of environmental control within the project.

Heap leach pad conceptual system design

A conceptual leach pad system was proposed based on information available in the literature about heap leaching (Piésold, 2012; Tech, 2012; Whitehorse, 2012; Ghorbani et al., 2016) and information obtained in the bench-scale leach testing performed in this project. The proposed heap leach pad was assumed to cover an area of 2 acres with four lifts/layers of CCR. The proposed system aims to manage the 1 million gallons (Mgal) (133,680 ft^3 or 3,785 m^3) of AMD available in the Crest Pond at the Hughes Hollow Impoundment at the Blacksville Number 2 Mine. Using the laboratory-measured hydraulic conductivity of the weathered CCR (1.14×10^{-5} ft/s or 3.48×10^{-4} cm/s), the volumetric flow rate of the AMD was obtained using Darcy's law, assuming a hydraulic gradient of 1 for simplicity (Equation 14). Time for a single cycle in the field (t) was calculated using Equation 15. More information about the proposed design can be found in the following sections.

$$Q=kAi \quad \text{(Equation 14)}$$

Where: Q = Volumetric flow rate, k = Hydraulic Conductivity, A = Cross-sectional area of flow, and i = hydraulic gradient

$$t = V/Q \quad \text{(Equation 15)}$$

Where: V = Volume, t = time, and Q = Flow rate

The proposed heap leach pad was assumed to cover an area of 2 acres (8,094 m^2) with four lifts/layers of CCR. Every lift was assumed to have a height of 10 ft (3 m), which makes a total heap height of 40 ft (12 m). This leach pad footprint is comparatively smaller in terms of size and capacity when compared to leach pad footprints reported in the literature for the extraction of other metals (in the range of 54 to 130 acres, e.g., gold) and lift heights in the range of 20 to 33 ft (6 to 10 m) (Roth et al., 2018; Lane et al., 2021; Tang and Esmaeili, 2021). Heap leaching low-grade ores for gold extraction are considered more established than CCR heap leaching. The proposed leach pad consists of the following layers: compacted foundation, geomembrane liner, gravel, a non-woven geotextile (1100 N; apparent opening size [AOS] of 0.006 inches or 0.15 mm), and CCR layer/s through which leachant would be introduced and allowed to flow. The gravel layer should contain the pipelines of the leachate collection system to collect and convey the leachate solution to the collection pond adjacent to the heap leach structure. More details are provided in the following subsections.

Foundation

The base foundation should be prepared by removing the topsoil and vegetation if necessary, compacting, and sloping. Depending on the site, grading may be required. A uniformly sloping area with a grade of 0.5% to 2.0% is considered ideal for a heap pad (Kappes, 2002). In this project, the heap pad was designed with a slope grade of 2%. This grade will allow for the leachate to flow toward the collection ditch on the side of the heap.

Liner system

To prevent leakage losses of the leachate through the bottom of the leach heap pad, a liner must be installed. The liner is also intended to reduce any negative environmental impact. Composite liners with drain fill are commonly preferred and used as pad liners heap leach practice (Piésold, 2012; Ghorbani et al., 2016). The most common liner system for heap leaching facilities consists of a composite geomembrane and underlying bedding material known for its low permeability (Tech, 2012). The proposed design in the current research consists of a 1.5-mm 60-mil double-sided textured geomembrane liner of low-level-density polyethylene (LLDPE). A geosynthetic clay liner (GCL) could also be placed under the geomembrane to provide a layer of very low hydraulic conductivity. The permeability of the GCL is typically in the range of 2.8×10^{-3} to 2.8×10^{-5} ft/day (1×10^{-6} to 1×10^{-8} cm/s) (Pyper et al., 2019). LLDPE was selected based on published literature (Piésold, 2012; Tech, 2012; Whitehorse, 2012; Ghorbani et al., 2016; Lane et al., 2021). LLDPE is known for its puncture and chemical resistance, high interface friction, excellent performance under high stresses, and flexibility. This material is known to elongate to support the settlement of the heap load, adapt to variable temperature, and install easily in cold climates (Piésold, 2012; Whitehorse, 2012; Lane et al., 2021).

Over liner

A layer of 1.5 to 3 ft (0.5 to 0.9 m) of crushed stone should be placed over the liner prior to CCR placement to prevent any possible liner damage during the CCR placement (Piésold, 2012; Lane et al., 2021). This layer will act as a drainage layer where the lateral collection network of pipes would be placed. In the current reach, a gravel layer approximately 1.7 ft (0.5 m) in height was considered.

Leachate collection system

The leachate collection system includes the following: i) pipes for lateral collection placed underneath the heap; ii) collection header pipes; and iii) leachate collection pond. A common practice in heap leaching is to use perforated pipes as the lateral collection system underneath heaps. The collection system is embedded within the overliner layer of coarse crushed ore (gravel in the current research work). The lateral collection pipes have a diameter of 2 to 4 inches (50 to 100 mm); the main collection header pipes in the system have a diameter of 18 inches (450 mm). These dimensions follow common practice according to the literature (César et al., 2014; Tech, 2017). The network of lateral collection pipes is placed underneath the pad to convey the PLS to the main collection header pipes, which discharge into the collection pond. Six (6) meters will separate each of the 15 lateral collection pipes across the pad (**Figure 2.4.2**).

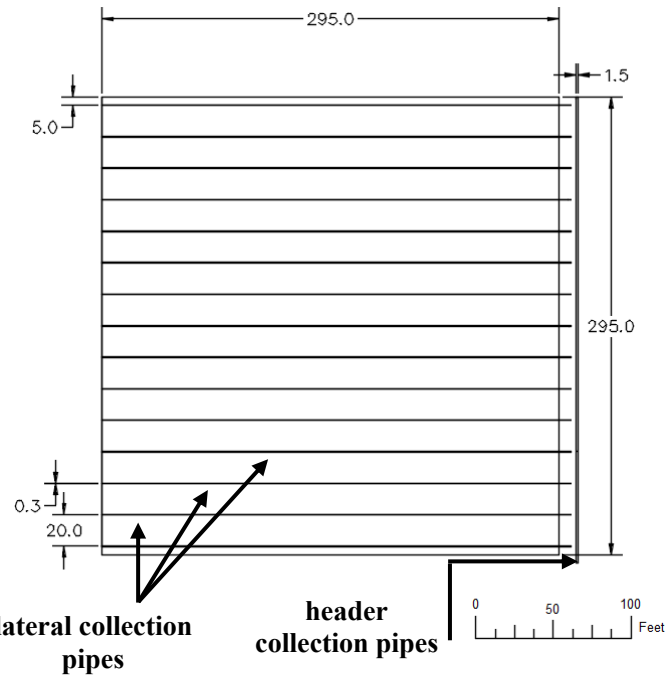


Figure 2.4.2: Leachate collection system for heap pad.

Ore layers

Four layers/lifts of weathered CCR to be constructed, using a conveyor stacking system, with a height of 10 ft (3 m) per lift and a side slope angle of 26.6 degrees (2:1 H: V). The CCR is assumed to be placed in its original condition in the field without further processing.

Irrigation system

The raw AMD available at the collection pond will be pumped to the top of the heap using a high-capacity centrifugal pump (e.g., Goulds 3196 ANSI Process Pump). The AMD will percolate in the heap at a volumetric flow rate of 450 gpm. The liquid will be introduced to the heap via a main supply line of 4 to 5-inch-diameter tubing. The main supply line feeds lateral lines that are 0.5 to 0.6 inches (1.3 to 1.5 cm) tubing. Standard spray wobbler sprinklers will spread the leach solution over the heap's surface. Coarse droplets control but do not eliminate evaporation with a coverage diameter of approximately 50 ft (15 meters). This coverage diameter results in a coverage area of approximately 1,900 ft^2 (177 m^2). It is common to place wobblers in a 6 × 6-meter pattern along the heap surface (Kappes, 2002). This placement pattern would ensure a slight overlap of their coverage area and consistent solution distribution. By dividing the heap area of 2 acres (87,120 ft^2) by the coverage area of a single sprinkler (1,900 ft^2 or 177 m^2), approximately 49 wobbler sprinklers are needed to cover the top surface of the heap. Given the coverage area of a single sprinkler and the calculated application rate, the application flow rate of each sprinkler should be approximately 9 to 10 gpm (**Figure 2.4.3**).

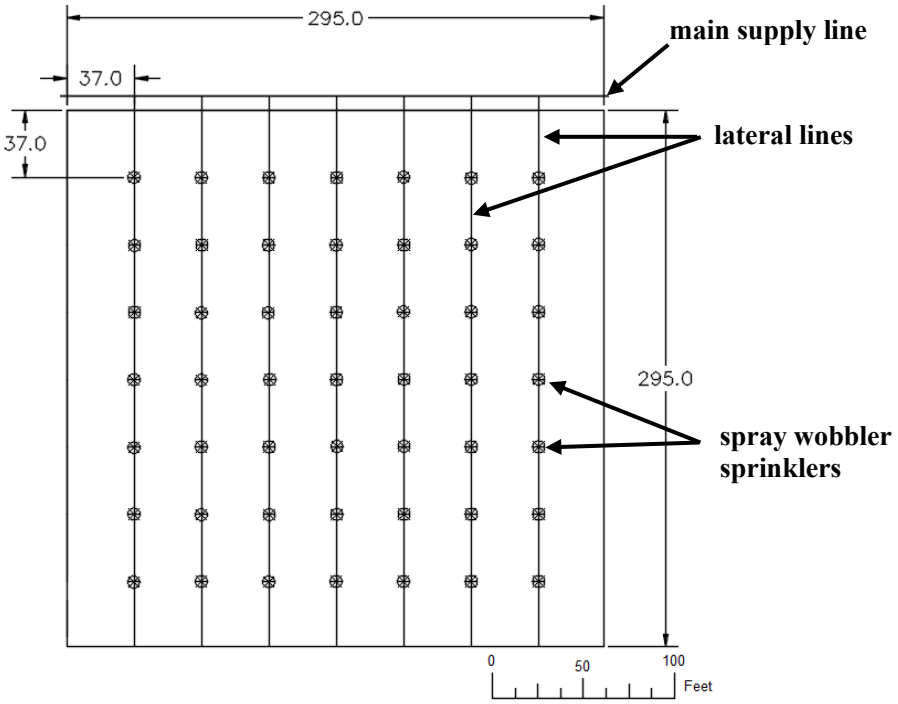


Figure 2.4.3: Irrigation pattern and system for heap pad.

Application flow rate

The volumetric flow rate of the AMD was obtained using Darcy's law and found to be 1 cfs (450 gpm). This is equal to an application flow rate of 5×10^{-3} gpm/ft^2 (12 l/hr/m^2), and the time for a single leaching cycle was approximately 4 days. Reported application flow rate in the literature may vary depending on the ore type, permeability, zones of low permeability, leachant used, and the condition of the ore (e.g., crushed and agglomerated), chemical reactions within the heap, and other complex aspects (the rate of washing off the mineral of interest of the ore) (Kappes, 2002; John, 2011; Ghorbani et al., 2016). Kappes (2002) reported different application flow rates for various gold recovery projects. The study reported that the application flow rate for crushed ore can be in the range of 3×10^{-3} to 9×10^{-3} gpm/ft^2 (7 to 20 l/hr/m^2). They also reported an average application flow rate in the range of 0.037 gpm/ft^2 to 0.048 gpm/ft^2 (8.3 l/hr/m to 10 l/hr/m^2) in other run-of-mine heaps. The calculated application flow rate for this project aligns with the application rates documented in published literature.

Task 2.5 Technical and economic analysis

Methodology

The economic assessment aimed to evaluate the feasibility of processing low-grade REE CCR (263.383 mg/kg or 238.937 g/US ton) at the proposed field-scale volume (approximately 11,150 US tons or 10,115 metric tons) via heap leaching. Primary components that were included in calculating the capital cost (CapEx) and operating cost (OpEx) are provided in **Figures 2.5.1 and 2.5.2**, respectively. The CapEx and OpEx breakdown was evaluated for four different scenarios that could be adopted for the leach pad. The four scenarios alternate between the CCR crushing and air injection through the ore as they factors were reported in literature to influence leaching efficiency (Geidel, 1979; Zhang et al., 2018; Yang, 2019a; Allen et al., 2019; Yang and Honaker, 2020; Jain et al., 2021). The four scenarios/options are: i) no crushing and no air injection, ii) no crushing and air injection, iii) crushing and no air injection, and iv) crushing and air injection.

Costs for most components included within the CapEx categories, as well as REE oxide prices, were determined through published literature (**Tables 2.5.1** through **2.5.4**). OpEx categories of energy consumption and labor and maintenance were assumed to be 10% and 5% of capital cost, respectively (Peters et al., 2003; Dimitriou, 2013; Zhang and Honaker, 2018). Chemical, including lime and polymer, consumption costs were calculated based on a nine-year average price of chemical consumption costs available for two WVDEP AMD treatment plants (T&T and A34) (**Table 2.5.3**). The information about prices were obtained through personal communications with the WVDEP Office of Special Reclamation (OSR). T&T is located in Preston County, WV, near the Monongalia County border, and A34 is situated in Mount Storm, Grant County, WV. Both facilities operated by the WVDEP to neutralize contaminated water at an average flowrate of 1,400 gpm and 300 gpm. Respectively. Average AMD inflow for the T&T was obtained from sampling by the West Virginia Water Research Institute (WVWRI) in an active characterization project with the WVDEP Office of Abandoned Mine Lands and Reclamation (AML). Average AMD inflow for the A34 Plant was obtained from the WVDEP OSR staff. The values of the flowrates were converted to annual volume of AMD treated and used to determine the cost of lime and polymer needed to treat 1 Mgal of collected AMD as assumed in this project.

The income from REE sales was determined by multiplying the REE concentration within the collected leachate by the volume of leachate by the unit price (US $/kg) of individual REE oxides available in the literature (**Table 2.5.4**). The average unit price of individual REE oxides for the available prices was used in the calculations. REE concentration within the leachate was assumed to be the same as the laboratory-measured value, as the assumed CCR: AMD ratio in the field was kept constant during the bench-scale testing in the lab.

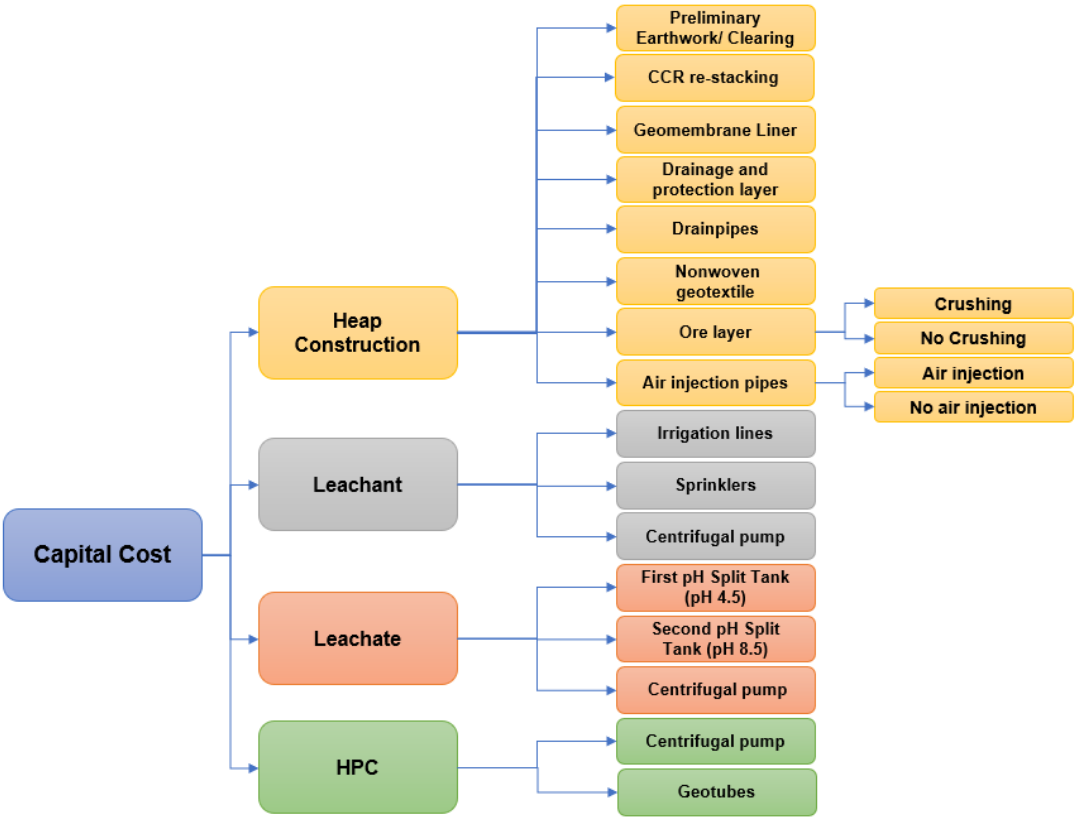


Figure 2.5.1: Components of the capital cost in the economic analysis.

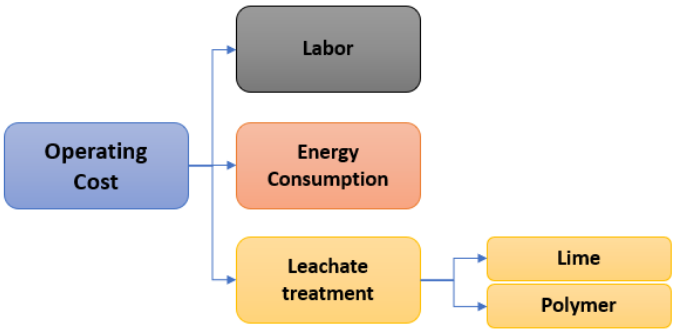


Figure 2.5.2: Components of the operating cost in the economic analysis.

Table 2.5.1: Costing for design parameters based on 2025 prices and values reported in the published literature (Leach pad and processing).

Installation/ Design aspects	Capacity and price details	Cost	References
Leach Pad			
Preliminary Earthwork/ Clearing	$/m^2	$1.00	(Kappes, 2002)
	$/m^2	$19.10*	(Smith et al., 2014)
Geomembrane Liner	$/m^2	$9.81	(Smith et al., 2014)
	$/m^2	$7.87*	(HOP, 2025)
	$/m^2	$1.50	(Kappes, 2002)
	$/m^2	$1.50	(Kappes, 2002)
Drainpipes	75-100 mm perforated flexible tubing $/m^2	$0.50*	(Dlamini, 2015)
	Perforated flexible tubing (price per 10 ft)	$16.00	(LOWE'S, 2025)
	Perforated flexible tubing 100 mm (4inches) $/100 feet ($/30 m)	$97.9	(menards, 2025)
	Perforated flexible tubing 450 mm (18 inches) $/100 feet $/30 m	$4,645.6*	(Ewing, 2025)
Non-woven geotextile	$/m^2	$4.95*	(Paramount Materials, 2025)
	$/m^2	$160	(Silt Management Supplies, LLC., 2025)
Drainage and protection layer	$/m^2	$0.50	(Dlamini, 2015)
	$/m^2	$4.3*	(Angi, 2025)
Processing			
Ore layer/crushing	Crusher Feeder (Solid capacity of 488 mtph)	$18,682*	(Allen et al., 2019)
	Cone Crusher (Solid capacity of 488 mtph)	$773,357	(Allen et al., 2019)
	Cone Crusher	$411,200*	(Aishred, 2025)
Aeration Unit	$/unit	$6,446	(Tezyapar Kara et al., 2024)
	Lobe Blower/ Max flow rate of 4460 ft^3/min	$36,301*	(pdblowers, 2025)

* Used in calculations

Table 2.5.2: Costing for design parameters based on 2025 prices and values reported in the published literature (Irrigation and air injection lines and equipment).

Installation/ Design aspects	Capacity and price details	Cost	References
Irrigation and Air Injection Lines			
Air injection pipes	$/m^2	$0.50*	(Dlamini, 2015)
	(25 feet) Natural Polyethylene Tubing	$4.98	(The HOME DEPOT, 2025)
Irrigation line	$/m^2	$0.60*	(Dlamini, 2015)
Equipment			
CCR re-stacking with a conveyor	Heavy-duty Belt conveyor	$4,500	(Honaker et al., 2021)
	Feed Conveyor/ Belt Conveyor (175,200 mtpy)	$68,000	(Ziemkiewicz, 2021)
	Conveyor (1 ton -1000 tons per hour)	$1,200*	(Alibaba, 2025)
	Conveyor	$6,477	(Gilmore Kramer, 2025)
Sprinklers	SpinNet Sprinkler w/Check Valve	$3.10*	(Dripdepot, 2023)
High-capacity centrifugal pump	Screw Pump (314 gpm)	$88,000	(Ziemkiewicz, 2021)
	PLS Feed Pump (312 gpm)	$45,000*	(Ziemkiewicz, 2021)
	Centrifugal Pump (690 gpm Max)	$24,940	(PumpProducts, 2019)
	Pumps Centrifugal	$14,181	(Zhang and Honaker, 2018)
pH Split Tanks	Baffled Tank (10,700 gallons)	$42,000*	(Ziemkiewicz, 2021)
	PLS Feed Tank (10,000 gallons)	$43,000	(Ziemkiewicz, 2021)
	Mix Tank (23,775.5 gallons)	$64,942	(Zhang and Honaker, 2018)
Composite Geotextile Geotubes	Dewatering bag (15'× 45')	$1,500	(AIRE 1, 2025)
	Dewatering bag (15'× 30')	$1,100*	(AIRE 2, 2025)
	Dewatering bag (6'× 6')	$250	(AIRE 3, 2025)
	Non-Woven Geotextile Dewatering Bag (15'× 15')	$202	(Airgas, 2025)

* Used in calculations

Table 2.5.3: Lime and Polymer costs for two WVDEP AMD treatment sites (A34 and T&T).

Year	Lime and Polymer Costs	
	Sites	
	A34	TandT
2015	$86,668	203,397
2016	$113,036	175,873
2017	$172,247	159,653
2018	$169,315	159,561
2019	$100,085	166,613
2020	$66,149	158,394
2021	$37,501	160,851
2022	$161,370	144,980
2023	$97,759	168,053
Average	$111,570	166,375

Table 2.5.4: Individual REE oxides prices based on literature.

REE (Oxides)	**References**		
	Das et al., 2018	Ziemliewicz, 2023	
	(2010-2014) average price	2016 Price	2022 Price
	Cost (US $/kg)		
Scandium Oxide	$6,719.0	$4,200.0	$2,000.0
Yttrium Oxide	$87.4	$6.0	$10.0
Lanthanum Oxide	$40.8	$2.0	$1.0
Cerium Oxide	$40.8	$2.0	$1.0
Praseodymium Oxide	$144.0	$2.0	$100.0
Neodymium Oxide	$136.0	$42.0	$125.0
Samarium Oxide	$87.4	$2.1	$3.0
Europium Oxide	$2,106.0	$150.0	$30.0
Gadolinium Oxide	$136.0	$32.0	$50.0
Terbium Oxide	$1,826.0	$400.0	$1,000.0
Dysprosium Oxide	$885.0	$230.0	$300.0
Holmium Oxide	$859.0	$53.0	$ --
Erbium Oxide	$223.0	$34.0	$50.0
Thulium Oxide	$1,500.0	$ --	$ --
Ytterbium Oxide	$470.0	$28.7	$ --
Lutetium Oxide	$3,525.0	$796.6	$ --

-- Not available

Results

Economic analysis has been reported in the literature for REE extraction through different processes (e.g., flotation) and from different ores (e.g., fly ash) (S. Das et al., 2018; O'Brien and Alonso, 2025). However, to the best of the project team's knowledge, there is currently no industrial-scale application to extract REEs through CCR heap leaching. Therefore, the current economic assessment was performed based on information obtained through bench-scale CCR leaching performed in the lab and information available in the literature (**Tables 2.5.1 through 2.5.4**).

The capital and operational cost breakdown was evaluated for four different options/scenarios that could be adopted for the heap pad, and they are presented in **Figures 2.5.3 and 2.5.4 and Tables 2.5.5 and 2.5.6**, respectively. The evaluation of the four scenarios revealed that crushing the material is the most cost-effective component. The two scenarios involving material crushing had the highest capital cost. The lowest capital cost was associated with the scenario that does not include any crushing or air injection. This scenario is considered the most economical, upon which the hypothesis of the bench-scale leaching test (Chapter 3) was built. The calculated capital cost of the different scenarios is lower than capital cost estimates reported in the literature for extracting other metals through heap leaching (e.g., gold) (Roth et al., 2018; Lane et al., 2021), as the extraction of such metals through heap leaching is considered more established. The income from REE sales was calculated and determined to be $12,987 (**Table 2.5.7**). This value represents the price that corresponds to one leaching cycle in the field, and not the total revenue generated through the project. No other assumptions or conclusions were made, as further testing is required to determine the most suitable operational approach to achieve high revenue that could offset the capital cost and ensure future profitability. Scandium is one of the two most expensive REEs according to literature (Das et al., 2018), and it made up approximately 85% of the total price in this research work.

The results of Phase 2 of the drum leaching tests showed that the use of no-cost engineering controls, specifically planned wetting/drying periods, is likely to result in sustained leaching. An additional two-fold increase in TREE concentration was achieved through the extended four-month drying period. Based on the results, flushing the weathered refuse with AMD every 4 months could increase income by $3,430 (**Table 2.5.7**). Flushing one lift of weathered refuse 3 times a year, in addition to the first leaching cycle, makes a total income of $23,277. Considering the same scenario for 3 more lifts, the total income would be $93,108 from four stacked lifts per year.

Table 2.5.5: Capital cost estimates for four different heap pad scenarios.

CAPEX/ Design Parameters	Options/ Scenarios			
	Option 1	Option 2	Option 3	Option 4
	No crushing and no air injection	No crushing and air injection	Crushing and no air injection	Crushing and air injection
Leach Pad				
Preliminary earthwork/ clearing	$154,353	$154,353	$154,353	$154,353
Geomembrane liner	$63,700	$63,700	$63,700	$63,700
Drainpipes (100 mm)	$4,047	$4,047	$4,047	$4,047
Drainpipes (450 mm)	$13,937	$13,937	$13,937	$13,937
Non-woven geotextile	$40,065	$40,065	$40,065	$40,065
Drainage and protection layer	$34,804	$34,804	$34,804	$34,804
Processing				
Crusher feeder	$0	$0	$18,682	$18,682
Cone crusher	$0	$0	$411,200	$411,200
Aeration unit	$0	$36,301	$0	$36,301
Irrigation and Air Injection Lines				
Air injection pipes	$0.00	$4,047	$0.00	$4,047
Irrigation lines	$4,856	$4,856	$4,856	$4,856
Equipment				
CCR re-stacking with a conveyor	$1,200	$1,200	$1,200	$1,200
Sprinklers	$142.60	$142.60	$142.60	$142.60
High-capacity centrifugal pump	$135,000	$135,000	$135,000	$135,000
pH split tanks	$84,000	$84,000	$84,000	$84,000
Composite geotextile geotubes	$1,100	$1,100	$1,100	$1,100
Total Cost	$537,205	$577,553	$967,087	$1,007,435

Table 2.5.6: Operating cost estimates for four different heap pad scenarios.

Operating expenditure (OpEX)	Options/ Scenarios			
	Option 1	Option 2	Option 3	Option 4
	No crushing and no air injection	No crushing and air injection	Crushing and no air injection	Crushing and air injection
Energy Consumption ($/year)	$53,720	$57,755	$96,709	$100,743
Maintenance and Labor ($/year)	$26,860	$28,878	$48,354	$50,372
Lime and Polymer Consumption ($/year)	$467	$467	$467	$467
Total Cost	$81,048	$87,100	$145,530	$151,582

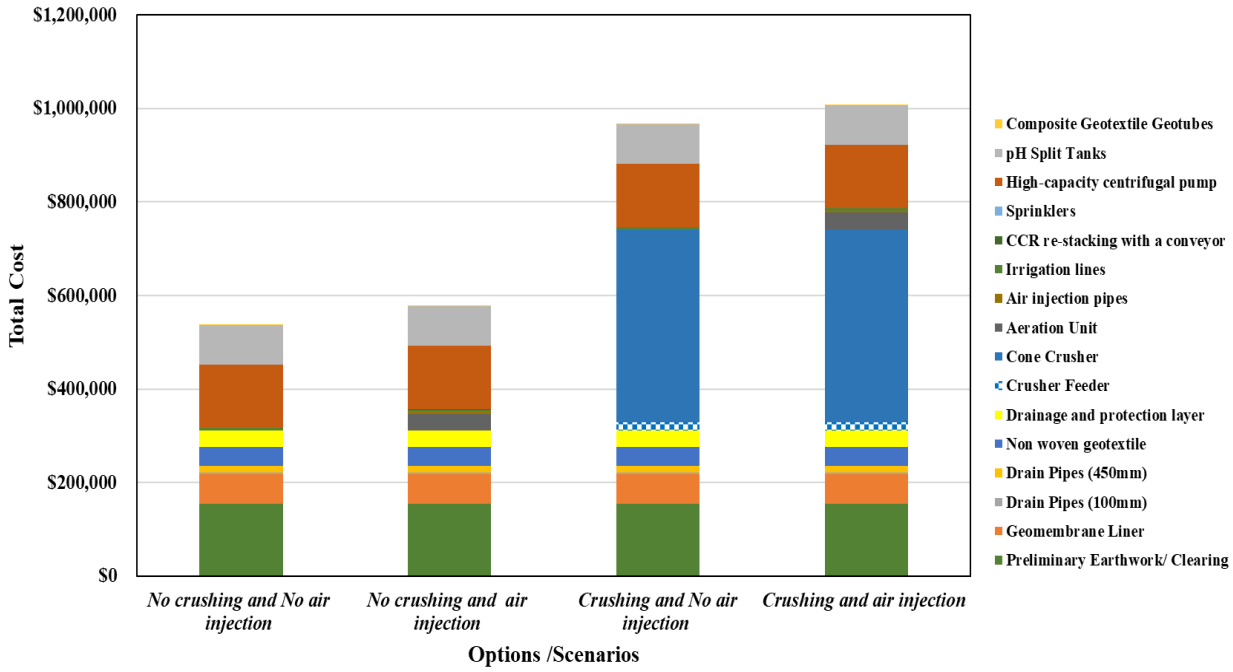


Figure 2.5.3: Capital cost estimates for four different heap pad scenarios.

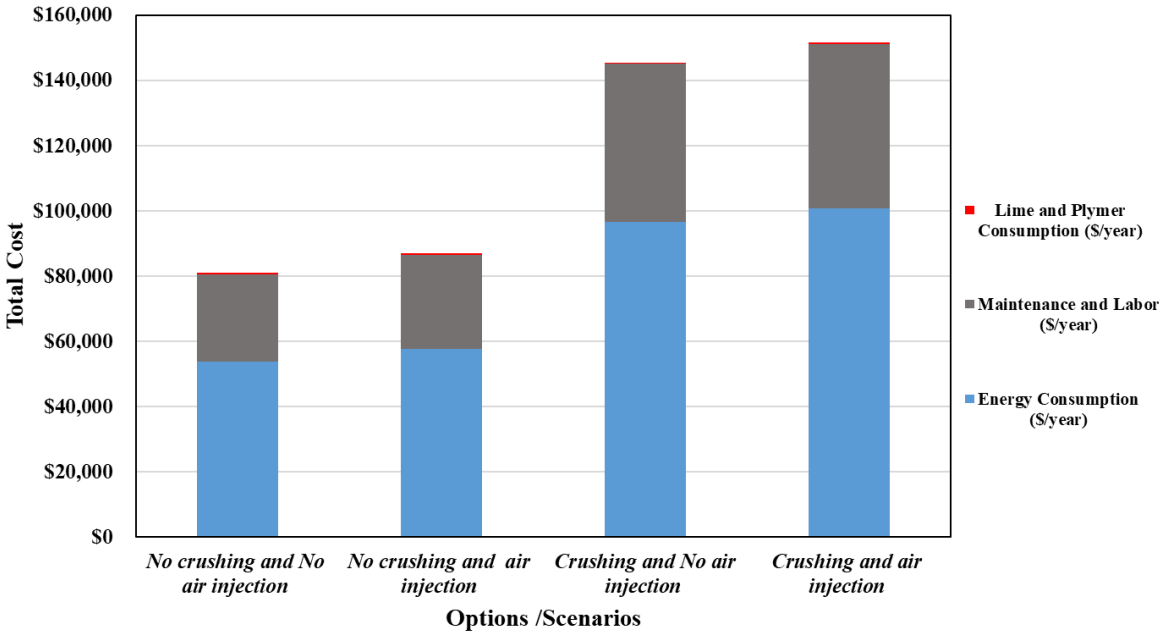


Figure 2.5.4: Operating cost estimates for four different heap pad scenarios.

Table 2.5.7: Cost of individual REEs contained in 1 million gallons of leachate after two leaching cycles that are approximately 4 months apart.

Individual REE	Phase 1- Leaching cycle 1	Phase 2 - Leaching cycle 2
	Cost	
Scandium	$11,023	$12,961
Yttrium	$107	$213
Lanthanum	$15	$30
Cerium	$63	$117
Praseodymium	$60	$111
Neodymium	$369	$675
Samarium	$33	$59
Europium	$199	$344
Gadolinium	$63	$106
Terbium	$197	$341
Dysprosium	$477	$815
Holmium	$82	$140
Erbium	$47	$80
Thulium	$83	$142
Ytterbium	$78	$129
Lutetium	$92	$152
Total Price	$12,987	$16,417

CONCLUSIONS

The experimental results successfully evaluated the hypothesis of this Project. Bench-scale leaching tests conducted to achieve the goal of the Project have confirmed that rare earth element (REE) and critical mineral (CM) concentrations in acid mine drainage (AMD) can be increased when AMD is used to leach coarse coal refuse (CCR) to develop a REE/CM pregnant leaching solution (PLS).

The Project successfully demonstrated that CCR can be managed to provide an economically attractive REE feedstock while controlling its long-term acid mine drainage (AMD) liability. We identified that leaching primarily occurred during the first leaching cycle, making the REE compounds readily available due to past weathering exposure. The discovery that weathered refuse has the best potential for REE extraction was a remarkable finding, as this refuse otherwise was discounted because it visually looked as the most exhausted type of the three coal refuse materials evaluated. Along with REE/CM, major metals (MM) (e.g., iron, aluminum) were also leached during the process.

Additional work conducted during the drum leaching tests provided more valuable conclusions. The extended drying period of approximately 4 months allowed for additional pyrite oxidation and doubles the amount of TREE within the PLS discharge. These findings are of particular relevance for abandoned, or closed and reclaimed coal mines, primarily due to the availability of the two major components: weathered refuse containing REE/CM and pyrite generating AMD. The implementation of heap leaching for manufacturing REE/CM at such sites could serve as a sustainable practice, helping to achieve multiple benefits, such as the responsible management

of tailing piles for REE/CM materials and mitigating the long-term environmental consequences of acid mine drainage generation.

We believe that the findings of this project support further expanding the overall REE/CM investigation into a pilot-scale heap leach demonstration using weathered CCR. Concurrent bench-scale testing to optimize individual site operational characteristics is advised before progressing to field-scale application. During this step, the essential criterion to determine the optimal drying duration can be determined for repeating maximizing TREE loads in the PLS.

The numerical modeling through PLAXIS LE showed that PLS flow within the heap structure was steady throughout the permeable and weathered coal refuse. Limit-equilibrium analysis for slope stability concluded that a balanced and surface uniform irrigation combined with slope toe reinforcement, results in a substantial role to maintaining slope stability.

We developed a site selection criteria process to assist with the selection of coal mine refuse sites that have beneficial or favorable site ground topography, deposit, and other characteristics to aid in the development of an engineering and operational design. Selecting the best candidate for constructing a leach pad was made possible through multi-criteria decision-making techniques (e.g. Analytical Hierarchy Process [AHP]). Blacksville #2 is recommended as the best option for any future potential operational scale-up of this project. Coal refuse tailings and AMD at the Crest Pond, available at the Hughes Hollow Impoundment, can be managed and used as part of the implemented design, which adds additional environmental measures to the site.

Abandoned coal mines are not considered a point source of pollution under the Clean Water Act because their source of pollution is not regulated. Therefore, their discharge creates a negative impact on groundwater and streams for extended periods. The developed criteria process could be easily applied to identify other sites suitable for leaching implementation, based on site characteristics and coal refuse age.

A significant conclusion to our research indicates that a design strategy can be applied to a coal refuse-based heap-leaching process to extract REEs and Critical Materials (CM) while ensuring pyrite oxidation through intentional drying periods, thereby maximizing REE production while exhausting the pyrite within the refuse resulting in minimizing the AMD environmental legacy.

REFERENCES

Agarwal, A., Datta, M., Ramana, G., and Satyakam, R. (2018). *Improving the slope stability of municipal solid waste dumps using reinforced soil berms: A case study*. 18–25.

AIRE 1. (2025). *Dewatering Bag*. https://www.aireenvironmental.com/product/dewatering-bag/?attribute_pa_size=15x45andgad_source=1andgclid=CjwKCAjwwLO_BhB2EiwAx2e-37NoFMaioXT1CmCkLskCKCTu-b62tMdfHK1tcJKel40kBIb73YV40xoChr8QAvD_BwE

AIRE 2. (2025). *DEWATERING BAG*. https://www.aireenvironmental.com/product/dewatering-bag/?attribute_pa_size=15x30andgad_source=4andgclid=CjwKCAjwwLO_BhB2EiwAx2e-3616jq0x45TVmpT_l9o3XGT4ic6B7EJYns9Qy_q2AQZR9NGW_d4AXBoC3W0QAvD_BwE

AIRE 3. (2025). *Dewatering Bag*. https://www.aireenvironmental.com/product/dewatering-bag/?attribute_pa_size=15x30andgad_source=4andgclid=CjwKCAjwwLO_BhB2EiwAx2e-3616jq0x45TVmpT_l9o3XGT4ic6B7EJYns9Qy_q2AQZR9NGW_d4AXBoC3W0QAvD_BwE

Airgas. (2025). *UltraTech 15’ X 15’ Black Non-Woven Geotextile Dewatering Bag*. https://www.airgas.com/product/Safety-Products/Environmental/Spill-Control-%26-Containment/p/U179727-O/S?s_kwcid=AL!10136!3!699041718616!!!g!2325932807754!andutm_arg=SEM:Google:GSN%20-%20Items%20-%20Safety%20Products-Environmental-COGSTier70:GSN%20Item%20-%20Other%20Brands-150-1000-Safety%20Products-Environmental-COGSTier70:pla:pla:Airgas:welding_products::U179727-O%2FS::PLAandgad_source=1andgclid=CjwKCAjwwLO_BhB2EiwAx2e-3zGGoxbgJbMIHJAASdVGZ1Rp-cRfD3MMw7J5rQ1a_EZ7mhoZ7d2bjRoCrTYQAvD_BwE

Aishred. (2025). *Crusher*. https://www.aishred.com/product/cone-crusher.html?utm_origin=shoppingandsrsltid=AfmBOorRPHPMQrK9FpF2VeUORyVjL6mpNpIHCx5d_cWJvO6ivv8qKKqSsM0

Ait Brahim, J., Ait Hak, S., Achiou, B., Boulif, R., Beniazza, R., and Benhida, R. (2022). Kinetics and mechanisms of leaching of rare earth elements from secondary resources. *Minerals Engineering*, *177*, 107351. https://doi.org/10.1016/j.mineng.2021.107351

Akcil, A., and Koldas, S. (2006). Acid Mine Drainage (AMD): Causes, treatment and case studies. *Journal of Cleaner Production*, *14*(12–13), 1139–1145.

Alibaba. (2025). *Heavy Duty Long Distance Large Capacity Belt Conveyor Machine for Coal/stone/sand Gravel*. https://www.alibaba.com/product-detail/Heavy-Duty-Long-Distance-Large-Capacity_60779551027.html

Allen, L., Zhang, Z., Sarswat, P., and Free, M. L. (2019). *Economic Extraction, Recovery, and Upgrading of Rare Earth Elements from Coal-Based Resources*. Google Docs.

https://drive.google.com/file/u/0/d/1TD_Gtis41P13XfMD2-lpiPdqWNcbLZIZ/view?usp=drive_webandpli=1andusp=embed_facebook

Angi. (2025). *What Are Average Gravel Prices? [2025 Data]*. https://www.angi.com/articles/gravel-prices.htm

Apelt, T., Forrester, K., Short, M., and Stefan, L. (2017). Determination of optimum heap height from column leach tests: 1. Model development and initial results. *Mineral Processing and Extractive Metallurgy*, *126*(3), 146–156. https://doi.org/10.1080/03719553.2016.1196520

ASTM, I. (2008). Standard test method for accelerated leach test for diffusive releases from solidified waste and a computer program to model diffusive, fractional leaching from cylindrical waste forms. *ASTM C1308*.

Basta, M. M., Rabie, M. H., Mansour, M. A., and Elbanna, W. M. (2024). A COMPARATIVE STUDY BETWEEN SOIL NAILING AND BERMS FOR SLOPE STABILIZATION: PERFORMANCE, AND ANALYSIS. *Engineering Research Journal*, *183*(3), 65–88.

Bigham, J., and Nordstrom, D. K. (2000). Iron and aluminum hydroxysulfates from acid sulfate waters. *Reviews in Mineralogy and Geochemistry*, *40*(1), 351–403.

Bird, I. (2024). *Design And Implementation of Large-Scale Hard Rock AMD Dewatering and REE Production*.

Bouffard, S. C. (2008). Application of the HeapSim model to the heap bioleaching of the Pueblo Viejo ore deposit. *Hydrometallurgy*, *93*(3–4), 116–123.

Bouffard, S. C., and Dixon, D. G. (2009). Modeling pyrite bioleaching in isothermal test columns with the HeapSim model. *Hydrometallurgy*, *95*(3–4), 215–226.

Brookhian, M., Golkar Hamzee Yazd, H. R., and Tavousi, M. (2022). An investigation of acid–base accounting test to predict acid mine drainage at Sangan iron ore mine in Khaf, Iran. *Environmental Earth Sciences*, *81*(13), 344. https://doi.org/10.1007/s12665-022-10434-5

Cao, S., Zhou, C., Pan, J., Liu, C., Tang, M., Ji, W., Hu, T., and Zhang, N. (2018). Study on influence factors of leaching of rare earth elements from coal fly ash. *Energy and Fuels*, *32*(7), 8000–8005.

Cavallo, B., and Ishizaka, A. (2023). Evaluating scales for pairwise comparisons. *Annals of Operations Research*, *325*(2), 951–965.

César, C., Parra, D., and Mendoza, J. (2014). Geomembrane and pipe design issues in deeper heap leach pads. *Proceedings Heap Leach Solutions*, 167–179.

Colín-Torres, C. G., Murillo- Jiménez, J. M., Del Razo, L. M., Sánchez-Peña, L. C., Becerra-Rueda, O. F., and Marmolejo-Rodríguez, A. J. (2014). Urinary arsenic levels influenced by abandoned mine tailings in the Southernmost Baja California Peninsula, Mexico. *Environmental Geochemistry and Health*, *36*(5), 845–854. https://doi.org/10.1007/s10653-014-9603-x

Currie, S., and Parra, D. (2010). *Leach pad design and construction issues in very steep slopes*. Proceedings of the 9th.

Daniels, W. L., Stewart, B. R., and Zipper, C. E. (2000). *Reclamation of Coal Refuse Disposal Areas*. (2018). 2018

Daniels, W. L., Stewart, B. R., and Zipper, C. E. (2018). *Reclamation of coal refuse disposal areas*.

D'Appolonia. (2009a). *Engineering and Design Manual: Coal Refuse Disposal Facilities*. US Department of the Interior, Mining Enforcement and Safety Administration.

D'Appolonia. (2009b). *Engineering and Design Manual: Coal Refuse Disposal Facilities*. US Department of the Interior, Mining Enforcement and Safety Administration.

Darko, A., Chan, A. P. C., Ameyaw, E. E., Owusu, E. K., Pärn, E., and Edwards, D. J. (2019). Review of application of analytic hierarchy process (AHP) in construction. *International Journal of Construction Management*, *19*(5), 436–452.

Das, B. (2010). *Principles of geotechnical engineering, 7th edn. Cengage Learning*.

Das, B. M. (2021). *Principles of geotechnical engineering*. Cengage learning.

Das, S., Gaustad, G., Sekar, A., and Williams, E. (2018). Techno-economic analysis of supercritical extraction of rare earth elements from coal ash. *Journal of Cleaner Production*, *189*, 539–551.

Dimitriou, I. (2013). *Techno-economic assessment and uncertainty analysis of thermochemical processes for second generation biofuels*.

Dixon, D., and Petersen, J. (2003). *Comprehensive modelling study of chalcocite column and heap bioleaching*. *6*, 493–516.

Dlamini, Z. (2015). *A techno-economic comparison of three process routes for the treatment of Gamsberg zinc ore*. http://hdl.handle.net/11427/13677

Dompierre, K., Castonguay, V., and Kelln, C. (2023). *3D seepage and slope stability assessment of a heap leach pad*.

Dripdepot. (2023). *Netafim SpinNet Sprinkler w/Check Valve*. https://www.dripdepot.com/spinnet-sprinkler-w-check-valve-diameter-18-feet-flow-rate-18-4-gallons-per-hour-trajectory-low

Eppes, M.-C. (Missy). (2022). Mechanical Weathering: A Conceptual Overview. In *Treatise on Geomorphology* (pp. 30–45). Elsevier. https://doi.org/10.1016/B978-0-12-818234-5.00200-5

Erickson, J., and Breckenridge, J. L. (2025). *Investigation of a Heap Leach Facility leak using Finite Element Seepage Analysis*.

Ewing. (2025). *Perforated flexible tubing (450 mm) $/30 m ($/100 feet)*. https://www.ewingoutdoorsupply.com/25201180-18-in-x-20-ft-corrugated-n-12slotted-perforated-pipe

Fabiańska, M., Ciesielczuk, J., Szczerba, M., Misz-Kennan, M., Więcław, D., Szram, E., Nádudvari, Á., and Ciesielska, Z. (2024). Weathering alterations of coal mining wastes geochemistry, petrography, and mineralogy, a case study from the Janina and Marcel Coal Mines, Upper Silesian Coal Basin (Poland). *International Journal of Coal Geology*, *281*, 104407.

Fosu, S., Owusu, C., Ntsiful, F., and Ackah, K. (2020). Determining Acid and Metalliferous Drainage Potential of Waste Rock on a Mine. *Ghana Mining Journal*, *20*(2), 49–59.

Fredlund, D. G., and Xing, A. (1994). Equations for the soil-water characteristic curve. *Canadian Geotechnical Journal*, *31*(4), 521–532.

Fredlund, D. G., Xing, A., and Huang, S. (1994). Predicting the permeability function for unsaturated soils using the soil-water characteristic curve. *Canadian Geotechnical Journal*, *31*(4), 533–546.

Fredlund, D.G., Rahardjo, H., and Fredlund, M.D. (2012). *Unsaturated soil mechanics in engineering practice*.

Free, M. (2020). *Economic Extraction, Recovery and Upgrading of Rare Earth Elements from Coal-Based Resources*. Univ. of Utah, Salt Lake City, UT (United States).

Gaikwad, R., and Gupta, D. (2007). Acid mine drainage (AMD) management. *Journal of Industrial Pollution Control*, *23*(2), 285–297.

Galla, V., van Zyl, D., Morrow, S., and Fourie, A. B. (2008). *Evaluating Unsaturated Flow of Heap Leach Materials in Large Diameter Column Tests* (pp. 193–206). Australian Centre for Geomechanics. Rock Dumps 2008: First International Seminar on the Management of Rock Dumps, Stockpiles and Heap Leach Pads, 2008 5-6 March, Perth. https://doi.org/10.36487/ACG_repo/802_17

Geidel, G. (1979). Alkaline and acid production potentials of overburden material: The rate of release. *Reclam. Rev.;(United States)*, *2*(3/4).

Ghorbani, Y., Franzidis, J.-P., and Petersen, J. (2016). Heap Leaching Technology—Current State, Innovations, and Future Directions: A Review. *Mineral Processing and Extractive Metallurgy Review*, *37*(2), 73–119. https://doi.org/10.1080/08827508.2015.1115990

Gilmore Kramer Company. (2025). *Conveyor*. https://gilmorekramer.com/pc-11-10-16-20-parts-conv-11ftoal-10ftlbed-16inwbelt-20inwbed-100852.html

Goepel, K. D. (2019). Comparison of judgment scales of the analytical hierarchy process—A new approach. *International Journal of Information Technology and Decision Making*, *18*(02), 445–463.

Hegazy, Y., Cushing, A., and Lewis, C. (2004). Physical, mechanical, and hydraulic properties of coal refuse for slurry impoundment design. *D'Appolonia Engineering*.

Honaker, R., Hower, J., Eble, C., Weisenfluh, J., Groppo, J., Rezaee, M., Bhagavatula, A., Luttrell, G., Bratton, R., and Kiser, M. (2014). Laboratory and bench-scale testing for rare earth elements. *Cell*, *724*, 554–3652.

Honaker, R., Werner, J., Yang, X., Zhang, W., Noble, A., Yoon, R.-H., Luttrell, G., and Huang, Q. (2021). *Pilot-scale testing of an integrated circuit for the extraction of rare earth minerals and elements from coal and coal byproducts using advanced separation technologies*. Univ. of Kentucky, Lexington, KY (United States).

Honaker, R., Zhang, W., Yang, X., and Rezaee, M. (2018). Conception of an integrated flowsheet for rare earth elements recovery from coal coarse refuse. *Minerals Engineering*, *122*, 233–240. https://doi.org/10.1016/j.mineng.2018.04.005

HOP. (2025). *25’ x 60’ 30-Mil LLDPE Pond Liner—HOPLDP25X060-30*. https://halfoffponds.com/half-off-ponds-25-ft-x-60-ft-30-mil-lldpe-pond-liner/?setCurrencyId=1andsku=HOPLDP25X060-30andgad_source=1andgclid=Cj0KCQjwy46_BhDOARIsAIvmcwN5CA7SSRy4qIEoJ3ksfxD80rMGVJn26uybqKDwm_6KBdAEbqsXFakaAkFVEALw_wcB

Houde, Z. R. (2024). *Acid Mine Drainage sludge and Rare Earth Element Hydraulic Preconcentrate precipitate filtration and dewatering characterization for enhanced dewatering*.

Huang, S., Barbour, S., and Fredlund, D. (1998). Development and verification of a coefficient of permeability function for a deformable unsaturated soil. *Canadian Geotechnical Journal*, *35*(3), 411–425.

Hudson-Edwards, K. A., Kemp, D., Torres-Cruz, L. A., Macklin, M. G., Brewer, P. A., Owen, J. R., Franks, D. M., Marquis, E., and Thomas, C. J. (2024). Tailings storage facilities, failures and disaster risk. *Nature Reviews Earth and Environment*, *5*(9), 612–630.

Iasillo, E., Rempel, C., and Holtzapple, A. (2013). Development of accurate metal production forecasts for a heap leach project using METSIM® dynamic simulation and defensible column leach testing data. *Heap Leach Solutions 2013*, 22–25.

Inabah, R. F., and Sukamta, S. (2025). Slope Stability Analysis with Bore Piles for Landslide Prevention Using Plaxis LE 2D. *TEKNIK*, *46*(2), 96–102.

Jain, K. R., Edraki, M., and McIntyre, N. (2021). Controls of Wetting and Drying Cycles on Salt Leaching from Coal Mine Spoils. *Water, Air, and Soil Pollution*, *232*(11), 472. https://doi.org/10.1007/s11270-021-05422-7

Jämsä-Jounela, S.-L. (2001). Current status and future trends in the automation of mineral and metal processing. *Control Engineering Practice*, *9*(9), 1021–1035.

Jedari, C., Palomino, A. M., and Drumm, E. C. (2018). Compressibility of fine coal refuse. In *IFCEE 2018* (pp. 455–462).

John, L. (2011). The art of heap leaching—The fundamentals. *Percolation Leaching: The Status Globally and in Southern Africa. Misty Hills: The Southern African Institute of Mining and Metallurgy (SAIMM)*, 17–42.

Kappes, D. W. (2002). Precious metal heap leach design and practice. *Proceedings of the Mineral Processing Plant Design, Practice, and Control*, *1*, 1606–1630.

Kay, D., and Panayides, S. (2023). *Automation of slope stability and rock berm support design*. SUT-OSIG.

Koerner, R. M. (2012). *Designing with geosynthetics-Vol. 1* (Vol. 1). Xlibris Corporation.

Kuppusamy, V. K., and Holuszko, M. (2022). Sulfuric acid baking and water leaching of rare earth elements from coal tailings. *Fuel*, *319*, 123738.

Lane, T., Harvey, T., Moritz, R., Samari, H., and Breckenridge, L. (2021). *PRELIMINARY ECONOMIC ASSESSMENT NI 43-101 TECHNICAL REPORT*. Granite Creek Mine Project Humboldt County, Nevada, USA

Lange, C. N., Camargo, I. M. C., Figueiredo, A. M. G. M., Castro, L., Vasconcellos, M. B. A., and Ticianelli, R. B. (2017). A Brazilian coal fly ash as a potential source of rare earth elements. *Journal of Radioanalytical and Nuclear Chemistry*, *311*(2), 1235–1241. https://doi.org/10.1007/s10967-016-5026-8

Leahy, M. J., Schwarz, M. P., and Davidson, M. R. (2006). An air sparging CFD model for heap bioleaching of chalcocite. *Applied Mathematical Modelling*, *30*(11), 1428–1444.

Li, X., Zhang, L., and Fredlund, D. (2009). Wetting front advancing column test for measuring unsaturated hydraulic conductivity. *Canadian Geotechnical Journal*, *46*(12), 1431–1445.

Lin, R., Howard, B. H., Roth, E. A., Bank, T. L., Granite, E. J., and Soong, Y. (2017). Enrichment of rare earth elements from coal and coal by-products by physical separations. *Fuel*, *200*, 506–520. https://doi.org/10.1016/j.fuel.2017.03.096

Lizama, H. M., Harlamovs, J. R., McKay, D. J., and Dai, Z. (2005). Heap leaching kinetics are proportional to the irrigation rate divided by heap height. *Minerals Engineering*, *18*(6), 623–630. https://doi.org/10.1016/j.mineng.2004.12.012

LOWE'S. (2025). *ADS 4-in x 10-ft Corrugated Perforated Pipe*. https://www.lowes.com/pd/ADS-4-in-x-10-ft-Corrugated-Perforated-Pipe/50163591?store=567andcm_mmc=shp-_-c-_-prd-_-plb-_-ggl-_-CRP_SHP_LIA_PLB_Online_C-D-_-50163591-_-local-_-0-_-0andgad_source=1andgclid=Cj0KCQjwqIm_BhDnARIsAKBYcmvwlJrebbm2A8gZs0fWIq-6Rnor6bGa7o4a5h-mIYTqDqCKduQ6gC4aAp6cEALw_wcBandgclsrc=aw.ds

Lupo, J. F. (2010). Liner system design for heap leach pads. *Geotextiles and Geomembranes*, *28*(2), 163–173.

Luttrell, G. H., Kiser, M. J., Yoon, R.-H., Bhagavatula, A., Rezaee, M., and Honaker, R. Q. (2016). *Concentrations of Rare Earth Elements Generated by US Coal Preparation Plants*. 35–41.

Marsden, J., and Botz, M. (2017). Heap leach modeling—A review of approaches to metal production forecasting. *Minerals and Metallurgical Processing*, *34*(2), 53–64.

McBride, D., Cross, M., and Gebhardt, J. E. (2012). Heap leach modeling employing CFD technology: A 'process' heap model. *Minerals Engineering, Computational Modelling*, *33*, 72–79. https://doi.org/10.1016/j.mineng.2011.10.003

McBride, D., Gebhardt, J., Croft, N., and Cross, M. (2018). Heap leaching: Modelling and forecasting using CFD technology. *Minerals*, *8*(1), 9.

Menards. (2025). *Perforated flexible tubing 100 mm (4inches) $/100 feet*. https://www.menards.com/main/plumbing/pipe-fittings/corrugated-pipe-fittings/4-x-100-yellow-8-slot-perforated-single-wall-corrugated-tubing/sw04x100y8slot/p-1642874324021793-c-9568.htm

Merkus, H. G. (2009). *Particle size measurements: Fundamentals, practice, quality* (Vol. 17). Springer Science and Business Media.

Nagar S, M., F A El-Sayed, W M Morsy, A H Mady, A M Mohamed, and K F Mahmoud. (2020). Capability of Uranium Heap Leaching From Gattar and El Missikat Area, Eastern Desert, Egypt: A Kinetic Approach. *Journal of Engineering and Applied Sciences Technology*, *2*(4), 1–7. https://doi.org/10.47363/JEAST/2020(2)115

Nasab, S. K., Hojat, A., and Fard, M. M. (2007). Technical factors for selecting optimum heap leach pad sites. *EandM. J*, 54–59.

Neupane, G., and Donahoe, R. J. (2013). Leachability of elements in alkaline and acidic coal fly ash samples during batch and column leaching tests. *Fuel, 10th Japan/China Symposium on Coal and C1 Chemistry*, *104*, 758–770. https://doi.org/10.1016/j.fuel.2012.06.013

NOAA. (2025). *National Oceanic and Atmospheric Administration (NOAA).* https://hdsc.nws.noaa.gov/pfds/

O'Brien, T. M., and Alonso, E. (2025). A simplified rare earth element mining project cost estimator-a new tool for evaluating future mine supply. *Mineral Economics*, *38*(2), 237–252.

Paramount Materials. (2025). *Mirafi 1100NC Geotextile Fabric—15' x 300' Roll—TenCate*. https://www.paramountmaterials.com/products/mirafi-1100nc-geotextile-fabric-15-x-300-roll-tencate?variant=51983241412andcountry=USandcurrency=USDandutm_medium=product_syncandutm_source=googleandutm_content=sag_organicandutm_campaign=sag_organicandsrsltid=AfmBOoqbo3maGicbSbjhccG9Tgjr6gyGzegnYL9u7_iob8m2GZ2EqcN4B64andgQT=1

pdblowers. (2025). *Blower*. https://www.pdblowers.com/product/824-rcs-rotary-lobe-blower/

Peters, M. S., Timmerhaus, K. D., and West, R. E. (2003). *Plant Design and Economics for Chemical Engineers* (5th ed.). McGraw-Hill.

Petersen, J., and Dixon, D. G. (2007). Modeling and optimization of heap bioleach processes. In *Biomining* (pp. 153–176). Springer.

Piésold, K. (2012). *FEASIBILITY DESIGN OF THE HEAP LEACH FACILITY*. *Casino Mining Corporation 2050-1111 West Georgia St. Vancouver, BC V6E 4M3*.

PLAXIS LE. (2023). *Bentley Systems* [Computer software]. https://www.bentley.com/software/plaxis-2d/

Pope, J., Bayless, E., Olyphant, G., and Branam, T. (2012). The role of efflorescent sulfate salts in Indiana's mine water quality. *Effects of Abandoned Mine Land Reclamation on Ground and Surface Water Quality: Research and Case Histories from Indiana*, 259–279.

Potter, G. M. (1981). Design factors for heap leaching operations. *Min. Eng.*, *33*(3), 277–281.

Pourverdi, A., Doulati Ardejani, F., Maghsoudy, S., Kafi, R., and Taherdangkoo, R. (2025). Coupled hydro-mechanical analysis and stabilization of a failing heap leaching structure. *Bulletin of Engineering Geology and the Environment*, *84*(11), 1–16.

PumpProducts. (2019). *Goulds 25SH10A1ZD3G2, Centrifugal Pump*. https://www.pumpproducts.com/goulds-25sh10a1zd3g2-centrifugal-pump-e-sh-m-group-series-100-hp-460-volts-3-phase-3500-rpm-2-1-2-discharge-3-suction-10-38-impeller-dppe-enclosure-690-gpm-max-465-ft-max-head.html?campaignid=1764756950andadgroupid=68060857119anddevice=candkeyword=25SH10A1ZD3G2andnetwork=gandmatchtype=andgad_source=1andgclid=CjwKCAjwwLO_BhB2EiwAx2e-34FNjxvhv1DFADMoHGWUYZ0D_nLyCdxJOrNcq3mPEJd_dae0LTxs2BoCNf4QAvD_BwE

Pyper, R., Seal, T., Uhrie, J. L., and Miller, G. C. (2019). Dump and heap leaching. *SME Mineral Processing and Extractive Metallurgy Handbook*, 1207–1224.

Qin, W., Li, W., Lan, Z., and Qiu, G. (2007). Simulated small-scale pilot plant heap leaching of low-grade oxide zinc ore with integrated selective extraction of zinc. *Minerals Engineering*, *20*(7), 694–700. https://doi.org/10.1016/j.mineng.2007.01.004

Quaranta, J. D., and Tolikonda, R. (2011). Design of non-woven geotextiles for coal refuse filtration. *Geotextiles and Geomembranes*, *29*(6), 557–566. https://doi.org/10.1016/j.geotexmem.2011.07.004

Quast, K., Xu, D., Skinner, W., Nosrati, A., Hilder, T., Robinson, D. J., and Addai-Mensah, J. (2013). Column leaching of nickel laterite agglomerates: Effect of feed size. *Hydrometallurgy*, *134–135*, 144–149. https://doi.org/10.1016/j.hydromet.2013.02.001

Reyes, A., Garma, P., and Parra, D. (2014). 3D slope stability analysis of heap leach pads using the limit equilibrium method. *Lima, Peru, InfoMine*.

Roth, D., Bernudez, B., McNaughton, J., Pennington, J. B., Smith, J., Sepulveda, D., and Baker, R. (2018). *Gold Bar Project-Form 43-101F1 Technical Report-Feasibility Study*.

Ruan, Z., Li, M., Gao, K., Zhang, D., Huang, L., Xu, W., and Liu, X. (2019). Effect of particle size refinement on the leaching behavior of mixed rare-earth concentrate using hydrochloric acid. *ACS Omega*, *4*(6), 9813–9822.

Saaty, T. L. (1977). A scaling method for priorities in hierarchical structures. *Journal of Mathematical Psychology*, *15*(3), 234–281.

Safari, V., Arzpeyma, G., Rashchi, F., and Mostoufi, N. (2009). A shrinking particle—Shrinking core model for leaching of a zinc ore containing silica. *International Journal of Mineral Processing*, *93*(1), 79–83.

Silt Management Supplies, LLC. (2025). *Non-Woven Geotextile Fabrics, Various Strengths and Sizes*. https://www.siltmanagementsupplies.com/non-ntpep-non-woven-needle-punched-geotextile-fabr.html?id=39297198andquantity=1

Skousen, J. G., Sexstone, A., and Ziemkiewicz, P. F. (2000a). Acid mine drainage control and treatment. *Reclamation of Drastically Disturbed Lands*, *41*, 131–168.

Skousen, J., Perry, E., Leavitt, B., Sames, G., Chisolm, W., Cecil, C., and Hammack, R. (2000b). Prediction of Water Quality at Surface Coal Mines. Chapter 4: Static Tests for Coal Mining Acid Mine Dainage Prediction in the Eastern US. *The National Mine Land Reclamation Center Located at West Virginia University*, 73–98.

Skousen, J. G., Ziemkiewicz, P. F., and McDonald, L. M. (2019). Acid mine drainage formation, control and treatment: Approaches and strategies. *The Extractive Industries and Society*, *6*(1), 241–249.

Skousen, J., Simmons, J., McDonald, L. M., and Ziemkiewicz, P. (2002). Acid–Base Accounting to Predict Post-Mining Drainage Quality on Surface Mines. *Journal of Environmental Quality*, *31*(6), 2034–2044. https://doi.org/10.2134/jeq2002.2034

Smith, M., Parra, D., and Asociados, A. (2014). Leach pad cost benchmarking. *Proceedings of Heap Leach Solutions*.

Smith, T. (2023). Condition and Modeling Assessment of Geomorphic Landform Design on Coal Refuse Impoundments. *Graduate Theses, Dissertations, and Problem Reports*. https://doi.org/10.33915/etd.11725

Soltani-Mohammadi, S., and Amini, M. (2013). Optimal site selection for heap leaching structures by the analytic hierarchy process (case study: Taft heap leaching structure, Iran). *Gospodarka Surowcami Mineralnymi*, *29*(1), 109–125.

Sophocleous, M. (2010). Understanding and explaining surface tension and capillarity: An introduction to fundamental physics for water professionals. *Hydrogeology Journal*, *18*(4), 811.

Stamboliadis, E., Alevizos, G., and Zafiratos, J. (2004). Leaching residue of nickeliferous laterites as a source of iron concentrate. *Minerals Engineering, Processing and Disposal of Minerals Industry Waste '03*, *17*(2), 245–252. https://doi.org/10.1016/j.mineng.2003.08.015

Steemson, M., and Smith, M. (2009). *THE DEVELOPMENT OF NICKEL LATERITE HEAP LEACH PROJECTS*.

Stevens, J. R. (2016). *Geotechnical testing and finite element modeling of geomorphic landform design with a multi-layer cap and cover system*. West Virginia University.

Stewart, B. R. (1990). *Physical and chemical properties of coarse coal refuse from southwest Virginia*.

Sun, Z., Xie, X., Wang, P., Hu, Y., and Cheng, H. (2018). Heavy metal pollution caused by small-scale metal ore mining activities: A case study from a polymetallic mine in South China. *Science of The Total Environment*, *639*, 217–227. https://doi.org/10.1016/j.scitotenv.2018.05.176

Tang, M., and Esmaeili, K. (2021). Heap leach pad surface moisture monitoring using drone-based aerial images and convolutional neural networks: A case study at the El Gallo Mine, Mexico. *Remote Sensing*, *13*(8), 1420.

Tech, T. (2012). *Heap Leach Facility Feasibility Design Eagle Gold Project*.

Tech, T. (2017). HEAP LEACH AND PROCESS FACILITIES PLAN. *EAGLE GOLD PROJECT*.

TenCate. (2025). *Mirafi®1100 N technical data sheet.* https://www.solmax.com/us/en/resources/mirafi-1100n-tds.

Tezyapar Kara, I., Wagland, S. T., and Coulon, F. (2024). Techno-economic assessment of bioleaching for metallurgical by-products. *Journal of Environmental Management*, *358*, 120904. https://doi.org/10.1016/j.jenvman.2024.120904

The HOME DEPOT. (2025). *1/4 in. O.D. x 0.170 in. I.D. x 25 ft. Natural Polyethylene Tubing*. https://www.homedepot.com/p/UDP-1-4-in-O-D-x-0-170-in-I-D-x-25-ft-Natural-Polyethylene-Tubing-T16007001/304185139

Tolikonda, R. (2010). *Nonwoven Geotextile Filtration Performance with Coal Refuse*.

Tolikonda, R., and Quaranta, J. D. (2012). Environmental factors affecting geotextile filter design in coal refuse impoundments. *International Journal of Mining, Reclamation and Environment*, *26*(2), 163–181.

Torres Hernandez, G. (2011). *Estimating the soil-water characteristic curve using grain size analysis and plasticity index*. Arizona State University.

Tyson, J. G. (2023). *Laboratory Experimentation and Numerical Modeling to Enhance Drainage in Geotextile Tubes*. West Virginia University.

USDOE. (2011). *Critical materials strategy*. DIANE publishing.

Van Staden, P., and Petersen, J. (2018). The effects of simulated stacking phenomena on the percolation leaching of crushed ore, Part 1: Segregation. *Minerals Engineering*, *128*, 202–214.

Vass, C. R., Noble, A., and Ziemkiewicz, P. F. (2019). The occurrence and concentration of rare earth elements in acid mine drainage and treatment by-products: Part 1—Initial survey of the Northern Appalachian Coal Basin. *Mining, Metallurgy and Exploration*, *36*(5), 903–916.

Wang, L., Yin, S., and Wu, A. (2021). Ore agglomeration behavior and its key controlling factors in heap leaching of low-grade copper minerals. *Journal of Cleaner Production*, *279*, 123705.

Wang, P., Sun, Z., Hu, Y., and Cheng, H. (2019). Leaching of heavy metals from abandoned mine tailings brought by precipitation and the associated environmental impact. *Science of The Total Environment*, *695*, 133893. https://doi.org/10.1016/j.scitotenv.2019.133893

Whitehorse, Y. (2012). *EAGLE GOLD PROJECT*.

Xiao, Y., Chen, Y., Feng, Z., Huang, X., Huang, L., Long, Z., and Cui, D. (2015). Leaching characteristics of ion-adsorption type rare earths ore with magnesium sulfate. *Transactions of Nonferrous Metals Society of China*, *25*(11), 3784–3790. https://doi.org/10.1016/S1003-6326(15)64022-5

Yang, X. (2019a). *Leaching characteristics of rare earth elements from bituminous coal-based sources*.

Yang, X. (2019b). LEACHING CHARACTERISTICS OF RARE EARTH ELEMENTS FROM BITUMINOUS COAL-BASED SOURCES. *Theses and Dissertations--Mining Engineering*. https://doi.org/10.13023/etd.2019.229

Yang, X., and Honaker, R. Q. (2020). Leaching Kinetics of Rare Earth Elements from Fire Clay Seam Coal. *Minerals*, *10*(6), 491. https://doi.org/10.3390/min10060491

Yang, X., Werner, J., and Honaker, R. (2019). Leaching of rare Earth elements from an Illinois basin coal source. *Journal of Rare Earths*, *37*(3), 312–321.

Yin, S., Wang, L., Chen, X., and Wu, A. (2021). Agglomeration and leaching behaviors of copper oxides with different chemical binders. *International Journal of Minerals, Metallurgy and Materials*, *28*, 1127–1134.

Yıldırım, B. C. (2019). *A New pairwise comparison scale for analytic hierarchy process*.

Zhang, W., and Honaker, R. Q. (2018). Rare earth elements recovery using staged precipitation from a leachate generated from coarse coal refuse. *International Journal of Coal Geology*, *195*, 189–199. https://doi.org/10.1016/j.coal.2018.06.008

Zhang, W., Yang, X., and Honaker, R. Q. (2018). Association characteristic study and preliminary recovery investigation of rare earth elements from Fire Clay seam coal middlings. *Fuel*, *215*, 551–560. https://doi.org/10.1016/j.fuel.2017.11.075

Zhu, C., Qu, S., Zhang, J., Wang, Y., and Zhang, Y. (2017). Distribution, occurrence and leaching dynamic behavior of sodium in Zhundong coal. *Fuel*, *190*, 189–197.

Ziemkiewicz, P. (2021). *Production of Rare Earth Products and Critical Minerals from Coal-Based Resources at an Engineering Prototype Scale* [National Energy Technology Lab U.S. Department of Energy].

Ziemkiewicz, P., He, T., and Noble, A. (2016). *Recovery of rare earth elements (REEs) from coal mine drainage*.

Ziemkiewicz, P., Hoffman, D., and Noble, A. (2023). *Development and Testing of an Integrated Acid Mine Drainage (AMD) Treatment and Rare Earth/Critical Mineral Plant*. West Virginia Univ., Morgantown, WV (United States).

Ziemkiewicz, P., Liu, X., and Noble, A. (2018). REE identification and characterization of coal and coal by-products containing high rare earth element concentrations. *Final Report, US Department of Energy, FE0026444-Final-Report-092618. Pdf*.

APPENDIX A – COLUMN LEACHING TESTS

Table 1A: Different sizes of columns used in the literature.

Reference	Size of Columns		Amount of material used
	Diameter (cm)	Length (cm)	Kg
(Allen et al., 2019)	4	30	0.65
(Wang et al., 2019)	4	19	0.018
(Nagar S et al., 2020)	5	100	-
(Iasillo et al., 2013)	7.5	160	10
(Neupane and Donahoe, 2013)	8.7	40.6	0.95
(Neupane and Donahoe, 2013)	8.7	40.6	1.125
(Stamboliadis et al., 2004)	10	100	11
(Quast et al., 2013)	12.5	200	5
(Qin et al., 2007)	20	400	100
(Steemson and Smith, 2009)	20	300 to 800	-
(Steemson and Smith, 2009)	20	300 to 800	-
(Allen et al., 2019)	20.32	182.88	50
(Apelt et al., 2017)	38	260	-
(Galla et al., 2008)	130	200	-
(McBride et al., 2012)	200	300	17,000



Figure 1A: Masterflex L/S digital pump used in the column leaching test.

Table 2A: Volumes of raw AMD, recirculated AMD, and H_2O_2 used as part of leachant in different columns (weeks 1 through 6).

Column	Week	Volume raw AMD (mL)	Volume recirc AMD (mL)	Volume H202 (mL)	Volume water (mL)
	1	1000	0	--	--
	2	400	600	--	--
	3	325	675	--	--
AMD-W	5-c1	360	640	--	--
	5-c2	200	800	--	--
	6-c1	20	980	--	--
	6-c2	200	800	--	--
	1	1000	0	--	--
	2	500	500	--	--
	3	325	675	--	--
AMD-F	5-c1	325	675	--	--
	5-c2	200	800	--	--
	6-c1	0	1000	--	--
	6-c2	160	840	--	--
	1	--	--	--	1000
	2	--	--	--	1000
	3	--	--	--	1000
DI-W	5-c1	--	--	--	1000
	5-c2	--	--	--	1000
	6-c1	--	--	--	1000
	6-c2	--	--	--	1000
	1	--	--	--	1000
	2	--	--	--	1000
	3	--	--	--	1000
DI-F	5-c1	--	--	--	1000
	5-c2	--	--	--	1000
	6-c1	--	--	--	1000
	6-c2	--	--	--	1000
	1	1000	0	0	--
	2	275	625	100	--
	3	275	625	100	--
H2O2-W	5-c1	300	600	100	
	5-c2	150	750	100	
	6-c1	0	900	100	
	6-c2	90	810	100	
	1	1000	0	0	--
	2	350	550	100	--
	3	320	580	100	--
H2O2-F	5-c1	410	490	100	--
	5-c2	200	700	100	--
	6-c1	10	890	100	--
	6-c2	110	790	100	--



Figure 2A. 250 mL of leachate collected from beakers after the termination of the test to be sent to analytical lab.

Table 3A: Volumes of raw and recirculated AMD used as part of the leachant in column AMD-R (10 leaching cycles).

Column	Cycle	Volume raw AMD (mL)	Volume recirc AMD (mL)
AMD-R	1	1000	0
	2	400	600
	3	50	950
	4	50	950
	5	0	1000
	6	110	890
	7	0	1000
	8	40	960
	9	25	975
	10	0	1000

Table 1A: Amount of CCR used to fill each of the two drums.

Drum #	Bucket +CCR (lb.)	Empty Bucket (lb.)	CCR (lb.)
Drum 1	25.52	1.83	23.7
	32.33	2.51	29.8
	33.65	1.85	31.8
	45.76	1.80	44.0
	29.27	2.18	27.1
	35.57	1.79	33.8
	41.31	2.14	39.2
	29.73	1.55	28.2
	31.62	1.56	30.1
	46.75	1.85	44.9
	18.40	1.85	16.6
	28.68	1.81	26.9
Sum			375.9
Drum 2	45.60	1.76	43.8
	20.18	2.57	17.6
	33.48	1.57	31.9
	34.00	2.21	31.8
	39.27	1.80	37.5
	40.05	1.85	38.2
	44.98	1.87	43.1
	41.90	1.60	40.3
	40.48	1.57	38.9
	41.90	1.57	40.3
Sum			363.5



Figure 3A: Leachate collected from discharge buckets after the end of the first cycle of the drum leaching tests (phase 1-leaching cycle 1).

Table 2A: Volumes of raw and recirculated AMD used as part of leachant in two drums-Phase 1 (weeks 1 through 3).

Drum #	Week	Volume raw AMD (L)	Volume recirc AMD (L)
Drum 1	1	22.7	0.0
	2	10.7	12.0
	3	1.60	21.1
Drum 2	1	22.7	0.0
	2	9.70	13.0
	3	1.20	21.5



Figure 4A: Leachate collected from discharge buckets at the end of the first leaching cycle (phase 2-leaching cycle 1).

Table 6A: Column leaching test TREE results.

Column	Week	Refuse TREE concentration (mg/kg)[1]	Leachant TREE concentration (ug/L)[2,3]	Leachate TREE concentration (ug/L)[4]	Increase in TREE concentration (ug/L)	Increase in TREE concentration (%)	Cumulative percent leached from solid (%)	TREE loading (lb/ac-ft)	TREE load (lb)
AMD-W	0	263.383	1,650	0	--	--	--	4	13
	1	--	1,650	5,810	4,160	252	1.58	16	47
	2	--	4,146	5,941	1,796	43	1.63	16	48
	3	--	4,547	5,719	1,173	26	1.55	15	46
	5-c1	--	4,254	--	--	--	--	--	--
	5-c2	--	4,906	--	--	--	--	--	--
	6-c1	--	5,638	--	--	--	--	--	--
	6-c2	--	4,906	5,881	975	20	1.61	16	48
AMD-F	0	281.31	1,650	0	--	--	--	4	13
	1	--	1,650	4,583	2,933	178	1.04	12	37
	2	--	3,116	4,050	934	30	0.85	11	33
	3	--	3,270	3,889	619	19	0.80	11	32
	5-c1	--	3,161	--	--	--	--	--	--
	5-c2	--	3,441	--	--	--	--	--	--
	6-c1	--	3,889	--	--	--	--	--	--
	6-c2	--	3,531	3,992	461	13	0.83	11	32
DI-W	0	263.383	0	0	--	--	--	0	0
	1	--	0	3,963	3,963	--	1.50	11	32
	2	--	0	2,565	2,565	--	0.97	7	21
	3	--	0	2,037	2,037	--	0.77	6	17
	5-c1	--	0	--	--	--	--	--	--
	5-c2	--	0	--	--	--	--	--	--
	6-c1	--	0	--	--	--	--	--	--
	6-c2	--	0	1,032	1,032	--	0.39	3	8
DI-F	0	281.31	0	0	--	--	--	0	0
	1	--	0	1,837	1,837	--	0.65	5	15
	2	--	0	1,297	1,297	--	0.46	4	11
	3	--	0	957	957	--	0.34	3	8
	5-c1	--	0	--	--	--	--	--	--
	5-c2	--	0	--	--	--	--	--	--
	6-c1	--	0	--	--	--	--	--	--
	6-c2	--	0	554	554	--	0.20	2	5
H_2O_2-W	0	263.383	1,650	0	--	--	--	4	13
	1	--	1,650	5,424	3,774	229	1.43	15	44
	2	--	3,844	5,816	1,972	51	1.58	16	47
	3	--	4,089	5,705	1,616	40	1.54	15	46
	5-c1	--	3,918	--	--	--	--	--	--
	5-c2	--	4,526	--	--	--	--	--	--
	6-c1	--	5,134	--	--	--	--	--	--
	6-c2	--	4,770	6,178	1,409	30	1.72	17	50
H_2O_2-F	0	281.31	1,650	0	--	--	--	4	13
	1	--	1,650	3,565	1,915	116	0.68	10	29
	2	--	2,538	3,570	1,032	41	0.68	10	29
	3	--	2,598	3,297	698	27	0.59	9	27
	5-c1	--	2,292	--	--	--	--	--	--
	5-c2	--	2,638	--	--	--	--	--	--
	6-c1	--	2,950	--	--	--	--	--	--
	6-c2	--	2,786	3,225.4	440	16	0.56	9	26

1. Refuse TREE concentrations from analytical results.
2. Week 0 leachant TREE concentrations from analytical results.
3. Week 1 and beyond leachant TREE concentrations estimated based on leachant blend volumes (raw AMD, recirculated AMD, H2O2).
4. Leachate TREE concentrations from analytical results.

Table 7A: Column leaching tests leachant and leachate pH readings.

Column	Cycle	Leachant pH	Leachate pH[1]	Leachate pH[2]
AMD-W	1	2.87	2.33	2.02
	2	2.45	2.36	2.02
	3	2.10	1.99	2.07
	4	1.94	1.84	--
	5	2.10	1.89	--
	6	1.97	1.93	--
	7	1.97	1.93	2.07
AMD-F	1	2.87	1.99	1.73
	2	1.95	2.17	1.81
	3	1.98	1.86	1.86
	4	1.84	1.72	--
	5	1.95	1.79	--
	6	1.82	1.82	--
	7	1.88	1.85	1.89
DI-W	1	4.54	2.18	2.07
	2	4.54	2.48	2.16
	3	5.75	2.12	2.19
	4	5.38	1.96	--
	5	5.38	1.97	--
	6	5.21	2.14	--
	7	5.21	2.12	2.27
DI-F	1	4.54	2.08	1.96
	2	4.54	2.35	2.04
	3	5.75	2.16	2.16
	4	5.38	1.96	--
	5	5.38	2.00	--
	6	5.21	2.19	--
	7	5.21	2.21	2.32
H_2O_2-W	1	2.87	2.21	2.00
	2	2.12	2.24	2.00
	3	2.07	1.97	2.05
	4	1.91	1.82	--
	5	2.03	1.85	--
	6	1.91	1.92	--
	7	1.90	1.92	2.01
H_2O_2-F	1	2.87	1.98	1.84
	2	2.06	2.07	1.83
	3	2.01	1.86	1.90
	4	1.88	1.75	--
	5	1.98	1.78	--
	6	1.86	1.84	--
	7	1.83	1.88	1.88

1. Leachate pH taken using the Mettler Toledo Seven 2 Go Pro while performing the column leaching test.
2. Leachate pH taken in the lab.

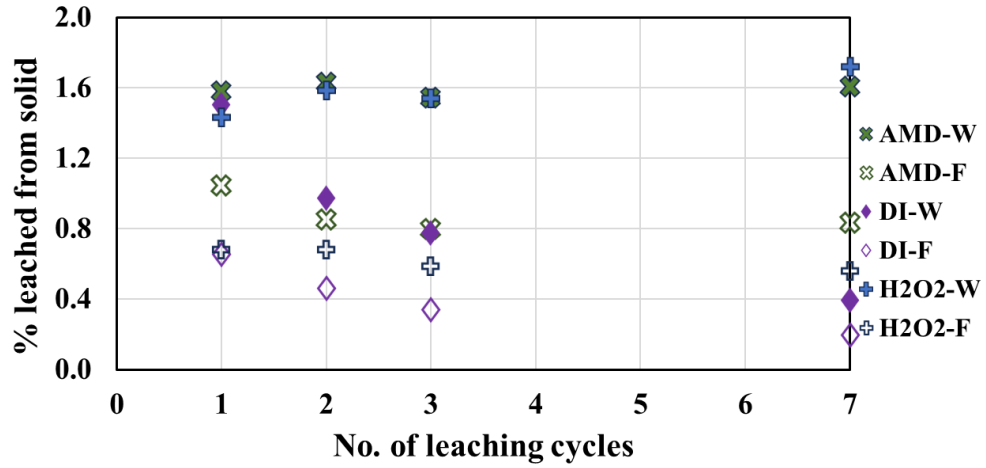


Figure 5A: Percent leached from solid in column leaching tests.

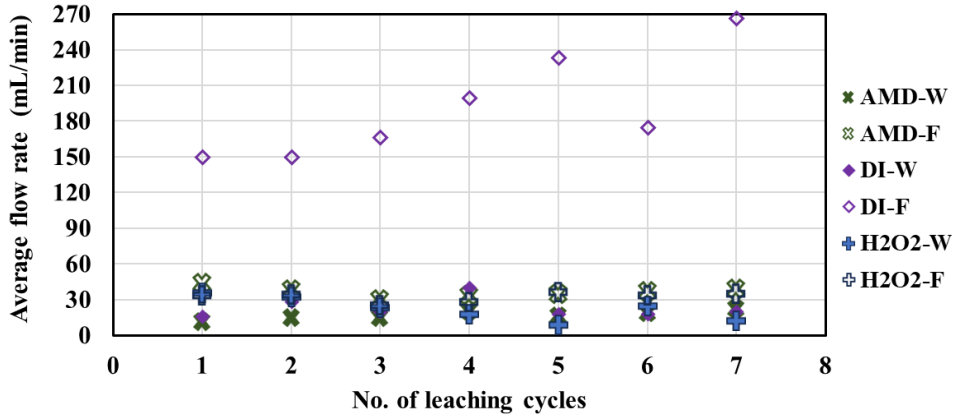


Figure 6A: Average outflow rate of leachant in column leaching tests.

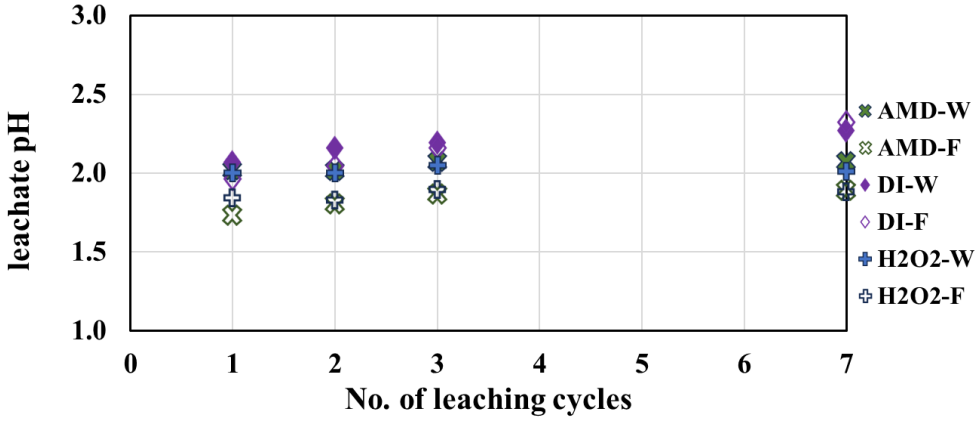


Figure 7A: pH of leachates collected from four columns over six weeks.

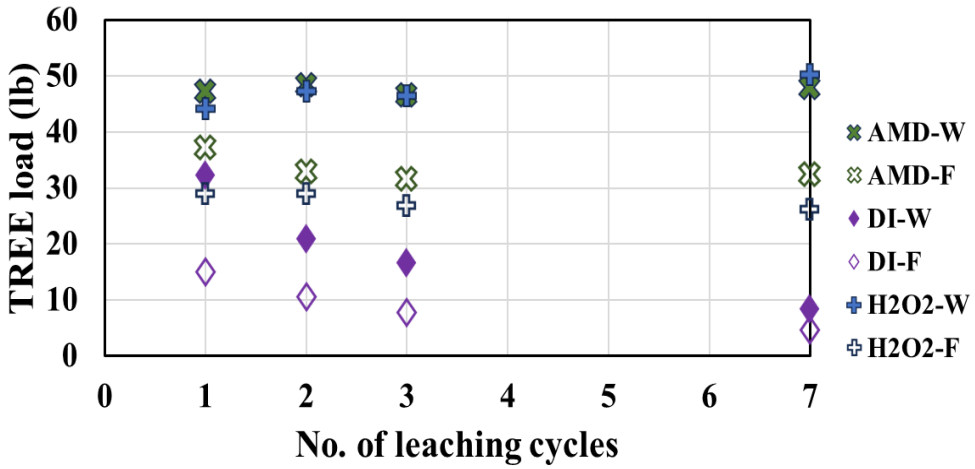


Figure 8A: TREE load determined based on column leaching tests results at field scale.

Table 8A: Leachate REE concentration from six columns – cycle 1.

Column	Increase REE Concentration (ug/L) / Week 1															
	Sc	Y	La	Ce	Pr	Nd	Sm	Eu	Gd	Tb	Dy	Ho	Er	Tm	Yb	Lu
AMD-W	410.7	787.7	259.0	928.5	144.3	702.9	206.4	46.8	234.3	34.3	198.5	34.4	90.7	11.0	61.8	8.4
AMD-F	42.9	77.2	426.7	1,197.4	155.8	656.3	146.9	28.9	112.6	11.7	48.5	6.3	13.3	1.2	6.5	0.6
DI-W	285.7	637.1	268.5	956.2	149.4	740.2	211.0	48.5	236.3	34.0	191.7	34.2	90.3	10.7	61.5	8.1
DI-F	45.4	127.0	213.2	639.0	90.0	420.7	101.0	20.5	83.9	10.1	47.9	7.3	17.5	1.8	10.4	1.3
H_2O_2-W	272.9	571.9	269.4	915.8	143.1	681.2	198.4	47.3	235.2	34.4	194.8	35.0	92.5	11.0	63.4	8.3
H_2O_2-F	13.9	26.7	279.6	777.4	103.0	446.7	101.5	20.0	81.1	8.4	35.3	4.8	9.9	0.9	5.2	0.4

Table 9A: Leachate REE concentration from six columns – cycle 2.

Column	Increase REE Concentration (ug/L) / Week 2															
	Sc	Y	La	Ce	Pr	Nd	Sm	Eu	Gd	Tb	Dy	Ho	Er	Tm	Yb	Lu
AMD-W	163.7	336.5	123.5	408.4	63.7	304.5	94.0	21.8	99.5	14.6	80.6	14.8	37.9	4.7	24.3	3.4
AMD-F	17.8	32.1	158.0	397.7	48.6	201.2	43.4	6.7	20.9	2.1	6.6	0.4	-0.7	-0.1	-0.9	-0.2
DI-W	185.4	438.6	184.9	639.2	97.5	478.0	132.0	29.2	137.6	19.5	108.9	19.1	50.2	5.9	33.9	4.6
DI-F	32.8	96.6	157.8	459.1	63.3	294.1	67.4	13.1	53.0	6.3	29.8	4.5	10.7	1.1	6.5	0.8
H_2O_2-W	185.0	381.6	161.8	493.5	69.1	333.1	93.6	19.6	87.7	12.3	69.3	11.9	29.6	3.5	18.2	2.7
H_2O_2-F	22.0	50.0	174.8	426.1	52.1	214.8	47.0	7.6	26.2	2.4	8.5	0.7	0.3	0.0	-0.5	-0.1

Table 10A: Leachate REE concentration from six columns – cycle 3.

Column	Increase REE Concentration (ug/L) / Week 3															
	Sc	Y	La	Ce	Pr	Nd	Sm	Eu	Gd	Tb	Dy	Ho	Er	Tm	Yb	Lu
AMD-W	92.1	241.6	70.8	256.3	41.1	219.1	60.4	12.7	62.9	9.2	50.6	9.0	25.0	2.7	17.2	2.0
AMD-F	8.9	24.0	90.7	250.1	33.4	143.6	30.9	5.3	22.4	1.8	5.4	0.6	1.3	0.0	0.3	-0.1
DI-W	132.7	352.8	145.7	513.9	77.8	386.5	105.0	23.0	109.4	15.2	85.4	15.1	39.6	4.6	27.0	3.6
DI-F	21.9	73.3	114.9	339.6	46.6	216.7	50.3	9.7	39.9	4.7	22.1	3.4	8.0	0.8	4.7	0.5
H_2O_2-W	115.9	306.9	112.2	393.8	61.0	285.0	81.0	18.3	87.6	12.5	70.8	11.9	31.8	3.7	21.0	2.7
H_2O_2-F	7.1	29.0	94.9	293.3	38.0	153.3	36.5	6.3	24.1	2.7	9.1	0.9	2.1	0.1	0.7	0.0

Table 11A: Leachate REE concentration from six columns – cycle 7.

Column	Increase REE Concentration (ug/L) / Week 6															
	Sc	Y	La	Ce	Pr	Nd	Sm	Eu	Gd	Tb	Dy	Ho	Er	Tm	Yb	Lu
AMD-W	95.0	146.7	76.4	183.7	35.4	197.2	51.2	13.1	60.4	8.5	52.2	9.2	25.1	2.9	15.8	2.1
AMD-F	27.7	30.5	59.6	116.2	19.8	122.6	27.1	5.7	21.8	3.0	16.5	2.3	4.5	0.6	2.8	0.3
DI-W	55.5	168.3	79.3	266.1	41.1	208.8	53.8	11.6	54.4	7.5	41.7	7.3	19.5	2.3	13.1	1.7
DI-F	10.1	42.1	69.5	195.2	26.8	125.9	28.6	5.7	23.1	2.8	13.6	2.1	5.0	0.5	2.7	0.4
H_2O_2-W	114.3	228.5	113.1	311.7	48.9	270.7	73.3	17.6	79.9	11.9	68.0	12.3	31.3	3.9	20.5	2.9
H_2O_2-F	23.4	24.4	61.2	136.5	20.3	104.4	21.7	5.3	18.9	2.3	12.4	2.0	3.7	0.5	2.4	0.3

Table 12A: Column leaching test TMM results.

Column	Week	Refuse TMM concentration (mg/kg)[1]	Leachant TMM concentration (mg/L)[2,3]	Leachate TMM concentration (mg/L)[4]	Increase in TMM concentration (mg/L)	Increase in TMM concentration (%)	Cumulative percent leached from solid (%)	TMM loading (lb/ac-ft)	TMM load (lb)
AMD-W	0	486,696.36	1,580	0	--	--	--	4,282	12,845
	1	--	1,580	5,669	4,089	259	0.84	15,363	46,089
	2	--	4,033	6,020	1,987	49	0.91	16,314	48,943
	3	--	4,577	5,699	1,122	25	0.85	15,444	46,333
	4	--	4,216	--	--	--	--	--	--
	5	--	4,875	--	--	--	--	--	--
	6	--	5,617	--	--	--	--	--	--
	7	--	4,875	5,711	836	17	0.85	15,477	46,430
AMD-F	0	479,451.08	1,580	0	--	--	--	4,282	12,845
	1	--	1,580	3,551	1,971	125	0.41	9,623	28,870
	2	--	2,566	3,364	799	31	0.37	9,116	27,349
	3	--	2,784	3,222	438	16	0.34	8,732	26,195
	4	--	2,688	--	--	--	--	--	--
	5	--	2,894	--	--	--	--	--	--
	6	--	3,222	--	--	--	--	--	--
	7	--	2,959	3,061	102	3	0.31	8,295	24,886
DI-W	0	486,696.36	0	0	--	--	--	0	0
	1	--	0	3,850	3,850	--	0.79	10,434	31,301
	2	--	0	2,871	2,871	--	0.59	7,780	23,341
	3	--	0	2,382	2,382	--	0.49	6,455	19,366
	4	--	0	--	--	--	--	--	--
	5	--	0	--	--	--	--	--	--
	6	--	0	--	--	--	--	--	--
	7	--	0	1,232	1,232	--	0.25	3,339	10,016
DI-F	0	479,451.08	0	0	--	--	--	0	0
	1	--	0	1,453	1,453	--	0.30	3,938	11,813
	2	--	0	1,139	1,139	--	0.24	3,087	9,260
	3	--	0	887	887	--	0.19	2,404	7,211
	4	--	0	--	--	--	--	--	--
	5	--	0	--	--	--	--	--	--
	6	--	0	--	--	--	--	--	--
	7	--	0	571	571	--	0.12	1,547	4,642
H_2O_2-W	0	486,696.36	1,580	0	--	--	--	4,282	12,845
	1	--	1,580	4,821	3,241	205	0.67	13,065	39,195
	2	--	3,448	6,317	2,869	83	0.97	17,119	51,357
	3	--	4,383	5,981	1,598	36	0.90	16,209	48,626
	4	--	4,063	--	--	--	--	--	--
	5	--	4,723	--	--	--	--	--	--
	6	--	5,383	--	--	--	--	--	--
	7	--	4,987	5,664	677	14	0.84	15,349	46,048
H_2O_2-F	0	479,451.08	1,580	0	--	--	--	4,282	12,845
	1	--	1,580	2,472	892	56	0.19	6,699	20,097
	2	--	1,913	2,877	964	50	0.27	7,797	23,390
	3	--	2,174	2,582	408	19	0.21	6,997	20,992
	4	--	1,913	--	--	--	--	--	--
	5	--	2,123	--	--	--	--	--	--
	6	--	2,314	--	--	--	--	--	--
	7	--	2,214	2,414	200	9	0.17	6,542	19,626

1. Refuse TMM concentrations from analytical results.
2. Week 0 leachant TMM concentrations from analytical results.
3. Week 1 and beyond leachant TMM concentration estimated based on leachant blend volumes (raw AMD, recirculated AMD, H_2O_2).
4. Leachate TMM concentrations from analytical results.

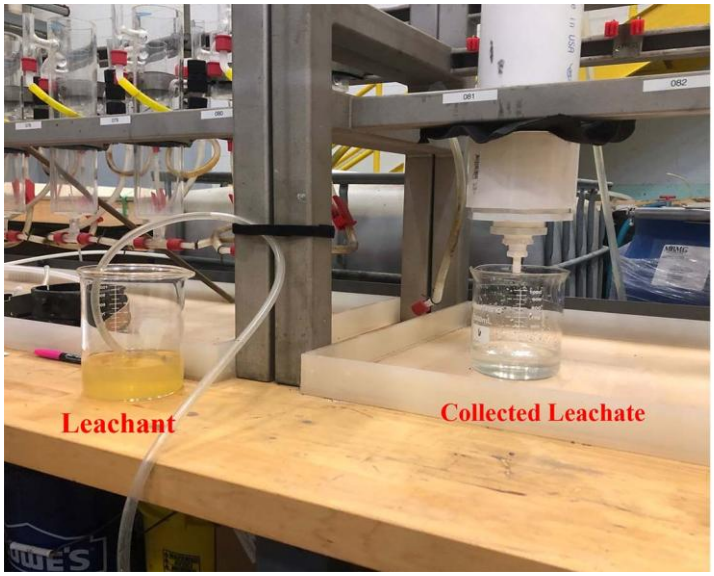


Figure 9A: Leachant (AMD) going into column AMD-R and collected leachate.

Table 13A: Leachant and leachate pH readings, alkalinity, and acidity (raw CCR).

Column	Cycle	Leachant pH	Leachate pH[1]	Leachate pH[2]	Alkalinity (mg/L)	Acidity (mg/L)
AMD-R	1	2.67	6.28	6.719	67.56	<4.092
	2	3.23	6.62	--	--	--
	3	6.22	6.64	--	--	--
	4	6.22	6.65	--	--	--
	5	6.65	6.91	--	--	--
	6	5.91	6.84	--	--	--
	7	6.84	6.95	--	--	--
	8	6.60	6.94	--	--	--
	9	6.70	6.97	--	--	--
	10	6.97	7.00	7.261	128.99	<4.092
DI-R	1	4.98	6.13	6.614	35.13	<4.092
	2	5.40	6.30	--	--	--
	3	5.98	6.67	--	--	--
	4	6.26	6.71	--	--	--
	5	6.38	6.69	--	--	--
	6	6.49	6.70	--	--	--
	7	6.40	6.82	--	--	--
	8	6.38	6.74	--	--	--
	9	6.40	6.90	--	--	--
	10	6.30	6.95	7.09	30.11	<4.092

1. Leachate pH taken using the Mettler Toledo Seven 2 Go Pro while performing the column leaching test.
2. Leachate pH taken in the lab.

Table 14A: Column leaching test results for raw CCR (TREE).

Column	Cycle	Refuse TREE concentration (mg/kg)[1]	Leachant TREE concentration (mg/L)[2,3]	Leachate TREE concentration (mg/L)[4]	Increase in TREE concentration (mg/L)	Increase in TREE concentration (%)	Cumulative percent leached from solid (%)	TREE loading (lb/ac-ft)	TREE load (lb)
AMD-R	0	417.16	488.6	0	--	--	--	1	4
	1	--	489	10	-479	-98	-0.11	1	4
	2	--	201	--	--	--	--	--	--
	3	--	34	--	--	--	--	--	--
	4	--	34	--	--	--	--	--	--
	5	--	10	--	--	--	--	--	--
	6	--	63	--	--	--	--	--	--
	7	--	10	--	--	--	--	--	--
	8	--	29	--	--	--	--	--	--
	9	--	22	--	--	--	--	--	--
	10	--	10	1	-9	-90	-0.12	0	0
DI-R	0	417.16	0	0	--	--	--	0	0
	1	--	0	6	6	--	0.00	0	0
	2	--	0	--	--	--	--	--	--
	3	--	0	--	--	--	--	--	--
	4	--	0	--	--	--	--	--	--
	5	--	0	--	--	--	--	--	--
	6	--	0	--	--	--	--	--	--
	7	--	0	--	--	--	--	--	--
	8	--	0	--	--	--	--	--	--
	9	--	0	--	--	--	--	--	--
	10	--	0	4	4	--	0.00	0	0

1. Refuse TREE concentrations from analytical results.
2. Week 0 leachant TREE concentrations from analytical results.
3. Week 1 and beyond leachant TREE concentration estimated based on leachant blend volumes (raw AMD and recirculated AMD).
4. Leachate TREE concentrations from analytical results.

Table 15A: Column leaching test results for raw CCR (TMM).

Column	Cycle	Refuse TMM concentration (mg/kg)[1]	Leachant TMM concentration (mg/L)[2,3]	Leachate TMM concentration (mg/L)[4]	Increase in TMM concentration (mg/L)	Increase in TMM concentration (%)	Cumulative percentage leached from the solid (%)	TMM loading (lb/ac-ft)	TMM load (lb)
AMD-R	0	488133.1	481.80	0	--	--	--	1	4
	1	--	481.80	1,778	1,296	269	0.00	1	4
	2	--	1260	--	--	--	--	--	--
	3	--	1,713	--	--	--	--	--	--
	4	--	1,713	--	--	--	--	--	--
	5	--	1,778	--	--	--	--	--	--
	6	--	1,635	--	--	--	--	--	--
	7	--	1,778	--	--	--	--	--	--
	8	--	1,726	--	--	--	--	--	--
	9	--	1,746	--	--	--	--	--	--
	10	--	1,778	2,097	319	18	0.00	5	14
DI-R	0	488133.1	0	0	--	--	--	0	0
	1	--	0	1351	1,351	--	0.00	4	11
	2	--	0	--	--	--	--	--	--
	3	--	0	--	--	--	--	--	--
	4	--	0	--	--	--	--	--	--
	5	--	0	--	--	--	--	--	--
	6	--	0	--	--	--	--	--	--
	7	--	0	--	--	--	--	--	--
	8	--	0	--	--	--	--	--	--
	9	--	0	--	--	--	--	--	--
	10	--	0	310	310	--	0.00	1	3

1. Refuse TMM concentrations from analytical results.
2. Week 0 leachant TMM concentrations from analytical results.
3. Week 1 and beyond leachant TMM concentration estimated based on leachant blend volumes (raw AMD and recirculated AMD).
4. Leachate TMM concentrations from analytical results.

Table 16A: Drum leaching test results (phases 1 and 2).

Drum #	Cycle #	Refuse TREE concentration (mg/kg)[1]	Leachant TREE concentration (µg/L)[2,3]	Leachate TREE concentration (µg/L)[4]	Increase in TREE concentration (µg/L)	Increase in TREE concentration (%)	Cumulative percent leached from solid (%)	TREE loading (g/m^3)	TREE load (kg)
Drum 1					Phase 1				
	0	311.1	1,147	0	--	--	--	1.14	4.2
	1	--	1,147	5,342	4,194	366	1.35	5.32	19.7
	2	--	3,365	4,572	1,207	36	1.10	4.56	16.9
	3	--	4,331	4,438	108	2	1.06	4.42	16.4
					Phase 2				
	4	--	4,105	8,826	4,721	115	2.47	8.80	32.5
	5	--	6,222	9,416	3,194	51	2.66	9.38	34.7
	6	--	7886	11000	3114	39	3.17	10.96	40.6
Drum 2					Phase 1				
	0	311.1	1,147	0	--	--	--	1.14	4.2
	1	--	1,147	3,549	2,402	209	0.77	3.54	13.1
	2	--	2,523	3,839	1,316	52	0.87	3.83	14.2
	3	--	3,650	3,723	74	2	0.83	3.71	13.7
					Phase 2				
	4	--	3,440	7,490	4,051	118	2.04	7.46	27.6
	5	--	5,576	8,323	2,747	49	2.31	8.29	30.7
	6	--	7153	10184	3030	42	2.90	10.15	37.6

1. Refuse TREE concentrations from analytical results.
2. Week 0 leachant TREE concentrations from analytical results.
3. Week 1 and beyond leachant TREE concentration estimated based on leachant blend volumes (raw and recirculated AMD).
4. Leachate TREE concentrations from analytical results

APPENDIX B – JAR TEST AND STATISTICAL ANALYSIS

Table 1B: TREE concentration correlated with three different leachants

Leachant	Recirc AMD	DI Water	Recic AMD + H_2O_2
Type of refuse	Increase in TREE concentration (µg/L)		
Weathered	4,160	3,963	3,774
	1,796	2,565	1,972
	1,173	2,037	1,616
	975	1,032	1,409
Fresh	2,933	1,837	1,915
	934	1,297	1,032
	619	957	698
	461	554	440

Table 2B: One-way ANOVA test results.

SUMMARY

Groups	*Count*	*Sum*	*Average*	*Variance*
Column 1	8	13049.54	1631.19261	1662367
Column 2	8	14242.1	1780.26288	1203316
Column 3	8	12855.54	1606.94189	1069228

ANOVA

Source of Variation	*SS*	*df*	*MS*	*F*	*P-value*	*F crit*
Between Groups	140933.8773	2	70466.9387	0.053724	0.947823	3.466800112
Within Groups	27544371.51	21	1311636.74			
Total	27685305.39	23				

Table 3B: Mann-Whitney test results.

SUMMARY	
n1	12
n2	12
n1*n2	144
n1+1	13
n2+1	13
Middle Term 1	78
Middle Term 2	78
R1	197
R2	103
U1	25
U2	119
U_stat	25
U_critical	42
Expected U (Mu)	72
Standard error of U	17.3
z	-2.72
p-value	0.003



Figure 1B: Jar test filtrate from each test.

The unit weight of the CCR determined using the reduced compaction energy was within the literature-defined range for reduced compaction energy.

Table 4B: Unit weight of CCR determined in published literature.

Literature	Year	Compaction Type	Compaction Energy ft-lb/ft^3 (kJ/m^3)	Density (g/cm^3)	Unit Weight (KN/m^3)
Current Project	2024	Standard	12,375 (592.5)	1.50	14.7
		Reduced	1,4160 (67.84)	1.23	12.1
Stevens	2016	Standard	12,375 (592.5)	-	15.4
		Reduced	1,4160 (67.84)	-	11.8
		Increased	24,749 (1,185)	-	14.3
Stewart	1990	-	-	1.61	15.8
Tolikonda and Quaranta, or/and Tolikonda	2012	Standard	12,375 (592.5)	-	18.8
		Reduced	1,4160 (67.84)	-	14.8
	2010	Increased	13,288 (636.2)	-	19.7
Hegazy et al.	2004	-	-	-	19.7
D'Appolonia	2009	-	-	-	18.0
Jedari et al.	2018	-	-	-	17.3

APPENDIX C – REFUSE SITE ASSESSMENT QUESTIONNAIRE FOR ACNR BLACKSVILLE NUMBER 2 MINE

Site Size

1- According to an aerial image of the site, the open-filled impoundment area is 1650 feet by 1700 feet. Is this the only open area with coarse coal refuse sitting on-site?
Response: There are no additional open coarse refuse areas on the site. There is a small 5-acre area southwest of Hughes Hollow and adjacent to the mine office in Wana, WV that contains some raw coal and pond cleanings. All other coarse refuse locations on site have been reclaimed.

2- Is the impoundment considered active? What is the permit number?
Response: The impoundment has not been completely abandoned.
MSHA Impoundment ID: 1211 WV30060-01
MSHA Mine ID: 46-01968
PA DEP CRDP No: 30950701
PA Dam Safety ID: D30-063
WV DEP Article 3: O101193 (Article 3 - U004684 is located downstream of the structure)

AMD Treatment

3- What is the AMD treatment protocol followed at the toe pond, and where is the treated water discharged into?
Response: The toe pond at the base of Hughes Hollow is no longer considered a pond and there is no AMD treatment at this location. However, water from Hughes Hollow gravity flows to what is considered the mine's "Beaver Pond". There is an active AMD treatment plant at the Beaver Pond that treats with hydrated lime. The AMD at the Beaver Pond is fed with water from the mine's Sedimentation Pond 2 and from a recirculation pump that is stationed on the west end of the Beaver Pond. Water from Hughes Hollow is mixed with the above-mentioned sources. A combination of pumps transfers water from the Beaver Pond to the mine's Freshwater Impoundment, located west of the Beaver Pond. The water within the Freshwater Impoundment is allowed to naturally decant into Dunkard Creek.

4- Is the permit for AMD treatment is different?
Response: A majority of the cap of Hughes Hollow is located in Pennsylvania and has the ID numbers listed in Question 2 above. A portion of the cap, in the southwest corner, is in West Virginia on WV DEP Article 3 Permit O101193. The AMD treatment system is located in West Virginia and is on WV DEP Article 3 Permit No. O1011193.

5- Have you ever had any problems containing the generated AMD?
Response: The mine has redundant pumps to handle large storm events and/or potential pump failures. Failed pumps could lead to AMD discharge.

6- Are there any prepared plans for cases of emergencies where the area receives unexpected amounts of rain?
Response: The mine has redundant pumps to handle large storm events and/or potential pump failures. The mine is seeking approval to install additional ditching on the east side of the cap to handle any overflow of the Low Gap Pond.

7- Are there any potential impacts from the area on local communities?
Response: There are no additional inherent potential impacts from this site that are not typical of coal refuse sites. There is an active EWP plan for this structure.

Topography

8- Are there any floodplain indicators in the area?
Response: The cap is well above any floodplain. Dunkard Creek, at the base of the structure, would have a floodplain.

9- What is the approximate slope of the area right at the moment before reclamation?
Response: The cap of the structure will be relatively flat with a minimum 1% grade before and following reclamation. The downstream face of the structure is benched with slopes of 2:1.

10- Does water drain naturally on-site with the given slope?
Response: In general, water naturally drains off the structure with the current slopes. Ruts and minor depressions will hold minimal water.

11- With the current slope, is there any water ponding on-site? Ponding does not include the known ponds within the impoundment area.
Response: Ruts and minor depressions will hold minimal water.

12- Are there any obvious places of settlement on site?
Response: None observed.

13- Is the CCR filling the impoundment compacted?
Response: General fill was placed in loose lifts. Structural fill, on the cap, has been compacted.

Hydrology

14- Regarding the area's hydrology, do we have an idea of how deep the underground water surface is?
Response: No answer was provided.

Construction materials sources

15- Is there any clay, sandy soil, and gravel available on-site?

Response: A soil survey report, for the general permit area, is attached for review.

Wildlife and Environmental Considerations

16- Are there any known sensitive species and habitats surrounding the area?
Response: A U.S. Fish and Wildlife Service species report is attached for review.

17- Does the solution containing ponds and ditches present any hazard to wildlife and birds?
Response: The ditches and ponds have not presented any known hazards to wildlife or birds. Water is treated to below effluent levels before it is discharged into any streams.

18- In the case of AMD containing pond failure, are there any nearby surface water or drinking water facilities that might be affected?
Response: No answer was provided.

19- How far is the nearest open surface water source? A river and/or a lake.
Response: The Pennsylvania Fork of Dunkard Creek is located 1,182 feet away from the structure. The decant of the Beaver Pond enters the West Virginia Fork of Dunkard Creek.

Meteorological Conditions:

20- Does short-term intense rainfall affect the size of ponds and ditches on site?
Response: All sediment control structures are designed to pass a 10 year/24 hour storm event.

APPENDIX D – REFUSE SITE ASSESSMENT QUESTIONNAIRE FOR ACNR LOVERIDGE MINE

Site Size

1- According to an aerial image of the site, the Loveridge impoundment area is 2112 feet by 1877 feet. Is this the only open area with coarse coal refuse sitting on-site?
Response: There are no additional open coarse refuse areas on the site. Response: The impoundment pictured below has been filled with coarse coal refuse and no longer receives refuse slurry. A second impoundment to the north of this site receives refuse slurry.

2- Is the impoundment considered active? What is the permit number?
Response: The site is an active coarse refuse pile and no longer considered an impoundment.
MSHA Mine ID: 46-01433
WV DEP Article 3: U007883



AMD Treatment

3- What is the AMD treatment protocol followed at the toe pond, and where is the treated water discharged into?
Response: There is an AMD at the toe pond that operates intermittently and treats with hydrated lime. The water in the toe pond is pumped to the Harvey Run II slurry impoundment.

4- Is the permit for AMD treatment is different?
Response: The permit for the AMD treatment site is the same as the refuse facility.

5- Have you ever had any problems containing the generated AMD?
Response: The mine has redundant pumps to handle large storm events and/or potential pump failures. Failed pumps could lead to AMD discharge.

6- Are there any prepared plans for cases of emergencies where the area receives unexpected amounts of rain?
Response: The mine has redundant pumps to handle large storm events and/or potential pump failures.

7- Are there any potential impacts from the area on local communities?
Response: There are no additional inherent potential impacts from this site that are not typical of coal refuse sites. There is an active EWP plan for this structure.

Topography

8- Are there any floodplain indicators in the area?
Response: The cap of the structure is well above the floodplain in elevation.

9- What is the approximate slope of the area right at the moment before reclamation?
Response: No response was provided.

10- Does water drain naturally on-site with the given slope?
Response: In general, water naturally drains off the structure with the current slopes. Ruts and minor depressions will hold minimal water.

11- With the current slope, is there any water ponding on-site?
Response: Ruts and minor depressions will hold minimal water.

12- Are there any obvious places of settlement on site?
Response: None observed.

13- Is the CCR filling the impoundment compacted?
Response: CCR being placed on the cap is placed in 2' thick loose lifts.

Hydrology

14- Regarding the area's hydrology, do we have an idea of how deep the underground water surface is?
Response: No answer was provided.

Construction materials sources

15- Is there any clay, sandy soil, and gravel available on-site?
Response: A soil survey report, for the general permit area, is attached for review.

Wildlife and Environmental Considerations

16- Are there any known sensitive species and habitats surrounding the area?
Response: A U.S. Fish and Wildlife Service species report is attached for review.

17- Does the solution containing ponds and ditches present any hazard to wildlife and birds?
Response: The ditches and ponds have not presented any known hazards to wildlife or birds. Water is treated to below effluent levels before it is discharged into any streams.

18- In the case of AMD containing pond failure, are there any nearby surface water or drinking water facilities that might be affected?
Response: No answer was provided.

19- How far is the nearest open surface water source? A river and/or a lake.
Response: Harvey Run Creek is located downstream of the structure approximately 1,100 feet from the top of the cap. Water entering Harvey Run would have to discharge from the toe pond prior to entering Harvey Run.

Meteorological Conditions:

20- Does short-term intense rainfall affect the size of ponds and ditches on site?
Response: All sediment control structures are designed to pass a 10 year/24 hour storm event.

APPENDIX E – ANALYTIC HIERARCHY PROCESS (AHP) CALCULATIONS

Table 1E. Pairwise comparison matrix of eight site selection criteria.

Criteria	Site Size	Topography	Environmental considerations	Haulage distance	CCR age	Construction materials source	Wildlife and vegetation	Meteorological conditions
Site Size	1	2	1/5	4	1/5	2	4	4
Topography	1/2	1	1/5	4	1/5	3	4	4
Environmental considerations	5	5	1	7	2	6	5	6
Haulage distance	1/4	1/4	1/7	1	1/7	1/2	1/2	1/2
CCR age	5	5	1/2	7	1	6	5	7
Construction materials source	1/2	1/3	1/6	2	1/6	1	1/3	2
Wildlife and vegetation	1/4	1/4	1/5	2	1/5	3	1	2
Meteorological conditions	1/4	1/4	1/6	2	1/7	1/2	1/2	1
SUM	**12.8**	**14.1**	**2.6**	**29.0**	**4.1**	**22.0**	**20.3**	**26.5**

APPENDIX F – GEOTECHNICAL MATERIAL CLASSIFICATION

Table 1F: Moisture content test results for the fresh CCR sample using an oven-drying method.

Container / Lid Number	CB4	CB5	CB6
Container Mass, g M_c	13.9	13.96	13.9
Container + Moist Specimen Mass, g M_{cms}	81.93	80.8	85
Initial Container Dry Specimen Mass, g	72.01	70.46	74.56
Secondary Container Dry Specimen Mass, g	71.99	70.45	74.54
Final Container Dry Specimen Mass, g M_{cds}	71.99	70.45	74.54
Mass of Water, g, $M_w = M_{cms} - M_{cds}$	9.94	10.35	10.46
Mass of Solids, g, $M_s = M_{cds} - M_c$	58.09	56.49	60.64
Water Content, %, $w = (Mw/Ms) \times 100$	**17.11**	**18.32**	**17.25**
Oven Temperature if Other Than 110 +/- 5°C	110	110	110
Remarks:	Time in Oven: 17 hr.		

Table 2F: Moisture content test results for the weathered CCR sample using an oven-drying method.

Container / Lid Number	CB1	CB2	CB3
Container Mass, g M_c	13.96	13.91	14.06
Container + Moist Specimen Mass, g M_{cms}	92.23	88.84	89.26
Initial Container Dry Specimen Mass, g	82.9	78.6	80.1
Secondary Container Dry Specimen Mass, g	82.89	78.6	80.08
Final Container Dry Specimen Mass, g M_{cds}	82.89	78.6	80.08
Mass of Water, g, $M_w = M_{cms} - M_{cds}$	9.34	10.24	9.18
Mass of Solids, g, $M_s = M_{cds} - M_c$	68.93	64.69	66.02
Water Content, %, $w = (M_w/M_s) \times 100$	**13.55**	**15.83**	**13.9**
Oven Temperature if Other Than 110 +/- 5°C	110	110	110
Remarks:	Time in Oven: 17 hr.		

Table 3F: Moisture content test results for the raw CCR using an oven-drying method.

Container / Lid Number	1	2	3
Container Mass, g M_c	13.96	13.95	13.82
Container+Moist Specimen Mass, g M_{cms}	58.69	65.73	66.42
Initial Container Dry Specimen Mass, g	55.96	62.56	62.5
Secondary Container Dry Specimen Mass, g	55.96	62.56	62.5
Final Container Dry Specimen Mass, g M_{cds}	55.96	62.56	62.5
Mass of Water, g, $M_w = M_{cms} - M_{cds}$	2.73	3.17	3.92
Mass of Solids, g, $M_s = M_{cds} - M_c$	42.00	48.61	48.68
Water Content, %, $w = (M_w/M_s)X100$	**6.50**	**6.52**	**8.05**
Oven Temperature	110	110	110
Remarks:	Time in Oven: 17 hr.		

Table 4F: Moisture content test results for the fresh CCR sample using an air-drying method.

Container / Lid Number	CB1	CB2	CB3
Container Mass, g Mc	13.91	13.89	13.95
Container + Moist Specimen Mass, g Mcms	85.3	81.79	84.88
Initial Container Dry Specimen Mass, g	77.78	75.52	77.4
Secondary Container Dry Specimen Mass, g	77.78	75.52	77.4
Final Container Dry Specimen Mass, g Mcds	77.78	75.52	77.4
Mass of Water, g, Mw=Mcms-Mcds	7.52	6.27	7.48
Mass of Solids, g, Ms=Mcds-Mc	63.87	61.63	63.45
Water Content, %, w=(Mw/Ms) ×100	**11.77**	**10.17**	**11.79**
Oven Temperature if Other Than 110 +/- 5°C	110	110	110
Remarks:	Time -air dried: 4 days		

Table 5F: Moisture content test results for the weathered CCR sample using an air-drying method.

Container / Lid Number	CB4	CB5	CB6
Container Mass, g Mc	13.91	13.91	14
Container + Moist Specimen Mass, g Mcms	83.14	83.92	82.09
Initial Container Dry Specimen Mass, g	74.7	76.49	73.99
Secondary Container Dry Specimen Mass, g	74.7	76.49	73.99
Final Container Dry Specimen Mass, g Mcds	74.7	76.49	73.99
Mass of Water, g, Mw=Mcms-Mcds	8.44	7.43	8.1
Mass of Solids, g, Ms=Mcds-Mc	60.79	62.58	59.99
Water Content, %, w=(Mw/Ms) × 100	**13.88**	**11.87**	**13.5**
Oven Temperature if Other Than 110 +/- 5°C	110	110	110
Remarks:	Time- air dried: 4 days		

Table 6F: Moisture content test results for the raw CCR using an air-drying method.

Container / Lid Number	4	5	6
Container Mass, g M_c	13.80	13.86	13.89
Container+Moist Specimen Mass, g M_{cms}	114.86	106	111.97
Initial Container Dry Specimen Mass, g	109.07	100.83	106.85
Secondary Container Dry Specimen Mass, g	109.07	100.83	106.85
Final Container Dry Specimen Mass, g M_{cds}	109.07	100.83	106.85
Mass of Water, g, $M_w=M_{cms}-M_{cds}$	5.79	5.17	5.12
Mass of Solids, g, $M_s=M_{cds}-M_c$	95.27	86.97	92.96
Water Content, %, $w=(M_w/M_s)X100$	**6.08**	**5.94**	**5.51**
Remarks:	Time -air dried: 4 days		

Table 7F: Specific gravity test results for the fresh CCR sample.

Container / Lid Number	CB1	CB2	CB3
Wt. of Pycnometer(g)	167.95	164.39	167.95
Sample + Pycnomter + Water(g)	695.52	690.8	694.76
Pycnometer + Water(g)	666.69	662.97	666.33
Wt. of Sample(g)	50.03	50.04	50.01
Specific Gravity	**2.33**	**2.22**	**2.27**

Table 8F: Specific gravity test results for the weathered CCR sample.

Container / Lid Number	CB4	CB5	CB6
Wt. of Pycnometer(g)	167.95	164.39	167.95
Sample + Pycnomter + Water(g)	692.44	688.59	690.64
Pycnometer + Water(g)	666.67	663.05	666.68
Wt. of Sample(g)	50	50	50.01
Specific Gravity	**2.04**	**2.02**	**1.91**

Table 9F: Specific gravity test results for the raw CCR sample.

Container / Lid Number	CB1	CB2	CB3
Wt. of Pycnometer(g)	167.67	159.71	164.37
Sample + Pycnomter + Water(g)	665.5	657.95	662.59
Pycnometer + Water(g)	720.5	713.1	716.24
Wt. of Sample(g)	100	100	100
Specific Gravity	**2.2**	**2.2**	**2.15**

Table 10F: Specific gravity of CCR from published studies.

Reference	**Specific Gravity (G_s)**
(Hegazy et al., 2004)	2.02
(D'Appolonia, 2009)	1.9 to 2.4
(Quaranta and Tolikonda, 2011)	2.54
(Zeng et al., 2008)	2.5
(Stevens, 2016)	2.19

Table 11F: GSD analysis data for all CCR samples.

Property	**Fresh**	**Weathered**	**Raw**
D10 (mm)	0.7	0.7	2.1
D30 (mm)	3	2.5	4.9
D50 (mm)	6	4.8	8.5
D60 (mm)	8.1	6	12.0
Passing No. 200, %	1.67	1.64	0.84
Cu	11.57	8.57	5.71
Cc	1.59	1.49	0.95

Table 12F: Sieve Analysis results of material passing No. 4 (4.75 mm) sieve for all CCR samples.

Property	Fresh	Weathered	Raw
D10 (mm)	0.4	0.45	0.70
D30 (mm)	1	1.4	1.50
D50 (mm)	1.6	2.2	2.30
D60 (mm)	2.2	2.5	2.60
Passing No. 200, %	1.02	1.56	1.58
Cu	5.5	5.56	3.71
Cc	1.14	1.74	1.24

Table 13F: GSD Data of CCR from published studies.

Reference	Grain Size				
	D10 (mm)	D30 (mm)	D50 (mm)	D60 (mm)	Passing No. 200 sieve (%)
(Hegazy et al., 2004))	<0.075	0.35	1.23	2.02	19.8
(D'Appolonia, 2009)	0.09	0.2	0.9	2	1.5
(Quaranta and Tolikonda, 2011)	-	3.65	6.5	8.45	1
(Zeng et al., 2008)	-	2	6	9	12
(Stevens, 2016) (2016)	0.525	1.73	4.33	6.85	3

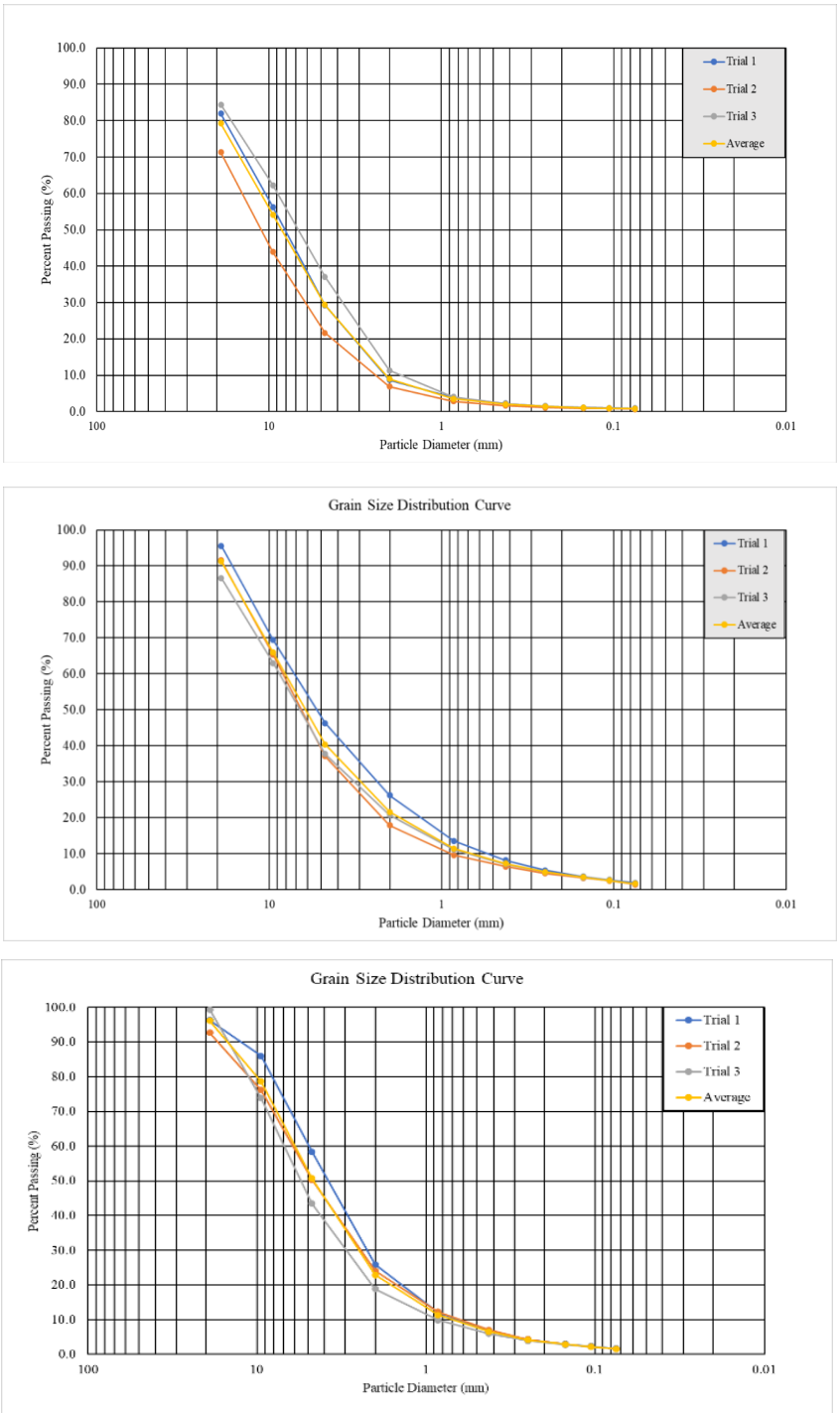


Figure 1F: Raw CCR (top), fresh CCR (middle), and weathered CCR (bottom) - particle size distribution curves.

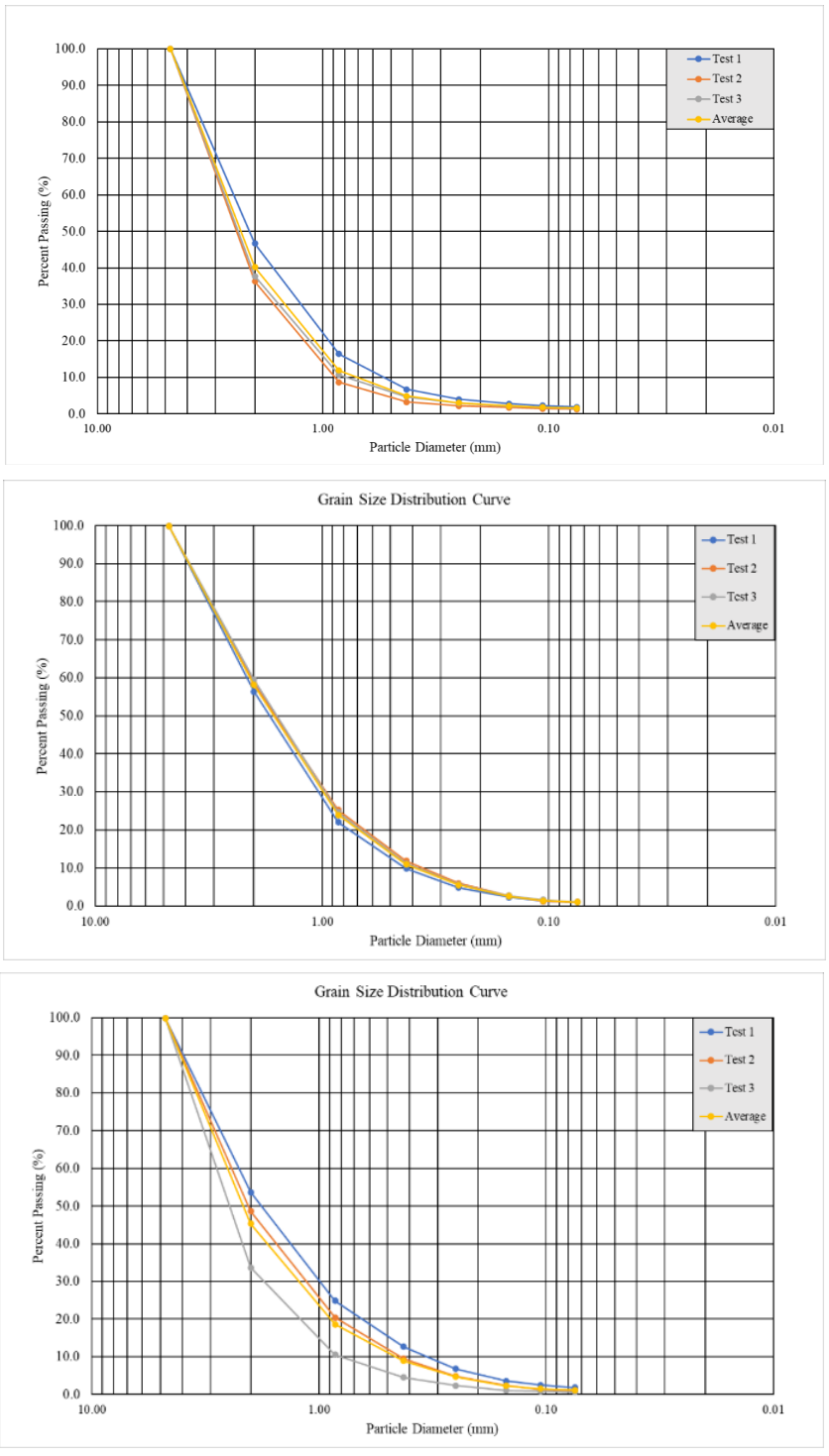


Figure 2F: Sieve analysis graphs of material passing sieve No.4 (4.75mm) For a) raw CCR (top), fresh CCR (middle), and weathered CCR (bottom).

Atterberg Limits

When water content is increased in fine-grained soils, soil behavior changes following the change in soil state from solid to semi-solid, plastic, and eventually liquid. Atterberg limits can tell a lot about the behavior of soils and other similar materials (B. M. Das, 2021). The Atterberg limit tests performed included the plastic limit (PL) and liquid limit (LL). The tests were performed on the fine portion of all CCR samples (raw, fresh, and weathered) according to ASTM standard test method D4318: Standard Test Methods for Liquid Limit, Plastic Limit, and Plasticity of soils. Four tests were conducted using the Liquid limit device following the Casagrande method to determine the liquid limit. Atterberg limits test results are presented in **Tables F14-F16 and Figure F3** for all CCR types.

The liquid limit was defined as moisture content at 25 blows, and it was found to be 21.9, 35.1, and 38.0 for the raw, fresh, and weathered CCR samples, respectively. The average plastic limits determined for the raw, fresh, and weathered samples were 16, 27, and 26, respectively. Using results from both liquid and plastic limit tests, the plasticity index for the raw, fresh, and weathered CCR samples was calculated to be 6, 8, and 12, which indicates a material with low and medium plasticity according to (B. M. Das, 2021). Calculated LL values are relatively larger than those of published references, while PL values are within the range of published studies (Table 18).

Table 14F: Plasticity index, liquid limit, and plastic limit determination – fine portion of the raw CCR sample.

Liquid Limit Test	**Test 1**	**Test 2**	**Test 3**	**Test 4**
Tin Number	CB-5	CB-6	CB-7	CB-8
Empty Container (g)	13.84	13.78	13.73	13.94
Container + Wet Sample (g)	40.51	42.04	36.83	32.38
Container + Dry Sample (g)	35.66	36.91	32.80	29.15
Moisture content w (%)	22.23	22.18	21.13	21.24
Weight of Water (g)	4.85	5.13	4.03	3.23
Number of Blows:	28.00	18.00	36.00	31.00
Liquid Limit:	**21.9**			
Plastic Limit Test	**Test 1**	**Test 2**	**Test 3**	
Tin Number	1	2	3	
Empty Container (g)	13.82	13.75	13.95	
Container + Wet Sample (g)	16.95	18.68	16.58	
Container + Dry Sample (g)	16.52	17.99	16.23	
Moisture content w (%)	15.93	16.27	15.35	
Weight of Water (g)	0.43	0.69	0.35	
Plastic Limit:	**16**			
Plasticity Index:	**5.9**			

Table 15F: Plasticity index, liquid limit, and plastic limit determination – fine portion of the fresh CCR sample.

Liquid Limit Test	**Test 1**	**Test 2**	**Test 3**	**Test 4**
Tin Number	CB1	CB2	CB3	CB4
Empty Container (g)	13.68	14.07	13.93	13.99
Container + Wet Sample (g)	24.64	26.86	27.97	27.52
Container + Dry Sample (g)	21.73	23.48	24.46	24.05
Moisture content w (%)	36.15	35.92	33.33	34.49
Weight of Water (g)	2.91	3.38	3.51	3.47
Number of Blows:	18	22	35	26
Liquid Limit:	**35.1**			
Plastic Limit Test	**Test 1**	**Test 2**	**Test 3**	
Tin Number	1	2	3	
Empty Container (g)	13.78	14.08	14.05	
Container + Wet Sample (g)	20.56	20.1	28.4	
Container + Dry Sample (g)	19.13	18.86	25.31	
Moisture content w (%)	26.73	25.94	27.44	
Weight of Water (g)	1.43	1.24	3.09	
Plastic Limit:	**27**			
Plasticity Index:	**8**			

Table 16F: Plasticity index, liquid limit, and plastic limit determination – fine portion of the weathered CCR sample.

Liquid Limit Test	**Test 1**	**Test 2**	**Test 3**	**Test 4**
Tin Number	CB-5	CB-6	CB-7	CB-8
Empty Container (g)	13.95	13.97	13.96	13.93
Container + Wet Sample (g)	26.55	30.22	26.96	30.44
Container + Dry Sample (g)	23.15	25.71	23.37	25.74
Moisture content w (%)	36.96	38.42	38.15	39.8
Weight of Water (g)	3.4	4.51	3.59	4.7
Number of Blows:	36	25	18	15
Liquid Limit:	**38**			
Plastic Limit Test	**Test 1**	**Test 2**	**Test 3**	
Tin Number	1	2	3	
Empty Container (g)	14	13.95	13.83	
Container + Wet Sample (g)	19.19	17.26	19.56	
Container + Dry Sample (g)	18.07	16.6	18.38	
Moisture content w (%)	27.52	24.91	25.93	
Weight of Water (g)	1.12	0.66	1.18	
Plastic Limit:	**26**			
Plasticity Index:	**12**			

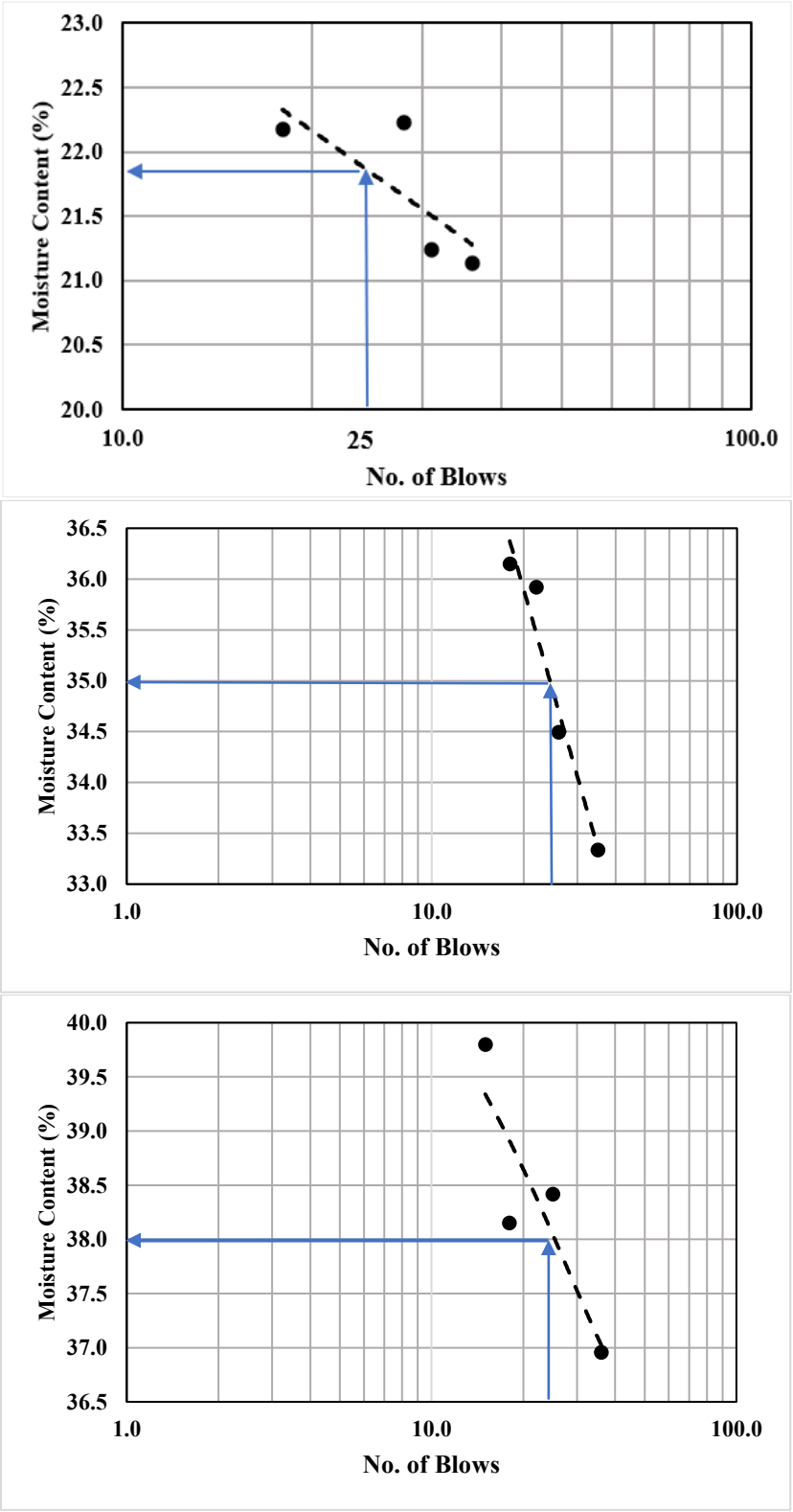


Figure 3F: Liquid Limit flow curve for the fine portion of the raw (top), fresh (middle), and weathered (bottom) CCR samples.

Table 17F: Atterberg limits of CCR in published studies.

Reference	LL	PL	PI
(D'Appolonia, 2009)	25-35%		<12%
(Quaranta and Tolikonda, 2011)	28.4	21.09	7.31
(Stevens, 2016)	30.1	26.1	4

Compaction Test

The first round of compaction test was conducted using Standard proctor compaction according to ASTM D698 to determine the maximum dry density of the CCR samples at a predetermined compaction energy of 12,375 ft-lb/ft^3 (592.5 kJ/m^3).

The second round of compaction tests was conducted for reduced compaction energies. The main goal of testing compaction under reduced energy was to simulate field conditions of heap leaching where the CCR is end-dumped with no external compaction. Compaction in the field would occur only when CCR particles are stacked together under their own weight and when water or other solutions (e.g., AMD) have settled on top of the CCR particles. Two different compaction energies were tested to model densities of loose (end dump) conditions and to compare a range of placement densities from optimum to loose (end dump) conditions.

The first reduced compaction condition test was completed following published literature (Quaranta and Tolikonda, 2011) by placing two layers of CCR in the compaction mold, where each layer was subjected to 4 blows using the compaction hammer (weight 5.5 lb (2.5 Kg) with a 12 in (30.4 cm) height of drop). The applied compaction energy was determined to be 1,416 ft-lb/ft^3 (67.84 kJ/m^3). The second reduced compaction test was performed by placing the compaction mold on a tray and dropping 5.5 lbs (2,500 g) of CCR from a table (dropping height of 6 feet), where it landed into the compaction mold by gravity under its own weight, which represents end dump condition (**Figure F4**). The applied compaction energy was determined to be 992 ft-lb/ft^3 (47.5 kJ/m^3).

Figures F5-F7 compare the standard and reduced energy curves for all CCR types. The results of the fresh CCR showed that the optimum dry unit weight was 15.55 KN/m^3 at an optimum moisture content of 16%. Results of the weathered CCR showed that the optimum dry unit weight was 15.40 KN/m3 at an optimum moisture content of 12.8 %. The reduced compaction energy of 1,416 ft-lb/ft^3 applied to fresh CCR resulted in an optimum dry unit weight of 14.4 KN/m^3 and an optimum moisture content of 22.8%. Meanwhile, optimum dry unit weight of 12.4 KN/m^3 and optimum moisture content of 13.7 % were obtained when the same reduced compaction energy was applied to the weathered refuse. Fresh CCR with a reduced compaction energy of 992 ft-lb/ft3 had an optimum dry unit weight of 11.3 KN/m^3 and an optimum moisture content of 10%. In contrast, weathered refuse was found to have an optimum dry unit weight of 11.8 KN/m^3 and a moisture content of 8% when the reduced compaction energy of 992 ft-lb/ft^3 was applied.

According to Das (2021), a higher compaction effort will result in a higher maximum dry unit weight and a lower optimum moisture content. Comparing the results from reduced compaction to the standard compaction showed that as the compaction effort was reduced to 1,416 ft-lb/ft^3, the optimum moisture content was increased, and the maximum dry unit weight of compaction was decreased for both samples (fresh and weathered). However, when no hammering was used in the third test, the optimum moisture content was decreased, which should not be the case in

reduced compaction tests. The refuse particles were not compacted under their own weight due to the small length of the specimen of 4.1 inches and dropping height of 6 feet. Thus, results from the third test (reduced compaction energy of 992 ft-lb/ft^3) were not considered in any further analysis. This test (reduced compaction energy of 992 ft-lb/ft^3) was not performed when the raw CCR was tested.

Testing the raw CCR showed that at a moisture content of 12.8%, the optimum dry unit weight was 16.7 kN/m^3. The optimum dry unit weight was 14.7 kN/m3 at an optimum moisture content of 19.5% with reduced compaction energy.

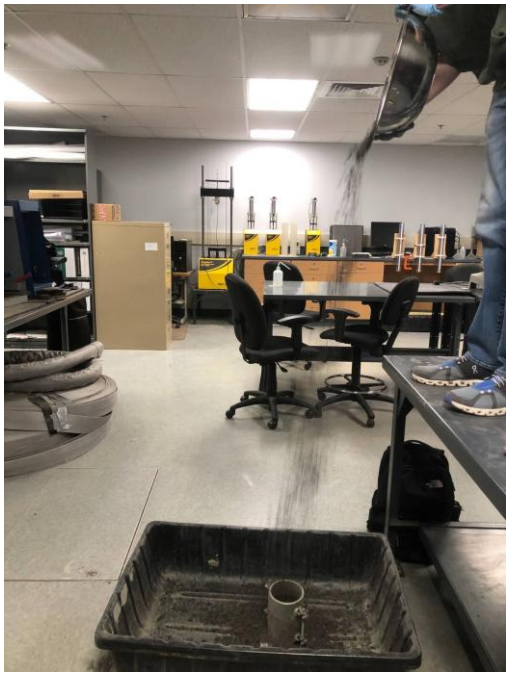


Figure 4F: Compaction mold sitting in a tray and CCR settling into the mold under its own weight by gravity to represent the end dump condition.

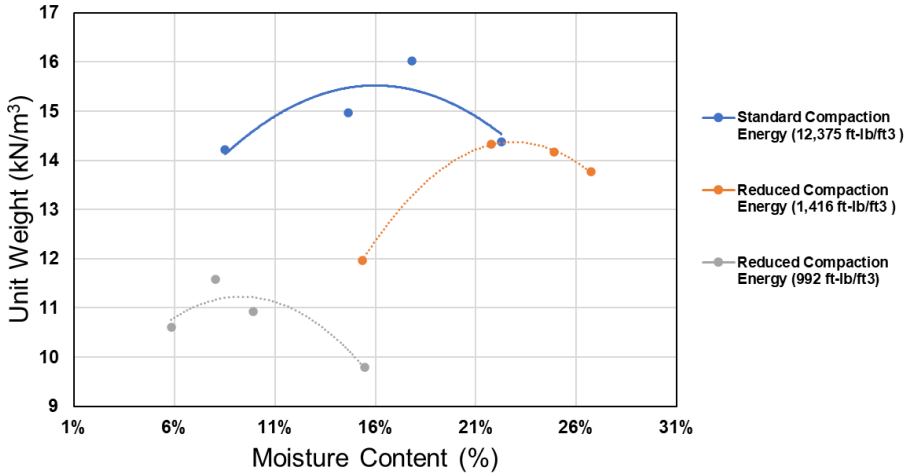


Figure 5F: Compaction curves of three different energies used with fresh CCR.

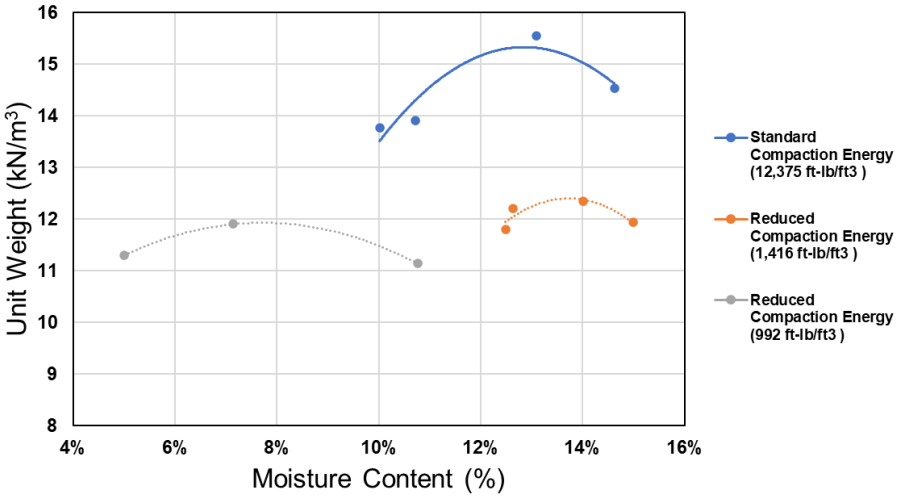


Figure 6F: Compaction curves of three different energies used with weathered CCR.

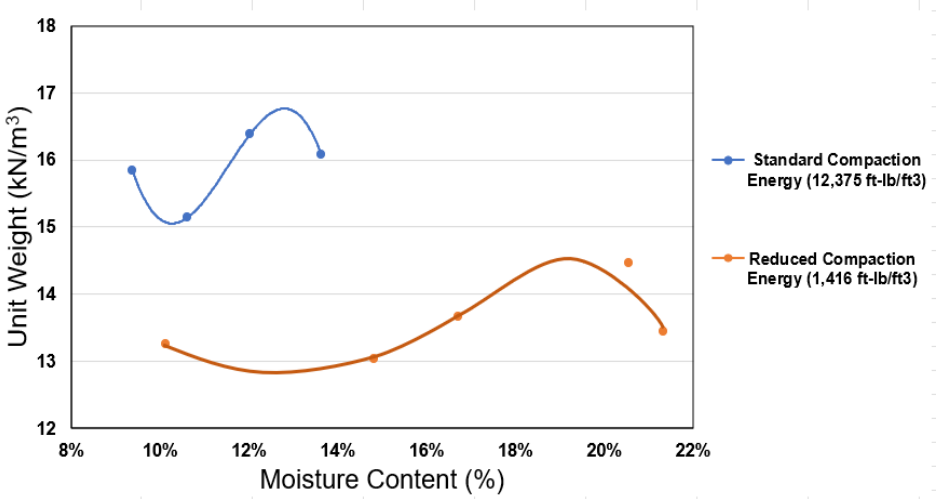


Figure 7F: Compaction Curves of two different energies used with fresh CCR.

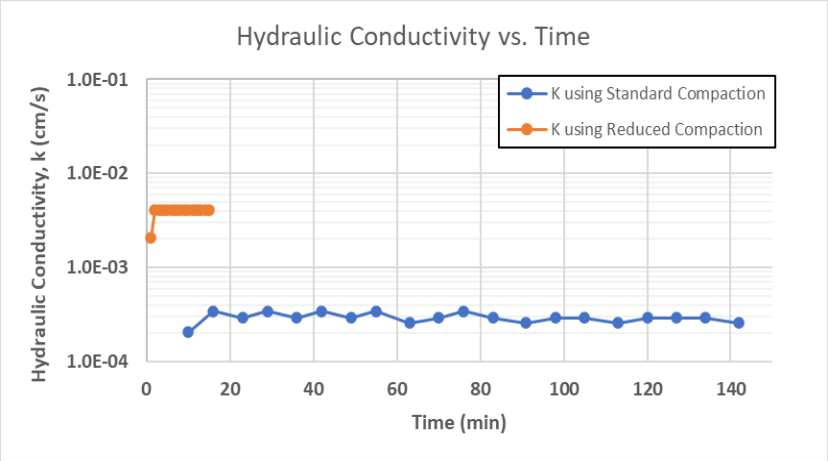


Figure 8F: Hydraulic conductivity of fresh CCR (Standard and Reduced Compaction).

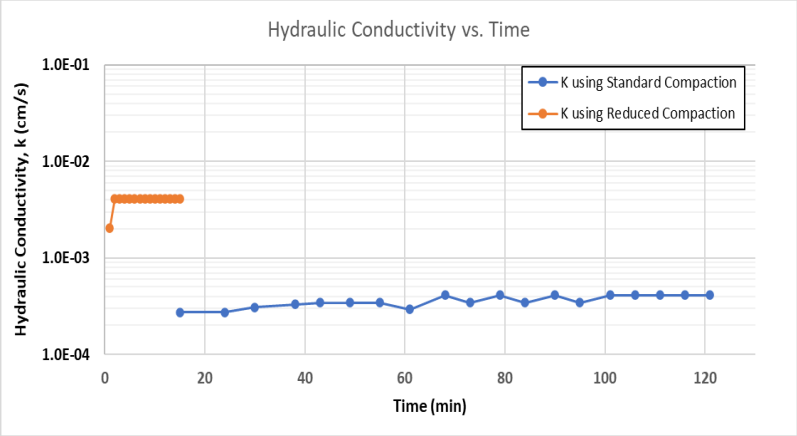


Figure 9F: Hydraulic conductivity of weathered CCR (Standard and Reduced Compaction).

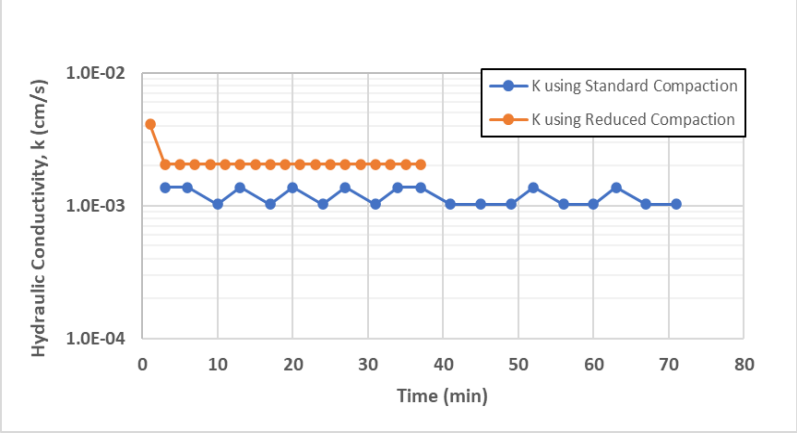
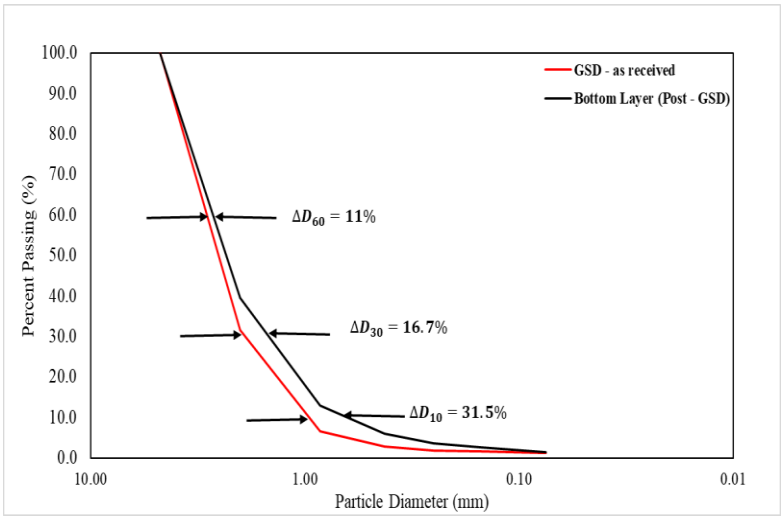
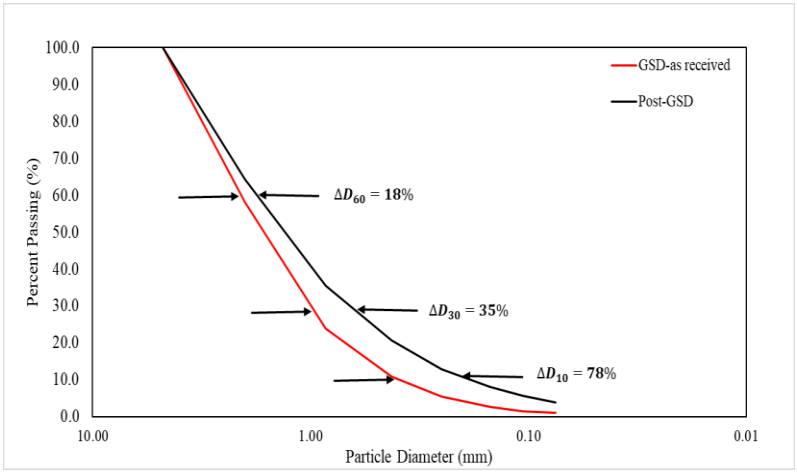


Figure 10F: Hydraulic conductivity vs. time of the raw CCR sample (Standard and Reduced Compaction).





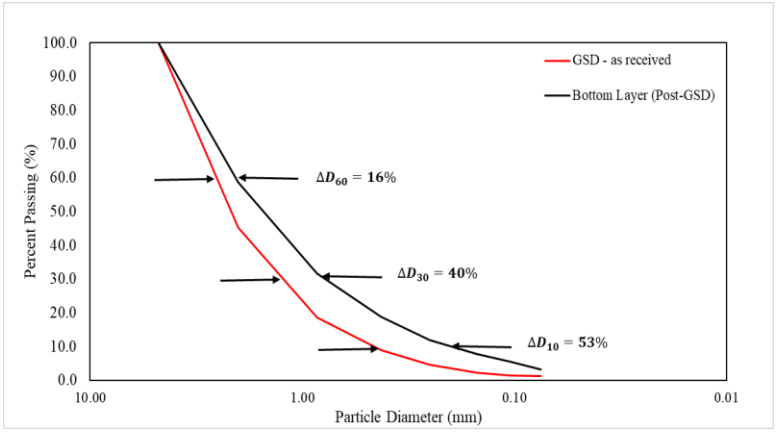


Figure 11F: Grading envelope for the bottom layer of the CCR sample (as received versus post-permeability GSD) – Reduced compaction: raw (top), fresh (middle), and weathered (bottom).

APPENDIX G – POSTER

Bench-scale Extraction of Rare Earth Elements from Appalachian Coarse Coal Refuse

Zainab S. Jawad[1], Nathan C. DePriest[2], Leslie C. Hopkinson[3], Rachel E. Spirnak[2], John D. Quaranta[4], Paul F. Ziemkiewicz[5]

[1]Graduate Research Assistant, Wadsworth Department of Civil & Environmental Engineering, West Virginia University, Morgantown, WV.
[2]West Virginia Water Research Institute, West Virginia University, Morgantown, WV
[3]Associate Professor, Wadsworth Department of Civil & Environmental Engineering, West Virginia University, Morgantown, WV.
[4]Professor, Wadsworth Department of Civil & Environmental Engineering, West Virginia University, Morgantown, WV.
[5]Tetra Tech, Morgantown, WV, USA

Background

- Coarse coal refuse (CCR) is a solid waste material generated during the coal preparation process [1,2]
- Previous research has found that the majority of Rare earth elements (REEs) are present in reject streams of coal preparation plants, especially CCR[3]
- REEs are essential components of many high-tech applications (e.g., electronic and health care)[3]
- CCR produces acidic mine drainage (AMD) with elevated metal (Fe, Al) and REE concentrations[2]

Research Hypothesis and Goal

Hypothesis: Recirculating AMD through CCR can accelerate pyrite oxidation to recover REE and exhaust major metals.

Research Goal: Evaluate the performance of leaching at bench-scale as a mechanism for the extraction of REEs from CCR in its field condition.

Methodology



Figure 1: Monongalia County Mine (also known as " Blacksville Number 2 Coal Mine ") (source: Google Earth)



Figure 2: Column leaching test setup (left) and drum leaching test setup (right).

Acknowledgment

The work described in this publication was supported by Grant/Cooperative Agreement Number S23AC00063 from the US Department of Interior, Office of Surface Mining Reclamation and Enforcement (OSMRE), Applied Sciences Program, and by in-kind support from Monongalia County Resources, Inc. (MCR), a subsidiary of American Consolidated Natural Resources (ACNR). Its contents are solely the responsibility of the authors and do not necessarily represent the official views of the OSMRE and ACNR.

Results: Columns leaching tests

- Best results – Weathered CCR with AMD as the leaching solution

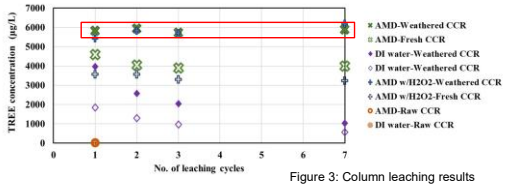


Figure 3: Column leaching results

Geotechnical Properties	CCR		
	Raw	Fresh	Weathered
Initial Moisture Content (%) - Oven dried	7.0	14.4	17.6
Initial Moisture Content (%) – air dried	5.4	11.3	13.1
D10 (mm)	2.0	0.7	0.7
D30 (mm)	5.0	3.0	2.5
D50 (mm)	8.1	6.0	4.8
D60 (mm)	12.0	8.1	6.0

Column	Paste pH
Weathered	4
Fresh	3
Raw	9

Results: Drum leaching tests

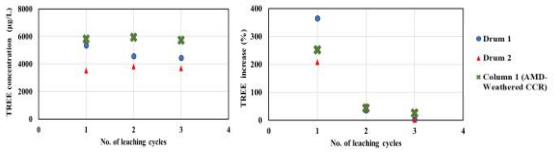


Figure 4: TREE concentration (left) and percentage TREE increase (right) in leachate-drum leaching (phase 1) and three cycles of column leaching

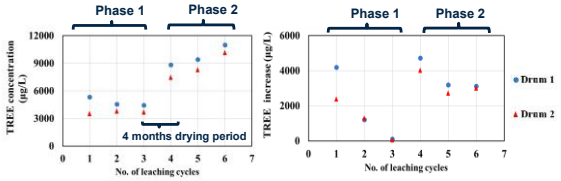


Figure 5: Drum leaching results: TREE content (left) and TREE increase in leachate (right)

Conclusions

The combination of AMD and weathered CCR offers the best opportunity for leaching REEs within the first leaching cycle. Maintaining an adequate drying period between flushing cycles may enable additional pyrite oxidation, REE compound accumulation on the solid surfaces, and improved leaching potential.

Applicability to Mining

The creation of sustainable REE sources in the long term is the primary value driver. Among the possible benefits of this work in terms of environmental controls are efficient refuse management and a controlled environment for AMD treatment, both of which are considered environmental hazards with no beneficial end use.

References

1- Wang P, Sun Z, Hu Y, Cheng H (2019) Leaching of heavy metals from abandoned mine tailings brought by precipitation and the associated environmental impact. Science of The Total Environment 695:133893. https://doi.org/10.1016/j.scitotenv.2019.133893.
2- Hudson-Edwards KA, Kemp D, Torres-Cruz LA, Macklin MG, Brewer PA, Owen JR, Franks DM, Marquis E, Thomas CJ (2024) Tailings storage facilities, failures and disaster risk. Nature Reviews Earth & Environment 5:612–630
3- Honaker R, Hower J, Eble C, Weisenfluh J, Groppo J, Rezaee M, Bhagavatula A, Lutrell G, Bratton R, Kiser M (2014) Laboratory and bench-scale testing for rare earth elements. Cell 724:554–3652